Ultimate Strength in Bending and Torsion of Prestressed Beams Reinforced with Longitudinal Steel Only

P. J. Wainwright

A Thesis submitted for the degree of Doctor of Philosophy

Department of Civil Engineering
The University of Aston in Birmingham

February 1972

Synopsis

Reported in this thesis are tests on 22 No. eccentrically prestressed rectangular beams. The beams were subjected to varying ratios of bending moment to torsion by means of a test-rig designed by the author. Experimental observations indicated 3 distinct modes of failure. The theoretical solutions proposed for all modes are based on the following generally accepted principles of structural analysis.

1) equilibrium of forces about a skew axis of bending
2) a compatability equation of linear strain distributed
3) linear stress-strain relationships for the concrete and the steel.

Failure in Mode 1 is assumed to be governed by the Cowan criteria of failure, whilst Modes 2 and 3 are dependent upon the modulus of rupture strength. The theory for Mode 1 allows for the inclusion of a dowel force at right angles to the steel where applicable. The theoretical solutions are compared with 131 experimental results of the author and other investigators.

An investigation was carried out into the behaviour of concrete under combined stresses. This involved the testing of 22 No. hollow cylinders and 20 No. split cubes under varying ratios of direct stress to shear stress. Tests were also carried out concerning the stress - strain relationship and the direct tensile strength of the concrete.

Acknowledgements

The author wishes to express his thanks to Mr. L. H. Martin, B.Sc., C.Eng., M.I.C.E., for his continual help, encouragement and advice throughout this project, and to Professor M. Holmes, B.Sc., Ph.D., C.Eng., F.I.C.E., F.I.Struct.E., F.I.Mun.E., for acting as advisor.

Thanks are due to Mr. W. Parsons, the Chief Technician in the Civil Engineering Department at the University of Aston and to his assistants, for their help during the experimental work. In particular the author would like to thank Mr. J. Hollins for the invaluable service provided during all of the tests carried out.

Special thanks are also due to Miss J. M. Baker who was responsible for the typing of the thesis, and to Miss P. C. Sage for her preparation of the drawings.

The Author

The author graduated from the Department of Civil Engineering at the University of Aston in 1968, after completing a 4 year sandwich course. The following 3 years have been spent in full time postgraduate study at the above department.

No part of this work has been submitted in support of an application for another degree or qualification.

Notation

A_{hc}	Cross-sectional area of hollow cylinder
A_{sl}	Cross-sectional area of lower layer of longitudinal steel
A_{su}	Cross-sectional area of upper layer of longitudinal steel
b	Bredth of section
C_l	Lever arm factor
D_l	Bond slip factor for lower layer of longitudinal steel
D_u	Bond slip factor for upper layer of longitudinal steel
d	Depth of section
d_l	Depth to lower layer of longitudinal steel
d_n	Depth of compressed concrete
d_u	Depth to upper layer of longitudinal steel
E_c	Young's modulus of elasticity of concrete
E_d	Dynamic modulus of elasticity of concrete
E_{sl}	Modulus of elasticity of lower layer of longitudinal steel
E_{su}	Modulus of elasticity of upper layer of longitudinal steel
E_{oc}	Initial tangent modulus of concrete
e	Eccentricity of prestressing steel
F_l	Dowel force in lower layer of longitudinal steel – Mode 1
F_u	Dowel force in upper layer of longitudinal steel – Mode 1
f'_c	Uniaxial cylinder compressive strength of concrete
f_{isl}	Stress in lower layer of longitudinal steel normal to the skew axis due to loading
f_{isu}	Stress in upper layer of longitudinal steel normal to the skew axis due to loading
f_m	Maximum direct compressive stress in the concrete normal to the axis of the beam due to bending moment – Mode 1
f_{mi}	Maximum compressive stress in the concrete normal to the skew plane due to loading – Mode 1

f_p	Direct compressive stress on a standard concrete cylinder
f_{r2}	Modulus of rupture strength of concrete – Mode 2
f_{r3}	Modulus of rupture strength of concrete – Modes 1 and 3
f_{psc}	Direct compressive stress on split cube
f_{sc}	Cube splitting stress
f_{sl}	Normal stress in lower layer of longitudinal steel due to applied bending moment
f_{su}	Normal stress in upper layer of longitudinal steel due to applied bending moment
f_{sp}	Split cylinder strength of concrete
f_t	Uniaxial tensile strength of concrete
f_{tp}	Apparent tensile strength of concrete
f_v	Maximum shear stress in the concrete, on a plane normal to the axis of the beam, due to applied torsional moment – Mode 1
f_{xhc}	Lateral stress on hollow cylinder
f_{yhc}	Direct compressive stress on hollow cylinder
G_c	Modulus of rigidity of concrete
G_l	Modulus of rigidity of lower layer of longitudinal steel
G_u	Modulus of rigidity of upper layer of longitudinal steel
J_{hc}	Polar moment of inertia of hollow cylinder
k_i	Direct stress distribution constant for concrete on a plane normal to the skew axis
k_m	Direct stress distribution constant for concrete on a plane normal to the axis of the beam
k_t	Torsional shear stress distribution constant for concrete on a plane normal to the axis of the beam
L_l	Lever arm of resistance of lower layer of longitudinal steel

L_u	Lever arm of resistance of upper layer of longitudinal steel
M	Applied bending moment – Mode 1
M_3	Applied bending moment – Mode 3
M_c	Bending moment at which first crack appears in soffit of beam – Mode 1
M_u	Ultimate moment of resistance in pure bending – Mode 1
M_{u3}	Ultimate moment of resistance in pure bending – Mode 3
m_l	Modular ratio for lower layer of longitudinal steel
m_u	Modular ratio for upper layer of longitudinal steel
P_{hc}	Direct axial load on hollow cylinder
P_s	Stress due to prestress at bottom of beam – Mode 1
P_{s2}	Stress due to prestress at centre of longer side of beam – Mode 2
P_{s3}	Stress due to prestress at top of beam – Mode 3
P_{tl}	Initial prestressing force in lower layer of longitudinal steel
P_{tu}	Initial prestressing force in upper layer of longitudinal steel
r_{hc}	Outer radius of hollow cylinder
T	Applied torsional moment – Mode 1
T_2	Applied torsional moment – Mode 2
T_3	Applied torsional moment – Mode 3
T_c	Torsional moment at which first crack appears in soffit of beam – Mode 1
T_{hc}	Torsional load on hollow cylinder
T_{u2}	Ultimate moment of resistance in pure torsion – Mode 2
T_{u3}	Ultimate moment of resistance in pure torsion – Mode 3
U_w	Uniaxial cube compressive strength of concrete

Z_2	Elastic section modulus – Mode 2
Z_3	Elastic section modulus – Mode 3
$\beta°$	Angle of inclination to the horizontal of the straight line failure envelope proposed by Cowan
$\gamma°$	Angle of inclination to the vertical of failure cracks in hollow cylinders
γ_h	Prestress factor developed by Hsu
ε_c	Direct compressive strain in standard concrete cylinder
ε_{cl}	Direct strain, due to applied bending moment, in concrete adjacent to lower layer of longitudinal steel
ε_{cm}	Maximum direct strain due to applied bending moment in concrete at top of beam
ε_{cu}	Direct strain, due to applied bending moment, in concrete adjacent to upper layer of steel
ε_{1hc}	Minimum principal strain in hollow cylinder
ε_{2hc}	Maximum principal strain in hollow cylinder
ε_{icl}	Strain in concrete, due to loading, on a plane normal to the skew axis, adjacent to lower layer of longitudinal steel
ε_{icm}	Maximum strain in concrete, due to loading, on a plane normal to the skew axis, at top of beam
ε_{icu}	Strain in concrete, due to loading, on a plane normal to the skew axis, adjacent to upper layer of longitudinal steel
ε_{il}	Strain due to loading, in a direction normal to the skew axis, in lower layer of longitudinal steel
ε_{iu}	Strain due to loading, in a direction normal to the skew axis, in upper layer of longitudinal steel

ε_{sl}	Direct strain, due to applied bending moment, in lower layer of longitudinal steel
ε_{su}	Direct strain, due to applied bending moment, in upper layer of longitudinal steel
ε_{uc}	"Peak" strain in concrete
ε_{xhc}	Lateral strain in hollow cylinder
ε_{yhc}	Direct axial strain in hollow cylinder
$\theta°$	Angle of inclination of the compression hinge in the top of the beam – Mode 1
$\theta°_2$	Angle of inclination of the compression hinge in the side of the beam – Mode 2
$\theta°_3$	Angle of inclination of the compression hinge in the bottom of the beam – Mode 3
$\theta°_c$	Angle of inclination of the first crack in the bottom of the beam – Mode 1
$\sigma_1, \sigma_2, \sigma_3$	Principal stresses – Octahedral stress theory
σ_c	Poisson's ratio for concrete
σ_x	Direct stress – Mohr's theory
σ_o	Octahedral direct stress
τ_{hc}	Shear stress on hollow cylinder
τ_{sc}	Shear stress on split cube
τ_o	Octahedral shear stress
τ_{xy}	Shear stress – Mohr's theory
ϕ_{hc}	Shear strain in hollow cylinder

CONTENTS

CHAPTER I

Introduction

The problem of torsion in concrete structural members has received very little attention until fairly recently. Although previously its presence had not been overlooked, its effects had often been minimized by the generously proportioned members designed by earlier working stress designs. When it was considered, many engineers planned structural frames to minimize the effects of torsion. The advent of ultimate strength design and liberalized load factors led to slenderer members in which secondary torsion effects were significant. In addition architects began to envisage new structural forms involving relatively high torsional stresses. Such structures include, free standing spiral staircases, edge beams of shells, plate and grid frameworks, and elevated roadways particularly those curved in plan.

Prior to the early sixties much of the research work carried out had been related to either plain, or reinforced concrete, in pure torsion. In practice, however, torsion very rarely occurs without either bending, or bending and shear. From a practical view point, therefore, it was important that a clear understanding of the interaction of these forces in structural concrete be obtained.

At this stage there had been very few investigations into the effects of torsion on prestressed concrete. With the growing use of prestressed concrete in the construction industry, especially where unusually large spans were involved, there was an ever increasing need for research to be undertaken within this field.

During the early sixties there was a growing awareness amongst engineers about the importance of torsion in concrete structures. Work was thus undertaken with the aim of drawing up design

recommendations for the use of reinforced concrete under combinations of bending, torsion, and shear. Despite this sudden growth of interest over the past few years there are still very few codes of practice that contain clauses on torsion.

Although our knowledge of the behaviour of reinforced concrete in this field is now quite considerable, there is still a dearth of information on prestressed concrete. The majority of research work undertaken in the last 10 years has been concerned with reinforced concrete. Regarding the small amount of work in the field of prestressed concrete, much of it was concerned with beams of I or T sections, leaving the relatively simpler problem of rectangular sections somewhat under-investigated. Naturally the author appreciates the fact that I and T sections are more common in practice, yet feels that a greater understanding of the basic problem is required.

1.1. Review of Previous Work

The first person to carry out work on torsion in any form was St. Venant[1] in 1853. Using the theory of elasticity, he obtained a rigorous solution for the stresses in a homogeneous rectangular member subjected to torsion. Even today his work is still used as a basis for many of the torsion theories for materials including plain, reinforced and prestressed concrete. In the case of plain concrete subject to torsion, failure is assumed to be reached when the maximum shear stress, and therefore the maximum principal tensile stress, is equal to the tensile strength of the concrete. In general, however, it has been shown that this elastic theory underestimates the strength of the concrete. This is because concrete is known to behave as an elastoplastic material. To account for this inelastic behaviour of concrete, theories were developed by Miyamoto,[2] Turner and Davies[3] and Marshall and Tembe[4] on the basis of different

idealized non-linear stress - strain curves for concrete. The membrane and sand-hill analogies developed by Nadai[5] have also been used in the analysis of torsional problems.

Tests on prestressed concrete subjected to pure torsion were first carried out in 1945 by Nylander[6] . He tested 15 uniformly prestressed rectangular beams, and used the maximum tensile stress criteria as the basis of his theoretical solution.

In 1953 Cowan and Armstrong [7] reported tests on, 3 uniformly prestressed, and 6 eccentrically prestressed, rectangular beams tested under pure torsion, pure bending, and various combinations of the two. These beams contained no transverse reinforcement, and failure in pure torsion occured immediately after the formation of the first crack. In pure bending, however, the beam was able to carry a much greater load than that at which the first crack appeared. For high ratios of M/T vertical cracks due to bending and inclined cracks due to torsion developed together, but on removal of the load only those cracks caused by the bending moment closed. Failure in this case was initiated by a diagonal tension fracture at the centre of the beam followed by a diagonal compression fracture on the opposite face. For low ratios of M/T, failure was very similar to that in pure torsion and generally less destructive than for high ratios. With eccentrically prestressed beams in pure torsion the first crack appeared at the top of the beam due to the low prestress.

In his theory Cowan assumed that failure was determined by the criterion of constant maximum tensile stress. For prestressed concrete in pure torsion he proposed an interaction equation of the form:-

$$\left(\frac{T}{T_p}\right)^2 - \frac{P_t}{K_E T_P} = 1$$

where T = Ultimate torsional load

T_P = Torsional strength of the plain concrete section

P_t = Prestress at critical section

K_E = Torsion moment constant based on Nadai's sand heap analogy

For the case of bending and torsion the equation takes the form

$$\left(\frac{T}{T_u}\right)^2 + \frac{K_b}{K_t}\left(\frac{M}{T}\right)\left(\frac{T}{T_u}\right) = 1$$

T_u = Strength in pure torsion

T = Applied torsional moment

M = Applied bending moment

K_b = Bending moment constant

K_t = Torsional moment constant

The second equation is based upon macroscopic stresses, and is not applicable to beams that show extensive cracking. It cannot therefore be used to determine the ultimate loads of beams subjected to combined bending and torsion.

During his analysis on prestressed concrete grillage beams, Reynolds[8] carried out tests on 12 rectangular eccentrically prestressed beams under varying ratios of bending and torsion. He found that the maximum principal tensile stress at the section where it first cracked was between 1.3 and 1.5 times the stress obtained from the split cylinder tests. He calculated the maximum principal tensile stress using the relationship developed by Cowan.

Paul Zia[9] carried out extensive tests in pure torsion on 68 pretensioned, rectangular, T, and I sections, with some plain sections and some reinforced. Zia observed that the crack angle at failure depended on the amount of prestress. The angle

(to the horizontal) was 45° for zero prestress and decreased with increase in prestress. For his failure criteria he proposed a modification to Cowan's, joining the intersection of the Coulomb limiting lines with the shear axis and the maximum tensile stress intercept with straight lines. His failure theory was based upon St. Venant's elastic torsion theory with which, in conjunction with a finite difference method,he was able to obtain a solution for all sections. His experimental results for rectangular and T sections agreed fairly well with his theory, but his results on I sections tended to show rather large discrepancy. He also reported that the ultimate strength of prestressed members with web steel was equal to the sum of the cracking moment of the member and the moment resisted by the web steel.

Gardner[10] tested 16 beams of eccentrically prestressed I section by the application of a bending moment which varied from 10% and 80% of the ultimate bending moment; the beams were then twisted until failure. In his plastic analysis he assumed that the prestress was uniform over the whole section, that the shear stress acted along the boundary lines at the boundary, and that the ultimate shear stress was that which would produce a principal tensile stress equal to the tensile strength of the concrete. His readings showed that whatever the distribution of direct stress,the distribution of the shear strain was the same at the top and bottom of the section, and that all gauges exhibited plasticity before failure. He concluded that within the range of the bending moments applied there was no significant variation in the ultimate torque. This was probably due to the fact that the very high compressive forces formed, enabled large shearing forces to be carried without large tensile stresses developing.

Reeves[11] in conjunction with Gardner's I beams carried out 3 series of tests on plain prestressed concrete T beams. The only difference between the beams of each series was the flange width. A predetermined bending moment was first applied, and the beam was then twisted till failure. His tests showed, that unlike the I beams of Gardner the twisting strengths were appreciably affected by bending moments. The torsional strength increased with the bending moment up to a point when the bending moment developed a direct tensile stress equal to that of the cylinder splitting strength. For greater bending moments the torsional strength decreased but did not drop below the pure twisting strength until approximately 80% of the ultimate bending moment was applied. He concluded that the ultimate tensile strain capacity of concrete was greater under favourable combined stress conditions than under pure states of stress. For any section as the bending moment is increased a point is reached at which the distribution of direct stress is approximately equal to that of prestress plus dead load only, and for a symmetrical section this will lead to a repetition of the torsional strength of the section. With an unsymmetrical section, however, this reversal of the direct stress will change the relationship between the direct stresses and the shear stresses, and thus change the torsional strength of the section. Reeves used a regression curve form of analysis to calculate the torsional strength of his beams.

Humphreys[12] carried out tests under pure torsion on 94 rectangular prestressed beams of varying cross section, some concentrically prestressed the remainder eccentrically prestressed. In all cases failure was caused by the sudden appearance of a diagonal tension crack, the angle of which tended to approach the horizontal

as the prestress was increased. It also became more apparent, as the amount of prestress was increased, that the crack on the opposite face was due to the compressive stresses on that face. He concluded that the torsional strength of a section increased with prestress until a certain limit was reached, after which it began to fall, suggesting a compression failure due to the combination of prestress and the compression component of torsion. The ultimate torsional strength of eccentrically stressed beams was governed by the same factors as concentrically stressed beams. His analysis was based on a finite difference method used in conjunction with the membrane anology.

Swamy[13] conducted tests on 20 hollow beams with comparison tests on prestressed solid and plain concrete hollow beams. The beams were uniformly prestressed and subjected to loads varying from pure torsion to pure bending. He concluded that the torsional resistance of a hollow beam may be increased by the addition of bending moment, until a bending moment of 65% of its ultimate is reached, after which it begins to decrease. He only obtained theoretical solutions for the cases of pure bending and pure torsion.

Van der Vlugt [14] carried out tests on rectangular concrete beams prestressed both longitudinally and vertically. He stated that there was a close agreement between the actual behaviour of the beam and the behaviour as predicted by the theory of elasticity.

Rowe[14] reported tests on prestressed concrete beams under combined bending and torsion, in which he noted that beams failing in pure torsion failed suddenly and that before failure there was some plasticity in the tension range. For a similar beam which was subjected to 75% of its ultimate bending moment and then twisted to failure, the principal tensile stress caused the

concrete to crack and immediately the bending caused spalling of the concrete in the top portion of the beam. The effect of a bending moment on the torsional strength is not noticed until the bending moment produces a uniform stress over the entire section. An increase in the torsional strength then occurs which decreases again when the net stress diagram is inverted.

Gersch and Moore[15] conducted a series of tests on prestressed I beams under pure torsion, from which they concluded that failure occurs when the ultimate tensile strength of the concrete is reached.

Amongst the specimens tested by Okada et al[16] under combined flexure and torsion were 10 uniformly prestressed rectangular beams. The beams contained no transverse reinforcement, and those tested under low M/T ratios failed at the appearance of a 45^{o} tension crack on the side of the beam. The crack on the opposite side was more inclined to the axis of the beam and appeared to be caused by compressive stresses. For those tested under higher M/T ratios a wedged shaped spalling of the concrete occurred in the top of the beam. His theoretical solution for the ultimate torsional resistance was based upon that proposed by Cowan. By assuming the critical section to be at the middle of the longer side he produced an interaction equation of the form shown below

$$\left(\frac{T}{T_u}\right)^2 + 0.287 \left(\frac{M_u}{T_u}\right) = 1$$

In his work on the effect of bending, torsion, and shear in prestressed concrete, Bishara[17] tested 24 beams of varying cross section. The beams, rectangular, I, or T in section, all contained shear reinforcement and were either eccentrically or uniformly prestressed. His theory was based upon St. Venant's theory of torsion and was used in conjunction with a finite difference method to obtain the failure moments.

Gausel's[18] work on prestressed concrete I beams involved the testing of 16 specimens under combined bending, torsion, and shear. He proposed 2 straight line interaction equations for conditions of combined bending and torsion.

$$\frac{T}{T_u} = 1$$

for values of $\frac{M}{M_u} \leq 0.9$

and $0.1 \frac{T}{T_u} + \frac{M}{M_u} = 1$

for values of $\frac{M}{M_u} > 0.9$

Khalil[19] tested 38 rectangular beams under varying ratios of bending moment to torsion. The prestress was applied either uniformly or eccentrically, and 15 of the specimens contained web reinforcement. He concluded that the maximum torsional capacity of the uniformly prestressed beams was achieved under pure torsion. The eccentrically prestressed beams on the other hand, achieved their torsional capacity under the action of an applied bending moment. Theoretically the value of this bending moment was that required to produce a uniform prestress across the whole of the section. In practice, however, it was found to be higher than this and was close to that value required to relieve the prestress in the bottom of the beam. For the unreinforced beams failing under low M/T ratios his theoretical analysis was based upon an elastic approach with a factor introduced to account for the semi-plastic behaviour of the concrete. In the case of those beams failing after the appearance of the first crack, an analysis, based on the equilibrium of the cracked section, was adopted.

As a result of torsion tests carried out on plain concrete, Hsu[20] proposed that failure was in the form of a skewed bending

mechanism. This is contrary to the belief of many investigators that failure of plain concrete under pure torsion is initiated by the formation of helical tension cracks. Hsu[21] has recently applied the skewed bending criteria to prestressed rectangular sections the results of which are shown in Fig. 1.1.1.compared with those of other experimenters. The factor $\sqrt{1 + 10\ P_t/f_c}$, which accounts for the effect of prestress, was derived for prestressed beams without stirrups.

Work has recently been carried out at North Carolina State University[22] on the effect of bending and torsion on prestressed rectangular beams. As a result, a square and tri-linear interaction curve were proposed for beams with and without reinforcement respectively.

Mukherjee and Warwaruk[23] reported tests on 52 rectangular prestressed beams tested under various ratios of bending, torsion, and shear. 28 beams were tested in bending and torsion and a correlation method used to determine the interaction curve.

The theoretical interaction curves of several of the authors referred to in this section are shown in Fig. 1.1.2.

1.2. Failure Criteria for Concrete under Combined Stresses

By comparison with that of metallic materials our knowledge of the structure of concrete is very limited. The plastic deformation of most ductile materials can be explained in terms of their physical structure. Brittle materials generally contain minute flaws within their structure which prevents their theoretical fracture strength from being reached.

Numerous theories have been proposed to explain the behaviour of concrete. Those based on the micro-structure of the cement contain empirical data and tend to be no more reliable or simpler than the semi-empirical macroscopic theories.

The combinations of principal stresses required to produce failure can be represented by a space model within the framework of the

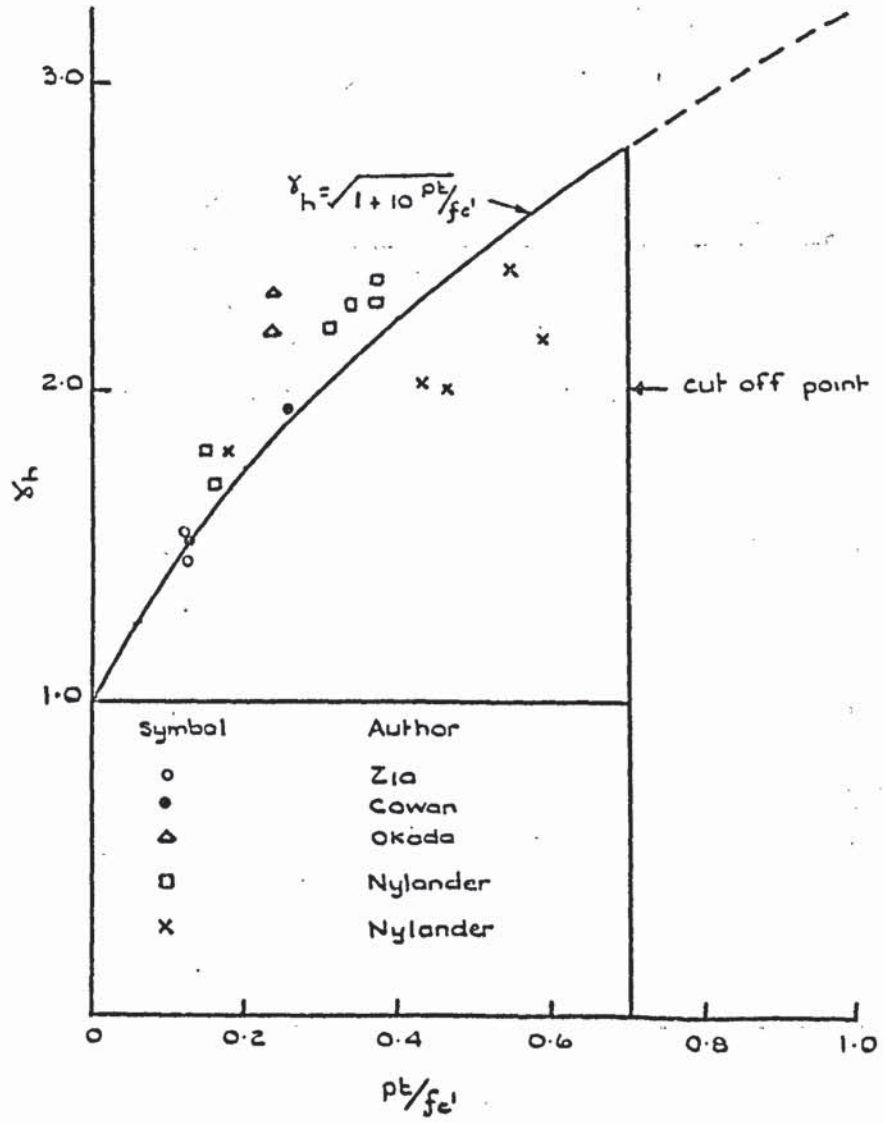

Fig. 1.1.1. Comparison of Hsu's theory with test results of other investigators

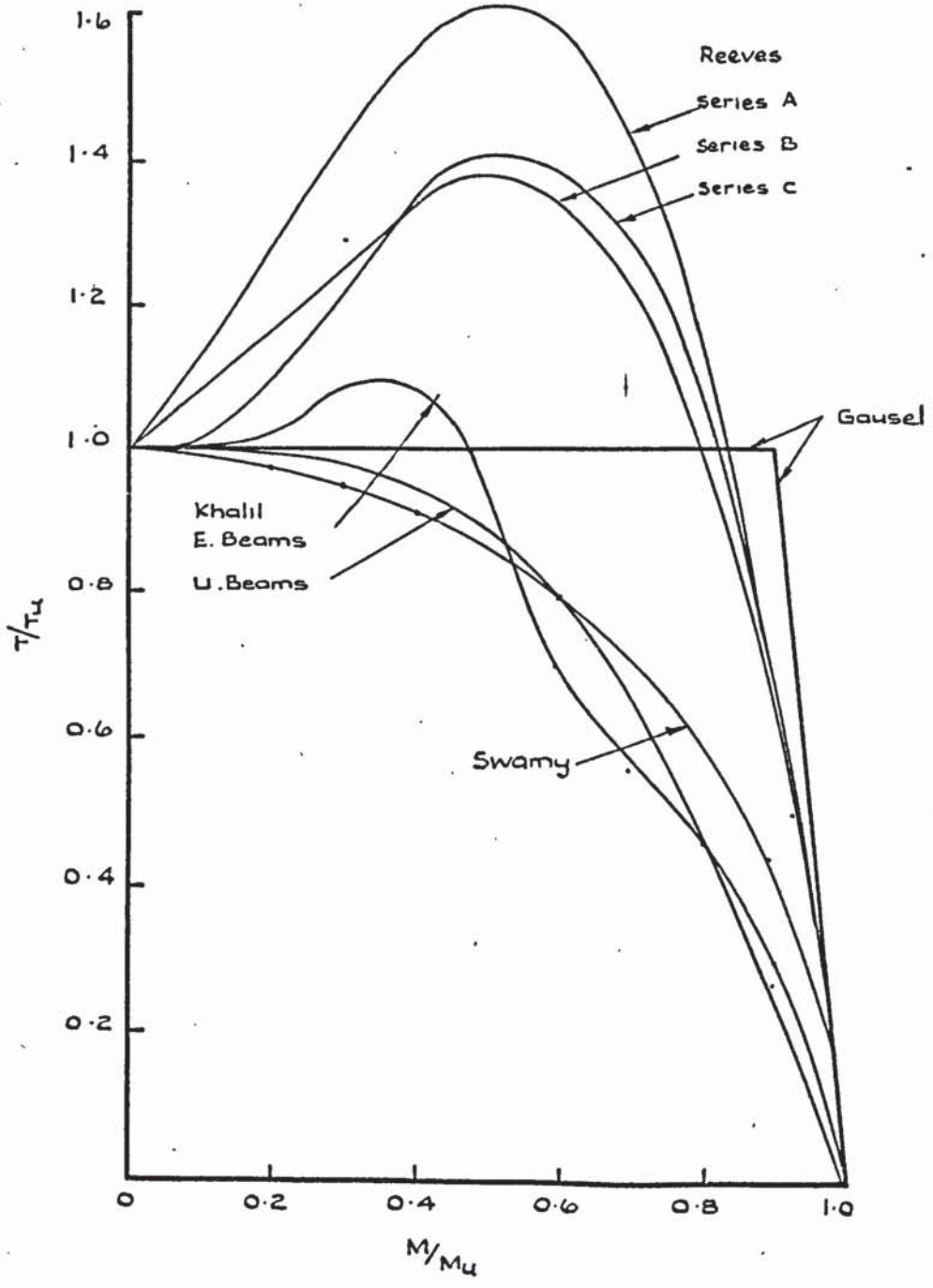

Fig. 1.1.2. Theoretical interaction curves for prestressed concrete in bending and torsion

3 principal stress axes, or two - dimensionally by Mohr circles. The surface of the space model, or the envelope of the Mohr circles, then constitutes the criterion of failure.

A summary of some of the macroscopic theories which have been proposed is now given:

1.2.1. Maximum Stress Theory

The theory generally attributed to W.J.M. Rankine [24], assumes that failure occurs if any direct stress exceeds a limiting value (f_{max}). The failure envelope to Mohr's circle (see Fig 1.2.1) can be represented by 2 straight lines parallel to the perpendicular axis and tangential to the stress circles C1, and C2. The theory has shown good agreement with experiments on the tensile and torsional strength of brittle materials, but it usually does not agree with experiments involving diagonal shear.

1.2.2. Maximum Strain Theory

St. Venant's [24] theory of maximum strain states that failure is determined by the maximum elastic strain.

$$|\varepsilon| \leq \varepsilon_{max}$$

This criteria does not agree well with experiments under combined stresses.

1.2.3. Internal Friction Theory

The theory proposed by Coulomb [24] is a modification of the Maximum Constant Shear Theory attributed to J. J. Guest. It is based on the conception of failure as a sliding action along planes inclined to the direction of the principal stresses. The assumed failure envelope consists of 2 straight lines tangential to both of the limiting Mohr's circles as shown in Fig. 1.2.2.

The theory advanced by Mohr [24] is a generalization of Coulomb's theory, the linear envelope being replaced by a curve

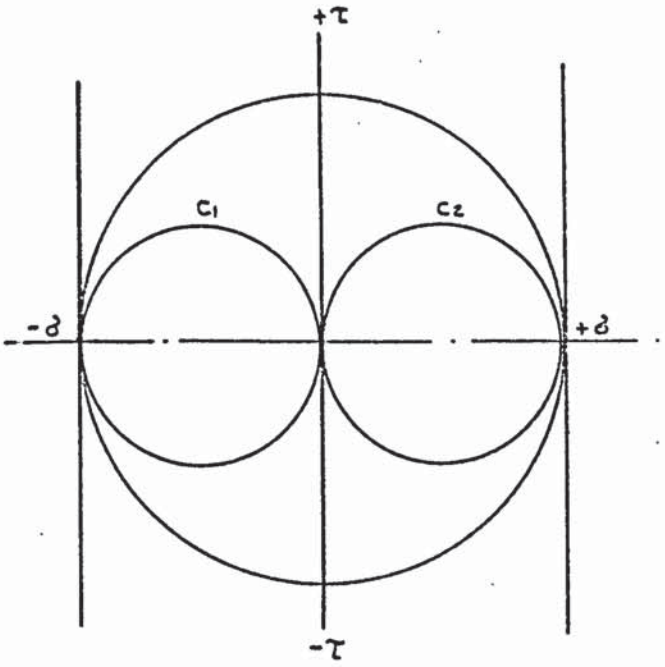

Fig. 1.2.1. Maximum stress theory

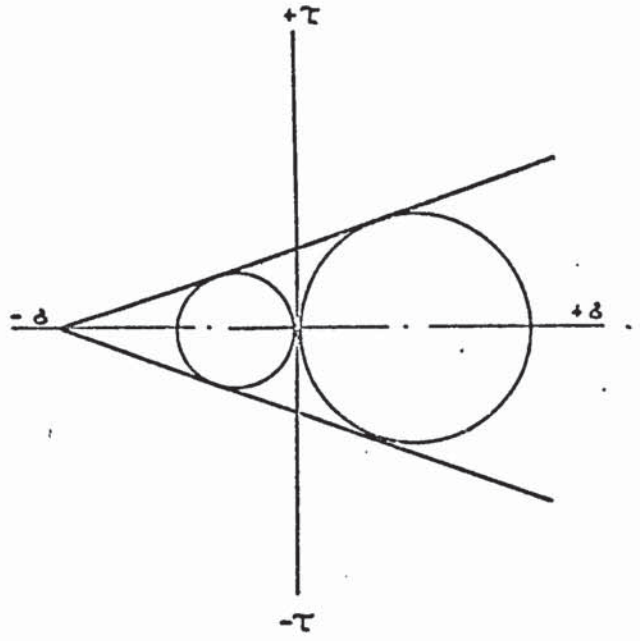

Fig. 1.2.2. Coulomb's internal friction theory

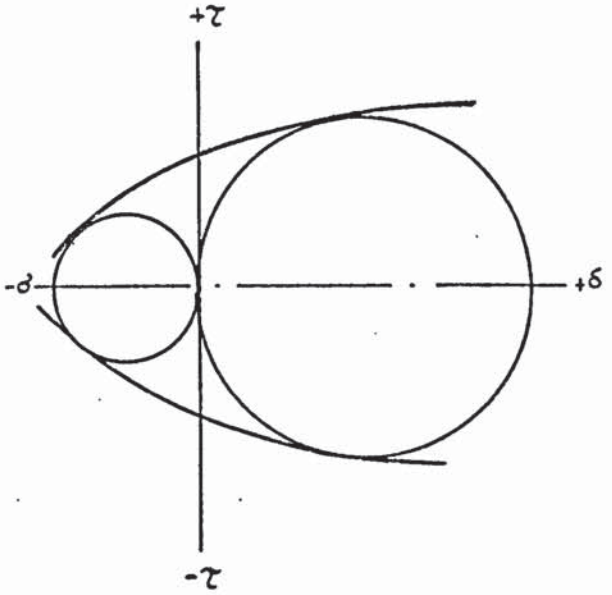

Fig. 1.2.3. Mohr's generalized maximum shear stress theory.

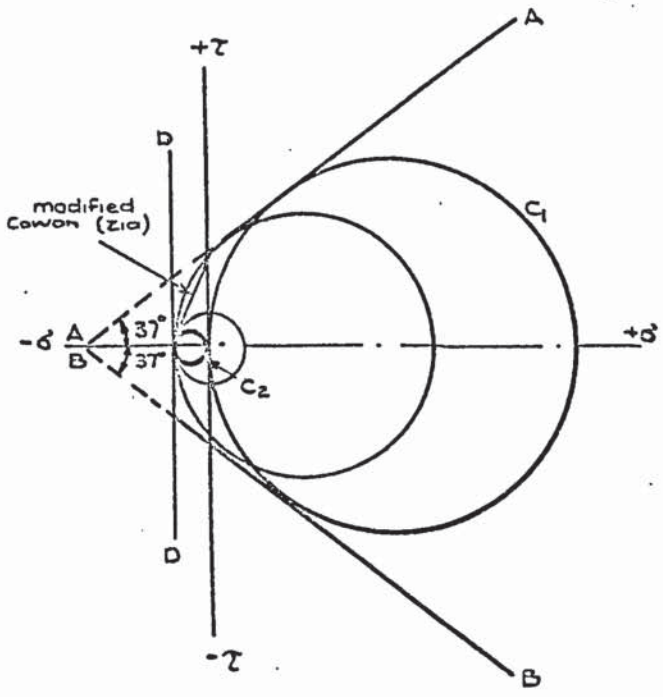

Fig. 1.2.4 Cowan & modified Cowan criterions of failure.

which often takes the form of a parabola. Both theories imply that the material behaves as a homogeneous body, and that there is a relation between the normal and shearing stresses in any plane, which governs the resistance to failure along that plane. Mohr's failure envelope is shown in Fig. 1.2.3 the equation of the line taking the form

$$\left(\frac{8\tau_{xy}}{f'_c}\right)^2 - \frac{8\sigma_x}{f'_c} - 1 = 0 \quad \text{if} \quad \frac{\sigma_x}{f'_c} < \frac{1}{4} \qquad \text{---- 1.2.1.}$$

$$\left(\frac{\sigma_x}{f'_c}\right)^2 - \frac{\sigma_x}{f'_c} + \left(\frac{2\tau_{xy}}{f'_c}\right)^2 = 0 \quad \text{if} \quad \frac{\sigma_x}{f'_c} > \frac{1}{4} \qquad \text{---- 1.2.2.}$$

σ_x = normal stress

τ_{xy} = associated shear stress

1.2.3. Cowan's Theory

By combining the maximum stress theory with the internal friction theory Cowan [25] obtained a failure envelope of the form shown in Fig. 1.2.4. The lines AA and BB are tangential to the maximum compressive stress circle C1 at an angle of 37° to the normal stress axis. The envelope is completed by the line DD drawn tangential to the stress circle C2 parallel to the shear stress axis. Mohr's circles tangential to the line DD represent stress combinations resulting in cleavage (tension) failure, whilst those tangential to the lines AA and BB indicate a shear (compression) failure.

P. Zia [9] proposed a modification to the Cowan criteria by joining the intersection of the Coulomb limiting lines with the shear axis and the maximum tensile stress intercept with straight lines (see Fig. 1.2.4.).

1.2.4. Leons Theory

A. Leon [26] derived a failure criteria by using a parabola as a continuous curved envelope for the Mohr theory of failure.

Mohr circles touching the envelopes at the apex of the parabola correspond to a cleavage failure, and Mohr circles touching the parabola elsewhere correspond to crushing failures

1.2.5. Octahedral Stress Theory

Bresler and Pister[27] suggested a criteria based on the octahedral stresses σ_o, τ_o where

$$\sigma_o = \frac{1}{3}(\sigma_1 + \sigma_2 + \sigma_3) \qquad \text{- - - - 1.2.4.}$$

$$\tau_o = \frac{1}{3}\sqrt{(\sigma_1 - \sigma_2)^2 + (\sigma_2 - \sigma_3)^2 + (\sigma_3 - \sigma_1)^2} \qquad \text{- - 1.2.5.}$$

Recent investigations have been directed towards the Griffith[28] crack theory, and Newman[29] has indicated a relationship between Griffith's theory and Leon's theory in the compression-tension zone.

1.3. Scope of Work

The experimental investigation involved the testing of 22 rectangular prestressed beams under varying ratios of bending moment and torsion.

The beams measuring 100 mm (4 in.) x 175 mm (7 in.) x 3000 mm (120 in.), were eccentrically prestressed by a single unbonded high tensile steel bar. The test length was reinforced in the longitudinal direction only, but transverse reinforcement was supplied at the extremities to prevent premature shear failure.

In addition to the main series of tests it was found necessary to carry out a number of subsidary tests. Twenty-two hollow cylinders, of identical mix to the prestressed beams, were tested under varying ratios of direct stress to shear stress. The object of the tests was to formulate a failure criteria for the concrete under states of biaxial stress. As a sequal to these tests a number of standard 150 mm (6 in.) cubes were split, and then

tested to failure under ratios of direct stress to shear stress. A series of tests on 150 mm (6 in.) diameter cylinders tested under direct compression were undertaken to determine a stress - strain relationship for the concrete. The results from these tests were also used to establish a value for the cylinder strength to cube strength ratio of the concrete. Experiments were also carried out into a method of obtaining the uniaxial tensile strength of the concrete.

Theoretical solutions have been produced for determining the ultimate strength of a prestressed rectangular beam under combined bending and torsion. The mode of failure of the beams can take 3 forms depending on the bending moment to torsion moment ratio. For each mode of failure a solution is proposed for determining the ultimate strength of the beam. Theoretical solutions are also proposed for the failure of hollow cylinders under combined direct stress and shear, and for the stress - strain relationship of the concrete.

Chapter 2

Experimental Methods

2.1. Introduction

The following chapter gives a detailed account of the experimental work carried out during the main series of tests on the prestressed beams. Reference is made to the type of concrete used, the casting details, prestressing details, test rig, and methods of instrumentation.

Details of a number of subsidary tests undertaken during and after the main series had been completed are reported in Chapter 6.

2.2. Materials Used

2.2.1. Cement

Ordinary Portland Cement supplied by the Blue Circle Group of Companies was used throughout the whole series of tests.

2.2.2. Aggregate

Zone III sand, and a 10 mm ($\frac{3}{8}$ in.) crushed aggregate were used for all specimens cast. The Midland Gravel Company supplied the quartzite aggregate which was obtained from the Perry Common Pit in Birmingham. Aggregate from the same batch was used in the casting of all but the last 4 beams. These beams, cast after the main series had been completed, were made from aggregate taken from a second batch. This additional supply of aggregate became necessary after the casting of a number of hollow cylinders had exhausted the original supply. Details of the sieve analysis for both batches are shown in Table 2.2. The necessary steps taken to allow for the obvious difference in the grading between the two are described in 6.1.3.

B.S. Sieve No. or Size		%
Retained	$\frac{3}{16}$	7.37
Retained	7	18.19
Retained	14	11.15
Retained	25	10.99
Retained	52	33.72
Retained	100	14.69
Passing	100	3.85

TABLE 2.1

Sieve Analysis Zone III Sand

B.S. Sieve Size		1st Batch	2nd Batch
		%	%
Retained	$\frac{3}{8}$	2.24	5.27
Retained	$\frac{3}{16}$	81.89	92.20
Passing	$\frac{3}{16}$	15.87	2.50

TABLE 2.2

Sieve Analysis Aggregate

2.3. Mix

The original mix used for the main series was a 1:1½:3 by dry weight ratio, with a water cement ratio of 0.5. All aggregate was thoroughly dried in the laboratory before being weighed.

2.4. Control Specimens

With each casting of a prestressed beam the following control specimens were made.

1) 3 No. 150 mm (6 in.) cubes to determine U_w the uniaxial cube compressive strength of the concrete.

2) 3 No. 300 mm (12 in.) x 150 mm (6 in.) diameter cylinders to determine the split cylinder strength f_{sp}.

3) 3 No. 300 mm (12 in.) x 150 mm (6 in.) diameter cylinders to determine f_t the uniaxial tensile strength.

4) 3 No. 300 mm (12 in.) x 150 mm (6 in.) diameter cylinders, capped 12 hours after casting with a mortar paste, and tested to determine f'_c the uniaxial cylinder compressive strength.

5) 2 No. 300 mm (12 in.) x 150 mm (6 in.) diameter cylinders, capped as before, and tested to determine E_c, the Youngs Modulus of Elasticity of the concrete. Testing was carried out in accordance with B.S. 1881 using electrical resistance strain gauges to measure the strains. Details of the type of gauges used, method of fixing and measuring are given in 2.10.2 and will not be repeated here.

6) 3 No. modulus of rupture beams measuring 100 mm (4 in.) x 175 mm (7 in.) x 1000 mm (40 in.). Hsu [20] has shown that the modulus of rupture decreases as the depth of the specimen increases, the variation being largely due to the change in strain gradient. The smaller the depth, the steeper the gradient and the higher the modulus of rupture. This phenomenon was also reported by Wright [30]

and the results of his tests and those of Hsu are shown in Fig. 2.1. As a result of these tests it was decided not to comply with the B.S.1881 recommendations for section sizes but to use a section identical to that of the main beam. This it was thought would eliminate any size effect and give a result which would be more applicable. All other conditions of the test were as those recommended in B.S. 1881 using a span to depth ratio of 4 with third point loadings. It should be noted that the mode of failure of the prestressed beam governed the way in which the modulus of rupture beam was tested. The specimens of beams failing in Modes 1 and 3 were tested with their larger dimension vertical, whilst those of beams failing in Mode 2 were tested with their smaller dimension vertical.

The moulds for the modulus of rupture beams were made from 13 mm ($\frac{1}{2}$ in.) plywood faced with a layer of "Formica". All other specimens were cast in steel moulds. Testing in all cases was carried out using a variable capacity Denison loading machine. The rate of loading for every specimen was in accordance with B.S.1881.

2.5. Steel

All beams were reinforced by a single longitudinal bar situated at a distance from the soffit of the beam equal to one third the depth. The bar, 22 mm ($\frac{7}{8}$ in.) in diameter, was of high tensile steel with properties as shown in Fig. 2.2. Both ends of the bar were threaded, one thread being extended to enable the prestressing jack to be attached. The threads were pressed and not taped into the metal, the effective thread diameter being approximately equal to the original blank diameter. The full strength of the trued bar was developed wherever the nut finished on the bar, the anchorage being completely positive without "take-up" on transfer of load. All bars along with nuts, washers, and end plates were supplied by McCalls Macalloy Ltd.,

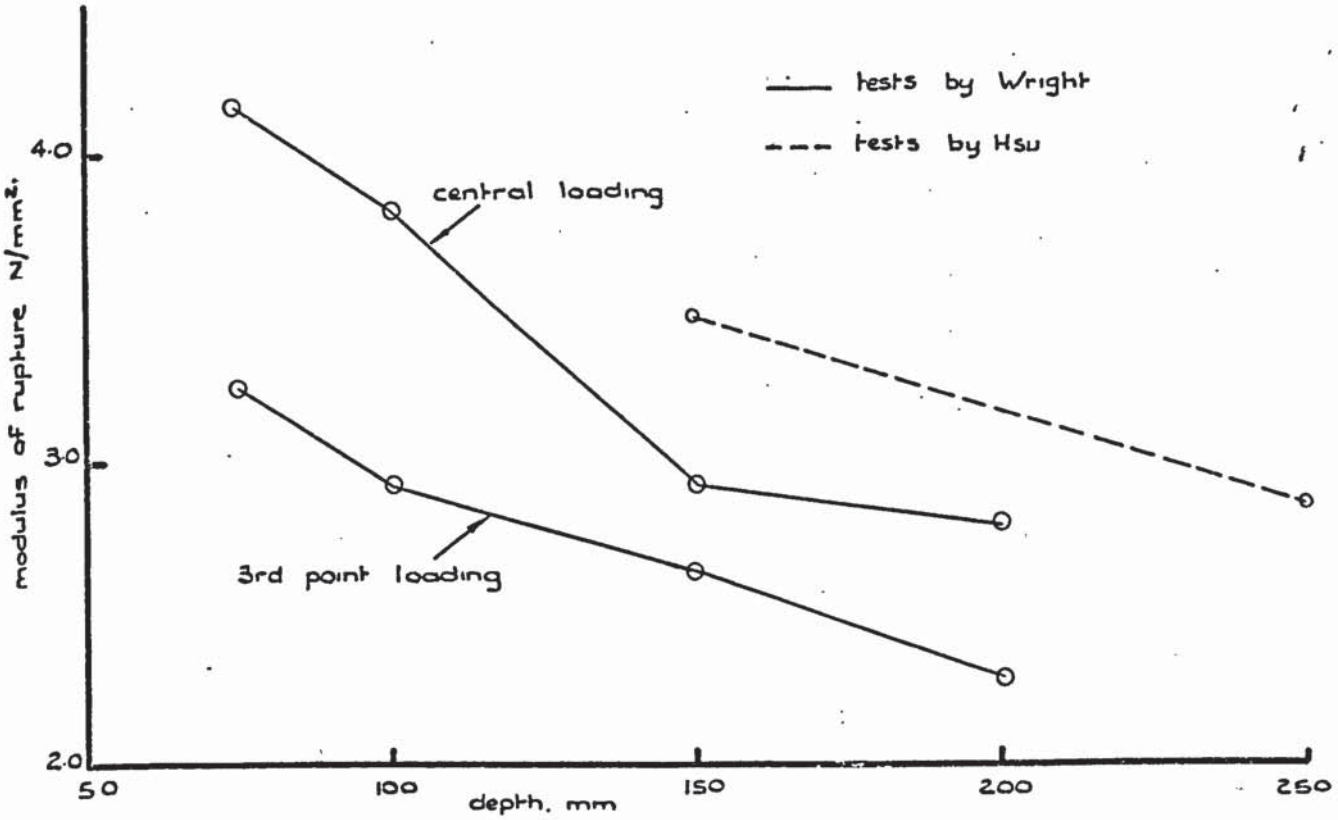

Fig. 2.1. Modulus of rupture as a function of the depth of the flexural specimen

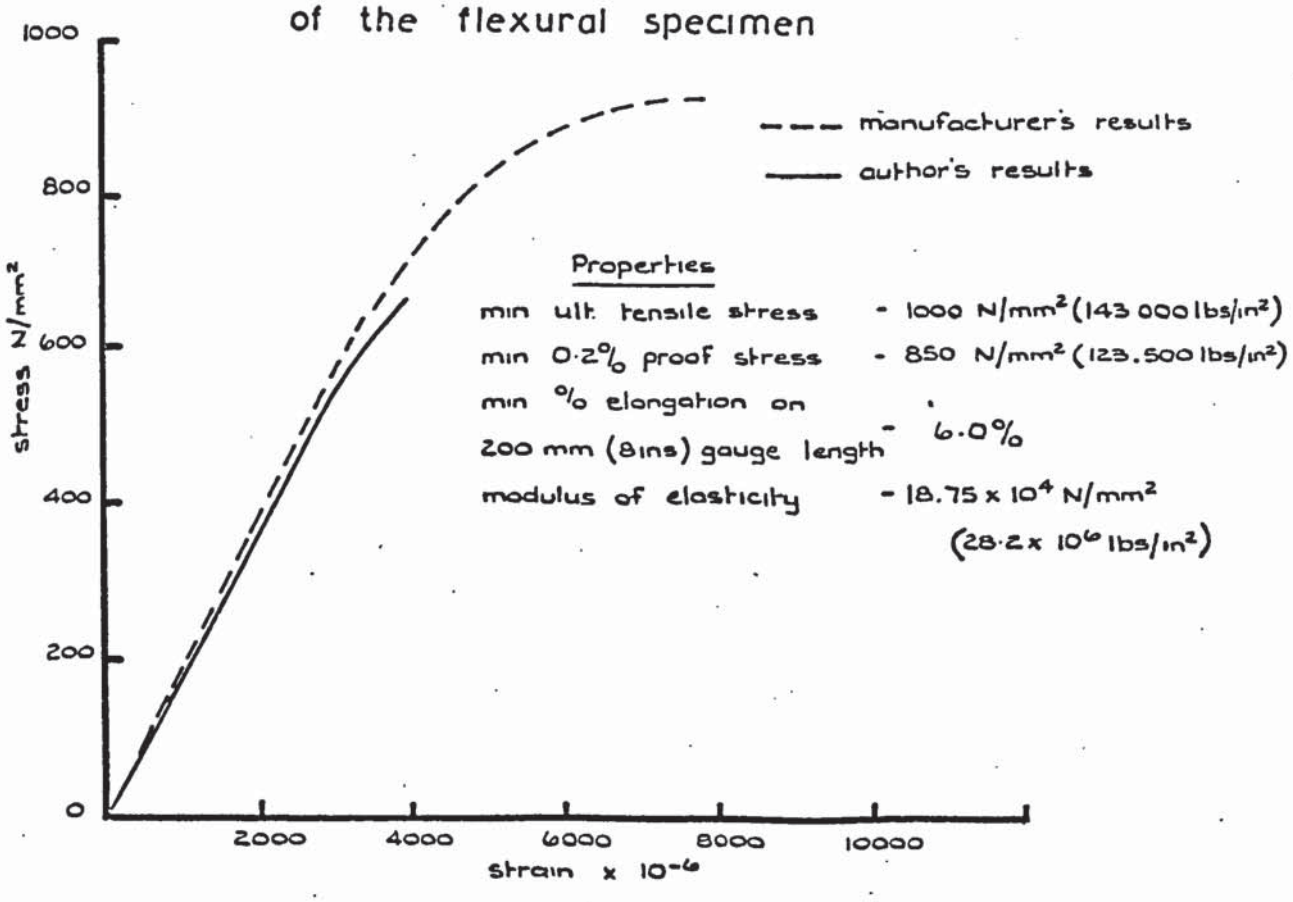

Fig. 2.2. Stress - strain curve for prestressing steel

Nominal shear reinforcement made from 6 mm ($\frac{1}{4}$ in.) mild steel bar was placed at either end of the beam. The reinforcing cage, 380 mm (15 in.) in length was necessary to prevent premature shear failure at either end of the beam between supports and loading points.

2.6. Beam Specimen

Casting of the main beam, measuring 100 mm (4 in.) x 175 mm (7 in.) x 3000 mm (120 in.) was carried out in a mould of similar construction to that used for the modulus of rupture beams. The combination of plywood lined with Formica proved to be very successful in giving a smooth accurate finish to the beam. It also had the added advantage of preventing the plywood from absorbing moisture from the wet concrete, hence minimising the effects of distortion due to warping. Regular checks were made on the condition of the mould before every cast, but very little maintenance was required throughout the whole series. Wooden ties, cut accurately to size, were placed across the top of the mould before casting to prevent any bulging occurring due to the weight of wet concrete.

Details of the beam sizes and reinforcement are shown in Fig. 2.3, and a view of the mould prior to casting is shown in Plate 2.1.

As the beams were to be prestressed post tensioned, it was necessary to produce a void in the beam through which the bar could be passed ready for stressing. To achieve this several methods of approach were attempted before a successful solution was reached. A detailed description of the three methods used follows:-

2.6.1. The Inflatable Rubber Tube

This involved the casting of an inflatable rubber tube into the beam, and removing it after initial setting had taken place. Holes 32 mm ($1\frac{1}{4}$ in.) in diameter were cut in both end sections of the

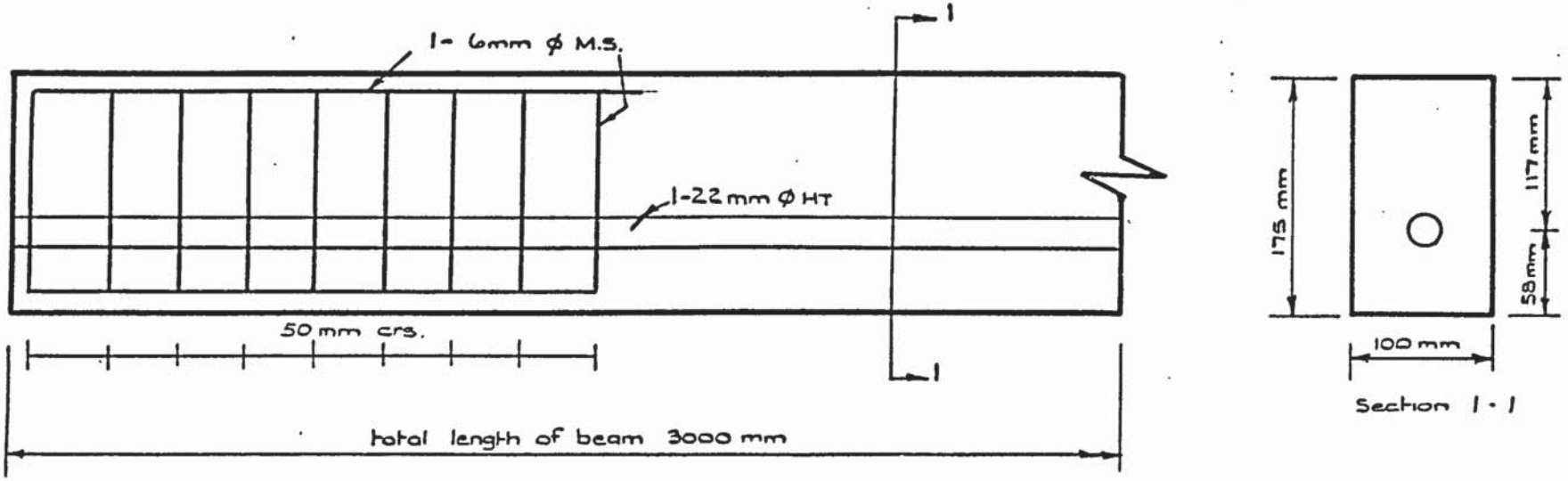

Fig. 2.3. Detail of prestressed concrete beams.

Plate 2.1. - Detail of mould prior to casting

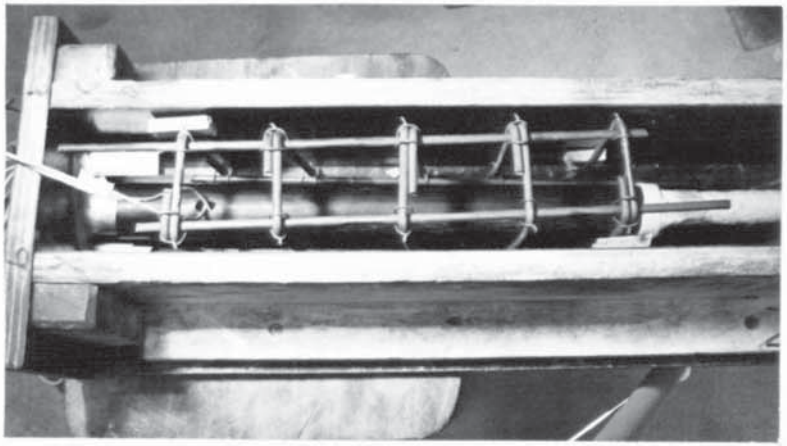

Plate 2.2 - Detail at end of mould
(bar cast in-situ)

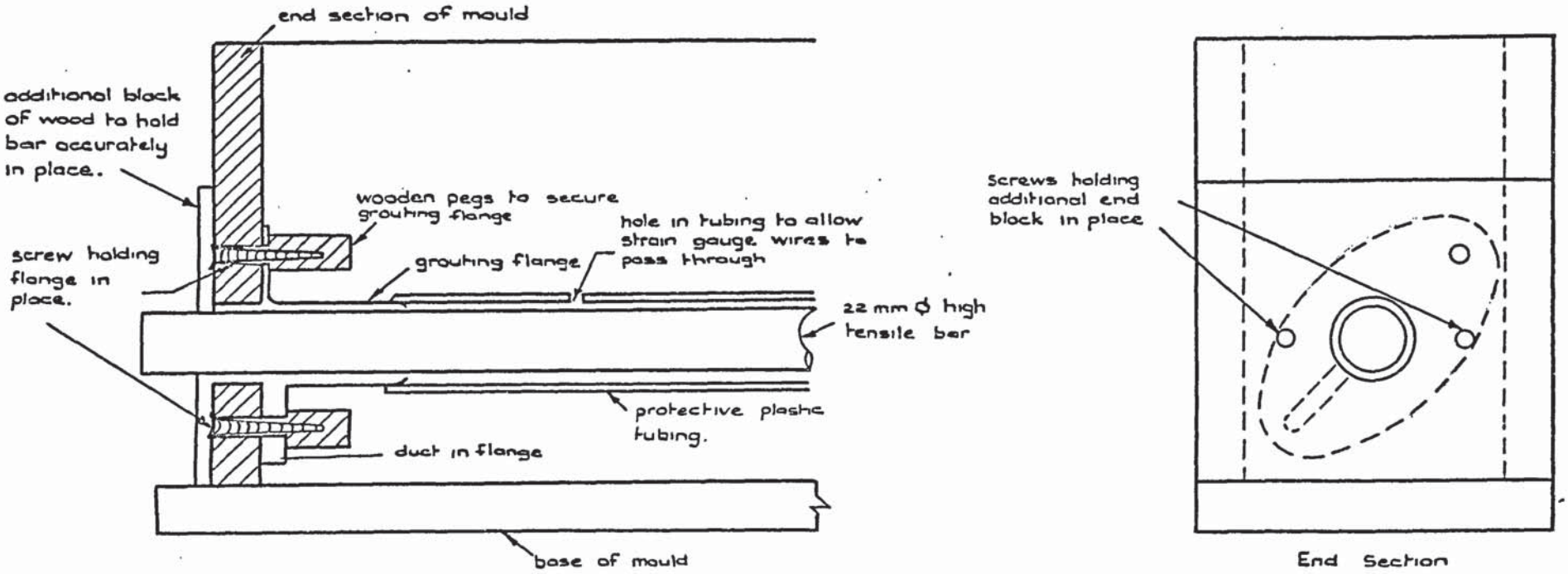

Fig. 2.4. End detail of mould.

mould, with centres at a distance from the base equal to one third the depth of the beam. Special grouting flanges (the purpose of which will be described later) were then accurately fixed to the inside of the sections. Fixing was effected by means of 2 screws and 2 wooden pegs passing through holes in the flange as shown in Fig. 2.4 and Plate 2.2. With the flanges in place, the rubber tube, 25 mm (1 in.) outside diameter with walls 6 mm ($\frac{1}{4}$ in.) thick was passed through the mould. By plugging one end with a piece of metal and inserting a valve in the other it was possible to inflate the tube, by means of a foot pump, to a diameter of 38 mm ($1\frac{1}{2}$ in.). The mould and tube were then well greased and a final check made on the position of the tube. All specimens were vibrated by means of a 25 mm (1 in.) diameter poker vibrator, and were cast in place in the curing tank. A careful watch was kept on the position of the tube during casting to ensure that it remained straight and horizontal. After 12 hours had elapsed the tube was deflated and removed from the beam and formwork on all specimens stripped. Although a void had successfully been formed in the beam its longitudinal profile had not remained horizontal, but had risen by a maximum distance of about 38 mm ($1\frac{1}{2}$ in.) at the centre. The wet concrete being forced under the tube during vibration was thought to have produced this effect.

A means of preventing the tube from rising during casting was now required which led to the second method of approach.

2.6.2. Inflatable Rubber Tube with Iron Bar

The inclusion of 13 mm ($\frac{1}{2}$ in.) diameter iron bar inside the tube would, it was thought, prevent the tube from floating on the wet concrete during casting. The added weight of the bar now required the tube to be supported by concrete blocks, placed at regular intervals along its length, to prevent sagging. This being done the same proceedure as described in 2.6.1 was carried out. A true, straight void was

produced allowing the prestressing bar to be easily inserted.

The testing and analysis of several of the early beams led to the hypothesis that the prestressing bar may be moving in the void during testing. Although the maximum allowable movement was comparatively small, it was felt that it may be having a large effect upon the distribution of the stress due to prestress. The exact location of the bar at the failure section was also considered to be important. The sagging of the beam after failure caused the bar to rise to the top of the void at the critical section. This prevented its exact position prior to failure from being measured. As a result of the above observations a third method of approach was decided upon.

2.6.3. Bar Cast In-Situ

By casting the prestressing bar in place it was thought that all possibilities of it moving during testing would be eliminated, and its exact location at the failure section would be able to be measured.

The mould, with grouting flanges in place, was set up as described previously. In order that the bar could be held rigidly in place 2 additional end sections were added to the mould as shown in Fig. 2.4. The 22 mm ($\frac{7}{8}$ in.) diameter holes drilled into these sections provided a tight fit between themselves and the bar, and when attached to the existing end sections, held the bar securely in place. To ensure that conditions in all beams throughout the series remained the same it was essential, with this method, to prevent any bond between the steel and concrete. This was effected by binding the bar in Syglass, a wax covered tape.

It was also felt that damage during stressing may be caused to the strain gauges attached to the steel. Previously with the bar free to move in the void the problem had not arisen. Protection was offered to the gauges by placing a 430 mm (17 in.) length of 38 mm

($1\frac{1}{2}$ in.) diameter plastic tubing over either end of the bar. The tubing was held in place by forcing it over the tapered end section of the grouting flange. A hole drilled in the top of each section of tubing allowed the strain gauge wires to be fed out. The bar was supported at intervals in the mould by means of thin pieces of wire attached to the wooden ties placed across the top of the mould.

Plate 2.2 shows in detail the end section of the mould prior to casting.

2.7. Curing Details

No seperate curing room was provided in the laboratory in which all casting was carried out. On previous occasions experimenters had cured all their specimens under wet Hessian in the open laboratory. Inherent in this system, however, were 2 main drawbacks:-

1) In order to maintain constant humidity conditions, the Hessian would need to be moistened manually daily. There would be no assurance of this being carried out especially at the week end.

2) With the ambient temperature fluctuations occuring throughout the year it would be difficult to maintain a constant temperature in the laboratory.

It was not considered practical to build a full size curing room, so a compromise between the 2 extremes was reached. A small tank, measuring 1230 mm (4 ft.) x 5000 mm (16 ft.) x 600 mm (2 ft.) high was constructed out of concrete blocks on the floor of the laboratory. One end, and the top of the tank, were left open to allow easy access during the casting and removal of the specimens. Coating the interior of the tank with a bitumen paint prevented absorbtion of moisture by the concrete blocks. Electrical strip heaters, connected to a thermostat and placed down either side of the tank provided the means of temperature control.

A removable wooden frame placed across the top of the tank was used to support the spraying mechanism. This consisted of a number of small lengths of 10 mm ($\frac{3}{8}$ in.) diameter copper tubing, connected in series by several lengths of flexible rubber tubing. The tubing at one end of the system was bent over to form a water tight joint, whilst that at the other was connected to an electrically operated water pump, immersed in a tank of water. Water, pumped through the system, emerged in the form of a fine spray via small holes punched in the copper tubing. An electrically operated timing mechanism, connected to the pump, ensured that equal amounts of water were supplied to the tank every day. A Sangamo 24 hour clock used in conjunction with a second more sensitive timing device, enabled water to be sprayed into the tank for a period of 30 seconds every 24 hours. Hessian sacks, lining the bottom of the tank, absorbed the water and helped to provide continuous moist conditions. After each spray the water tank was automatically filled by means of a simple ball-cock arrangement.

The above mentioned system enabled constant temperature and humidity conditions to be maintained within the tank for as long as was necessary.

After casting,the open end of the tank was covered with a concrete block, and the top with a double layer of polythene stretched over a wooden framework. A thermohygrograph placed in the tank recorded constant temperature and humidity conditions of 20°C and 99% respectively. Plate 2.3 shows the curing tank just prior to casting. The removable spraying system and top covering can be seen resting at the back of the tank.

All specimens remained in the tank for 28 days after casting before being removed and prepared for testing on the 30th day. A 2

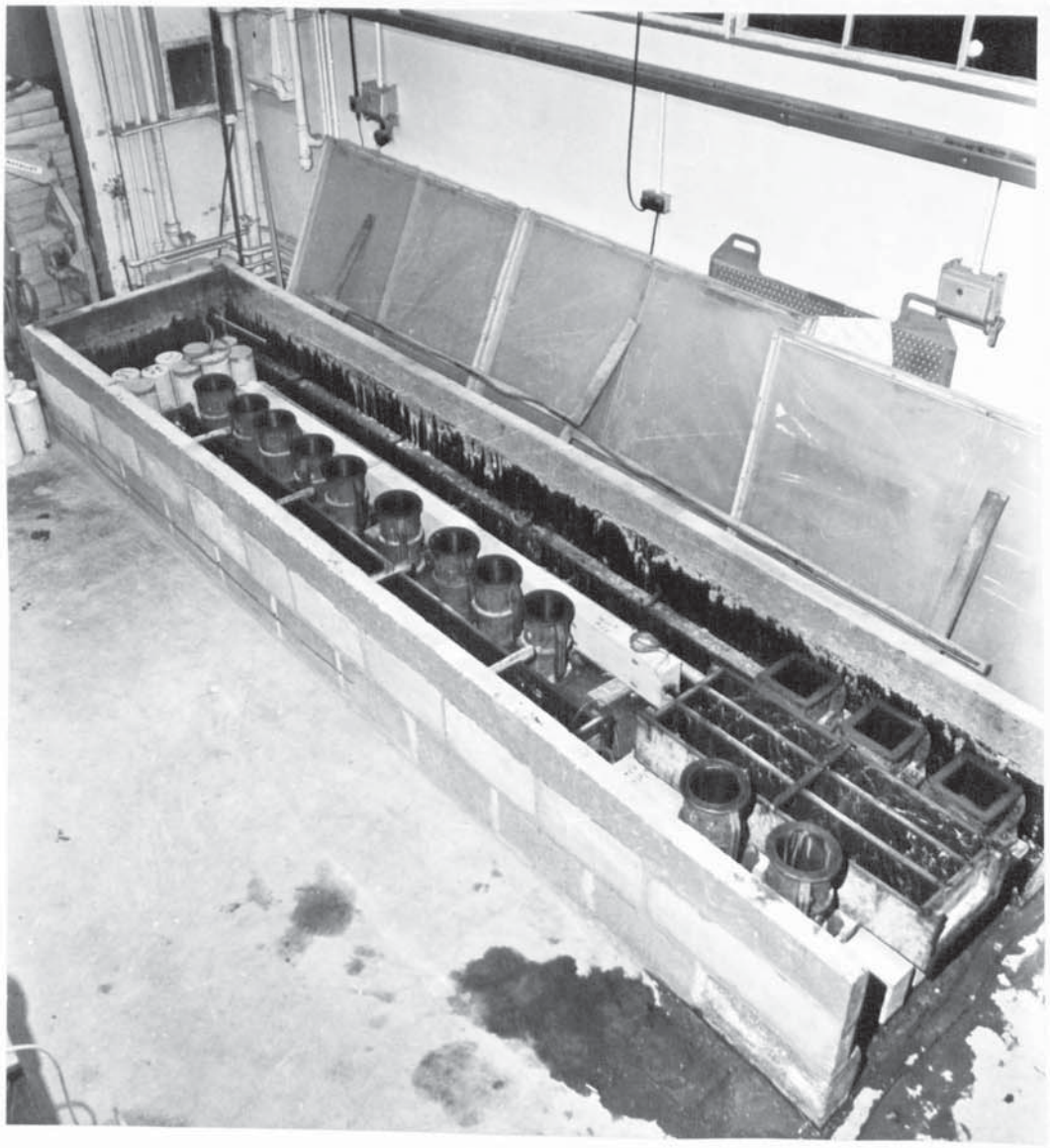

Plate 2.3. - General layout of curing tank

week cycle of testing and casting was maintained throughout the whole series of tests. On removal of a beam from the tank for testing a second was immediately cast. This meant that at any one time there were always 2 beams plus control specimens in the tank.

2.8. Prestressing Details

There are 2 basic methods of prestressing which are normally available to the engineer. The first involves the use of a high tensile steel strand, and the second that of a high tensile steel bar.

In the first case a number of cold-drawn high tensile steel wires are grouped together, either parallel or helically, to form a tendon. The tendons, used either singularly or in groups, are then stressed by means of hydraulic jacks. With many of the methods available each tendon in a group has to be stressed individually, and a wedge type anchorage is usually used.

The second method incorporates a single high tensile steel bar and usually a threaded end anchorage.

In practice, the first method is the more commonly used. The tendons are able to take much higher stresses than the single bar. Their uneven outward appearance also helps form a good bond between the steel and the concrete. Such a bond is particularly important in prestressed pretensioned concrete. With the single bar, however, prestressing is a much simpler process. The fact that only one bar has to be stressed minimizes errors due to stressing, and the threaded anchorage is more convenient and effective than the wedge type.

As a result it was decided to use the second of the 2 techniques, employing a single 22 mm ($\frac{7}{8}$ in.) diameter high tensile steel bar. The capacity of the bar was almost twice that necessary to produce the required prestress, but was the smallest one available from the manufacturers.

The techniques involved in stressing the beam differ slightly depending upon the method used for forming the cavity. This difference is, however, only concerned with the positioning of the bar before stressing. It is therefore proposed to discuss in detail the method used on the earlier beams. Reference will then be made to the slight variations involved for beams with the bar cast in-situ.

On the 28th day after casting, the beam, along with all its control specimens was removed from the curing tank. Strain gauges were then glued (as described in 2.10) to both the steel and the concrete, after which the bar was carefully inserted into the void. During this process a close watch was kept on the wires leading to the strain gauges on the steel. Tape wrapped round the thread of the bar prevented it from becoming burred. The bar was held in its correct position in the void by means of 150 mm (6 in.) x 150 mm (6 in.) x 13 mm ($\frac{1}{2}$ in.) end plates attached to the ends of the beam. The 2 wooden pegs, used previously to hold the grouting flanges in place, were now employed to take the 2 end plate securing screws.

The grouting flange, as its name suggests, was originally designed to allow grout to be injected into the cavity after stressing. This could be done by removing one of the end plate securing screws giving access to a groove in the flange. Grout could then be pumped through this hole, via the groove, and into the duct. In this case, as the bar was to be left unbonded, the flanges were used to serve a different purpose. Use was made of the groove in the flange to allow the strain gauge wires to be fed out through one of the screw holes in the end plate. This having been done the beam was placed on the floor, supported along its whole length, and initial readings on all strain gauges taken. The beam was then supported at either end and a second set of readings taken to determine the stresses due to self weight.

Stressing was carried out using a 450 kN (45 ton) capacity hydraulic jack Mark VIII supplied by Mcalls Macalloy Ltd. The bar was positioned in the beam so that at least 100 mm (4 in.) of thread was showing at the jacking end. At the other end it was necessary to have at least a full nut length plus 6 mm ($\frac{1}{4}$ in.) of thread, and no unthreaded bar showing. Once this position had been achieved the nuts and washers were placed on either end and tightened by hand. The jack was capable of stressing bars of between 22 mm ($\frac{7}{9}$ in.) and 35 mm ($1\frac{3}{8}$ in.) in diameter, the size of the hexagon insert placed in the bevel housing governing the size of the bar. With the appropriate insert in position, (see Plate 2.4(A)) the bevel housing was held in place on the bar, whilst the jack was suspended in the correct position by means of a small winch mounted on the trolley. The drawbar was then turned on to the bar for a minimum distance of $1\frac{3}{4}$ bar diameters, and the drawbar nut run up to the back face of the jack and tightened (see Plate 2.4(B)). A check was made on the bevel tightening gear to ensure that it was free to rotate, before stressing was commenced.

The pressure gauge, supplied with the jack to read the applied load was only capable of measuring to within 5 kN ($\frac{1}{2}$ ton). This was considered insufficient for the accuracy of work to be carried out, and use was made of strain gauges attached to the prestressing bar. This system enabled an accuracy of 9 N (2 lb) to be obtained, as well as allowing the prestressing force, at any stage during the test, to be determined.

As the load was applied the nut was run-up by means of the bevel gear (see Plate 2.4(C)). At the correct load, shown by the strain gauge readings, loading was ceased and the nut tightened. A small drop in the needle on the pressure gauge showed that the nut was fully tightened and was taking up the load. An approximate check on the applied load was also made by measuring the extension of the bar. This was

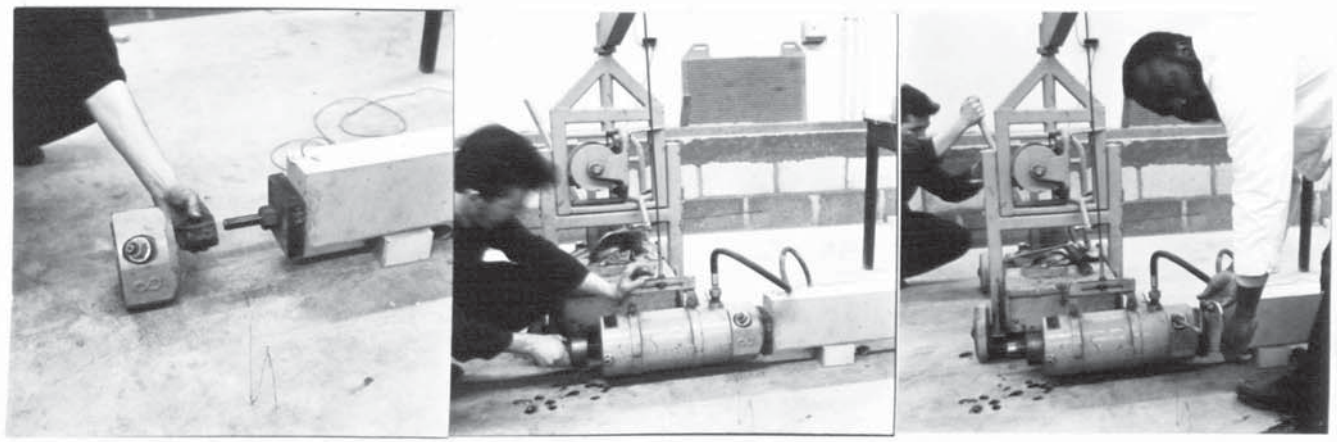

(A) (B) (C)

Plate 2.4. - Stages of prestressing

achieved by measuring, with a ruler, the movement of the drawbar nut relative to the back face of the jack. A third set of strain gauge readings was then taken, afterwhich the pressure was gently released, allowing the jack and bevel gear to be removed. A further set of readings taken at this stage, gave an indication of any change in stress produced due to complete transfer taking place.

The stressing proceedure, for beams containing the bar cast in-situ, was a somewhat simpler operation. The bar being already fixed in position eliminated the needs of securing the end plates to the beam, and feeding the strain gauge wires out via the cavity. The proceedure was otherwise identical to that mentioned above.

Eccentric prestressing causes an upwards deflection in the beam, which, in this case was in the order of 3 mm ($\frac{1}{10}$ in.) at centre span. This phenomenon, it was thought, might cause a reduction in prestress due to friction along the length of the bar, which would only occur in those beams containing the bar cast in-situ. The amount of free movement in the pre-formed void of the other beams would prevent any frictional forces from being set up. As a check on this, 2 sets of 3 gauges were placed close to either end of the bar. Any marked difference between the 2 sets of readings would indicate a loss in prestress. The results show, however, that no such loss occurred, probably because of the small spans and deflections involved.

2.9. Test Rig.

Testing was carried out within a large permanent portal testing rig constructed from I sections. Resting on the base of the rig, and running approximately at right angles to it, were 2 more I sections placed side by side. These 2 sections formed a base measuring 760 mm (2ft-6in.) x 6100 mm (20 ft) long upon which all the testing was carried out.

The beams were tested over a span of 2500 mm (8ft-3in.), the bending moment being applied through a spreader beam, with a distance of 1950 mm (6 ft-6 in.) between loading points.

The nature of the tests to be undertaken required that the beam be free from both lateral and torsional restraints. The 4 bearing pads shown in Fig. 2.5 were designed to achieve this aim. Free rotation of the beam was supplied by means of small roller bearings placed between the plates. The faces of the plates were machined to a predetermined radius, allowing beams of up to 300 mm (12 in.) in depth to be tested in the rig. Beams of any smaller depth could be accommodated for by placing packing pieces between the pads and the beam. The size of the packing pieces being such, that the centre of rotation of the beam, coincided with the centre of the circle described by the radius to which the plates were machined. The bottom bearing pad A was also supplied with rollers to eliminate any lateral restraints during bending.

Point loading was effected by 25 mm (1 in.) diameter rods, resting in grooves cut in each of the 4 bearing pads. The width of the groove was made slightly larger than depth and thus contact between the plates and the rod was only made at the top and bottom extremities.

Torsion was applied through collars placed around either end of the beam. The colars, shown in Fig. 2.6.(A), were made from 45 mm ($1\frac{3}{4}$ in.) x 25 mm (1 in.) mild steel bars, bolted and welded together. Special mild steel packing pieces, shown in Fig. 2.6(A), were designed to enable the beam to be placed easily and accurately at the centre of the collar. With the collar held approximately in place the 2 rectangular packing pieces were placed around adjacent faces of the beam. The size to which they had been machined

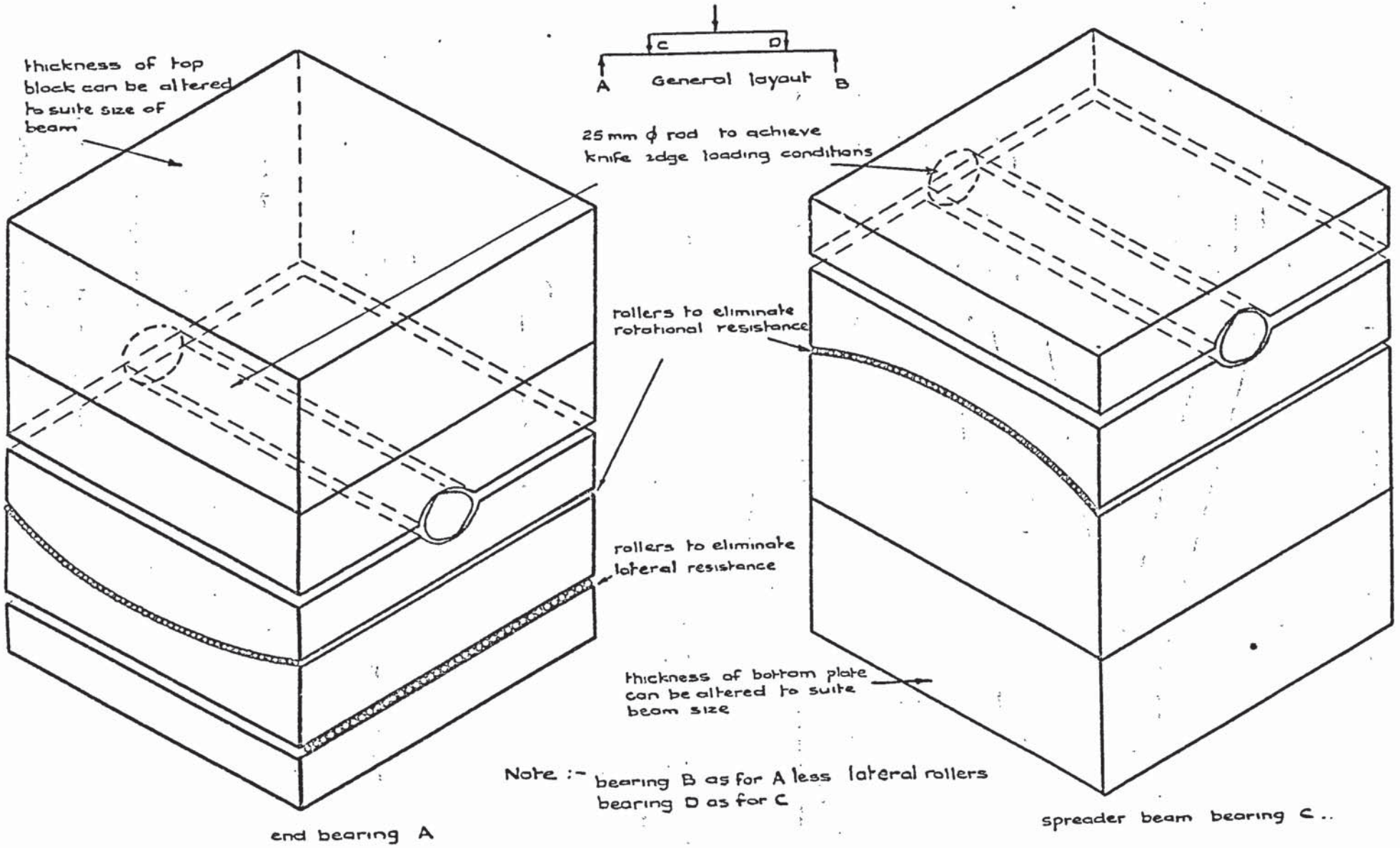

Fig. 2.5. Bearing points details

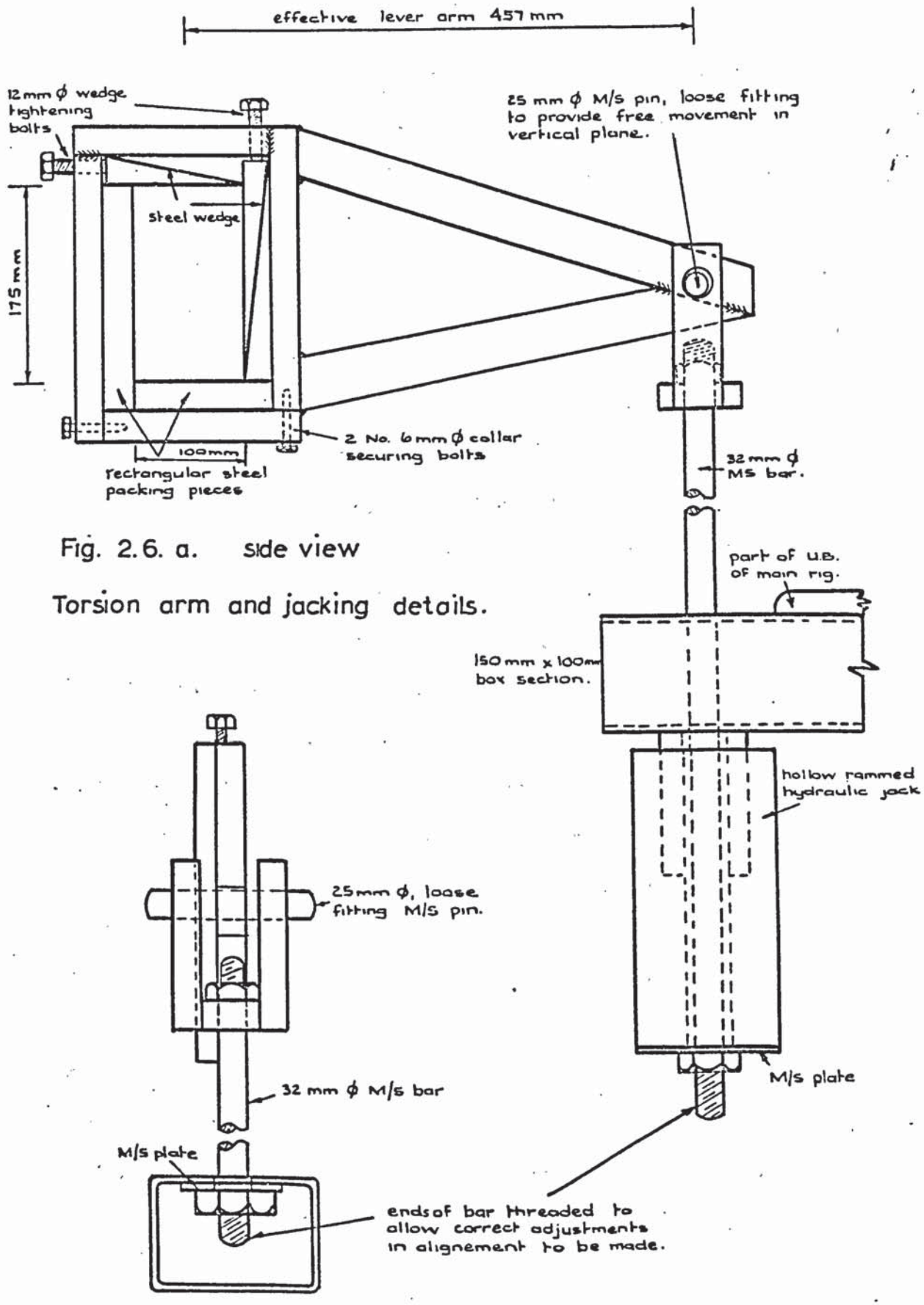

Fig. 2.6. a. side view

Torsion arm and jacking details.

Fig. 2.6. b. front view.

Details of arrangement at fixed end.

ensured that the axis of the beam coincided with the centre of the collar. The remaining pieces, consisting of 2 pairs of wedges, were then inserted in their respective spaces. The wedges were tightened against the beam by a bolt, threaded through the collar, and pressing against the thick end of one of the wedges in a pair. The effective lever arm of the collar was 457 mm (18 in.).

The load was transmitted to the collar by a 32 mm ($1\frac{1}{4}$ in.) diameter mild steel bar, attached as shown in Figs. 2.6(A) and 2.6(B). The loose fitting 25 mm (1 in.) diameter mild steel pin allowed the bar to rotate freely in the vertical plane ensuring that it remained vertical as the load was applied. Two brackets, made from 150 mm (6 in.) x 100 mm (4 in.) mild steel box section, and attached to the underside of the main rig, supplied the reaction to the torsional load. The bar at the fixed end passed freely through a hole in the bracket, and contact between the two was completed by a bolt screwed onto the end of the bar tightening against a mild steel plate. (See Fig. 2.6(B)). The load was applied through a 300 kN (30 ton) capacity hydraulic jack with hollow ram and a 127 mm (5 in.) stroke. The jack was held in position on the bar by a bolt and mild steel plate as shown in Fig. 2.6(A).

The accuracy of the pressure gauge supplied with the jack was considered insufficient, and a tensile proving ring was used to measure the applied load. The 50 kN (5 ton) capacity ring had a mean sinsitivity of 0.03 kN (7 lb) per division. Its calibration chart is shown in Fig. 2.7. Connection between the ring and the bar was made by universal joints to ensure the transmission of a pure axial load.

The bending moment was applied via a 1000 kN (100 ton) capacity hydraulic jack. The load, transmitted through a load cell, was measured on an automatic recording device to an accuracy of

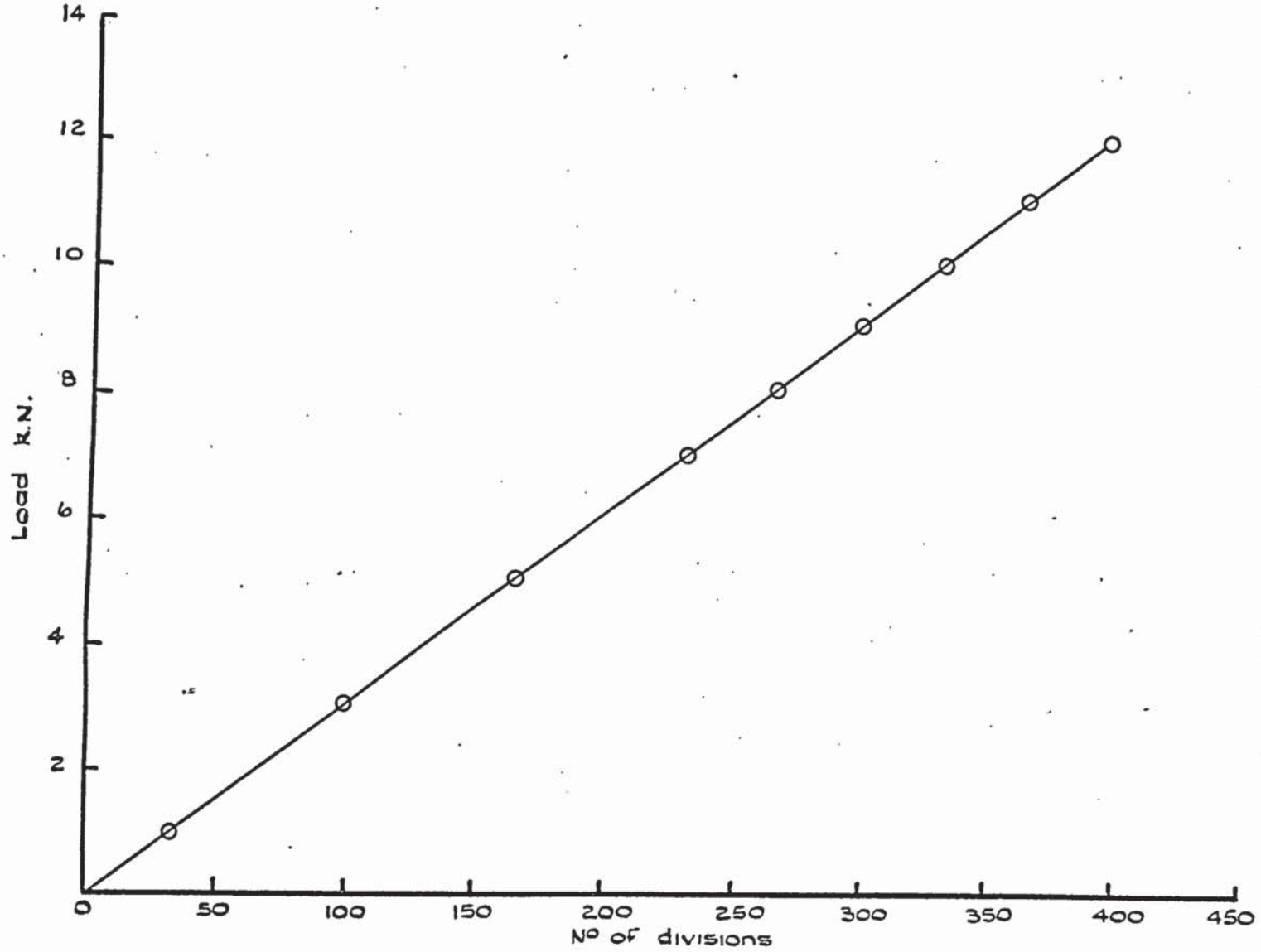

Fig. 2.7. Proving ring calibration chart

1.25 kN (0.125 tons).

The general layout of the rig is shown in Plates 2.5 and 2.6.

2.10. Instrumentation

2.10.1. Steel Strains

Electrical resistance strain gauges were used to measure all strains on the steel. The type of gauges used throughout the investigation were Tinsley linear foil gauges, with a 6 mm ($\frac{1}{4}$ in.) gauge length and a nominal resistance of 100 ohms. The sensitivity of the gauges necessitated great care being taken when attaching them to the steel. Consequently the manufacturers specifications were followed closely. Initially the metal was sanded bright with wet and dry paper. The surface was then degreased and neutralized with trichloroethane and a 10% solution of ammonia respectively. Eastman 910 Adhesive, in conjunction with Eastman 910 Catalyst Hardener, was used to bond the gauges to the steel. The gauges were affixed with the aid of a Sellotape strip and the application of light finger pressure for about 1 minute. Bonding was complete and the gauges ready for testing within 4 minutes of application.

Bad results, near yield, with reinforced concrete have been reported by some investigators using Eastman adhesive. The author felt, however, for 2 reasons, that the use of Eastman in this case would produce satisfactory results. Firstly, it was not expected that the steel would be near yield at failure of the beam. Secondly, the surface finish on much of the steel used in reinforced concrete tends to be rather rough and pitted. In this case it is felt that the use of Budd G.A.2 cement is advisable. After sanding, the finish produced on the steel used in this

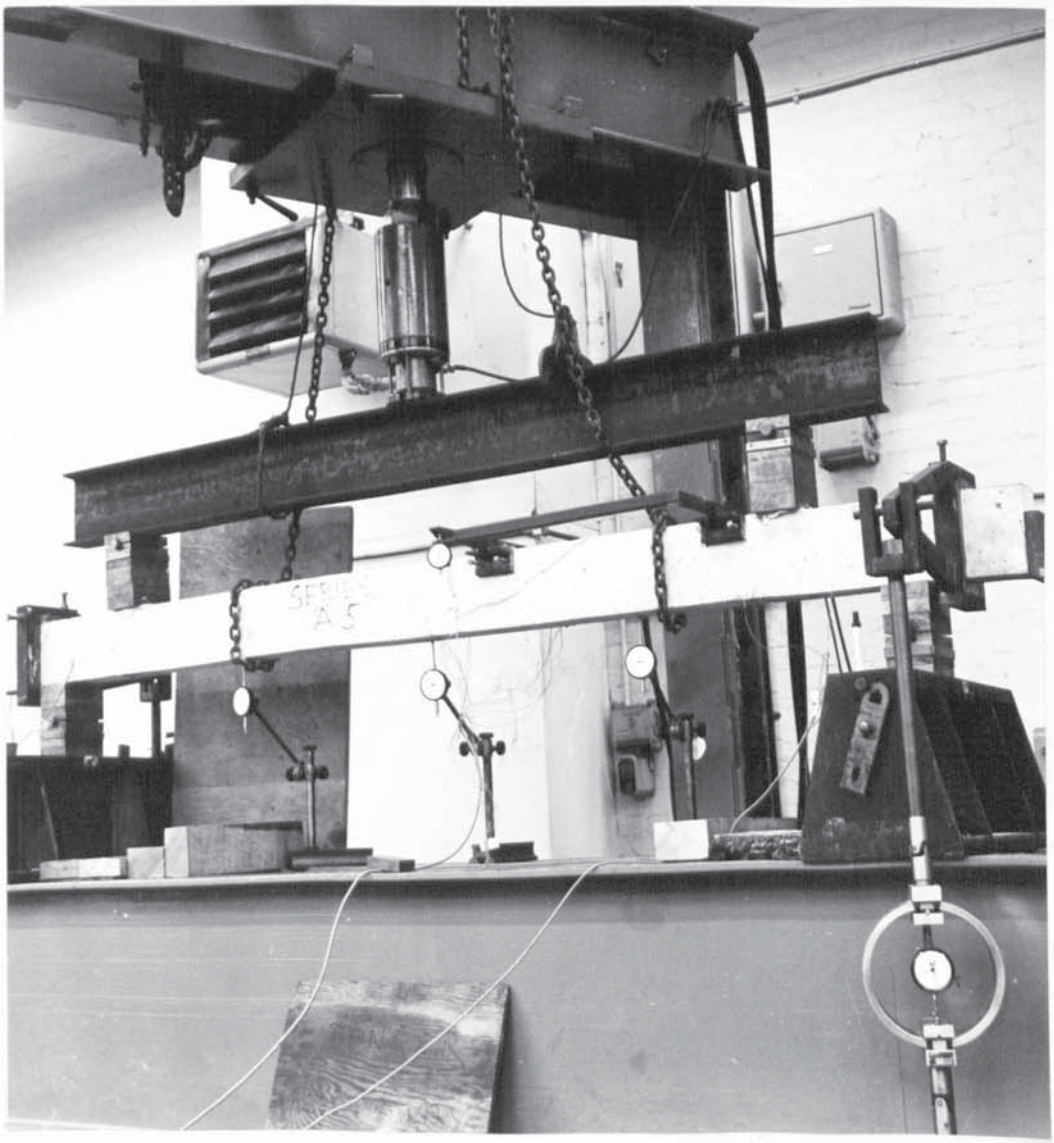

Plate 2.5 - General layout of rig, front view

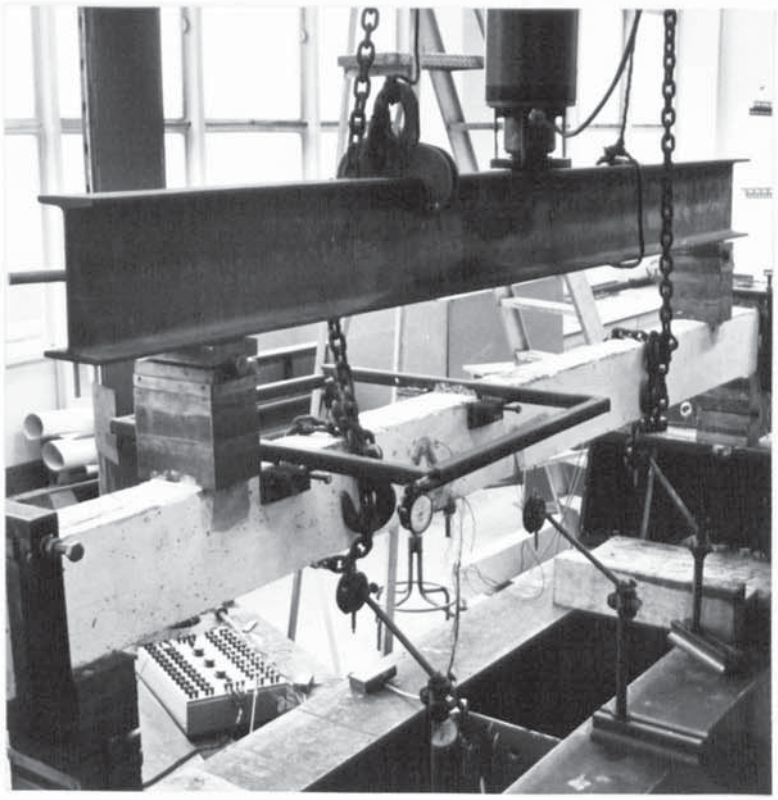

Plate 2.6. - View from back of rig

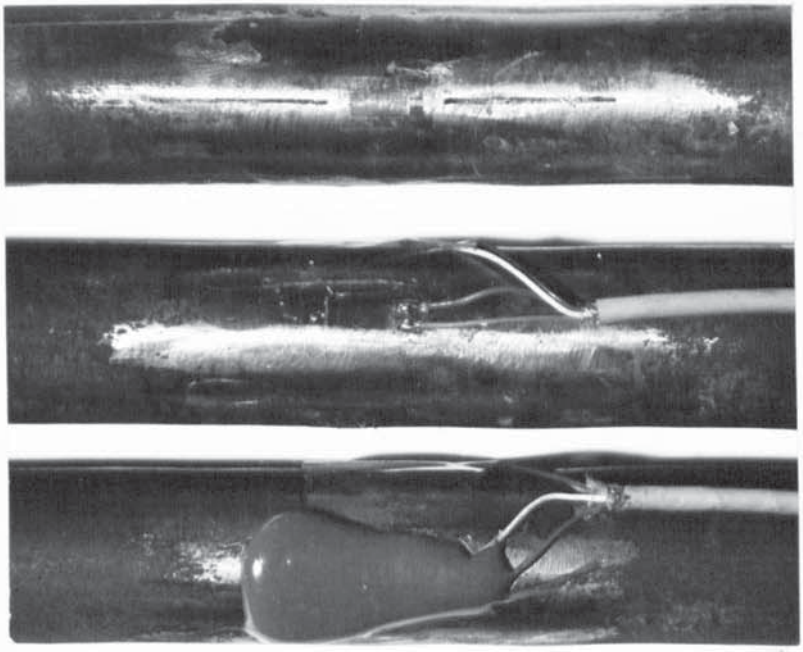

Plate 2.7. - Method of strain gauge application

investigation was very smooth, providing a very satisfactory surface for the Eastman. At one stage during the course of the experiments supplies of Eastman became exhausted, and it was necessary to make use of the Budd G.A.2 cement. Strains recorded using this glue tended to be as much as 50% below those expected and as a result a seperate test was carried out to investigate this phenomenon. Part of a prestressing bar was tested under pure axial tension, strains being recorded by 6 gauges, 3 adhered by Budd G.A.2 cement, and 3 by a new supply Eastman cement. The results were in agreement with those obtained from the beam tests. The error was thought to be due to the layer of glue existing between the steel and the gauge. The authors' lack of experience with this type of glue had probably caused him to leave too thick a layer. All remaining gauges were bonded to the steel using the newly obtained supply of Eastman cement.

The gauges on the early beams were positioned at the centre of the bar, 4 of them being placed at equidistant points around its circumference. In order to measure any loss in prestress in those bars cast in-situ, 2 sets of 3 gauges were placed close to either end of the bar. The final test also contained a further set of 3 gauges placed at the mid-span of the bar. It was felt that the increase in stress due to bending may not be recorded by those gauges placed at the extremities, and as a check the above step was taken.

Electrical wires from a multicore minature cable were soldered to the exposed tags of the gauges, and a resistance box used to check the condition of the gauges and the connections. Waterproofing was then carried out using a 2 component rubber-like epoxy resin, Gagekote 5. The resulting fluid mixture was easily

applied to the gauges without fear of damaging them, and dried within 6 hours at 75°F to a tough flexible film. Its use with beams containing the precast void was simply to protect the gauges as the bar was being inserted. Plate 2.7 shows in detail the various stages involved in applying the gauges.

Gauge positions and respective coloured wires were noted before casting so that connection to the strain recorder could be easily carried out. The same strain recorder was used to measure both steel and concrete strains and a description of it is given in the next section.

2.10.2. Concrete Strains

Strains were measured by a combination of mechanical and electrical resistance gauges. Felt backed Tinsley strain gauges, Type 6E, with a nominal gauge length of 16 mm ($\frac{5}{8}$ in.) were used on the first 2 beams but were found to give rather erratic results. With a maximum aggregate size of 10 mm ($\frac{3}{8}$ in.) the strain, recorded over such a small gauge length, could easily be effected by the position of pieces of aggregate within this length. Type 7A gauges, whose gauge length of 48 mm ($2\frac{1}{2}$ in.) was greater than 4 times the maximum aggregate size, were then used. Mechanical strain readings were taken using Demec spots fixed to the surface of the beam over gauge lengths of 4 in. and 8 in. Strains to an accuracy of 20 and 10 microstrains respectively could be measured using this system.

Gauges forming 60° rosettes were used to measure the maximum principal stresses. Additional gauges placed along the axis of the beam recorded stresses due to prestress. The gauge position having been carefully marked out, the areas in question were sanded to remove any bad surface characteristics. A quick drying dental cement, F.88, was used to fix both the gauges and the

Demec spots to the surface of the concrete. Wires of the same type used on the steel gauges were then soldered to exposed tags and the circuit checked using the resistance box.

All wires, from gauges on both the steel and the concrete, were led to an extension box, type 48 U, designed to be used in conjunction with a Peekel B.105 strain recorder. The recorder automatically converts resistance changes into microstrains. This arrangement has the advantage that only 1 dummy gauge is needed to complete the Wheatstone circuit for every 24 active gauges. The concrete dummy was attached to a 150 mm (6 in.) concrete cube, and was replaced everytime there was a significant change in the gauge factor of a particular batch of gauges. A short length of prestressing steel was used to attach the steel dummy to, which was waterproofed in the same manner as before. Both dummies were kept close to the specimens during the tests in order that temperature compensation was adequate. Leads from both dummy and active gauges were of the same length to prevent any inaccuracies occurring due to electrical inbalance. It was possible, using this system, to measure the strains to within 1 microstrain.

2.10.3. Mechanical Dial Gauges

Deflection readings were taken at selected points on the soffit of the beams using Batty type CL.5 gauges with a range of 50 mm (2 in.) and a sensitivity of 0.01 mm (0.0004 in.) per division. Points at mid-span and 600 mm (24 in.) either side, on the longitudinal axis of the beam, were selected to determine the vertical deflections.

2.10.4. Angular Rotation Measurements

Several methods of measuring the angular rotation of the beam were considered, including the mirror-telescope system and the

differential transformer transducer as used by Hsu [31] The mirror telescope was considered rather clumsy and the method adopted by Hsu required somewhat expensive equipment. A simple, but precise method was needed, which necessitated the taking of as few readings as possible. The one finally decided upon was that shown in Fig. 2.8. A pair of cranked arms, made from 25 mm (1 in.) square box section, were clamped to the beam at selected points, the distance between the arms being fixed at 600 mm (24 in.). Clamping was effected by 2 small pieces of angle iron welded to the arm as shown. Two bolts, passing through the angle and bearing upon a 6 mm ($\frac{1}{4}$ in.) steel plate, secured the arm in place. Adjustments could be made via the bolts to ensure that the apparatus was positioned both centrally and perpendicularly across the section of the beam. The relative movement between the arms was measured using 2 Batty type C-15 gauges with a range of 25 mm (1 in.) and sensitivity of 0.002 mm (0.00008 in.) per division. A split clamp arrangement on either end of each arm held the gauges securely in place. Using the average readings from both gauges it was possible to measure the angular rotation to within 1.1×10^{-7} radians per mm.

Deflections due to a constant bending moment would cause equal, but opposite movements in both gauges. The average reading therefore would remain unchanged and all movements due to flexure would be effectively eliminated.

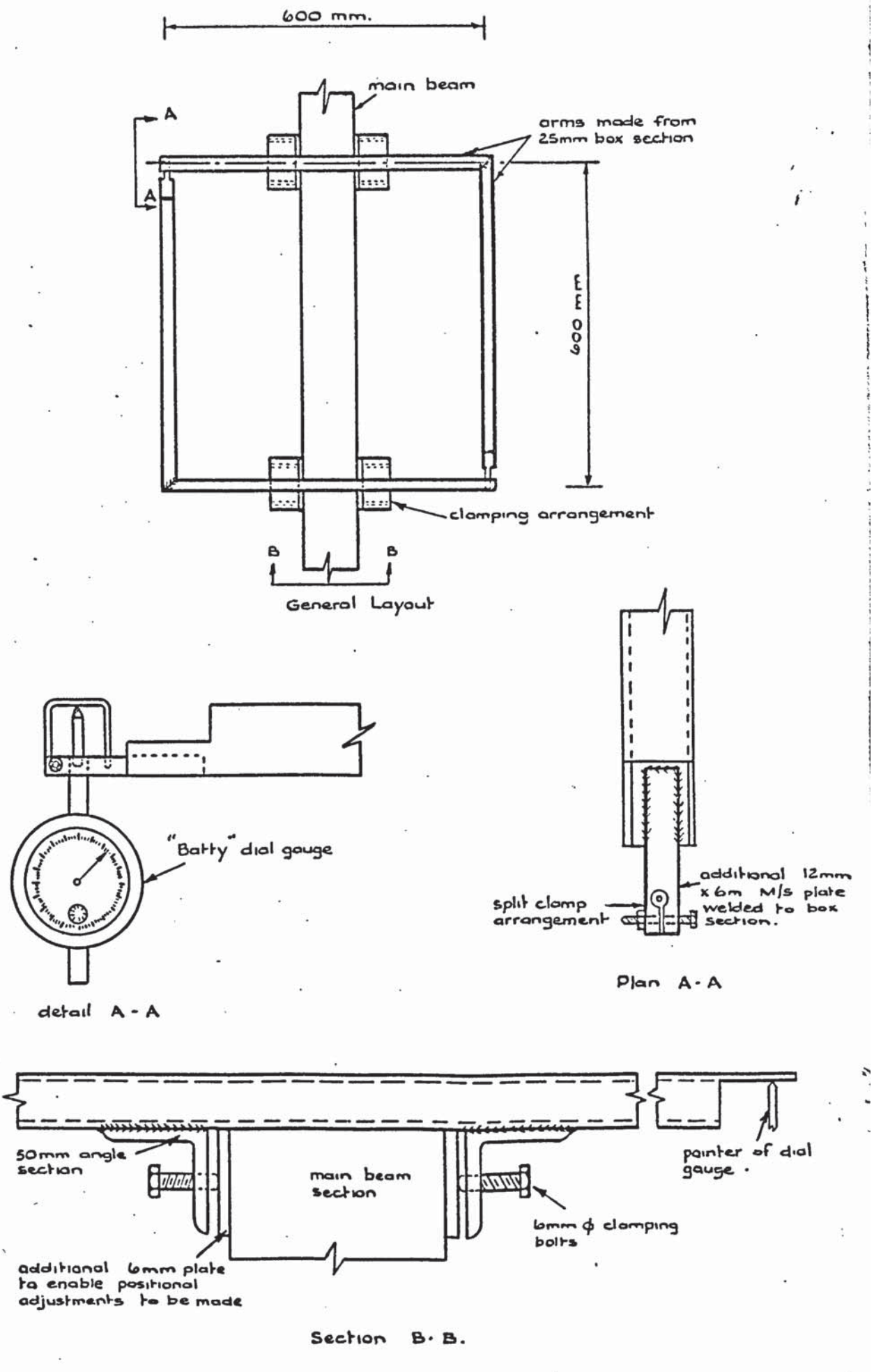

Fig . 2. 8. Angular rotation apparatus

Chapter 3

Experimental Observations

3.1. Introduction

The following chapter is concerned with the observations recorded during the testing of the prestressed beams. The behaviour pattern of many of the beams was found to be very similar, and it is not proposed to describe, in detail, each individual test. The experimental failure loads are presented in tabular form in Tables 3.1 and 3.2 and in graphical form in Fig. 3.1. Graphs of all relevant readings recorded throughout the tests have also been plotted.

3.2 Sequence of Loading

A small bending moment was first applied to the beam in order to stabilize the test rig, and a torsional moment of approximately 50% of the expected ultimate was then added. The bending moment was then increased to a predetermined value and the torsional moment gradually increased until failure. The increments of loading were reduced from 2kN to $\frac{1}{4}$ kN as failure was approached.

In general, the time required between loading increments, to record all relevant readings and examine the beam for cracks, was about 15 minutes. The overall length of time of the test was usually about 3 hours.

3.3 Description of Tests

S.A.1.

Due to the arrangement of the test rig (see Plate 2.5) it was not possible to obtain a condition of pure torsion. The application of a torsional load to the beam induced a hogging bending moment within its length. The torsion arms were, however, placed very close to the bottom bearing pads and the resulting hogging

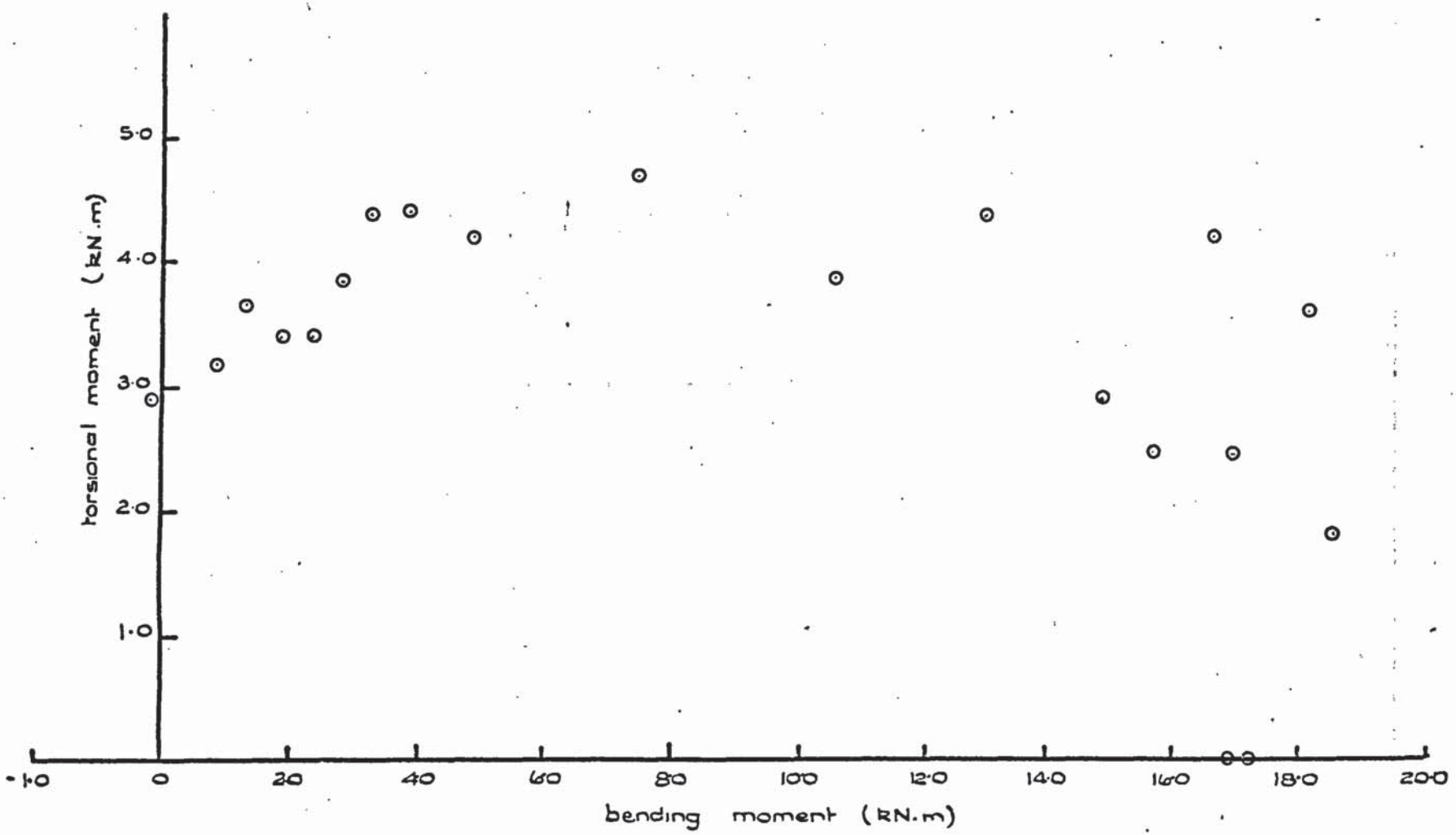

Fig. 3.1. General pattern of authors results.

Beam No.	U_w N/mm^2	f'_c N/mm^2	f_{sp} N/mm^2	f_r N/mm^2	E_c N/mm^2 x 10^4	P_{tl} kN	Ult. Bending Moment kN.m	Ult. Torsion Moment kN.m
1	48.24	30.30	1.93	3.04	2.88	153	-0.15	2.86
2	46.37	35.01	1.26	2.61	3.81	146	0.86	3.18
3	43.80	28.44	1.50	3.10	2.56	142	1.30	3.63
4	51.22	38.41	2.92	3.50	3.07	114	1.89	3.40
5	53.07	43.49	2.52	3.32	3.05	159	2.43	3.40
6	52.24	39.96	2.11	3.90	2.68	146	2.87	3.85
7	52.02	40.03	2.37	3.59	3.02	131	3.29	4.42
8	61.50	41.28	3.19	3.58	2.60		3.83	4.42
9	60.94	42.06	3.26	3.26	2.85		4.96	4.19
10	57.26	41.27	2.92	3.92	2.96	138	7.53	4.76
11	56.14	38.33	2.50	3.57	2.62	137	13.23	4.38
12	54.12	31.32	2.25	3.64	2.48	145	18.99	0
13	57.33	37.39	2.72	3.46	2.92	144	16.70	4.20
14	56.18	37.55	2.61	3.52	2.73	142	18.19	3.63
15	52.63	34.70	3.40	3.12	2.23	140	19.84	1.12
16	49.84	41.83	3.39	3.61	2.47	141	17.20	0
17	55.47	40.68	2.85	3.18	2.63	143	18.59	1.80
18	54.87	45.67	2.94	4.44	2.70	138	15.70	2.47
19	49.21	36.34	2.18	2.90	3.26	138	17.08	2.47
20	47.21	37.79	2.50	3.32	3.39	143	10.60	3.86
21	45.86	44.52	2.79	3.30	3.31	142	14.91	2.95
22	44.89	35.72	3.10	3.23	2.99	138	16.95	0
Av.	52.29	38.28	2.60	3.41	2.87	141		
%Coeff Var.	10%	12%	22%	11%	13%	6%		

TABLE 3.1.

Author's Experimental Results S.I. Units

Beam No.	U_w psi	f'_c psi	f_{sp} psi	f_r psi	E_c psi x 10^6	P_{tl} kips.	Ult. bending moment kips.ins.	Ult. Torsion Moment kips.ins.
1	6995	4394	280	441	4.18	34.35	-1.28	25.27
2	6724	5077	183	378	5.52	32.71	7.64	28.10
3	6351	4124	217	449	3.71	31.86	11.53	32.14
4	7427	5570	423	508	4.45	25.61	16.75	30.12
5	7695	6306	365	482	4.42	35.72	21.52	30.12
6	7575	5794	306	566	3.88	32.80	25.43	34.09
7	7543	5804	344	520	4.38	29.44	29.10	39.14
8	8917	5986	462	519	3.77		33.87	39.14
9	8836	6098	472	473	4.13		43.87	37.12
10	8302	5984	423	568	4.29	31.01	66.64	42.14
11	8141	5558	362	517	3.80	30.85	117.09	38.42
12	7847	4541	326	528	3.59	32.61	168.02	0
13	8313	5422	395	501	4.23	32.29	147.75	37.20
14	8146	5445	379	510	3.96	31.98	160.99	32.14
15	7632	5032	493	453	3.23	31.47	175.57	9.89
16	7227	6065	491	523	3.58	31.80	152.25	0
17	8043	5899	413	461	3.81	32.11	164.53	15.96
18	7956	6622	427	644	3.92	30.95	138.98	21.83
19	7136	5269	316	420	4.73	31.01	151.12	21.83
20	6845	5479	362	482	4.92	32.09	93.83	34.17
21	6650	6455	405	478	4.80	32.02	131.99	26.07
22	6509	5179	448	468	4.34	31.00	150.00	0
Av.	7582	5550	377	495	4.17	31.68		
%Coeff Var.	10%	12%	22%	11%	13%	6%		

TABLE 3.2

Author's Experimental Results Imperial Units

moment was only 5% of the ultimate torsional moment.

The load was seen to drop off at the appearance of the first cracks. When this occurred the load was quickly released to prevent complete disrupture of the beam from taking place. Diagonal tension cracks on the top and the sides of the beam were present after the load had been released. Although great care was taken to detect the occurance of cracks during loading, failure was so sudden that it was not possible to determine at which point the first crack appeared. The crack pattern did indicate, however, that had loading been continued, disruptüre would have taken place by rotation about a compression hinge in the bottom of the beam.

This type of failure has not been recorded previously in prestressed concrete, although it was reported by Collins et al[32] in reinforced concrete. Such a failure will be referred to as a Mode 3 failure as discussed in Section 4.1.

S.A.2.

The failure of this beam, tested under an M/T ratio of 0.27, was sudden and explosive and complete disrupture of the specimen took place before the loads could be released. An examination of the beam showed diagonal tension cracks on the top and sides with the formation of a compression hinge on the bottom face indicating a Mode 3 failure.

S.A.3.

A further increase in the applied bending moment, producing an M/T ratio of 0.48, resulted in a different mode of failure. Failure was initiated by the formation of diagonal tension cracks on the upper and lower faces as well as on the front face of the beam. Rotation then occurred about a compression hinge on the back face of the beam. This type of failure will be referred to as a Mode 2 failure as discussed in Section 4.1.

S.A.4.

Despite an increase in the bending moment to torsion ratio

to 0.56. the failure mechanism was that of Mode 3. It was possible to release the loads before complete collapse had occurred and diagonal tension cracks could be clearly seen on the top and on both sides of the beam.

S.A.5.

Tested under an M/T ratio of 0.72 the failure mechanism was similar to that of beam No. S.A.3. Loading was ceased at the occurance of the first cracks which appeared on both the upper and lower faces as well as on the front face of the beam.

S.A.6.

Up to this stage of testing all beams had been cast with a void formed by an inflatable rubber tube. It was thought however, that the prestressing bar may be moving within the void during testing. As a check, holes, leading to the void, were cast at regular intervals into the front face and soffit of the beam. By means of a specially designed depth micrometer it was possible to record both the lateral and vertical movement of the bar during testing. Readings were taken at each increment of loading.

Failure was of the Mode 2 type, the diagonal tension crack on the front face being propogated by one of the holes used for locating the position of the prestressing bar. The M/T ratio in this case was 0.74. Readings on the depth micrometer indicated that the bar remained in position throughout the test.

S.A.7, 8, 9, 10.

In each successive test the bending moment to torsion ratio was increased from 0.74 to 1.58 and the mode of failure remained that of Mode 2. With each increase in bending moment the failure became more explosive due to the sudden release of the prestress. It was clear, however, that the failure mechanism was one of rotation about a diagonal

compression hinge on either the front or back face of the beam.

S.A.11.

The M/T ratio of 3.0 in this case was substantially greater than that of previous tests. During the application of the bending moment tension cracks appeared in the soffit of the beam and travelled a small distance vertically up the side faces. The torsion moment was then carefully applied until failure, which was once again explosive, and occurred without any warning. A close examination of the fragments revealed a diagonal compression hinge on the back face indicating a Mode 2 failure.

S.A.12, 16.

The test on S.A.12 was carried out under the action of bending moment only. Cracks appeared in the soffit and the lower extremities of the side faces sometime before failure. The initial vertical movement of the cracks up the sides of the beam tended to be rather rapid for a small increase in bending moment. As failure was approached, however, it was often difficult to detect any increase in their length. At a bending moment of 20.4 kN.m. (180.2 kips. ins.) there appeared to be a slight spalling of the concrete on the top of the beam indicating the beginning of a possible compression failure. It was not clear, however, at this stage whether infact this apparent spalling was simply a result of the whitewash flaking off the beam. In addition it was noticed that there was a large amount of lateral movement in one of the top loading pads. A small increase in the load resulted in the total collapse of the rig due to excessive movement of the bearing pad. A close examination of the beam revealed that all the bending cracks had closed up due to the effect of prestress. It was therefore decided to make a slight modification to the rig and repeat the test using the same

beam. The complex bearing pads used previously were replaced by a simple plate and roller arrangement. Such an arrangement could only be used for the pure bending test as it did not allow free rotational movement of the beam to take place.

On commencement of the test it was noted that none of the strain gauges were recording their original values. This was to be expected as the beam had previously been subjected to a load close to its predicted collapse load. It was nevertheless decided to continue with the test as a means of proving the rig. The cracks began to re-open after the first increment of loading and failure occurred at a moment of 18.99 kN.m (168.02 kips. ins.) The failure mechanism was clearly one of a compression failure of the concrete in the top of the beam.

Due to the fact that the failure bending moment was lower than that at which the rig had previously collapsed it was dicided to repeat the test using the modified bearing pads. Beams No's. S.A.16, and 22 were tested under pure bending moment and failed in a similar manner to that of S.A.12.

S.A.13.

This beam was subjected to a bending moment to torsion ratio of 4.0. No cracks were visable until approximately 80% of the ultimate torsion moment had been added. The cracks appeared as the bending moment was being applied, and were first noticed in the soffit of the beam running approximately at right angles to its axis. For further increase in load the cracks began to move up both the front and back faces of the beam. This initial vertical direction was maintained for a distance of approximately 40 mm ($1\frac{1}{2}$ ins.) after which the cracks became inclined to the beam's axis. Shear cracks between the supports and loading points were also visable at the high

bending moment values. Shear reinforcement placed in this section of the beam prevented premature failure from taking place.

With increase in the torsional load the cracks continued to increase in the inclined direction, their rate of increase becoming greater as the ultimate load was approached. Failure was explosive with a large amount of disruption taking place. This disruption was due not only to the sudden release of prestress but also to the sudden release of the high bending moment. This caused the beam to bow upwards resulting in the appearance of tensile cracks on its top face.

The crack pattern was very complex, and even after a close examination it was very difficult to decide which of the cracks had initiated failure. It was apparent, however, that a compression failure had occurred in the concrete in the top of the beam. Such a failure is known as a Mode 1 failure as described in Section 4.1.

S.A.14.

This beam, tested under an M/T ratio of 5.0, had a failure pattern very similar to that of the previous beam although disruption was not as complete. The increase in crack length under the torsional load was not quite so apparent in this case, and in fact after several increments of loading there was no detectable increase in their lengths. After a torsional moment of 2.15 kN.m (19.00 kips. ins.) had been reached there was an obvious increase in the rate of change of angle of twist and compressive strain. It was therefore thought that the beam was close to failure and it was considered unsafe to record any more Demec readings. As the torsional moment was increased it was noticed that both the deflection and rotation gauges were continually moving whilst the load itself was held steady to allow readings to be taken. Failure occurred at a torsional moment of 3.63 kN.m. (32.14 kips. ins.).

The resulting crack pattern showed tensile cracks on the bottom and sides of the beam with a wedged shaped spalling of the concrete on the top face. The failure mode was therefore considered to be Mode 1.

S.A.15.

Results from this test were not used in the analysis due to the fact that the rig collapsed before complete failure had taken place. The reason for collapse was similar to that occurring in S.A.12, the excessive lateral movement of the upper supports, due to the high bending moment, making the rig unstable. As a result the pads were modified slightly as shown in Fig. 3.2. The upper plate, containing one half of the groove used for the point loading arrangement (see Fig. 2.5) was removed and replaced by a flat plate. The 25 mm (1 in.) diameter rods were then placed on top of this plate producing a simple roller support. It was hoped that any lateral movement would now be taken up by the rollers. It is important to note that the centre of rotation of the beam still had to coincide with the centre of rotation of the rollers as had been the case previously. The thickness of the roller plus the flat plate was therefore equal to the thickness of that plate which had been removed.

The test was then repeated using the original beam, but was only used as a means of testing the apparatus. The only readings that were taken, therefore, were those of the failure loads. The above arrangement proved to be successful, failure of the beam occurring as in the previous test.

S.A.17, 18

The failure mechanism of both these beams, tested under M/T ratios of 10.3 and 6.6 respectively, was very similar to that of S.A.14, both beams failing in Mode 1.

The remaining tests were used to fill important gaps which existed in the range over which the beams had been tested. In some cases

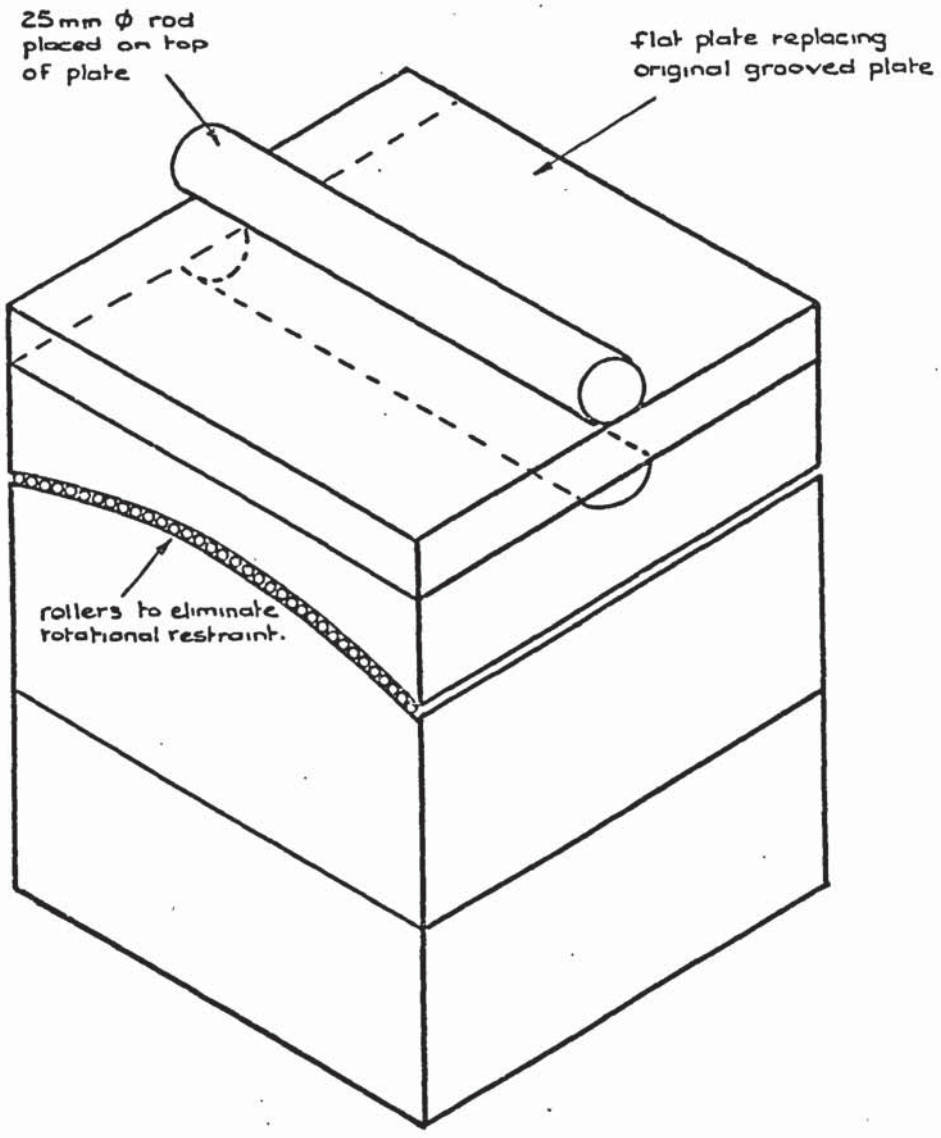

Fig. 3.2. Modified spreader beam bearings C & D

the test was a repeat of a previous test whose results were in some doubt. In all cases (with the exception of S.A.22) only readings of deflection, rotation, and ultimate load were taken. It was felt at this stage that all relevant information concerning the strains in the concrete had been obtained from previous tests. Beam Nos. S.A.19, and 21 failed in a typical Mode 1 fashion and S.A.20 failed in Mode 2.

S.A.22.

The main purpose of this test was to try and verify the relationship between the strain in the steel and the concrete at the same level in the beam. A knowledge of this relationship was required to determine the value of the Bond Slip Factor referred to in 4.2.3. There was also some doubt as to whether the strain readings in the steel, recorded in all previous tests, were in fact a true representation of the strain in the steel at its central section. The reason for this was that previously the steel strains had been recorded by 2 sets of 3 gauges placed at the extremities of the bar. Due to the fact that the bar was unbonded it was thought that the strain may not be constant along its length, but it may be greater at the centre as a result of the effect of the bending moment. A further set of 3 gauges were therefore added to the bar at its central section. The addition, at this section, of the plastic tubing required to protect the gauges (see 2.6.3.) meant that there would be a weakness in the beam at this point. However, the main purpose of the test was not to determine the ultimate bending strength of the beam. It was therefore considered acceptable to weaken the beam at this section.

The results of the strain readings taken throughout the test indicated that the strain in the steel was constant throughout its length.

The failure mechanism was very similar to that of the previous 2 pure bending tests and its ultimate strength was very close to that of S.A.16.

3.4. General Pattern of Results

Fig. 3.1 shows the general pattern of the results plotted in graphical form. It can be seen that the addition of a small amount of bending moment increases the torsional resistance of the beam. During this stage the beams are failing in Mode 3. After about 25% of the ultimate bending moment has been applied the mode of failure changes to Mode 2 and the torsional resistance is then little affected by the increase in bending moment. This trend continues until about 90% of the ultimate bending moment has been reached at which point the torsional resistance is reduced, the beams are then failing in Mode 1.

3.5 Crack Angles

The crack patterns of all beams tested under combined bending moment and torsion are shown in diagramatic form in Fig. 3.3 to 3.8. They are also shown in pictorial form in Plates 3.1, 2 and 3.

In order to assist in the detection of the cracks during testing all beams were painted with a thin coat of whitewash. For those beams failing in Modes 2 and 3, it would have been beneficial to locate the exact point at which the first crack appeared.

As mentioned in Section 3.2 this was not possible as the crack usually appeared on 3 faces of the beam almost simultaneously. It was however possible, in some cases, to release the loads before complete disrupture occurred which greatly assisted the plotting of the crack patterns. The fact that the beams contained no transverse reinforcement meant, that if complete failure was allowed to take place, the specimen would become rather badly damaged. It was then very difficult to distinguish between those cracks produced after failure, and those which had initiated failure.

3.5.1. Beams Failing in Mode 3

For these beams failing under low M/T ratios the critical

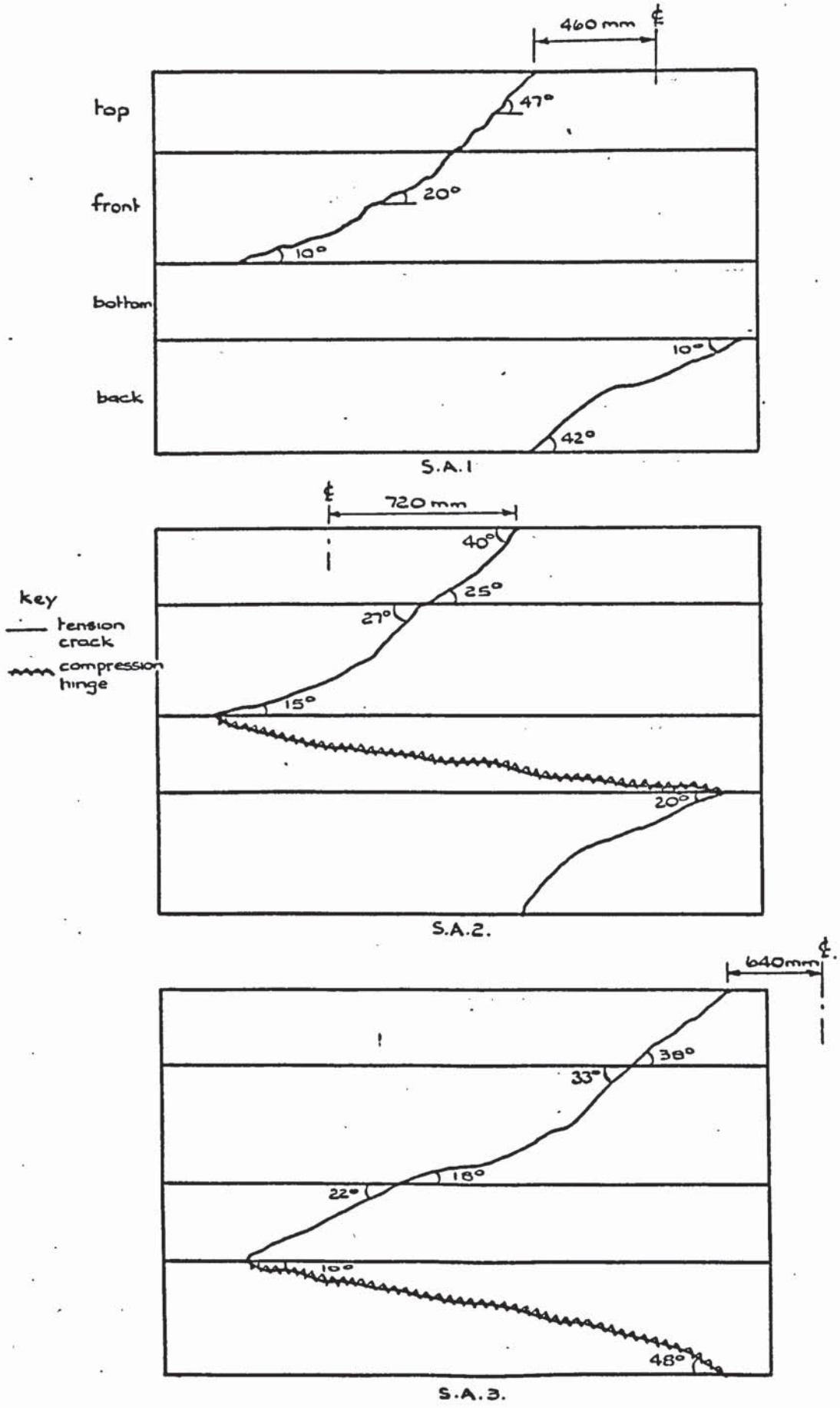

Fig. 3.3. Crack patterns at failure

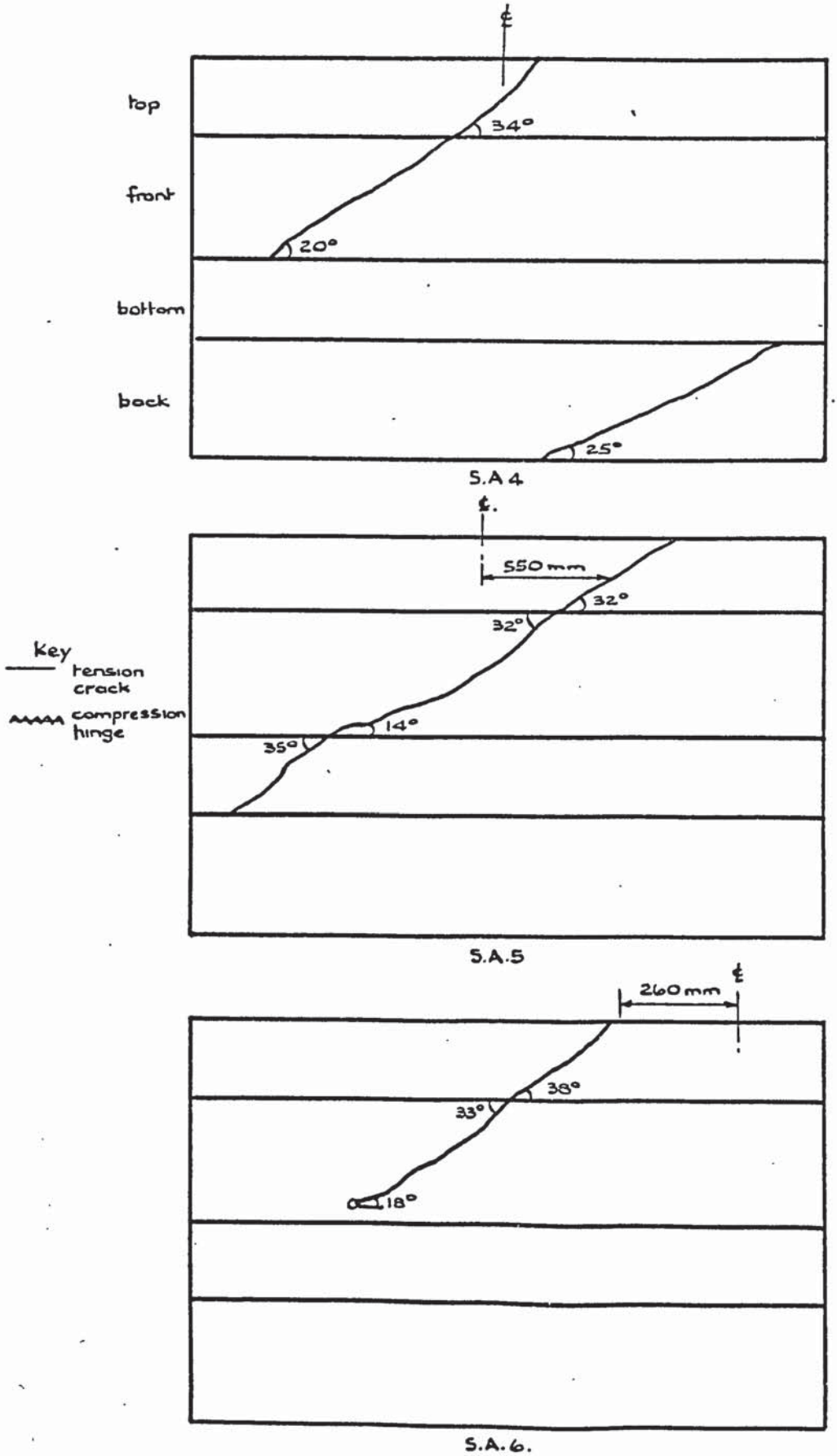

Fig. 3.4. Crack patterns at failure.

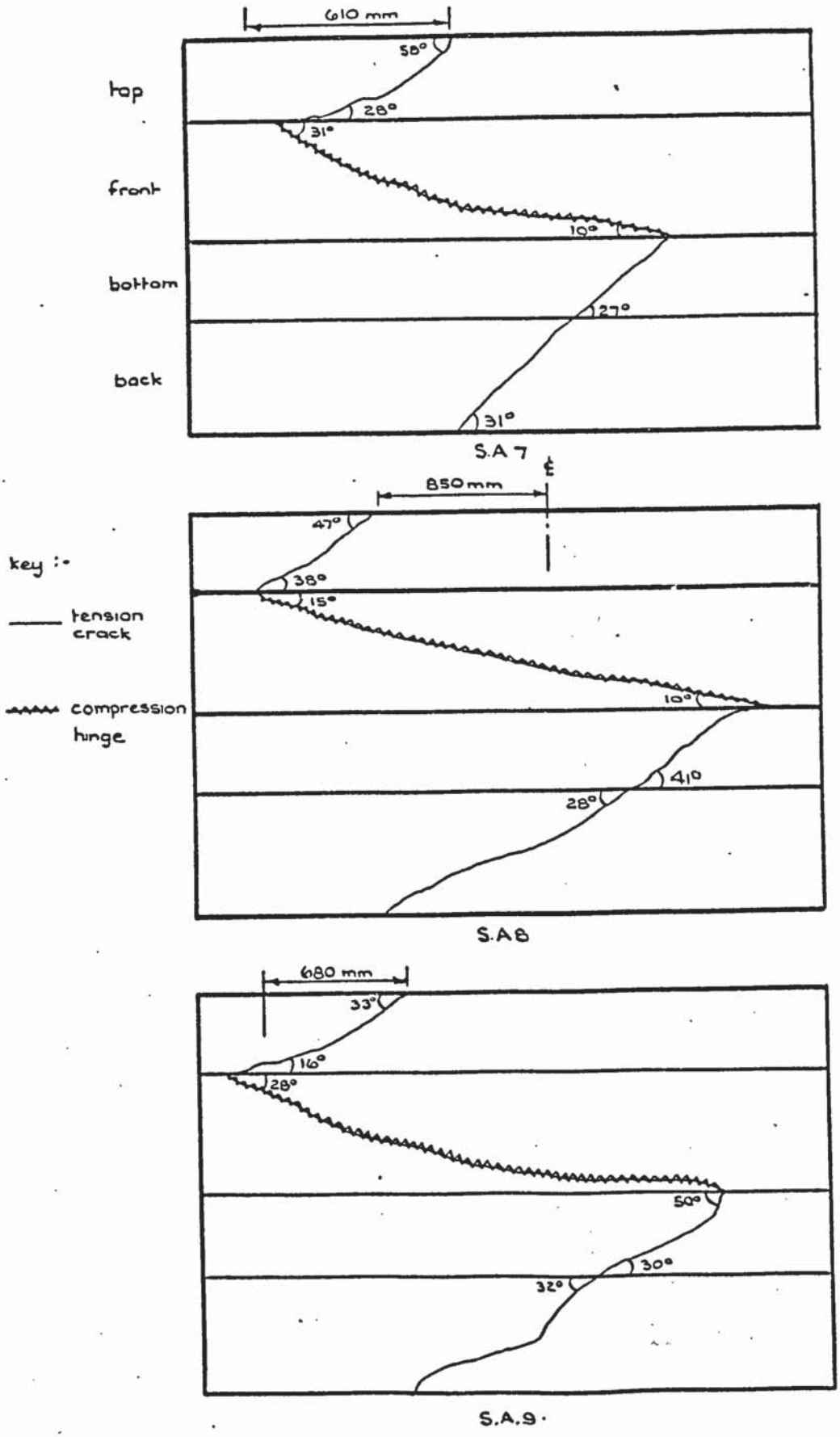

Fig. 3.5 Crack patterns at failure.

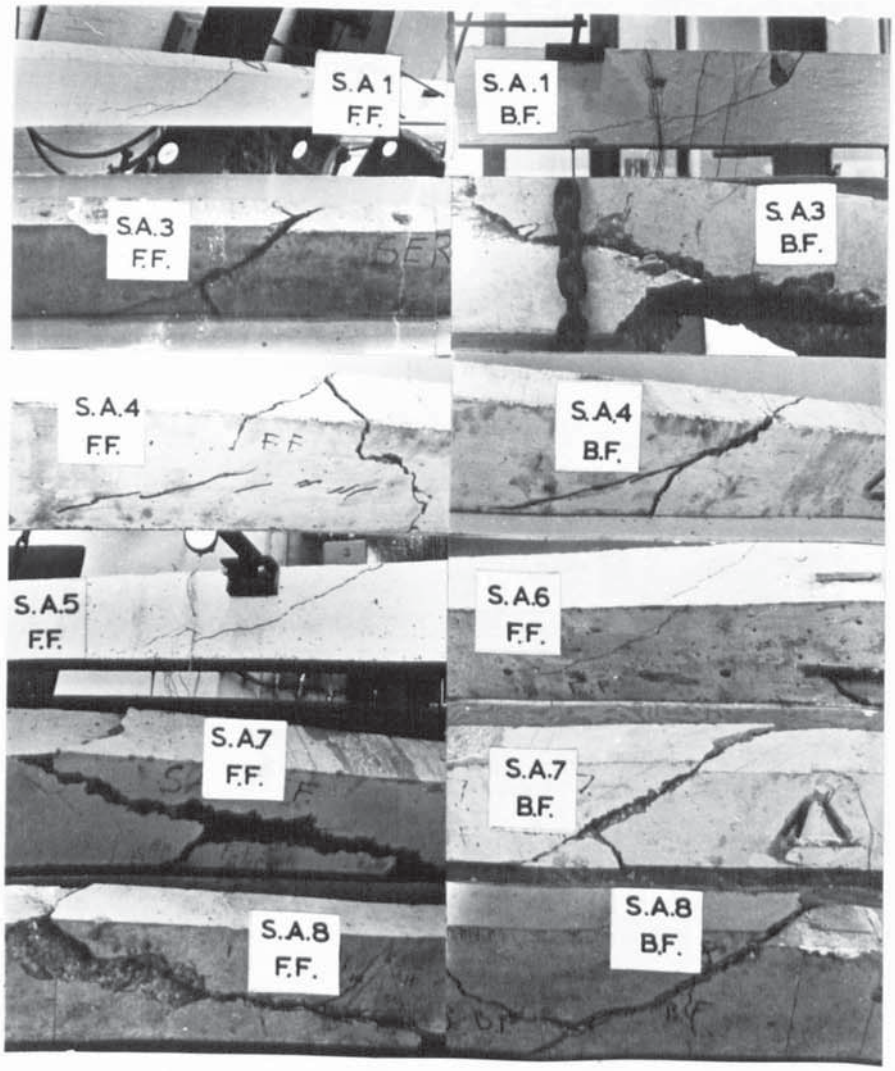

Plate 3.1 – Typical failure patterns of prestressed beams

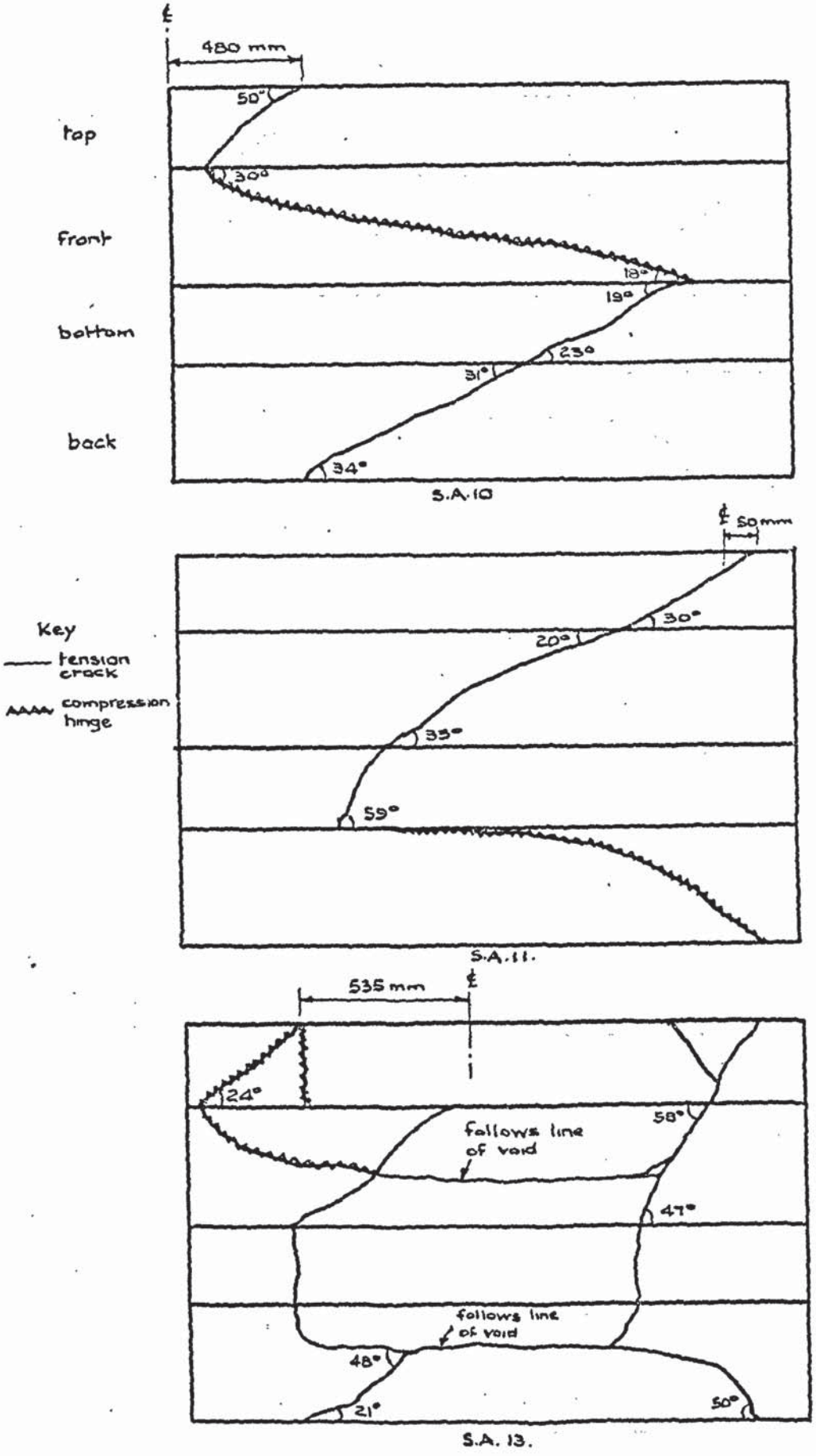

Fig. 3.6. Crack patterns at failure

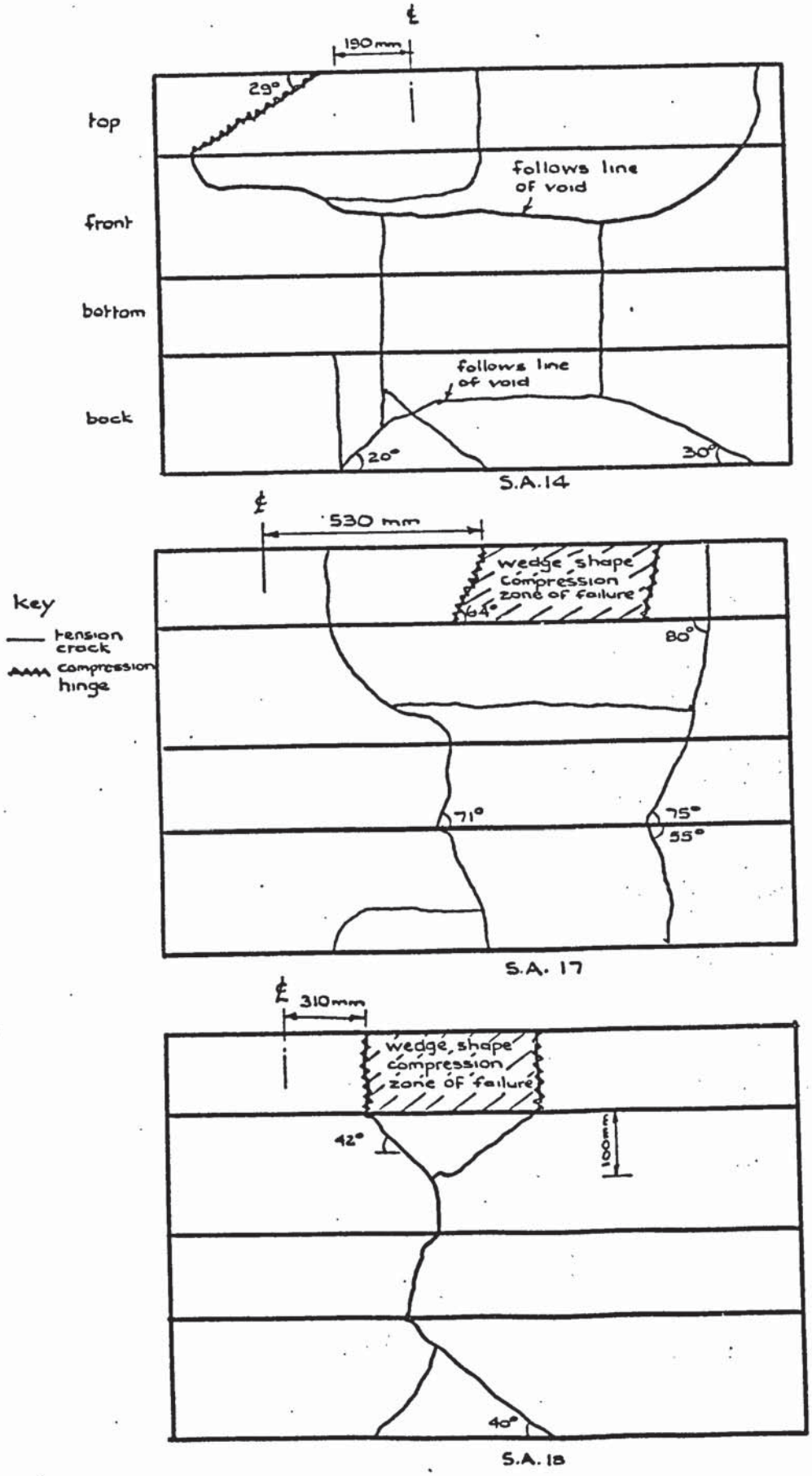

Fig. 3.7. Crack patterns at failure.

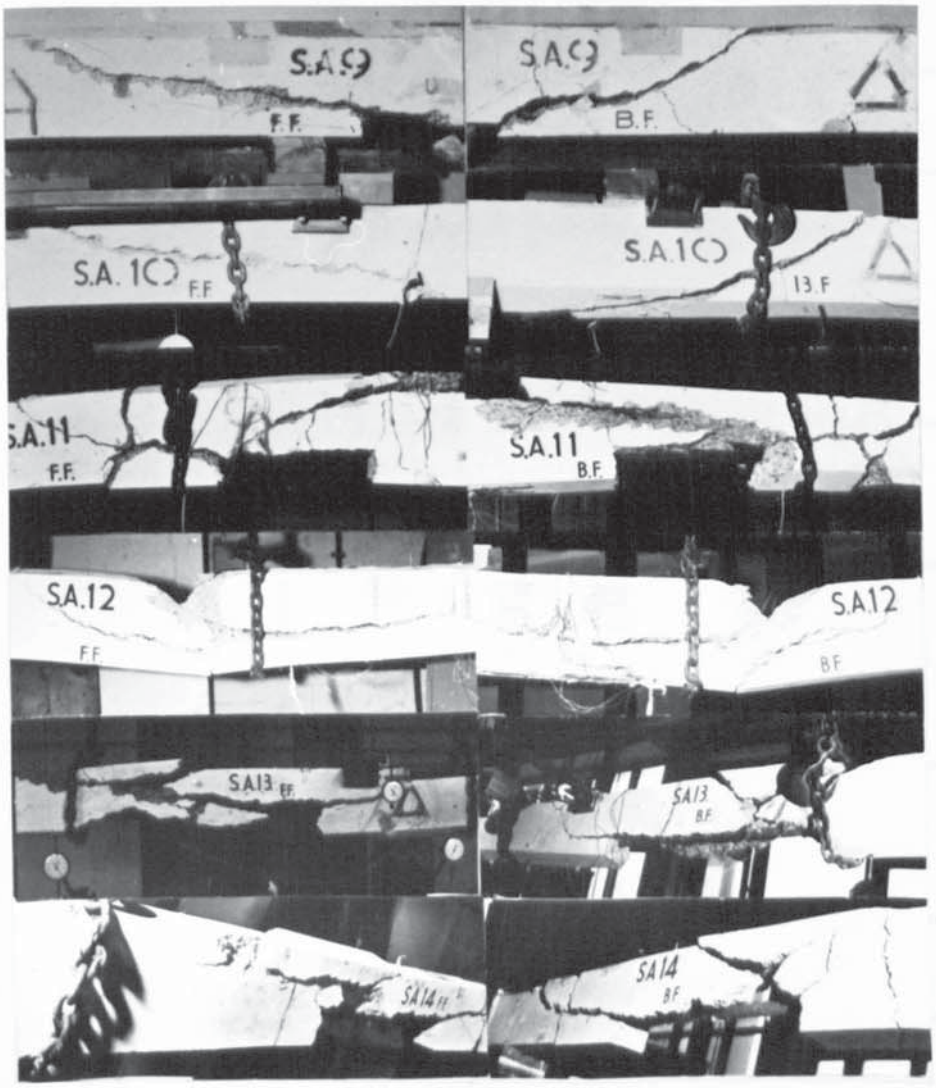

Plate 3.2 - Typical failure patterns of prestressed beams

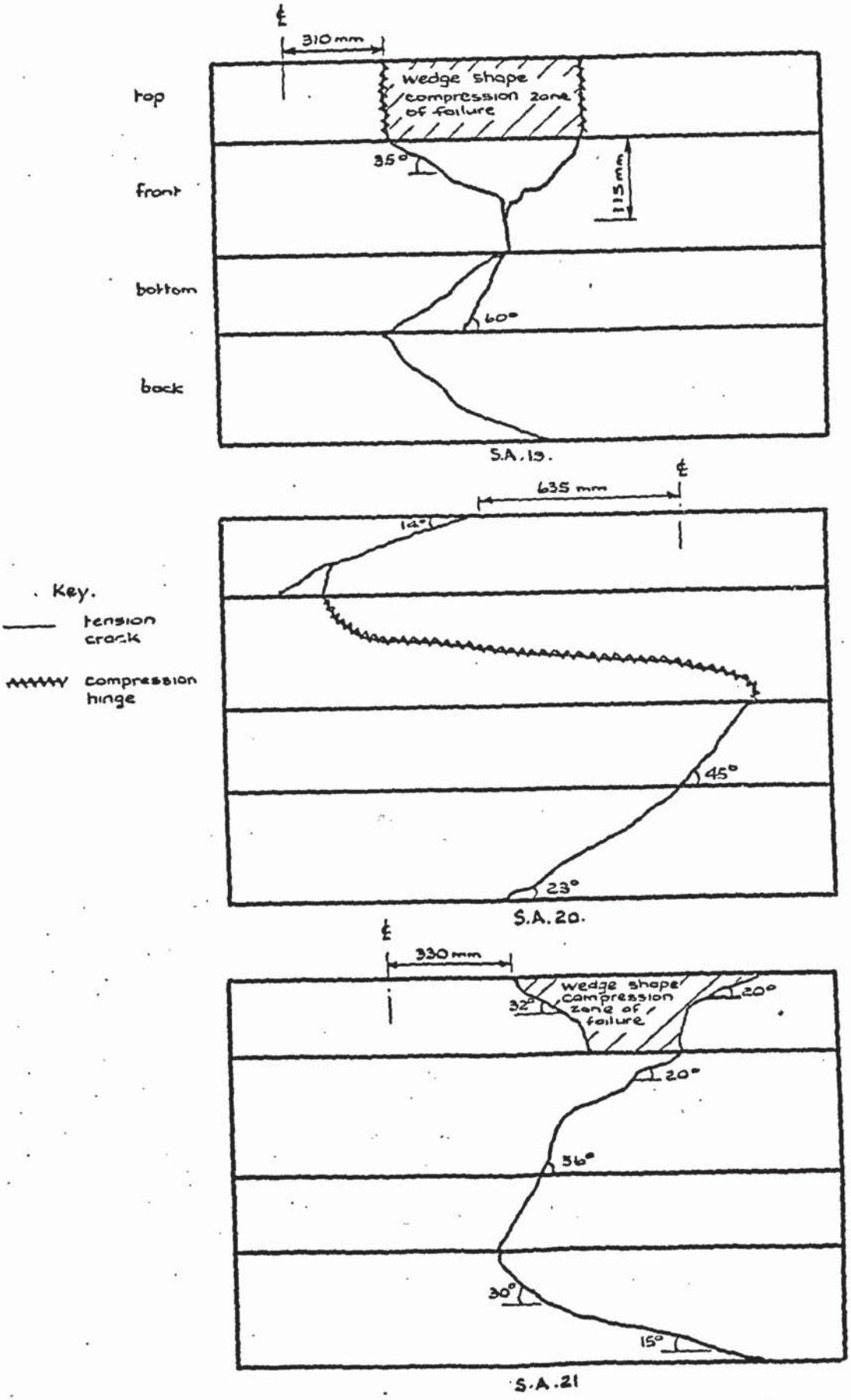

Fig. 3.8. Crack patterns at failure.

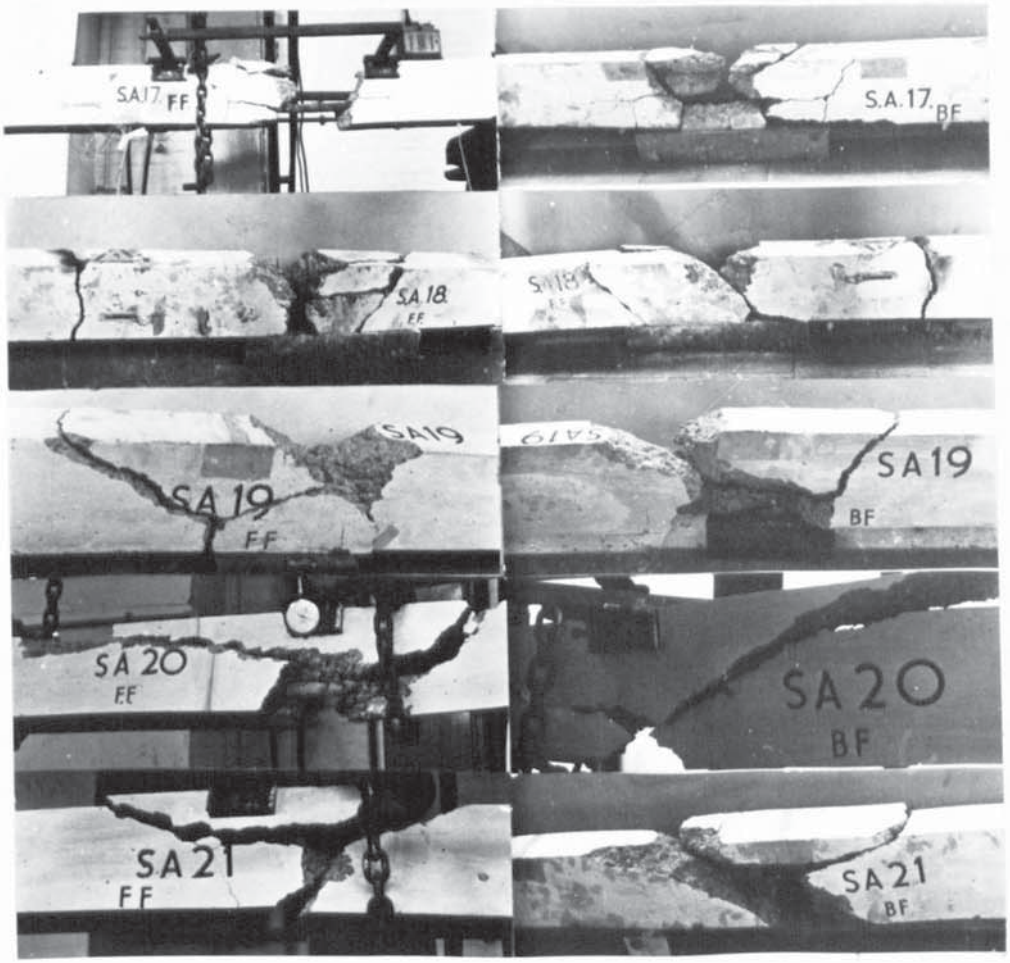

Plate 3.3 - Typical failure patterns of prestressed beams

section is at the top of the beam. At this point the compressive stresses due to bending and prestress are low.

For beam No. S.A.1 tested under almost pure torsion the crack inclination on the top of the beam was very nearly 45°. This was to be expected as the stresses, at this point, due to bending moment and prestress were almost zero. The conditions were, therefore, similar to that of plain concrete under pure torsion, the crack angle being 45° as predicted by the theory of maximum principal stresses. The addition of a compressive stress in this zone reduces the angle of inclination of the principal compressive stresses. The crack inclination is therefore reduced as shown in beams S.A.2, and S.A.4.

3.5.2. Beams Failing in Mode 2

These beams, tested under a higher M/T ratio than those of Mode 3, failed by rotation about a compression hinge on the side of the beam. Observations have shown that failure occurs immediately after the formation of inclined tension cracks on the remaining 3 faces.

The crack inclination, on the vertical face opposite to that on which the compression hinge forms, can be seen to vary across the depth of the beam. This is a result of the variation in compressive stresses produced by the bending moment and the eccentric prestress. For low bending moments the compressive stresses due to prestress in the bottom of the beam are predominant. The crack inclination here is therefore less, and increases as it travels towards the top of the beam as shown in Nos. S.A. 3, 5, and 6. For higher bending moments, the prestress in the bottom begins to be relieved and the crack inclination at this point begins to increase. The compressive stresses, due to bending moment, in the top of the beam now become more predominant and the crack angle begins to

decrease at this point. This variation through the depth of the beam is, however, small and in many cases it can be considered almost constant. Even in the cases of S.A.3, 5, and 6, where the inclination at the soffit of the beam is small, the crack travels only a relatively small distance before its inclination becomes almost constant. In the case of S.A.10 the resultant compressive stresses due to bending moment and prestress are equal in both the top and bottom of the beam. The beam can therefore be considered to be uniformly prestressed and the crack angle is, as expected, nearly constant.

3.5.3. Beams Failing in Mode 1

The failure mechanism of these beams was one of rotation about a compression hinge in the top face of the beam. In all cases failure was of a violent nature due to the sudden release of the high stresses imposed by the bending moment and prestress. As a result the specimen was often badly damaged making it difficult to locate the true failure cracks.

The cracks on the bottom of the beam can be seen to be almost at right angles to the longitudinal axis. This phenomenon is due to the sequence of loading, as at this stage only the bending moment is being applied. The cracks on the side faces are vertical to begin with which is again due to the application of the bending moment. However, the addition of a twisting moment and the increase in compressive stresses due to bending moment as the crack travels towards the top of the beam causes it to deviate from its vertical path. This angle, although difficult to determine after failure has occurred, is thought to increase as the bending moment increases, and becomes 90° for the case of pure bending.

In Nos. S. A. 18 and 19 the crack travels vertically up the side of the beam before meeting the wedge shape compression zone of failure in the top of the beam. The inclination of the compression hinge on the top face is also shown to increase for an increase in the bending moment. This is again due to the increase in compressive stresses at this point, and in many cases the angle is 90° which is the case for pure bending.

3.6. Maximum Principal Strains

The maximum principal strains occurring in the concrete were recorded by 60° strain gauge rosettes located at various points on the beams. The position of the gauges, which were dependent upon the expected mode of failure of the beams, are shown in Fig. 3.9 to 3.11.

Fig. 3.12 shows the maximum principal tensile strain, recorded in the top of those beams failing in Mode 3, plotted against the applied torsional moment. In general the graphs are straight lines indicating elastic conditions to failure.

The maximum tensile strains recorded on the longer side of those beams failing in Mode 2 are shown in Fig. 3.13. The initial tensile strain recorded under zero torsion moment is due to the effects of the prestress.

With reference to Figs. 3.12 and 3.13, if it is considered that failure occurs when the curve either finishes or becomes non-linear then the strain in the concrete at this load can be determined. Knowing the E value of the concrete and assuming a linear stress-strain relationship the maximum principal tensile stress at this point can be found. This is shown in Table 3.3 and compared with the modulus of rupture values for the respective beams. As can be seen, in the majority of cases, the maximum recorded stress is approximately equal to twice that of the modulus

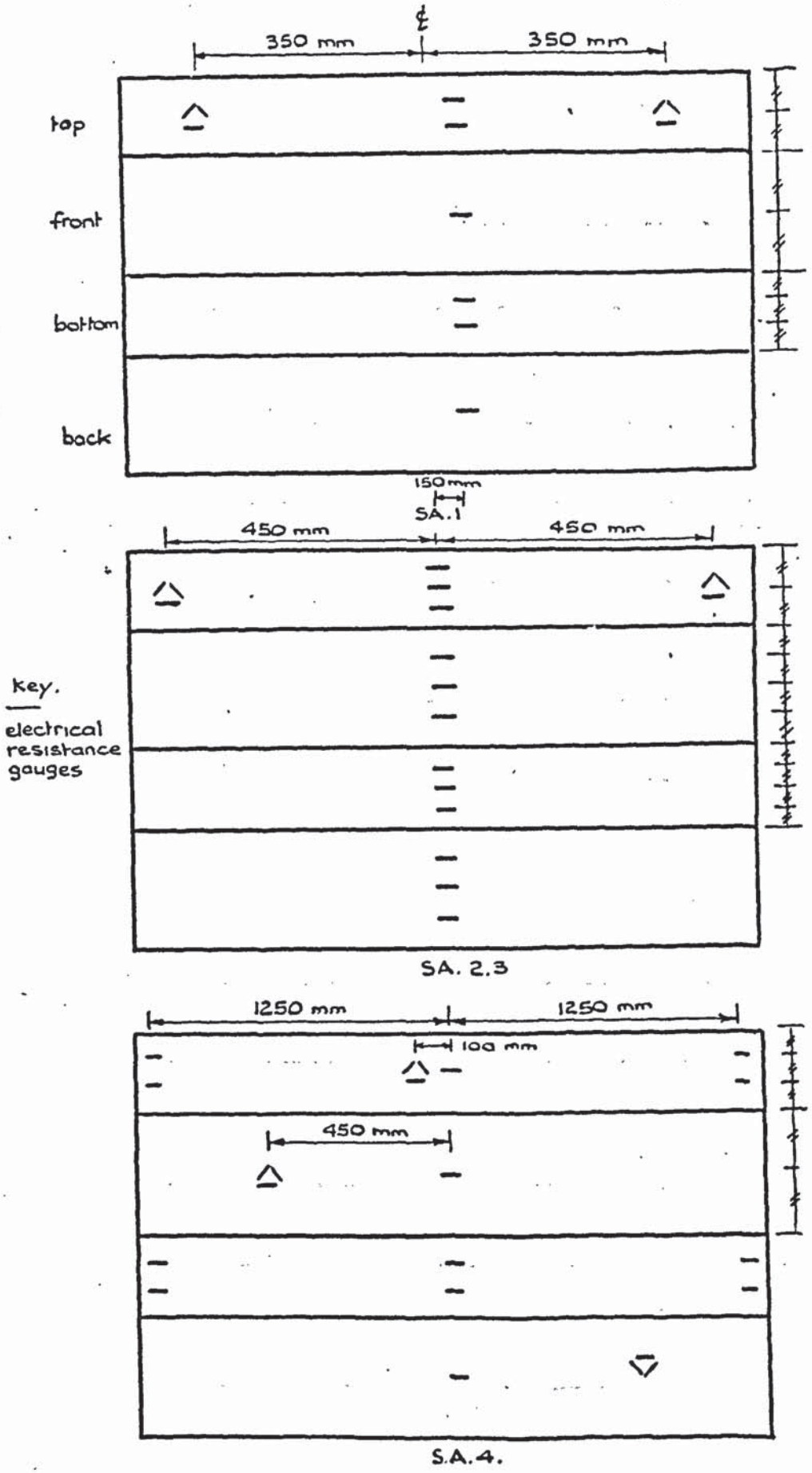

Fig. 3.9. Gauge locations

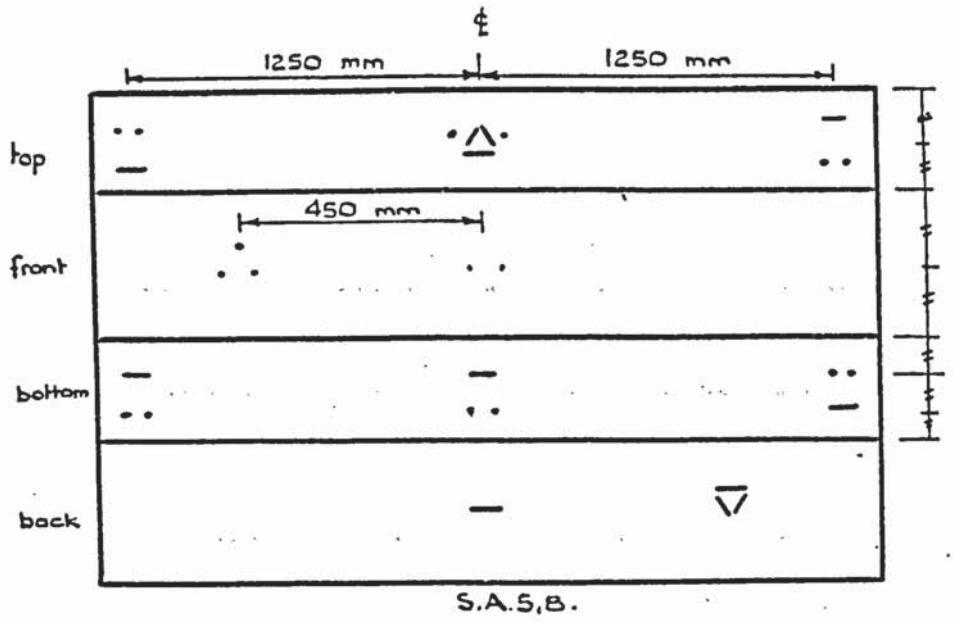

S.A.5,8.

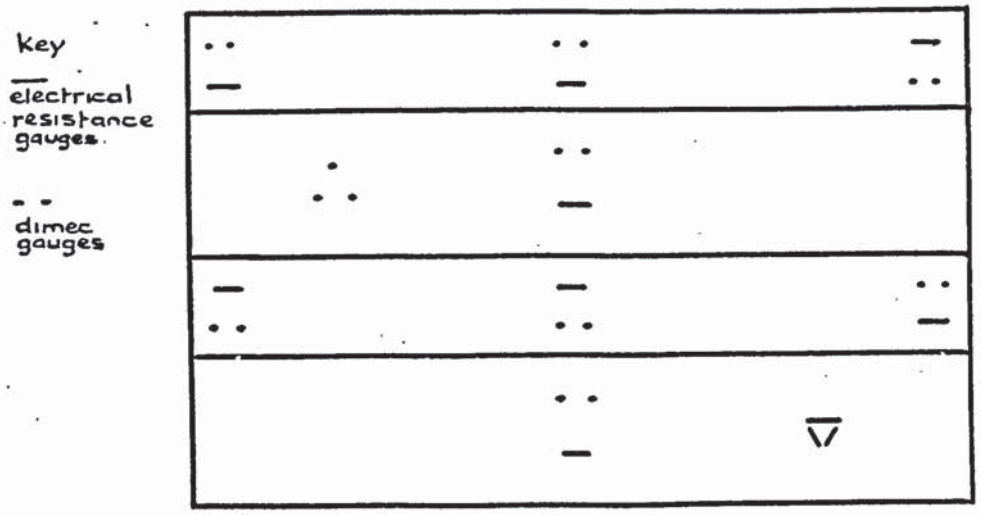

S.A. 6, 7.

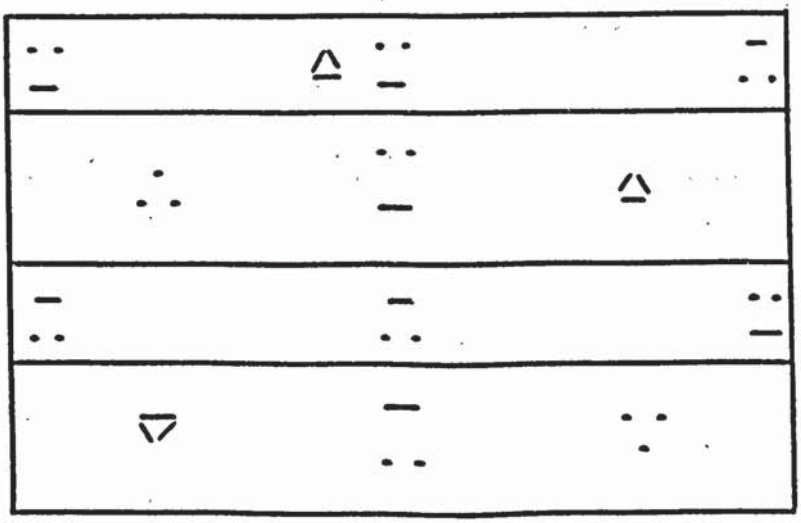

S.A. 9, 10, 11, 13

Fig. 3.10 Gauge locations

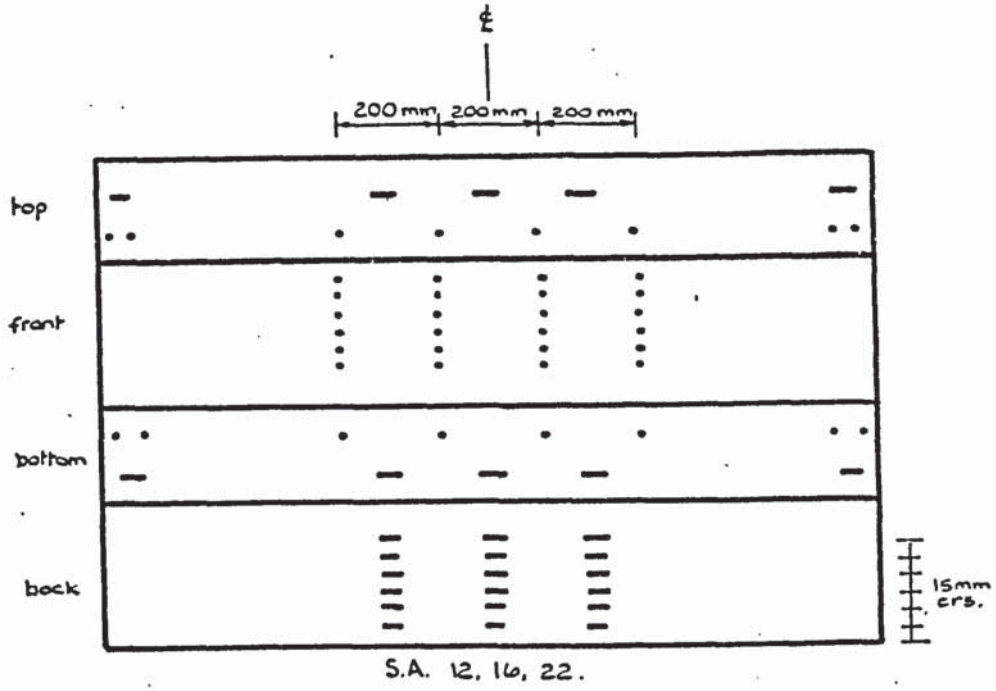

S.A. 12, 16, 22.

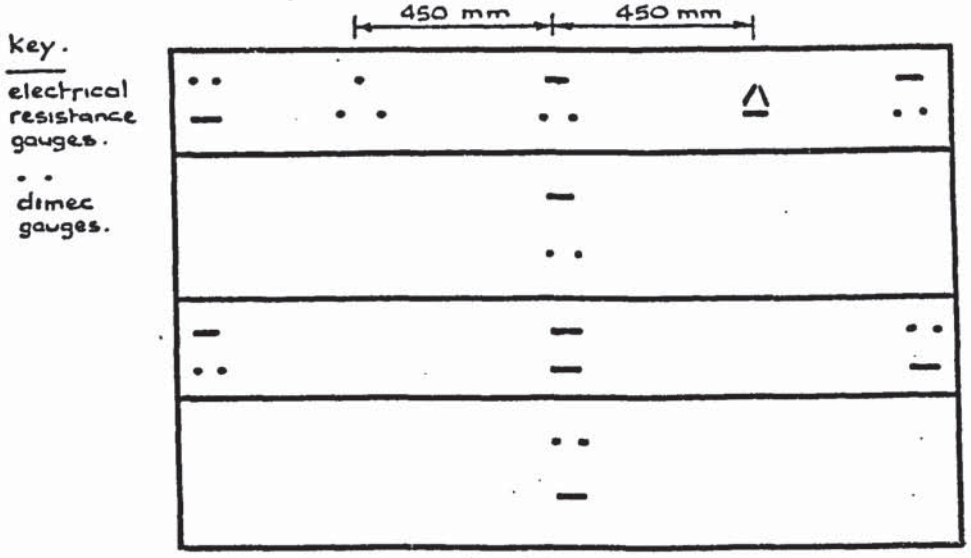

S.A. 14, 17, 18

Fig. 3.11. Gauge locations

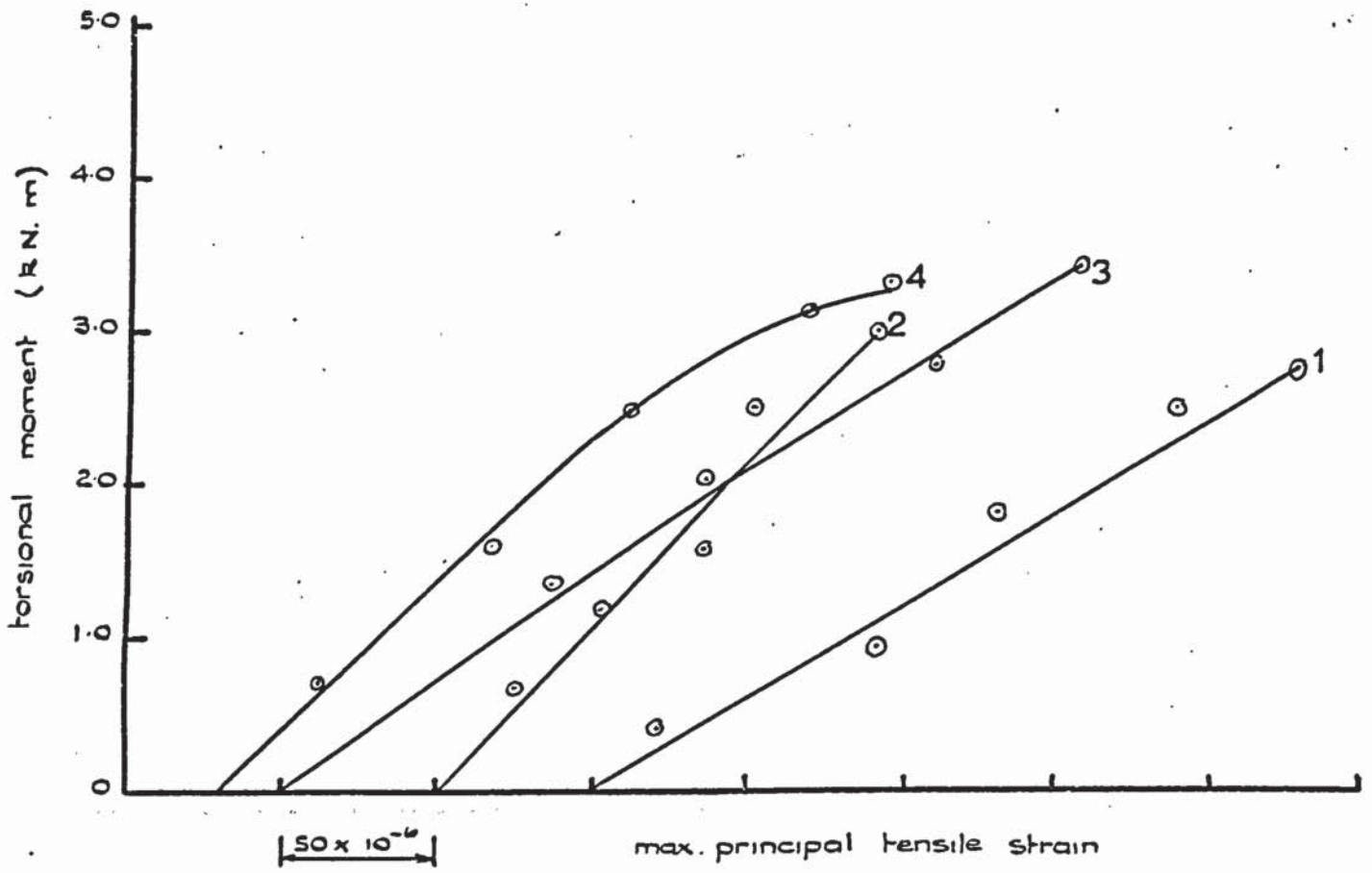

Fig. 3.12 Relationship between torsional moment and principal tensile strain in top of beam. Mode 3.

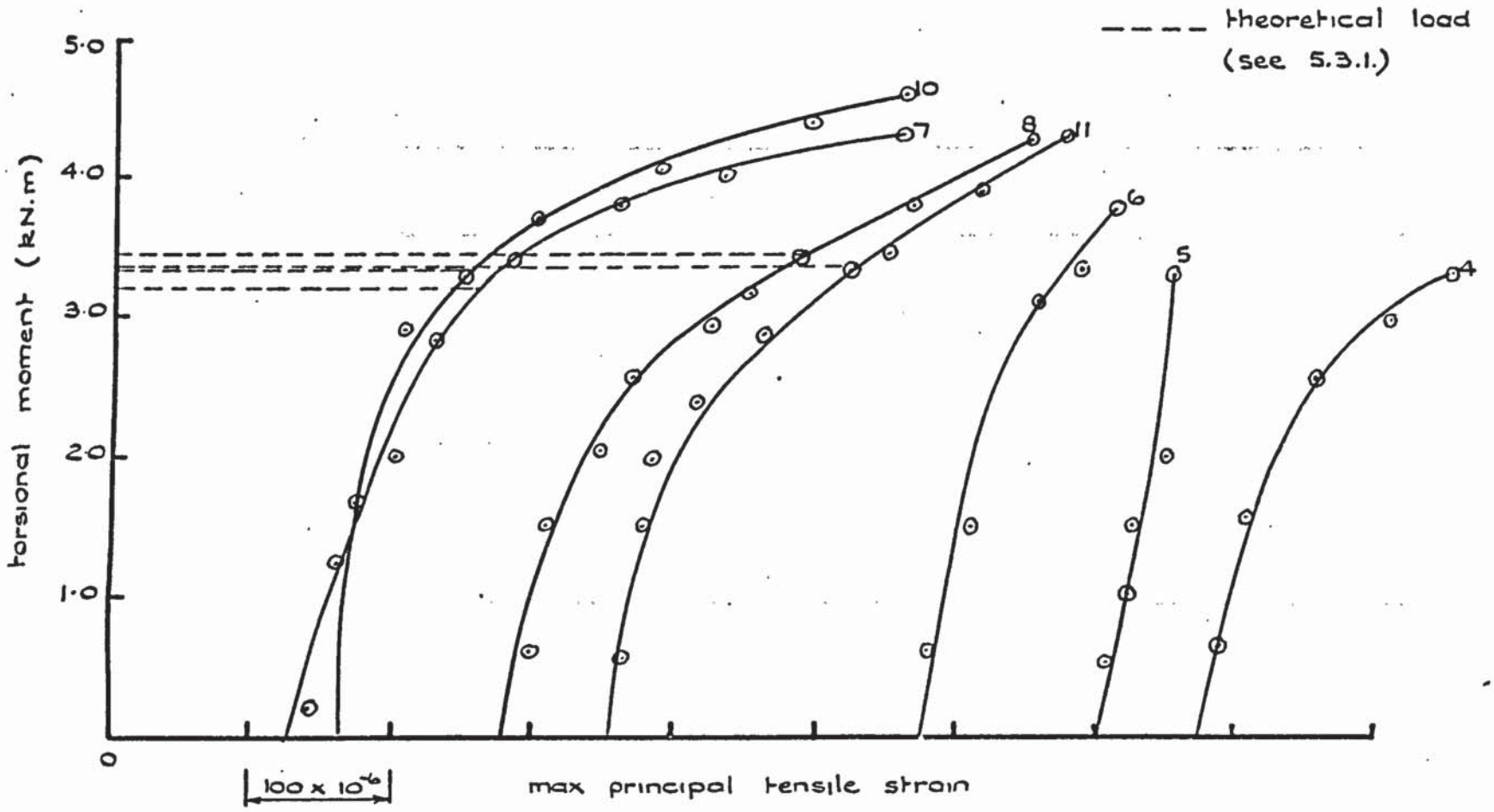

Fig. 3.13 Relationship between torsional moment and principal tensile strain in side of beam. Mode 2.

Beam No.	Max recorded tens.stress at assumed failure N/mm^2 (lbs/in^2)	Modulus of rupture N/mm^2 (lbs/in^2)
1	6.49 (941)	3.04 (441)
2	5.33 (773)	2.61 (378)
3	6.66 (965)	3.10 (449)
4	7.68 (1113)	3.50 (508)
5	7.62 (1105)	3.32 (482)
6	8.03 (1164)	3.90 (566)
7	7.55 (1095)	3.59 (520)
8	5.20 (754)	3.58 (519)
10	4.44 (644)	3.92 (568)
11	3.93 (570)	3.57 (517)

TABLE 3.3. Comparison of maximum recorded tensile stress with modulus of rupture value for beams failing in Modes 2 and 3.

of rupture value. This is possibly due to the fact that all the strains were recorded at the centre of either the shorter or longer sides. According to the classical elastic theory of torsion as proposed by St. Venant,(33) the shear stresses are zero at the corners of the rectangle, and a maximum at the centre of the longer side. It is possible that before failure occurs the mean stress across the face of the rectangle must be approximately equal to the modulus of rupture value of the concrete. The additional load required to produce this state of stress could probably account for the high strains recorded at the centre of the sides.

The fact that in some cases strains have been recorded after the slope of the curve becomes non-linear is probably due to the appearance of microcracks beneath the gauges.

The author would like to point out, however, that in his opinion, the readings taken in tension using the electrical resistance gauges tend to be very suspect. In many cases readings were recorded on the top face of the beam during stressing which indicated that the tensile strength of the concrete had been exceeded. A close examination of the surface of the concrete revealed no signs of cracking. Such results may be due to the presence of small shrinkage cracks which may open slightly on the application of a load. Although not detectable to the eye these cracks may be large enough to effect the readings on the strain gauges.

The maximum principal compressive strains recorded in the top of those beams failing in Mode 1 are shown in Fig. 3.14. The graphs show linearity until the cracking bending moment is reached. The maximum strain recorded was 3650 microstrains in beam No. S.A.22. Although this was not the beam in which the maximum bending moment was attained, the high strain recorded was probably due to the fact that the strain

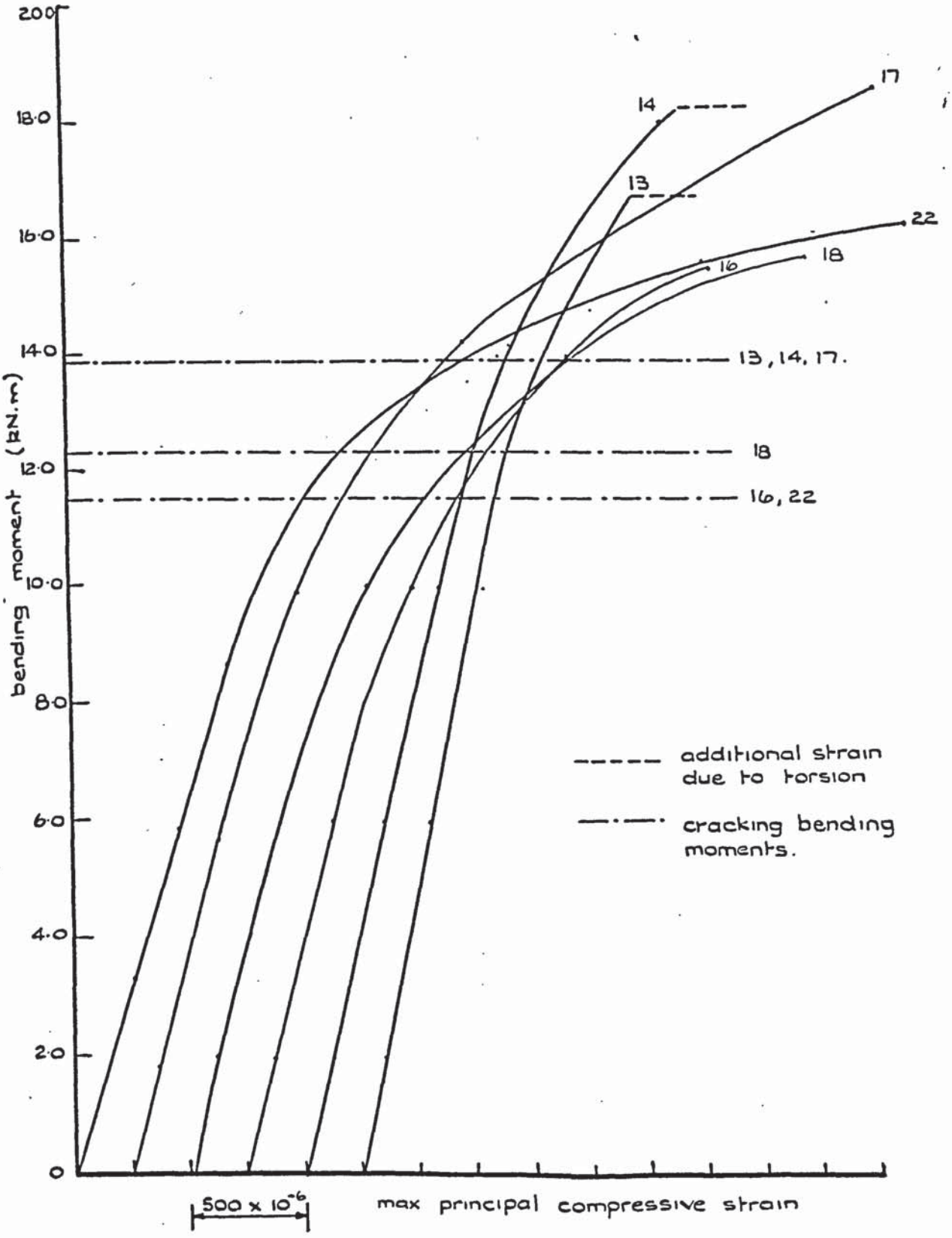

Fig 3.14. Relationship between bending moment and principal compressive strain in top of beam Mode 1.

gauges were located directly over the compression zone of failure. In those beams where this did not occur the strain recorded may be considerably less than that in the actual failure zone.

3.7. Angle of Rotation

Fig. 3.15 shows the angle of twist plotted against the torsional moment for all beams tested under combined bending and torsion. The results of S.A.1 have been omitted due to the fact that original apparatus used to measure the rotation was too flexible yielding unsatisfactory results.

As can be seen the angle of rotation of all beams failing in Modes 2 and 3 is very similar, the lines remaining straight until just before failure. Cracking does not occur in these beams until the ultimate load is reached. It can therefore be deduced from these results that the torsional stiffness of the beam before cracking is not influenced by the presence of flexure. The stiffness is considerably reduced in those beams in which cracking due to flexure occurs before failure.

3.8. Central Deflection

The variation of central deflection with bending moment for all beams is shown in Fig. 3.16. Readings were taken at 3 points on the soffit of the beam as described in 2.10.3. The difference in readings between the central gauge and the average of the 2 outer gauges gives a value of the central deflection relative to the movement of the 2 outer gauges. Using this method it was hoped to eliminate any errors introduced by an overall movement in the beams vertical position. Resultant readings showed, however, that no such movement occurred, and the central deflections plotted are those actually recorded by the central gauge.

Results show that the central deflection increases with the bending moment, the curve becoming non-linear at the point at which

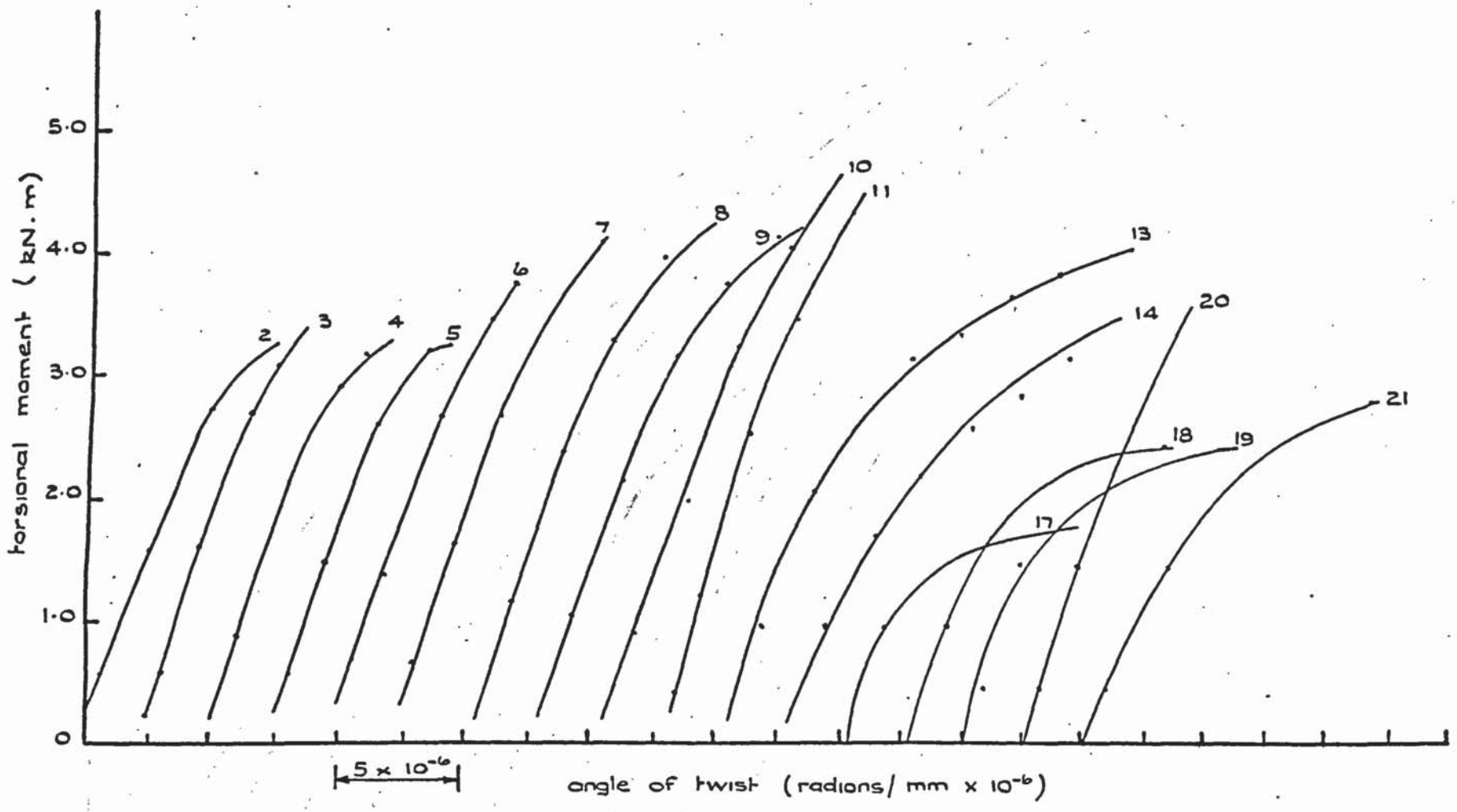

Fig. 3.15. Relationship between torsional moment and angle of twist.

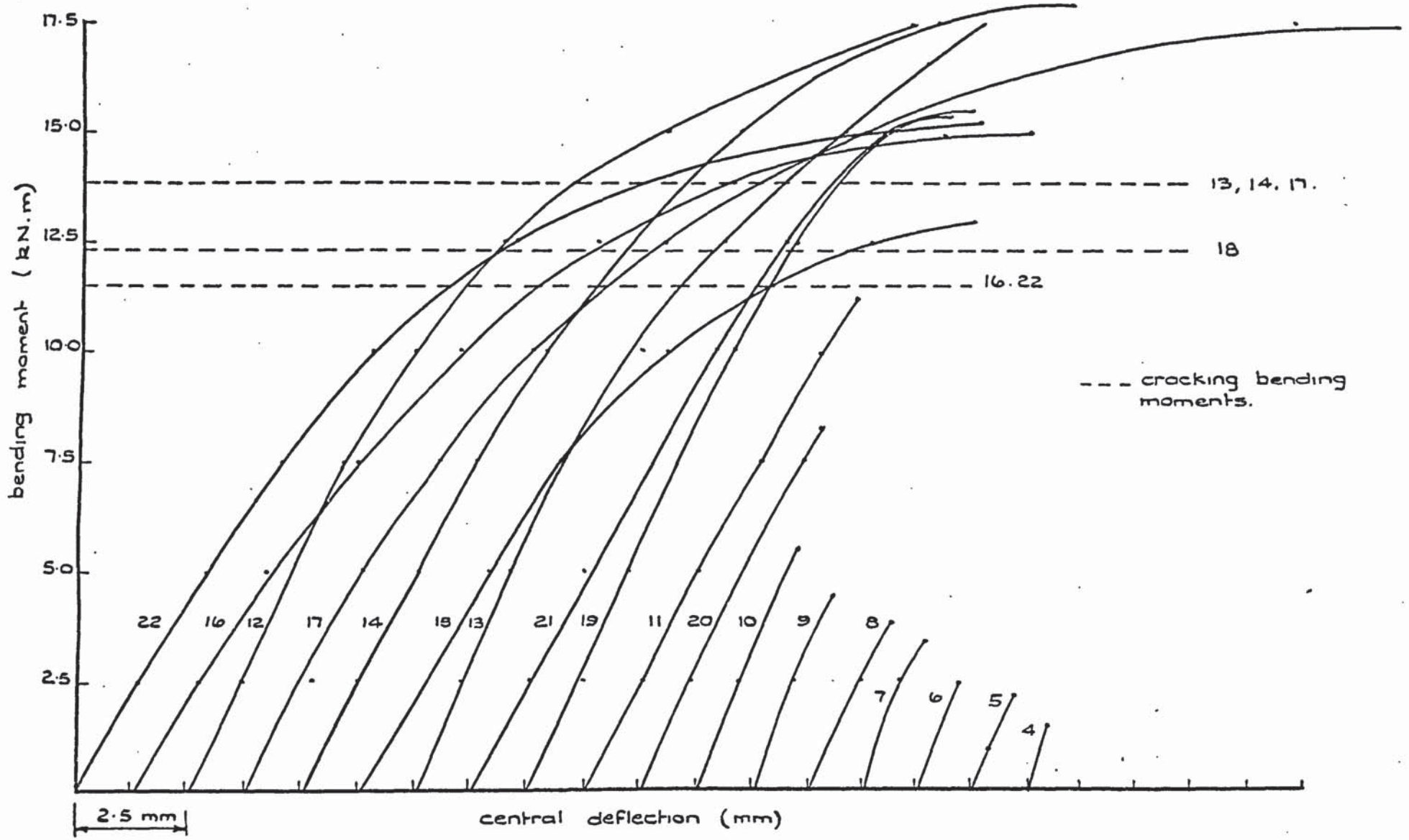

Fig. 3.16. Variation of central deflection with applied bending moment

cracking occurs in the bottom of the beam.

3.9. Steel Strains

The percentage reinforcement in all beams tested in this series was 2.2%. This resulted in an over-reinforced section, and consequently the steel did not approach yield during any of the tests.

An analysis of the longitudinal strains recorded in the steel is given in Table 3.4. It shows that the strain increase is greater under the application of a high bending moment.

Fig. 3.17 represents the increase in longitudinal steel strain plotted against the applied bending moment for beams tested under bending moment only. The slope of these curves can be seen to change at a point approximately equal to that at which the first crack appears. At this point there is a redistribution of stresses causing a sudden increase in the steel strains.

3.10. Relationship Between Strain in Concrete and Steel at the Same Level

The variation in strains in the steel and the concrete with change in bending moment for beam S.A.16 tested under pure bending is shown in Fig. 3.18. The distribution of the concrete strains through the depth of the beam can be seen to be linear up to failure. It is clear, however, that the increase in strain due to bending in the steel and the concrete at the same level is not the same. The increase in steel strain is considerably smaller than that in the concrete due to the fact that the steel is unbonded. The ratio between the two strain increases is shown also in Fig. 3.18 and can be seen to reduce as the applied bending moment increases. These factors and the factors taken from the other pure bending tests have been plotted against M/Mult in Fig. 4.2.7. The results have been used to determine a value of the Bond Slip Factor referred to in 4.2.3.

Beam No.	M/T	Strain Readings (microstrains)	
		Initial	Final
1	0.05	2362	2367
2	0.27	2413	2433
3	0.36	1962	1973
4	0.56	1674	1696
5	0.71	Gauges damaged	
6	0.75	1651	1679
7	0.74	1797	1858
8	0.87	Gauges attached with Budd Cement	
9	1.18		
10	1.58	1896	2007
11	3.02	1886	2082
12	∞	Rig Collapse	
13	3.97	1975	2528
14	5.01	1956	2605
15		Rig Collapse	
16	∞	1944	2768
17	10.31	1964	3008
18	6.37	1893	2595
19	6.92	1914	No Readings Taken
20	2.75	1962	
21	5.06	1959	
22	∞	1889	2563

TABLE 3.4. Analysis of Steel Strains

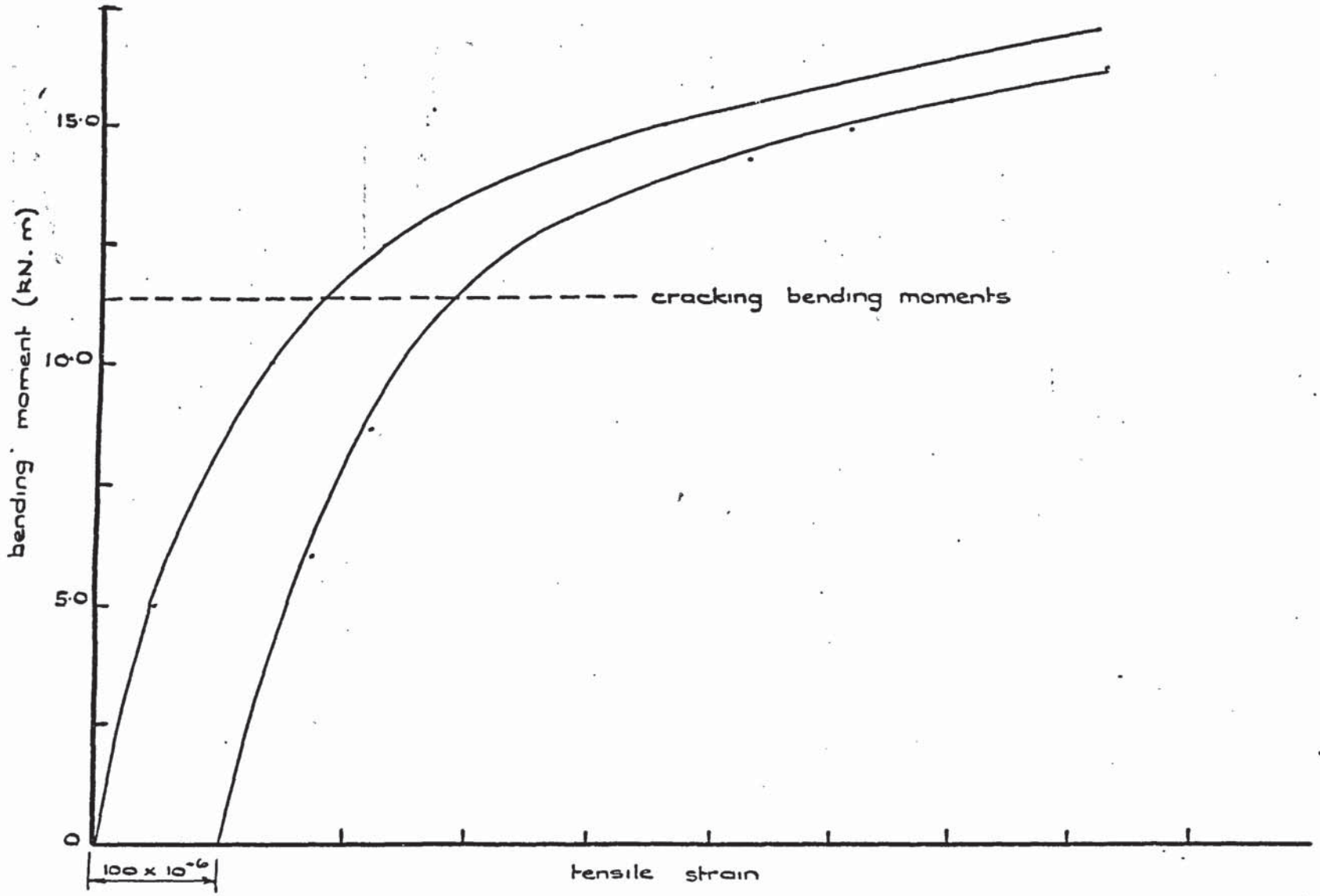

Fig. 3.17. Increase in steel strain under applied bending moment

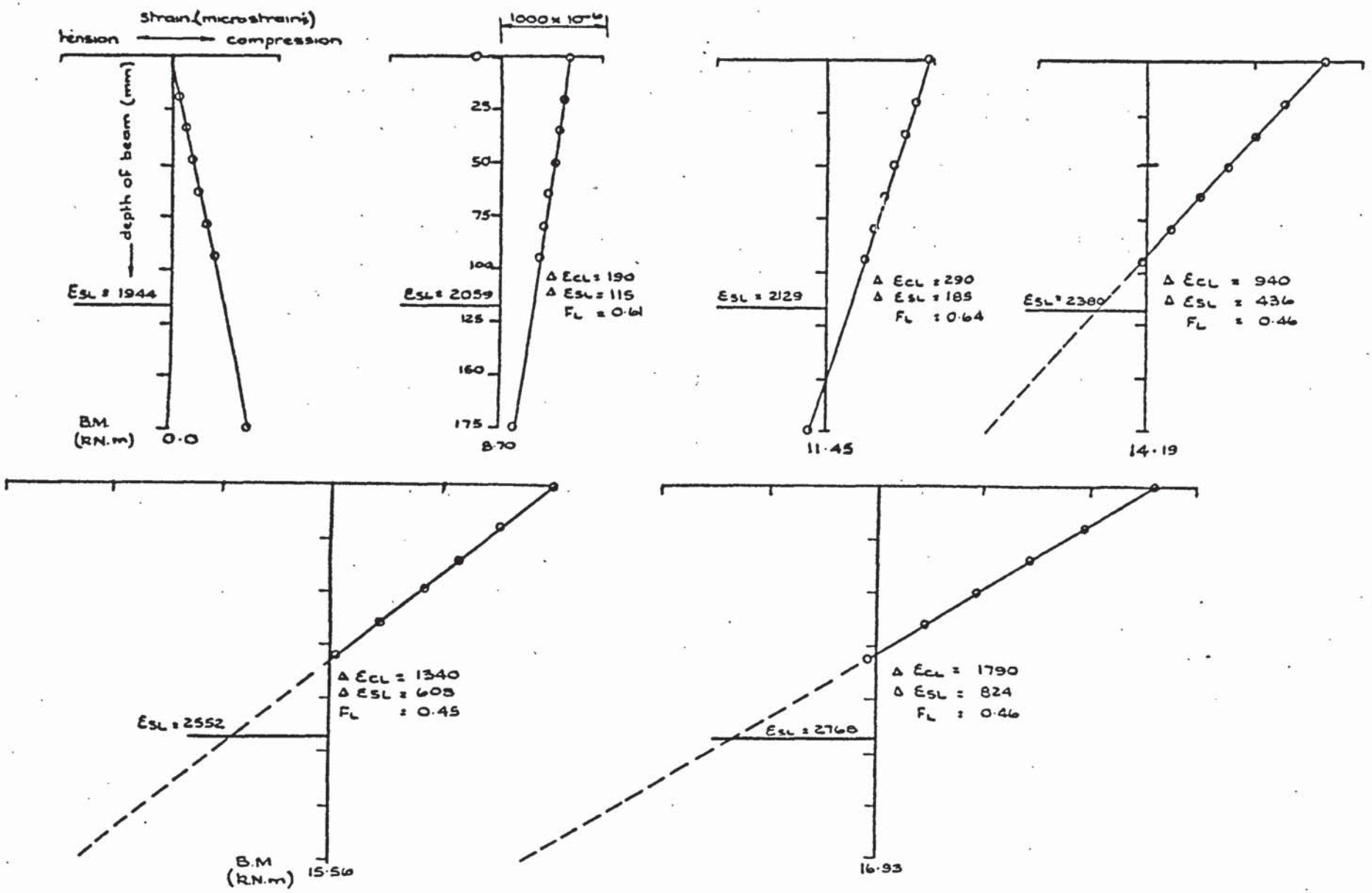

Fig. 3.18. Relationship between increase in steel and concrete strains at the same level -beam No. S.A.16

Chapter 4

Theoretical Analysis

4.1. Introduction

For a prestressed rectangular beam loaded under combined bending and torsion its ultimate load is assumed to correspond to 1 of 3 modes of failure. In all cases the opening of inclined tension cracks permits rotation of the member about an axis in the compression zone, generally referred to as the "compression hinge". The location of this hinge is determined by the ratio of the forces acting on the section, the shape of the cross-section, and the nature of the prestressing force (i.e. eccentric or concentric). If the hinge forms on the top face of the beam then, using the notation adopted by Lessig [34] it is referred to as a Mode 1 failure. This occurs when the M/T ratio is high, the compressive stresses in the top of the beam due to bending being predominant. For lower M/T ratios the hinge forms on one side of the beam and is known as a Mode 2 failure. In some instances, when the M/T ratio is low, the hinge forms in the bottom of the beam and it is then known as a Mode 3 failure. In general, however, this will only take place when the prestress in the top of the beam is low, which is the case in a eccentrically prestressed beam.

For all modes, the failure mechanism is considered to be one of a bending action about the inclined "compression hinge" or skew-axis. This skew bending approach was originally suggested by Lessig [34] for reinforced members and more recently by Hsu [20, 21] for plain, and prestressed concrete.

4.2. Mode 1

The high bending moments present when this type of failure occurs are responsbile for the beam showing extensive cracking

before failure. The theoretical solution proposed here is based, therefore, upon the equilibrium of a cracked section.

The method of approach is dependent upon the presence of dowel forces in the prestressing steel which effect the distribution of the shear stresses in the compressed concrete. For those beams in which the steel is left unbonded in a void, somewhat larger in diameter than the bar, the dowel action will not take place. If, on the other hand, the bar is bonded, or as in the case of the author's beams, the bar is unbonded but cast in place, then dowel forces will be set up in the steel. In practise the majority of prestressed beams contain bonded bars and they will therefore have dowel forces set up within them. The format of the theoretical solution for those beams containing a dowel force is also dependent upon the position of the steel within the section.

4.2.1. Failure Theories For Beams Containing a Dowel Force

For simplicity, those beams which contain more than 1 layer of steel in the tension zone at failure have been treated seperately from the remainder. The more complex solution for a beam with 2 layers of steel in the tension zone is developed fully. The solution involves the formation of a general failure theory, which in turn necessitates an additional calculation to determine dn, the depth of the compressed concrete. The overall analysis is considerably simplified for those beams containing only 1 layer of tensile reinforcement.

4.2.1.1. General Theory of Failure For Beams Containing 2 Layers of Tensile Reinforcement

The ultimate carrying capacity of the beam is assumed to be reached when failure of the concrete, in the compression zone, has taken place. The concrete is subjected to direct stresses due to bending, and shear stresses due to the torsional moment. Failure

under these conditions of combined stresses is assumed to be governed by the Cowan[25] criteria of failure referred to in 1.2.3. This is conveniently expressed in terms of the direct stresses and shear stresses acting in directions parallel and normal to the axis of the beam respectively. The distribution of the direct stresses is taken as a parabola with maximum ordinate at the top fibre of the beam as shown in Fig. 4.2.1. The distribution of the shear stresses in the compressed concrete is also taken as a parabola as shown in Fig. 4.2.1. The dowel forces in the steel produce this type of shear stress distribution which is comparable to that occuring in a member under simple flexure.

With reference to Fig. 4.2.1 concerning the dowel forces.

The value of the force in each layer of steel is assumed to be proportional to its distance from the centre of rotation of the beam. This distance, or lever arm, is taken as the same as that produced under conditions of pure bending moment. Although this is not strictly correct the error introduced is assumed to be small.

Taking moments about an axis through the centroid of the compressed concrete, and parallel to the length of the member.

$$T = F_u L_u + F_l L_l \qquad \text{-------- 4.2.1.1.}$$

But $F \propto L$

$$\therefore \quad F_u = \frac{L_u}{L_l} F_l \qquad \text{-------- 4.2.1.2.}$$

NOTE The suffix (1) referring to Mode 1 has, for ease of typing, been omitted from all terms in this section.

Substituting for F_u in 4.2.1.1.

$$T = \frac{L_u}{L_l} F_l L_u + F_l L_l$$

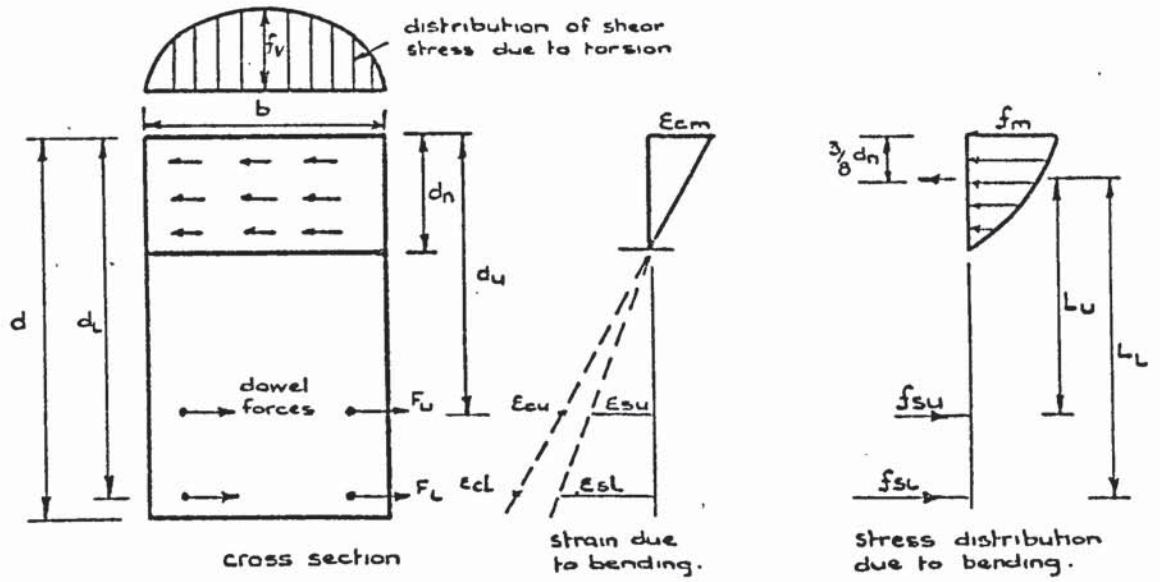

Fig. 4.2.1. Stress and strain distribution due to loading on a plane normal to the axis of the beam - Mode 1- dowel force

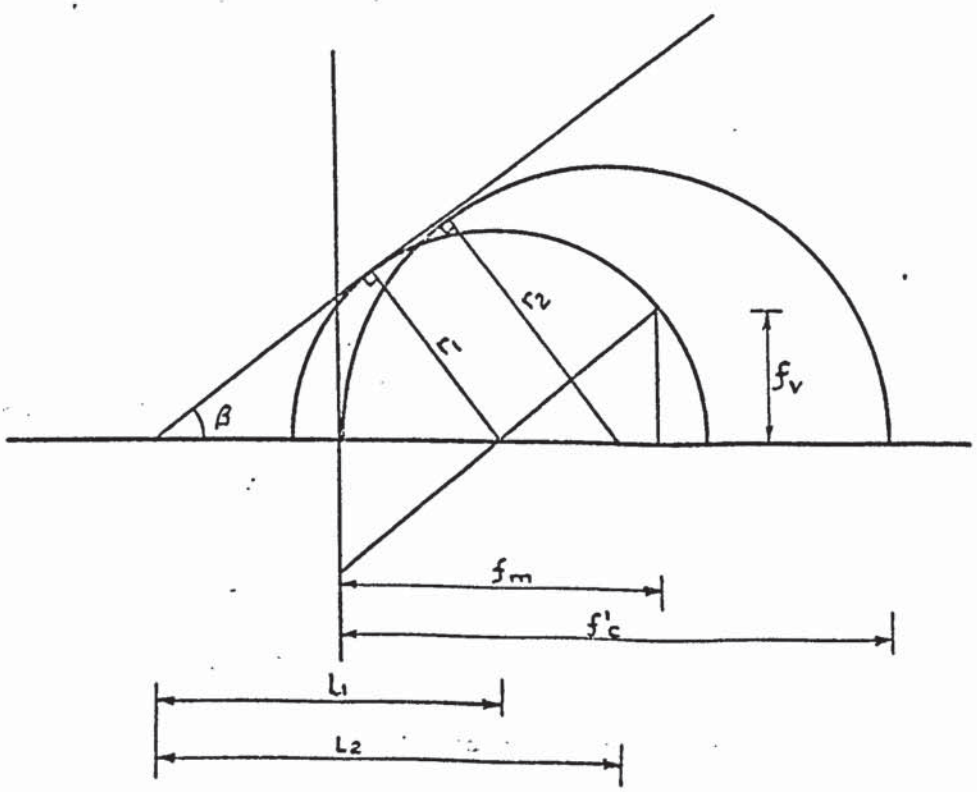

Fig. 4.2.2. Failure criteria for concrete, envelope tangent to the stress circle for uniaxial compression.

$$\therefore \quad F_1 = \frac{T}{L_1 + L_u^2/L_1} \qquad \text{------ 4.2.1.3.}$$

and $$F_u = L_u \frac{T}{L_1 (L_1 + L_u^2/L_1)} \qquad \text{------ 4.2.1.4.}$$

$$F_1 + F_u = \frac{T(L_1 + L_u)}{(L_1^2 + L_u^2)} \qquad \text{------ 4.2.1.5.}$$

The theory proposed by Cowan is shown in 2 dimensional form in Fig. 4.2.2.

With reference to Fig. 4.2.2.

By similar Δ's

$$\frac{r_1}{l_1} = \frac{r_2}{l_2} \qquad \text{------ 4.2.1.6.}$$

also

$$r_1 = \sqrt{\left(\frac{f_m}{2}\right)^2 + f_v^2}$$

and $$r_2 = \frac{f'_c}{2}$$

$$l_2 - l_1 = \frac{f'_c}{2} - \frac{f_m}{2}$$

$$\therefore \quad l_2 = l_1 + \frac{f'_c}{2} - \frac{f_m}{2}$$

substituting for r_1, r_2, and l_2 in 4.2.1.6.

and rearranging

$$l_1 = \frac{\left(\sqrt{\left(f_m/2\right)^2 + f_v^2}\right)\left(f'_c/2 - f_m/2\right)}{\left(f'_c/2 - \sqrt{\left(f_m/2\right)^2 + f_v^2}\right)} \qquad \text{------ 4.2.1.7.}$$

$$\sin \beta = \frac{r_1}{l_1}$$

substituting for r_1 and l_1 and rearranging

$$\frac{f_v}{f_c'} = \frac{\left(\frac{1 - \sin\beta}{2}\right)}{\sqrt{\left(\frac{f_m}{2f_v}\right)^2 + 1 - \frac{f_m}{2f_v}\sin\beta}} \qquad \text{------ 4.2.1.8.}$$

Taking moments of the forces about an axis through the centroid of the lower steel and perpendicular to the length of the member (See Fig. 4.2.1.)

$$M + P_{tu}\,(d_1 - d_u) + A_{su}\,f_{su}\,(d_1 - d_u) = k_m\,b\,d_n\,L_1\,f_m \qquad \text{------4.2.1.9.}$$

The strain distribution in the concrete due to bending is assumed linear across the depth of the section. If the steel is unbonded then the strain in the steel will be less than the strain in the adjacent concrete. This phenomenon will be discussed in greater detail in 4.2.3. The steel strains will therefore be reduced by a factor, the value of which will depend on whether the steel is in the tension or compression zone.

The assumption concerning the strain distribution is not consistent with that made in 4.2.1.2.regarding the distribution on the skew axis. To obtain a more rigorous solution a linear strain distribution on the skew axis should be considered (as in 4.2.1.2) and the strains then resolved on to the perpendicular axis. The term involving f_{su} does, however, tend to be small and may be ignored in many cases without involving a great amount of inaccuracy. The author feels, therefore, that the complexity of the solution involved, when considering the linear relationship on the skew axis, is not warranted in this case. A linear stress-strain relationship in the steel and the concrete has also been assumed in order to simplify the approach. A non-linear relationship has been considered in the relat-

ively simpler cases where there is only 1 layer of steel in the tension zone. The resulting solutions have proved to yield very similar results to these involving a linear relationship.

From Fig. 4.2.1, therefore, we have

$$\varepsilon_{sl} = D_l \varepsilon_{cl} \text{ and } \varepsilon_{su} = D_u \varepsilon_{cu} \qquad \text{------ 4.2.1.10.}$$

also assuming a linear stress-strain relationship

$$\varepsilon_{sl} = \frac{f_{sl}}{E_{sl}}, \quad \varepsilon_{su} = \frac{f_{su}}{E_{su}} \text{ and } \varepsilon_{cm} = \frac{f_m}{E_c}$$

from the geometry of the figure

$$\frac{\varepsilon_{cm}}{d_n} = \frac{\varepsilon_{cu}}{(d_u - d_n)}$$

Substituting for ε_{cu}, ε_{su}, and ε_{cm} and rearranging

$$\therefore \quad f_{su} = \frac{D_u f_m (d_u - d_n) m_u}{d_n} \qquad \text{------ 4.2.1.11.}$$

Substituting for f_{su} in 4.2.1.9 and rearranging

$$f_m = \frac{M + P_{tu}(d_l - d_u)}{k_m b d_n L_l - \dfrac{D_u A_{su} m_u (d_u - d_n)(d_l - d_u)}{d_n}} \qquad \text{------ 4.2.1.12.}$$

Taking moments of forces about an axis through the centroid of the lower steel and parallel to the length of the member (see Fig.4.2.1.)

$$T = k_t b d_n L_l f_v - F_u (L_l - L_u)$$

substituting for F_u from 4.2.1.4 and rearranging

$$f_v = \frac{T(1 + B)}{k_t b d_n L_l} \qquad \text{------ 4.2.1.13.}$$

where

$$B = \frac{L_u (L_l - L_u)}{(L_l^2 + L_u^2)}$$

Substituting for f_v from 4.2.1.13 into the L.H.S. of 4.2.1.8 and

rearranging

$$T = \frac{k_t\, b\, d_n\, L_1\, f_c' \left(\frac{1 - \sin\beta}{2}\right)}{(1+B)\left(\sqrt{\left(\frac{f_m}{2f_v}\right)^2 + 1} - \frac{f_m \sin\beta}{2f_v}\right)} \quad \text{------ 4.2.1.14}$$

The value of f_m, and f_v in 4.2.1.14 can be calculated from 4.2.1.12 and 4.2.1.13.

Inorder to determine the torsional capacity, therefore, it is necessary to know both the applied torsion moment and bending moment. This, however, is not uncommon in practice when all the working loads are known and the size of the section is required.

The value of β recommended by Cowan is 37° and substituting this into 4.2.1.14

$$T = \frac{k_t b\, d_n\, L_1}{(1+B)} f_c' \left\{\frac{0.2}{\sqrt{\left(\frac{f_m}{2f_v}\right)^2 + 1 - 0.3\left(\frac{f_m}{f_v}\right)}}\right\} \quad \text{------ 4.2.1.15.}$$

The value of d_n required to solve 4.2.1.15 is calculated using the method described in 4.2.1.2.

4.2.1.2. The Solution for d_n for Beams Containing 2 Layers of Tension Reinforcement

The solution proposed is based upon the equilibrium of a cracked section about a skew axis. The strain distribution in the concrete due to loading, across the depth of the skew failure plane, is taken as linear as mentioned in 4.2.1.1.

The strain, normal to the skew plane in the concrete adjacent to the steel, consists of a normal strain due to bending combined with a shear strain due to the dowel force. It is necessary to find the

resultant strain acting normal to some plane inclined at θ degrees to the vertical. The angle θ corresponds to the inclination of the skew axis (or compression hinge) formed in the top of the beam at failure.

If we consider a small element of the concrete adjacent to the steel, see Fig. 4.2.3, we have a direct strain ε_x due to bending, plus a shear strain γ due to the dowel force. Using Mohr's[35] strain circle (see also Fig. 4.2.3) it can be shown that the normal strain ε_i on a plane inclined at θ° is given by

$$\varepsilon_i = \tfrac{1}{2}(\varepsilon_x + \varepsilon_y) + \tfrac{1}{2}(\varepsilon_x - \varepsilon_y)\cos 2\theta + \frac{\gamma}{2}\sin 2\theta$$

But in this case $\varepsilon_y = 0$

$$\therefore \varepsilon_i = \tfrac{1}{2}\varepsilon_x(1 + \cos 2\theta) + \frac{\gamma \sin 2\theta}{2}$$

$$\varepsilon_i = \varepsilon_x \cos^2\theta + \gamma \sin\theta \cos\theta \qquad \text{------ 4.2.1.16.}$$

For the concrete adjacent to the lower steel ε_{cl} is represented by ε_x in equation 4.2.1.16. Also the shear strain in the concrete is equal to the shear strain in the adjacent steel, as it is assumed that no slip occurs between them in this direction.

Now γ = shear strain = $\dfrac{\text{shear stress}}{G}$

$$\text{Shear stress} = \frac{\text{shear force}}{\text{cross sectional area}}$$

The shear force corresponds to the dowel force in the steel

$$\therefore \gamma = \frac{F_1}{A_{sl} G_1}$$

$\therefore$ from 4.2.1.16

$$\varepsilon_{icl} = \varepsilon_{cl}\cos^2\theta + \frac{F_1}{A_{sl} G_1}\sin\theta\cos\theta \qquad \text{------ 4.2.1.17.}$$

Also from the geometry of Fig. 4.2.4

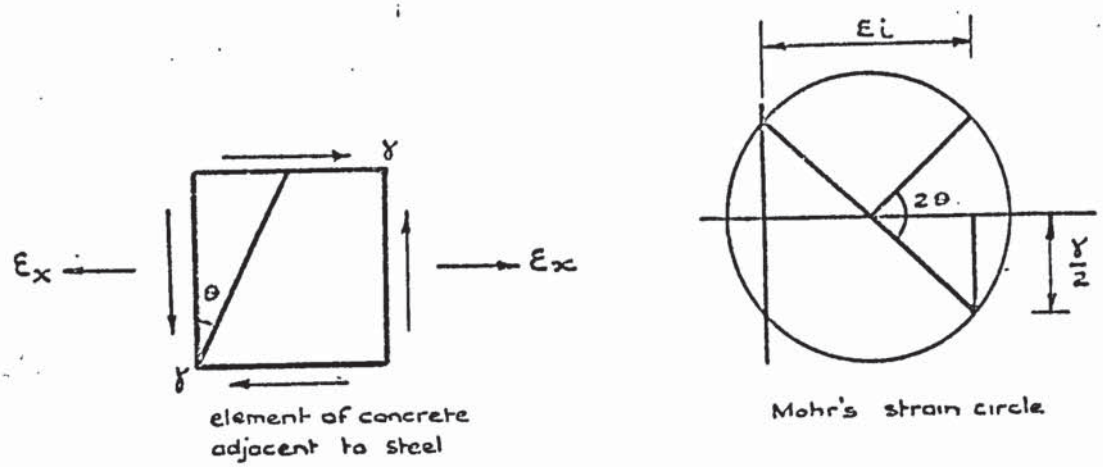

Fig 4.2.3. Analysis of strains in concrete adjacent to steel.

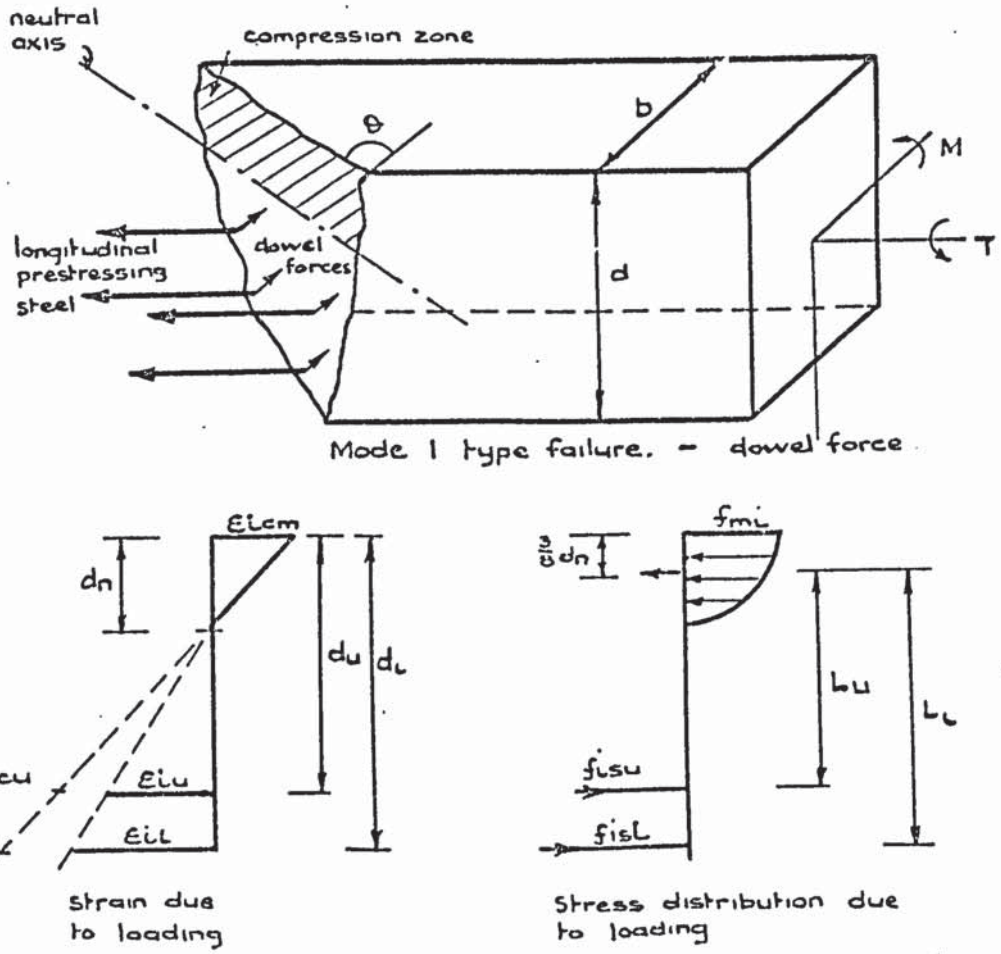

Fig. 4.2.4. Stress and strain distribution due to loading on a plane normal to the skew axis. Mode 1 - dowel force.

$$\frac{\varepsilon_{icm}}{d_n} = \frac{\varepsilon_{icl}}{(d_1 - d_n)}$$

Substituting for ε_{icl} into 4.2.1.17

$$\therefore \quad \frac{\varepsilon_{icm}\,(d_1 - d_n)}{d_n} = \varepsilon_{cl} \cos^2\theta + \frac{F_1}{A_{sl}G_1} \sin\theta \cos\theta \qquad \text{------ 4.2.1.18.}$$

Now from 4.2.1.10

$$\varepsilon_{cl} = \frac{\dot{\varepsilon}_{sl}}{D_1}$$

and assuming a linear stress-strain relationship in both the steel and the concrete

$$\varepsilon_{icm} = \frac{f_{mi}}{E_c} \text{ and } \varepsilon_{sl} = \frac{f_{sl}}{E_{sl}}$$

substituting for ε_{icm}, ε_{cl} and ε_{sl} in 4.2.1.18 and rearranging

$$f_{sl} = D_1 \left\{ \frac{f_{mi}\,(d_1 - d_n)m_1}{d_n \cos^2\theta} - \frac{F_1 \tan\theta\, E_{sl}}{A_{sl}G_1} \right\} \qquad \text{------ 4.2.1.19.}$$

similarly

$$f_{su} = D_u \left\{ \frac{f_{mi}\,(d_u - d_n)\,m_u}{d_n \cos^2\theta} - \frac{F_u \tan\theta\, E_{su}}{A_{su}G_u} \right\} \qquad \text{------ 4.2.1.20.}$$

Considering the equilibrium of the forces normal to the skew axis (see Fig. 4.2.4.)

Compressive forces = Tensile forces

$$\frac{k_i\, b\, d_n\, f_{mi}}{\cos\theta} = (A_{sl}\, f_{sl} + A_{su}\, f_{su}) \cos\theta + (P_{tl} + P_{tu})\cos\theta + (F_1 + F_u)\sin\theta$$

------- 4.2.1.21.

Substituting in 4.2.1.21 for f_{sl} and f_{su}

$$\frac{k_i b d_n f_{mi}}{\cos\theta} = D_l A_{sl}\cos\theta\left\{\frac{f_{mi}(d_l-d_n)m_l}{d_n\cos^2\theta} - \frac{F_l\tan\theta E_{sl}}{A_{sl}G_l}\right\} +$$

$$D_u A_{su}\cos\theta\left\{\frac{f_{mi}(d_u-d_n)m_u}{d_n\cos^2\theta} - \frac{F_u\tan\theta E_{su}}{A_{su}G_u}\right\} + (P_{tl}+P_{tu})\cos\theta +$$

$$(F_l + F_u)\sin\theta \text{ ------ 4.2.1.22.}$$

Taking moments of the forces normal to the skew axis about the centre of the lower layer of steel (See Fig. 4.2.4.)

$$M\cos\theta+T\sin\theta = \frac{k_i b d_n f_{mi} L_l}{\cos\theta} - P_{tu}(d_l-d_u)\cos\theta - A_{su}f_{su}(L_l-L_u)\cos\theta -$$

$$F_u(L_l-L_u)\sin\theta \text{ ------ 4.2.1.23.}$$

Substituting for f_{su}, and F_u in 4.2.1.23 and simplifying

$$M\cos\theta+T\sin\theta = \frac{k_i b d_n f_{mi} L_l}{\cos\theta} - P_{tu}(d_l-d_u)\cos\theta -$$

$$\frac{D_u A_{su}(d_l-d_u)(d_u-d_n)f_{mi}m_u}{d_n\cos\theta} + \frac{(R.D_u-1)T\sin\theta(L_l-L_u)L_u}{(L_l+L^2_{u/L_l})L_l}$$

------ 4.2.1.24.

where $R = \frac{E_{su}}{G_u} = \frac{E_{sl}}{G_l}$ ------ 4.2.1.25.

Although it is appreciated that $E_{su} \neq E_{sl}$ and $G_u \neq G_l$ the change in E with increase in stress is assumed to equal the change in G. This assumption helps to simplify the final solution.

Rearranging 4.2.1.24.

$$f_{mi}\left\{\frac{k_i b d_n L_l}{\cos\theta} - \frac{D_u A_{su}(d_l-d_u)(d_u-d_n)m_u}{d_n\cos\theta}\right\} = M\cos\theta + T\sin\theta + P_{tu}(d_l-d_u)\cos\theta -$$

$$\frac{(R.D_u-1)T\sin\theta(L_l-L_u)L_u}{(L_l^2 + L_u^2)}$$

------ 4.2.1.26.

Substituting for F_u, F_l, E_{su}/G_u, E_{sl}/G_l, in 4.2.1.22

and rearranging

$$f_{mi}\left\{\frac{k_i b d_n}{\cos\theta} - \frac{D_l A_{sl}(d_l-d_n)m_l}{d_n\cos\theta} - \frac{D_u A_{su}(d_u-d_n)m_u}{d_n\cos\theta}\right\} = (P_{tl}+P_{tu})\cos\theta -$$

$$\frac{T\sin\theta}{(L_l^2+L_u^2)}\ (L_l(R.D_l-1) + L_u(R.D_u-1)) \quad \text{------ 4.2.1.27.}$$

Substituting for f_{mi} from 4.2.1.26 into 4.2.1.27, multiplying throughout by $d_n \cos\theta$ and simplifying

$$k_i b d_n^2(1-L_l R_d) = D_l A_{sl}(d_l-d_n)m_l + D_u A_{su}(d_u-d_n)m_u(1-(d_l-d_u)R_d) \quad \text{------ 4.2.1.28.}$$

where $$R_d = \left\{\frac{(P_{tl}+P_{tu})-C_d(L_l(R.D_l-1)+L_u(R.D_u-1))}{M+T\tan\theta+P_{tu}(d_l-d_u)-C_d(R.D_u-1)(L_l-L_u)L_u}\right\} \quad \text{------ 4.2.1.29.}$$

and

$$C_d = \frac{T\tan\theta}{(L_l^2+L_u^2)} \quad \text{------ 4.2.1.30.}$$

also

$$L_l = d_l - C_l d_n \text{ and } L_u = d_u - C_l d_n \quad \text{------ 4.2.1.31.}$$

C_l is a factor depending on the distribution of the compressive stresses in the concrete. Therefore, knowing the value of θ (the solution for which is given in 4.2.4) d_n can be determined, by iteration, from equation 4.2.1.28.

4.2.1.3. <u>General Theory of Failure for Beams Containing 1 Layer of Tensile Reinforcement</u>

The solution proposed here is applicable to beams containing only 1 layer of steel in the tension zone. The beams may or may not contain steel in their compression zone. For beams, such as those uniformly prestressed, where steel is present in the compression zone, then

the following assumptions are made.

1) The compressive force resisted by the upper steel is ignored.

2) The dowel force resisted by the upper steel is ignored. This assumption is based on the fact that the lever arm L_u is small in comparison with that of L_1.

From equation 4.2.1.5, therefore, the dowel force becomes

$$F_1 = \frac{T}{L_1} \qquad \text{------ 4.2.1.32.}$$

Substituting $A_{su} = 0$ in 4.2.1.12

$$f_m = \frac{M + P_{tu}(d_1 - d_u)}{k_m b d_n L_1} \qquad \text{------ 4.2.1.33.}$$

and substituting $L_u = 0$ in 4.2.1.13

$$f_v = \frac{T}{k_t b d_n L_1} \qquad \text{------ 4.2.1.34.}$$

$\frac{f_m}{f_v}$ in equation 4.2.1.14 becomes

$$\frac{\left(M + P_{tu}\,(d_1 - d_u)\right) k_t}{T\, k_m} \qquad \text{------ 4.2.1.35.}$$

and 4.2.1.15 reduces to

$$T = k_t b\, d_n\, L_1\, f_c' \left\{ \frac{0.2}{\sqrt{\left(\frac{f_m}{2f_v}\right)^2 + 1} \quad - 0.3\left(\frac{f_m}{f_v}\right)} \right\} \qquad \text{------ 4.2.1.36.}$$

For beams containing no steel in the top (as in the author's) the term P_{tu} in equation 4.2.1.35 is eliminated.

4.2.1.4. The Solution for d_n for Beams Containing 1 Layer of Tension Reinforcement

The solution derived in section 4.2.1.2 is greatly simplified by the 2 assumptions referred to in 4.2.1.3. The derivation of the final equation is identical to that described in 4.2.1.2 and it is only

proposed here to eliminate the relevant terms from the equations in question.

We have therefore

$$L_u = A_{su} = 0$$

Substituting for L_u in 4.2.1.30

$$C_d = \frac{T \tan \theta}{L_1^2} \qquad \text{------ 4.2.1.37.}$$

Substituting for L_u and C_d in 4.2.1.29

$$R_d = \left\{ \frac{(P_{tl} + P_{tu}) - L_1 C_d (R.D_1 - 1)}{M + T \tan\theta + P_{tu}(d_1 - d_u)} \right\} \qquad \text{------ 4.2.1.38.}$$

Substituting for R_d and A_{su} in 4.2.1.28

$$k_i b d_n^2 (S_d) = D_1 A_{sl} (d_1 - d_n) m_1 \qquad \text{------ 4.2.1.39.}$$

where

$$S_d = (1 - L_1 R_d) = 1 - \left\{ \frac{L_1 (P_{tl} + P_{tu}) - (R.D_1 - 1) T \tan\theta}{M + T \tan\theta + P_{tu}(d_1 - d_u)} \right\} \qquad \text{------ 4.2.1.40.}$$

Dividing 4.2.1.39 throughout by bd_1^2

$$k_i \left(\frac{d_n}{d_1}\right)^2 S_d = \frac{D_1 A_{sl} m_1}{b d_1} - \frac{D_1 A_{sl} m_1}{b d_1} \left(\frac{d_n}{d_1}\right)$$

dividing throughout by $2k_i$ and rearranging

$$\frac{1}{2} \left(\frac{d_n}{d_1}\right)^2 + \frac{G_d}{2k_i S_d} \left(\frac{d_n}{d_1}\right) - \frac{G_d}{2k_i S_d} = 0$$

where

$$G_d = \frac{D_1 A_{sl} m_1}{b d_1}$$

$$\therefore \quad \frac{d_n}{d_1} = -\left(\frac{G_d}{2k_i S_d}\right) + \sqrt{\left(\frac{G_d}{2k_i S_d}\right)^2 + \frac{G_d}{k_i S_d}} \qquad \text{------ 4.2.1.41.}$$

4.2.1.41 is again solved by iteration. The negative sign before the square root in equation 4.2.1.41 is inadmissible as it yields a negative value for d_n. For those beams containing no top steel P_{tu} is eliminated from equation 4.2.1.40.

Substituting for d_n, therefore, in equation 4.2.1.36 the torsional resistance T of the beam can be determined.

4.2.2. Failure Theories for Beams Containing No. Dowel Force

As was the case for beams containing a dowel force, the beams containing more than 1 layer of steel in the tension zone are treated seperately from the remainder. The derivation of many of the formulas here are similar to those developed in 4.2.1, and much of it will be eliminated to prevent duplication.

4.2.2.1. General Theory of Failure for Beams Containing 2 Layers of Tensile Reinforcement

Cowan's theory of failure on the perpendicular axis is again taken as the failure criteria.

The distribution of shear stresses in the compressed concrete is the basic difference between these beams and those containing a dowel force. The absence of the dowel forces means that the resistance to rotation is provided entirely by the compression concrete. The shear stresses are therefore assumed to be distributed according to Nadai's (5) Sand Heap analogy as shown in Fig. 4.2.5. This plastic theory is assumed to be applicable in this case because of the high compressive stresses present in the concrete. Although it is realized that the conditions are not purely plastic it is felt that this theory is more applicable than the torsion theories proposed in 4.2 and 4.3 for modes 2, and 3. The distribution of the direct stresses is the same as that proposed in 4.2.1.1 and is also shown in Fig. 4.2.5.

Considering the equilibrium of the moments about an axis

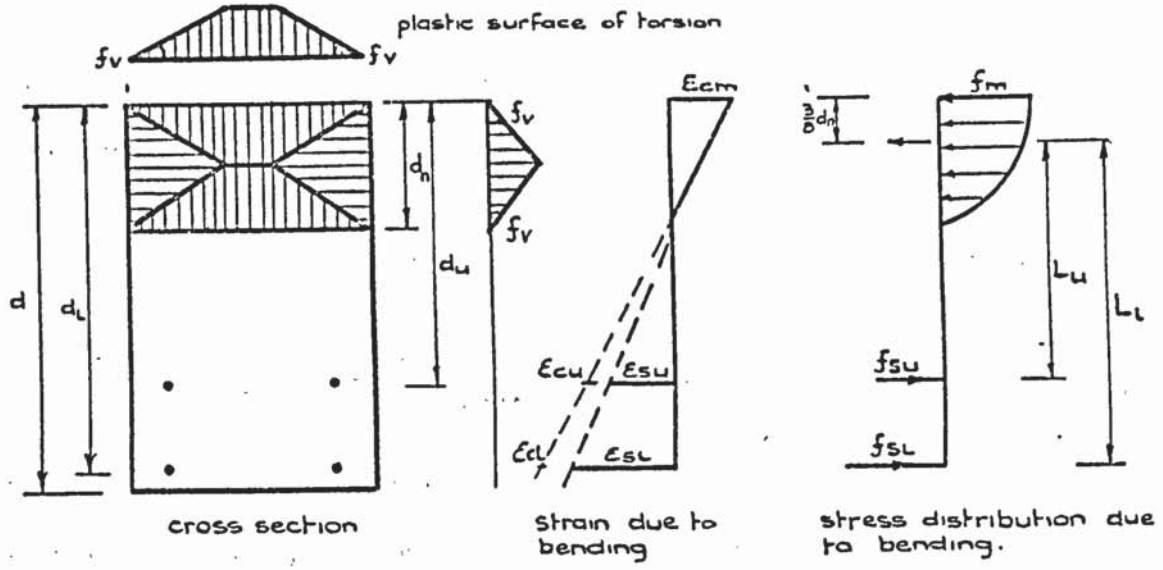

Fig. 4.2.5. Stress and strain distribution due to loading on a plane normal to the axis of the beam. Mode 1.- no dowel force.

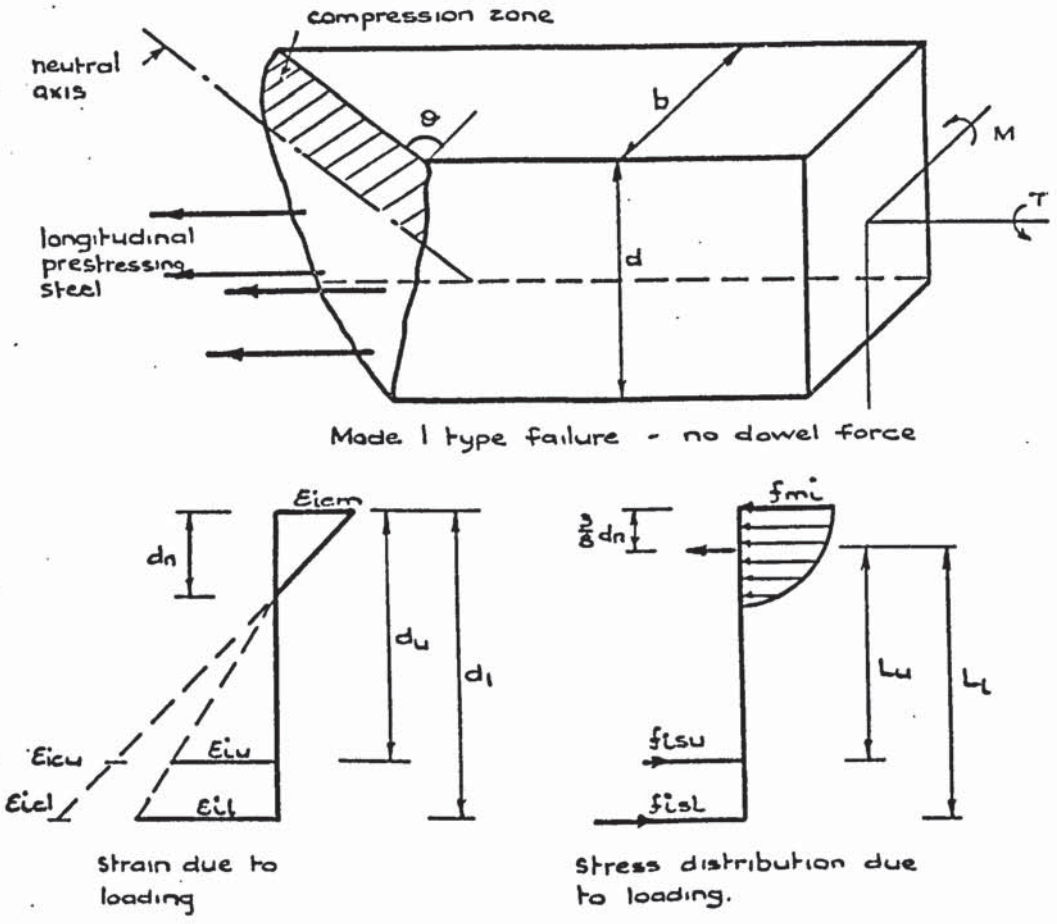

Fig. 4.2.6. Stress and strain distribution due to loading on a plane normal to the skew axis. Mode 1.- no dowel force.

parallel to the length of the member, the torsional resistance T is given by:-

$$T = \frac{b^2}{2}\left(d_n - \frac{b}{3}\right) f_v \quad \text{. . . for } d_n > b \qquad \text{------ 4.2.2.1.}$$

$$T = \frac{d_n^2}{2}\left(b - \frac{d_n}{3}\right) f_v \quad \text{... for } d_n < b \qquad \text{------ 4.2.2.2.}$$

Taking moments of the forces about an axis through the centroid of the lower steel, and perpendicular to the length of the member, the equation is identical to that of 4.2.1.12. i.e.

$$f_m = \frac{M + P_{tu}(d_1 - d_u)}{k_m b d_n L_1 - \dfrac{D_u A_{su} m_u (d_u - d_n)(d_1 - d_u)}{d_n}} \qquad \text{------ 4.2.2.3.}$$

Equation 4.2.1.8 derived from Cowan is also applicable here, and substituting for f_v from 4.2.2.1 or 4.2.2.2, into the L.H.S. of the equation and rearranging

$$T = \frac{b^2}{2}\left(d_n - \frac{b}{3}\right) f_c' \left\{ \frac{0.2}{\sqrt{\left(\frac{f_m}{2f_v}\right)^2 + 1} - 0.3\left(\frac{f_m}{f_v}\right)} \right\} \qquad \text{---- 4.2.2.4.}$$

where $d_n > b$

or

$$T = \frac{d_n^2}{2}\left(b - \frac{d_n}{3}\right) f_c' \left\{ \frac{0.2}{\sqrt{\left(\frac{f_m}{2f_v}\right)^2 + 1} - 0.3\left(\frac{f_m}{f_v}\right)} \right\} \qquad \text{---- 4.2.2.5.}$$

where $d_n < b$

Knowing d_n, therefore, values of f_m and f_v from 4.2.2.1. through 4.2.2.3. can be substituted into the relevant equation above to find T.

4.2.2.2. The Solution for d_n for Beams Containing 2 Layers of Tension Reinforcement

As is the case in 4.2.1.2 the solution proposed is based on the equilibrium of a cracked section about a skew axis.

With reference to Fig. 4.2.6. Considering the equilibrium of the forces on the skew plane we have

Compressive forces = Tensile forces

$$\frac{k_i b d_n f_{mi}}{\cos\theta} = (A_{sl} f_{sl} + A_{su} f_{su}) \cos\theta + (P_{tl} + P_{tu}) \cos\theta \qquad \text{------ 4.2.2.6.}$$

This is comparable with equation 4.2.1.21 if the term due to the dowel force is omitted. If the same assumptions concerning the strain distribution are made, then from equation 4.2.1.19

$$f_{sl} = \frac{D_l f_{mi} (d_l - d_n) m_l}{d_n \cos^2\theta} \qquad \text{------ 4.2.2.7.}$$

and from 4.2.1.20

$$f_{su} = \frac{D_u f_{mi} (d_u - d_n)\, m_u}{d_n \cos^2\theta} \qquad \text{------ 4.2.2.8.}$$

Substituting for f_{sl} and f_{su} in 4.2.2.6

$$\frac{k_i b d_n f_{mi}}{\cos\theta} = \frac{D_l A_{sl} f_{mi} (d_l - d_n) m_l}{d_n \cos\theta} + \frac{D_u A_{su} f_{mi} (d_u - d_n) m_u}{d_n \cos\theta} + (P_{tl} + P_{tu}) \cos\theta$$

------ 4.2.2.9.

Taking moments of the forces normal to the skew axis about the centre of the lower steel

$$M\cos\theta + T \sin\theta = \frac{k_i b d_n L_l f_{mi}}{\cos\theta} - P_{tu}(d_l - d_u) \cos\theta - A_{su} f_{su} (d_l - d_u) \cos\theta$$

---- 4.2.2.10.

Substituting for f_{su} and rearranging

$$f_{mi} = \cos\theta \left\{ \frac{M\cos\theta + T\sin\theta + P_{tu}(d_1 - d_u)\cos\theta}{k_i b d_n L_1 - \dfrac{D_u A_{su}(d_u - d_n)(d_1 - d_u)m_u}{d_n}} \right\} \quad \text{------ 4.2.2.11.}$$

Multiplying 4.2.2.9 by d_n/f_{mi}, substituting for f_{mi} from 4.2.2.11 and rearranging

$$k_i b d_n^2 \left\{1 - L_1 R_d\right\} = D_1 A_{s1}(d_1 - d_n)\, m_1 + D_u A_{su}(d_u - d_n)\, m_u(1 - (d_1 - d_u)R_d) \quad \text{------ 4.2.2.12.}$$

Where $R_d = \dfrac{(P_{t1} + P_{tu})}{M + T\tan\theta + P_{tu}(d_1 - d_u)}$ ------ 4.2.2.13.

Equation 4.2.2.11 and 4.2.2.13 are again comparable with 4.2.1.28 and 4.2.1.29, if the terms involving the dowel force are removed.

Solving 4.2.2.12 by iteration f_m and f_v can be found from equation 4.2.2.1 or 2, and 4.2.2.3. The torsional resistance T of the beam can then be determined by solving 4.2.2.4 or 5.

4.2.2.3. General Theory of Failure for Beams Containing 1 Layer of Tensile Reinforcement

For those beams containing steel in the compression zone, then as in 4.2.1.3, the compressive force resisted by this steel will be ignored. Equation 4.2.2.3 then reduces to

$$f_m = \frac{M + P_{tu}(d_1 - d_u)}{k_m b d_n L_1} \quad \text{------ 4.2.2.14}$$

P_{tu} is eliminated from 4.2.2.14 if there is no top steel. The remaining equations developed in 4.2.2.1 are applicable to the beams in this section.

4.2.2.4. The Solution for d_n for Beams Containing 1 Layer of Tension Reinforcement

By ignoring the compressive forces resisted by the upper steel, equation 4.2.2.12 reduces to

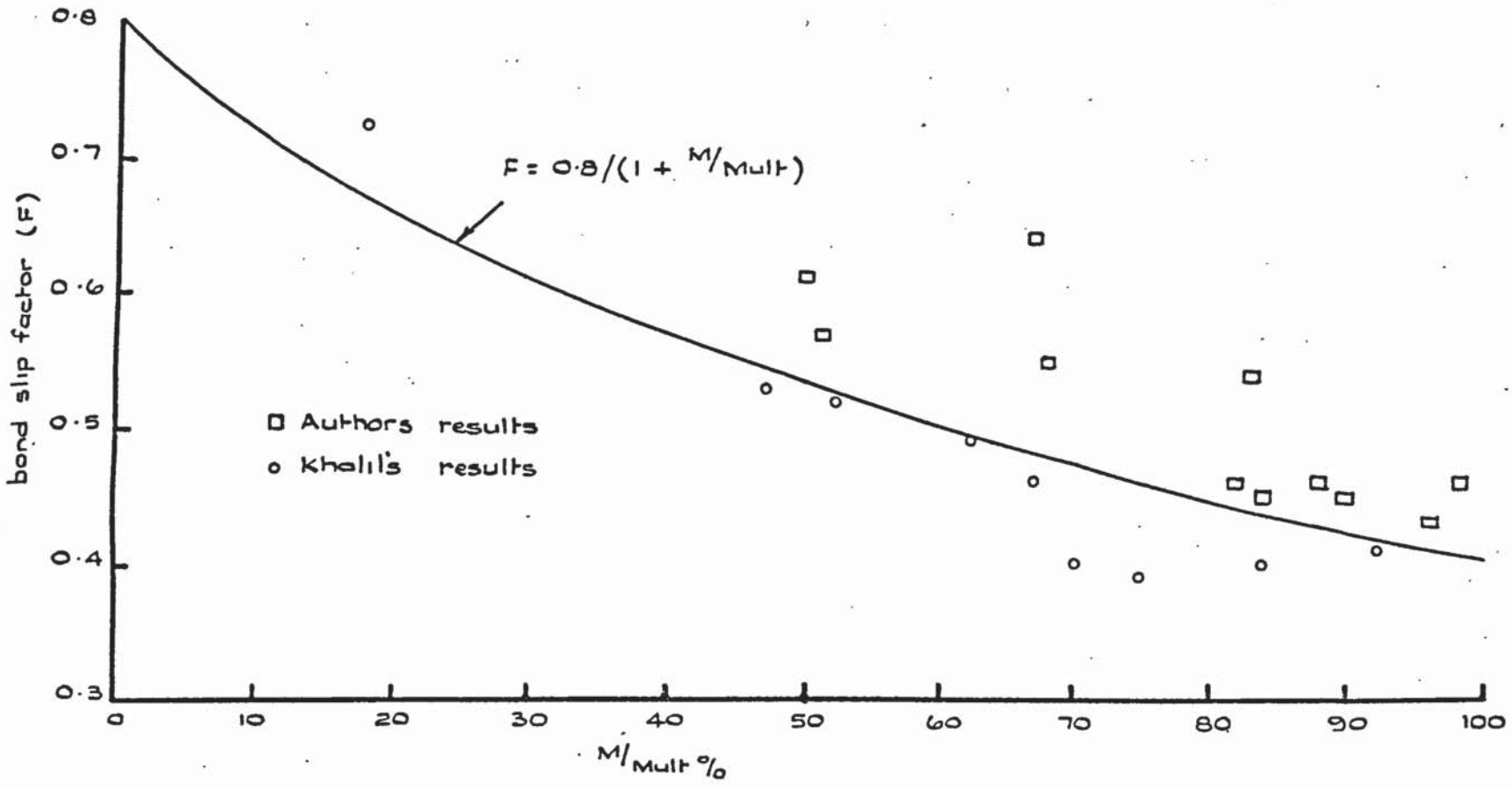

Fig. 4.2.7. Relationship between $^{M}/_{Mult}$ and the bond slip factor for steel in tension.

As can be seen the equation shows reasonable agreement with the experimental results of both the author's and Khalil's. The factor D_u for the upper layer of steel is assumed to equal D_1 if the upper layer is in the tension zone. The compressive forces resisted by the steel in the compression zone have been ignored in this analysis and there is therefore no need to consider a value for the factor governing these conditions. Khalil has, however, suggested that a value of 0.67 be used when accounting for compressive forces resisted by the steel.

4.2.4. The Solution For The Angle of Inclination of The Compression Hinge

A theoretical solution for the angle of inclination θ of the compression hinge in the top of the beam is proposed here. A value of θ is required to solve all the equations involving d_n referred to in this chapter.

In order to develop this theory the following assumptions have been made:

1) The angle of inclination of the compression hinge is controlled by the crack angle at the extreme fibres at the bottom of the section.
2) The crack inclination on the sides of the beam is assumed to be vertical. The crack inclination on the top and bottom of the beam will therefore be the same.
3) The M/T ratio at the first crack is assumed to be the same as that at ultimate.

The assumed failure plane is that shown in Fig. 4.2.8, and the derivation of the equation is very similar to that developed for Mode 3 in section 4.4.

Prior to cracking therefore, taking moments of the forces about the neutral axis of the failure plane.

External moments = Internal moment of resistance on the failure plane

$$\therefore T_c \sin\theta_c + M_c \cos\theta_c = \frac{bd^2}{6}\left(\frac{f_{r3} + P_s\cos^2\theta_c}{\cos\theta_c}\right)$$

rearranging

$$T_c = \frac{bd^2}{6} f_{r3} \frac{(1 + \tan^2\theta_c + \frac{P_s}{f_{r3}})}{(\tan\theta_c + \frac{M_c}{T_c})} \qquad \text{------ 4.2.4.1.}$$

This is comparable with equation 4.4.1 for Mode 3, the sign of the applied bending moment is reversed as the compression hinge is now in the top and not the bottom of the beam. The modulus of rupture value f_{r3} is the same for both Modes 1 and 3.

By a similar derivation to that explained in 4.4 the optimum value of θ_c can be found by differentiating T_c with respect to θ_c.

Thus

$$\tan\theta_c = -\left(\frac{M_c}{T_c}\right) + \sqrt{\left(\frac{M_c}{T_c}\right)^2 + \left(1 + \frac{P_s}{f_{r3}}\right)} \qquad \text{------ 4.2.4.2.}$$

This is again comparable with 4.4.4.

From assumptions 2, and 3 the above equation becomes

$$\tan\theta = -\left(\frac{M}{T}\right) + \sqrt{\left(\frac{M}{T}\right)^2 + \left(1 + \frac{P_s}{f_{r3}}\right)} \qquad \text{------ 4.2.4.3.}$$

A value of θ can therefore be obtained from equation 4.2.4.3.

4.2.5. <u>A Non-Linear Stress - Strain Relationship for Concrete Applied to Beams Containing a Dowel Force</u>

A non-linear stress - strain relationship has been developed for the concrete used throughout this investigation. Full details of the methods of testing and the derivation of the equation are given in section 6.4.

It is now proposed to develop the equations of failure for the author's beams using this non-linear relationship. Much of the derivation

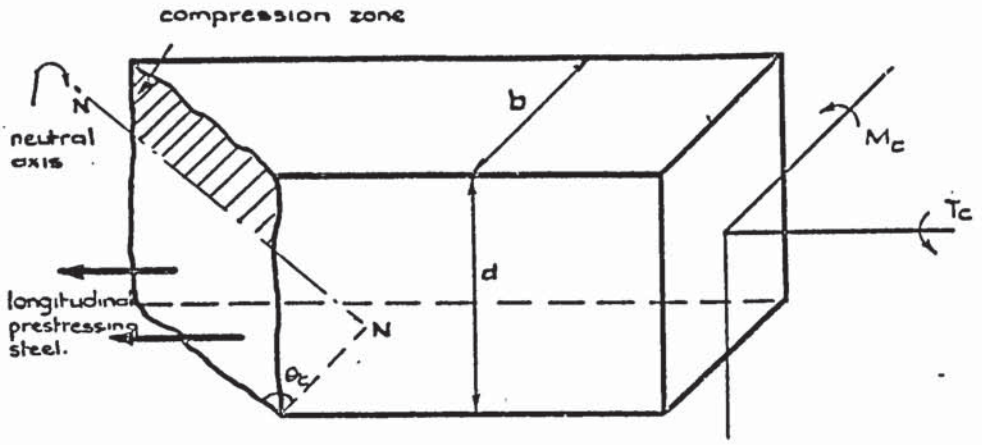

Fig. 4.2.8. Assumed failure plane at appearance of first crack. Mode 1.

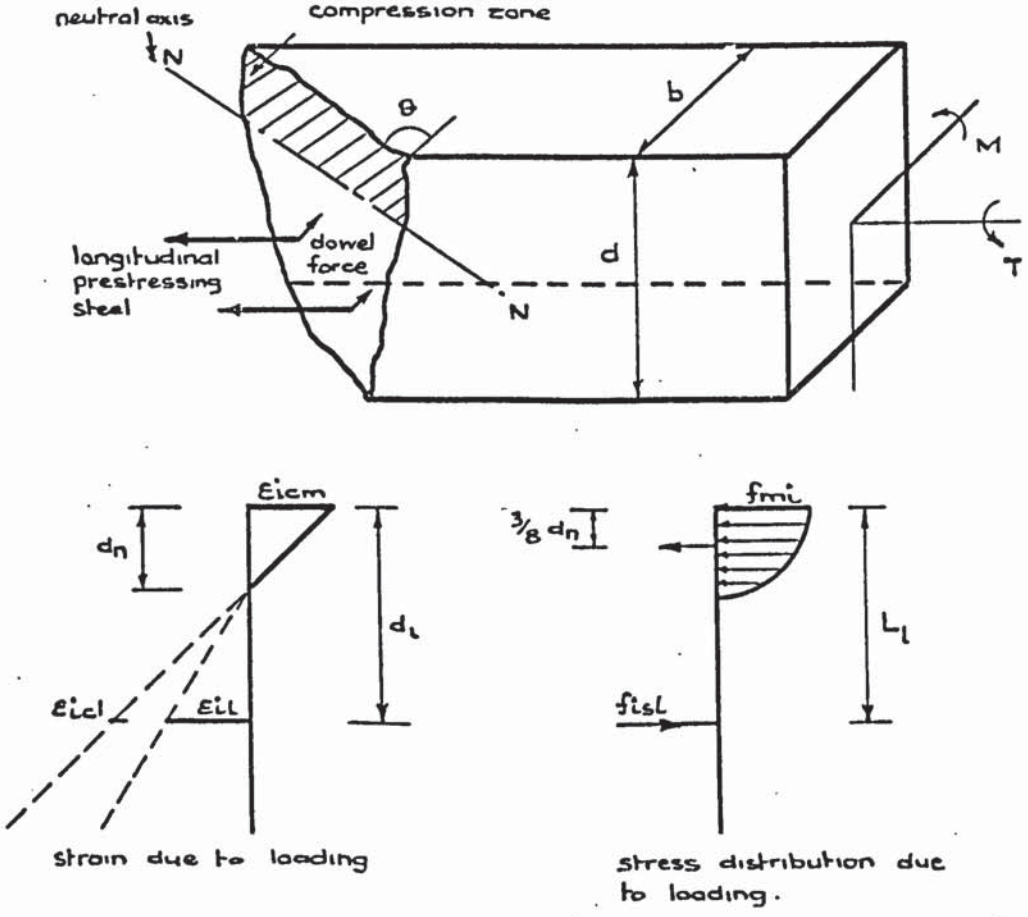

Fig. 4.2.9. Stress and strain distribution due to loading on a plane normal to the skew axis for Mode 1 including a dowel force and a non-linear stress-strain relationship for the concrete

is similar to that described in sections 4.2.1.3 and 4.2.1.4 where a linear relationship was used.

The general equations of failure are identical to those developed in 4.2.1.3 with the exception that all terms containing P_{tu} are eliminated. Thus equation 4.2.1.33 reduces to

$$f_m = \frac{M}{k_m\ b\ d_n\ L_1} \qquad \text{——— } 4.2.5.1.$$

and 4.2.1.35 becomes

$$\frac{f_m}{f_v} = \frac{M\ k_t}{T\ k_m} \qquad \text{——— } 4.2.5.2.$$

Equation 4.2.1.36 remains unchanged

The derivation of d_n is somewhat different from the method described previously. The assumptions, referred to in 4.2.1.2, concerning the strain distribution in the concrete, the bond slip factor, and the resultant strains in the steel are all applied here.

With reference to Fig. 4.2.9 therefore, assuming a linear strain distribution in the concrete on the skew axis, we have

$$\frac{\varepsilon_{icm}}{d_n} = \frac{\varepsilon_{icl}}{(d_1-d_n)}$$

$$\therefore \frac{d_n}{(d_1-d_n)} = \frac{\varepsilon_{icm}}{\varepsilon_{icl}} \qquad \text{------ } 4.2.5.3.$$

But from equation 4.2.1.17, concerning the resultant strain in the concrete adjacent to the steel on the skew axis, we have

$$\varepsilon_{icl} = \varepsilon_{cl} \cos^2\theta + \frac{F_1 \sin\theta \cos\theta}{A_{sl}\ G_1} \qquad \text{------ } 4.2.5.4.$$

Also from 4.2.1.10 concerning the bond slip factor

$$\varepsilon_{cl} = \frac{\varepsilon_{sl}}{D_1}$$

and assuming a linear stress - strain relationship in the steel

$$\varepsilon_{sl} = \frac{f_{sl}}{E_{sl}}$$

$$\therefore \quad \varepsilon_{cl} = \frac{f_{sl}}{E_{sl}\ D_1} \qquad \text{------ 4.2.5.5.}$$

Substitution for ε_{cl} in 4.2.5.4.

$$\varepsilon_{icl} = \frac{f_{sl}\ \cos^2\theta}{E_{sl}\ D_1} + \frac{F_1 \sin\theta \cos\theta}{A_{sl}\ G_1} \qquad \text{------ 4.2.5.6.}$$

Taking moments of the forces, normal to the skew axis, about the centre of the tensile reinforcement (See Fig. 4.2.9).

$$M \cos\theta + T \sin\theta = \frac{k_m\ b\ d_n\ L_1\ f_{mi}}{\cos\theta}$$

$$\therefore \quad f_{mi} = \frac{\cos\theta\ (M \cos\theta + T \sin\theta)}{k_m\ b\ d_n\ L_1} \qquad \text{------ 4.2.5.7.}$$

Taking moments of the forces, normal to the skew axis, about the centre of the compression zone (see Fig. 4.2.9).

$$M \cos\theta + T \sin\theta = P_{tl}\ L_1 \cos\theta + A_{sl}\ f_{sl}\ L_1 \cos\theta + F_1\ L_1 \sin\theta \quad \text{---- 4.2.5.8.}$$

But from 4.2.1.5 where $F_u = 0$ and therefore $L_u = 0$

$$F_1 = \frac{T}{L_1} \qquad \text{------ 4.2.5.9.}$$

Substituting for F_1 in 4.2.5.8 and rearranging

$$f_{sl} = \frac{M - P_{tl}\ L_1}{A_{sl}\ L_1} \qquad \text{------ 4.2.5.10.}$$

Substituting for F_1 from 4.2.5.9 and f_{sl} from 4.2.5.10 into 4.2.5.6 and rearranging

$$\varepsilon_{icl} = \frac{\cos\theta}{A_{sl}L_1}\left\{\left(\frac{M - P_{tl}L_1}{E_{sl}D_1}\right)\cos\theta + \frac{T\sin\theta}{G_1}\right\} \text{ ------ } 4.2.5.11.$$

Now the equation of the stress - strain curve for concrete under compression developed in section 6.4 is

$$\frac{\varepsilon_c}{\varepsilon_{uc}} = 1 \pm \sqrt{1 + \left(\frac{2 - S_c}{S_c}\right)\left(\frac{f_p}{f'_c}\right)^2 - \frac{2}{S_c}\left(\frac{f_p}{f'_c}\right)}$$

This equation was based on conditions occurring in a concrete cylinder under axial load only. The direct compressive stress is represented by f_p and the resulting strain by ε_c. If we now assume that the above equation is applicable to the conditions occurring in the compression zone normal to the skew axis in the prestressed beams, then ε_c can be represented by ε_{icm} and f_p by f_{mi}. The equation then becomes

$$\varepsilon_{icm} = \varepsilon_{uc}\left\{1 \pm \sqrt{1 + \left(\frac{2 - S_c}{S_c}\right)\left(\frac{f_{mi}}{f'_c}\right)^2 - \frac{2}{S_c}\left(\frac{f_{mi}}{f'_c}\right)}\right\} \text{ ------ } 4.2.5.12.$$

Where S_c represents the slope of the non-dimensional stress - strain curve (Fig. 6.4.4) at the point (0,0)

$$\therefore S_c = \frac{E_{oc}\,\varepsilon_{uc}}{f'_c}$$

Substituting for f_{mi} in 4.2.5.12, and substituting for ε_{icl} and ε_{icm} in 4.2.5.3, equation 4.2.5.3 can be solved for d_n by iteration. Knowing d_n, therefore, equation 4.2.1.36 can be solved for T.

The inclusion of a non-linear stress-strain relationship for the concrete adds to the complexity of the resulting equations.

Results taken from the author's experiments (see Table 5.5) have shown, however, that there is very little difference between the solutions obtained using a linear relationship and those using a non-linear relationship. It was not considered beneficial, therefore, to develop this approach for the more complicated cases of beams containing 2 layers of steel in the tension zone.

4.3. Mode 2

In order to develop the theory for this mode of failure the following assumptions will be made.

(1) The failure surface is initially considered to be a plane rectangle as shown in Fig. 4.3.1.

(2) As mentioned previously the failure mechanism is considered to be one of bending about a skew axis. For this reason therefore, the limiting tensile stress of the concrete will be taken as that measured from the modulus of rupture tests.

(3) Due to the eccentricity of the prestress, and the distribution of the stress due to bending, the resulting stress distribution across the depth of the section will not be uniform. The critical section is assumed to lie at the centre of the larger side (BC) of the rectangle. This is in agreement with the classical elastic theory of St. Venant[33]. It states that for a rectangular section under pure torsion the maximum shear stress occurs on the periphery at the middle of the longer sides of the rectangle.

(4) Failure occurs when the resulting tensile stress at the critical section reaches the limiting tensile stress of the concrete.

Now the apparent tensile strength of the section is equal to its modulus of rupture strength plus the component of the prestress normal to the failure surface at the critical section.

If we consider the forces due to prestress acting on a small dement as shown in Fig. 4.3.2.we have

Horizontal force due to prestress = P_{s2} x 1 (unit side)

Component of force normal to plane = $P_{s2} \cos \theta_2$

Resolving forces normal to plane

$$P_{s2} \cos \theta_2 = \frac{f_{tp} \times 1}{\cos \theta_2}$$

$$\therefore \quad f_{tp} = P_{s2} \cos^2 \theta_2$$

The apparent tensile strength of the section = $f_{r2} + P_{s2} \cos^2 \theta_2$

With reference to Fig. 4.3.1.

Taking moments of the forces about the neutral axis of the failure plane.

External moments = Internal moment of resistance on the failure plane

$$T_2 \sin \theta_2 = \frac{db^2}{6} \frac{(f_{r2} + P_{s2} \cos^2 \theta_2)}{\cos \theta_2}$$

rearranging

$$T_2 = \frac{db^2}{6} f_{r2} \frac{(1 + \tan^2 \theta_2 + P_{s2}/f_{r2})}{\tan \theta_2} \qquad \text{——— 4.3.1.}$$

This form of the equation is comparable to Mode 2 for plain concrete as shown by Martin[36] where $P_{s2}/f_{r2} = 0$

By differentiating T_2 with respect to θ_2 and equating to zero, the failure plane that corresponds to the minimum torsional resistance of the beam can be found

Thus from 4.3.1

$$\frac{dT_2}{d\theta_2} = \tan \theta_2 \frac{\left\{c_2\ 2 \sec^2 \theta_2 \tan \theta_2\right\} - \sec^2 \theta_2 \left\{c_2(\sec^2 \theta_2 + F_2)\right\}}{\tan^2 \theta_2} = 0$$

where $c_2 = \frac{db^2}{6} f_{r2}$

$$F_2 = \frac{P_{s2}}{f_{r2}}$$

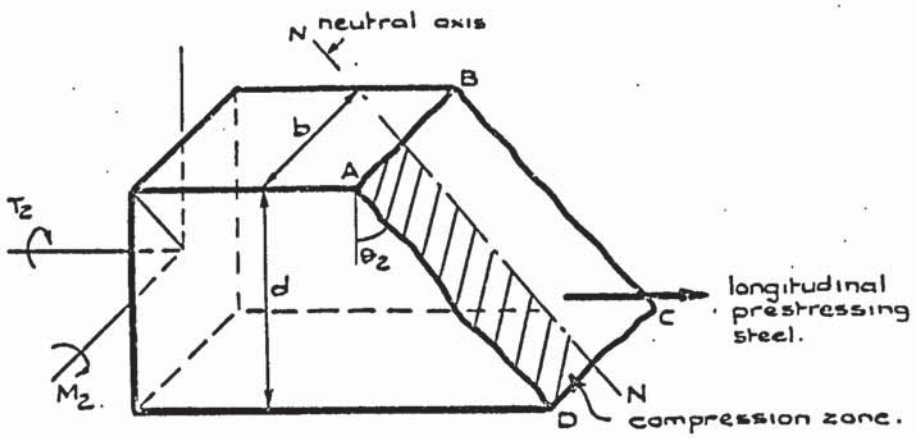

Fig 4.3.1. Mode 2. type of failure in prestressed concrete. (rectangular failure plane)

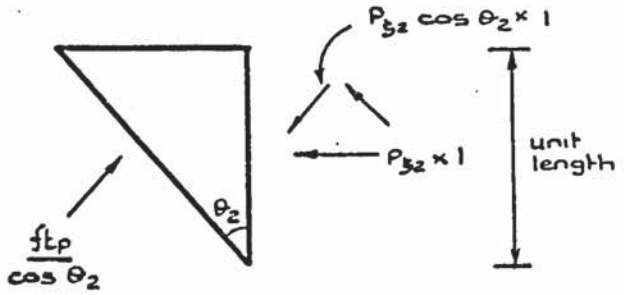

Fig. 4.3.2. The forces due to prestress on an element of the concrete - Mode 2.

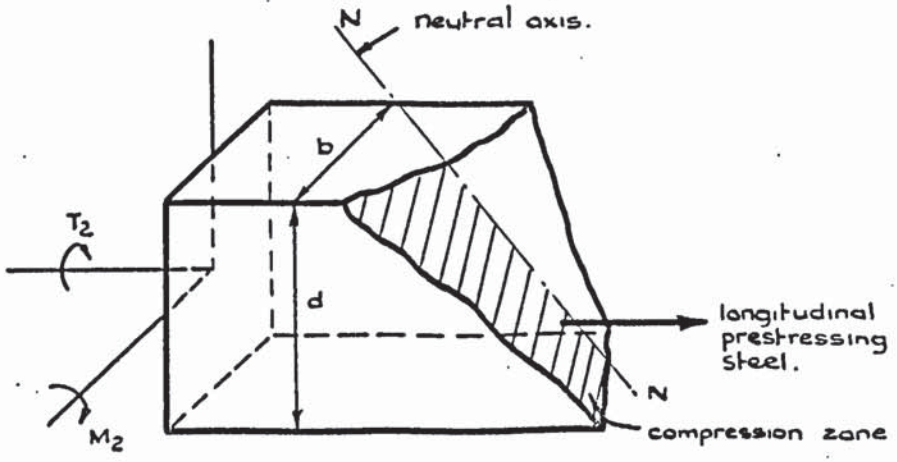

Fig. 4.3.3. Mode 2 type of failure in prestressed concrete (trapezoidal failure plane.)

$$\therefore \quad 2\,c_2 \tan^2\theta_2 \sec^2\theta_2 - \sec^2\theta_2 \left\{ c_2(\sec^2\theta_2 + F_2) \right\} = 0$$

simplifying

$$2\tan^2\theta_2 - \sec^2\theta_2 - F_2 = 0$$

but $\sec^2\theta_2 = 1 + \tan^2\theta_2$

$$\therefore \tan^2\theta_2 - 1 - F = 0$$

$$\tan\theta_2 = \sqrt{1 + \frac{P_{s2}}{f_{r2}}}$$

Substituting for $\tan\theta_2$ in 4.3.1

$$T_2 = \frac{db^2}{3} f_{r2} \sqrt{1 + \frac{P_{s2}}{f_{r2}}} \qquad \text{——— 4.3.2.}$$

or in the general interaction form of the equation

$$\frac{T_2}{T_{u2}} = 1 \qquad \text{——— 4.3.3.}$$

where

$$T_{u2} = \frac{db^2}{3} f_{r2} \sqrt{1 + \frac{P_{s2}}{f_{r2}}} \qquad \text{——— 4.3.4.}$$

or in the general case

$$T_{u2} = 2Z_2 f_{r2} \sqrt{1 + \frac{P_{s2}}{f_{r2}}} \qquad \text{——— 4.3.5.}$$

where Z_2 = elastic section modulus = $\frac{db^2}{6}$.

In tests subjecting plain rectangular sections to pure torsion Hsu[20] showed that close agreement could be obtained between experiment and theory if

$$T_{u2} = \frac{db^2}{3} (0.85\, f_{r2}) \qquad \text{——— 4.3.6.}$$

The factor of 0.85 was introduced based on Mohr's failure theory which reduces the modulus of rupture value under conditions of pure torsion.

Hsu[21] also applied the above theory to rectangular prestressed

sections under pure torsion and obtained a solution of the form

$$T_{u2} = \frac{db^2}{3} (0.85 f_{r2}) \sqrt{1 + \frac{P_{s2}}{0.85 f_{r2}}} \qquad \text{——— 4.3.7.}$$

Hsu assumed, as did the author in the preceding theory, that the failure plane was a rectangle. Experimental evidence has shown, however, that this plane is in fact distorted to a spiral form to produce a projected trapezium as shown in Fig. 4.3.3. This distortion may account for the need to introduce a factor such as the one of 0.85 adopted by Hsu.

Martin[36] has shown for plain concrete, by assuming the plane approximates to a trapezium, that this factor can be represented by the expression

$$\frac{1}{3 + (b/d)^{\frac{1}{2}}} \qquad \text{——— 4.3.8.}$$

If we assume that this factor is also applicable to prestressed concrete then 4.3.4 becomes

$$T_{u2} = \frac{1}{3 + (b/d)^{\frac{1}{2}}} db^2 \cdot f_{r2} \sqrt{1 + \frac{P_{s2}}{f_{r2}}} \qquad \text{——— 4.3.9.}$$

4.4 Mode 3

The theoretical analysis will be based on assumptions 1, 2, 4, used in the derivation of the Mode 2 equation. With regard to assumption 3 concerning the position of the critical stress, this will now be assumed to be at the top of the beam. The distribution of stresses, due to prestress and bending, across the width of the section AB (see Fig. 4.4.1) is uniform. Using the skew bending approach, therefore, the stress conditions in the extreme fibres (AB) at failure are assumed to be the same at all points.

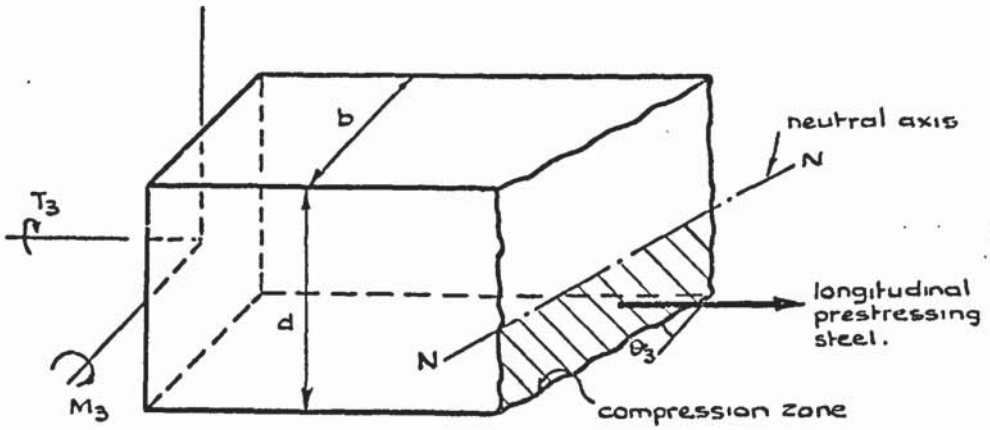

Fig. 4.4.1. Mode 3 type failure in prestressed concrete (rectangular failure plane.)

The apparent tensile strength at the critical section is taken as

$$f_{r3} + P_{s3} \cos^2 \theta_3$$

The derivation of the above equation is similar to that described in 4.3 for Mode 2.

With reference to Fig. 4.4.1. Taking moments of the forces about the neutral axis of the failure plane.

External moments = Internal moment of resistance on the failure plane.

$$T_3 \sin \theta_3 - M_3 \cos \theta_3 = \frac{bd^2}{6} \frac{(f_{r3} + P_{s3} \cos^2 \theta_3)}{\cos \theta_3}$$

rearranging

$$T_3 = \frac{bd^2}{6} f_{r3} \frac{(1 + \tan^2 \theta_3 + \frac{P_{s3}}{f_{r3}})}{(\tan \theta_3 - \frac{M_3}{T_3})} \qquad \text{------ 4.4.1.}$$

The optimum value of θ_3 corresponding to the minimum torsional resistance can be found by differentiating T_3 with respect to θ_3.

Thus from 4.4.1

$$\frac{dT_3}{d\theta_3} = \frac{(\tan\theta_3 - R_3)(2C_3 \sec^2\theta_3 \tan\theta_3) - \sec^2\theta_3 C_3(\sec^2\theta_3 + F_3)}{(\tan\theta_3 - R_3)^2} = 0$$

where

$$R_3 = \frac{M_3}{T_3}$$

$$C_3 = \frac{bd^2}{6} f_{r3}$$

$$F_3 = \frac{P_{s3}}{f_{r3}}$$

$$\therefore 2C_3 \sec^2\theta_3 \tan^2\theta_3 - 2C_3 R_3 \sec^2\theta_3 \tan\theta_3 - C_3 \sec^4\theta_3 - C_3 F_3 \sec^2\theta_3 = 0$$

simplifying

$$2 \tan^2\theta_3 - 2 R_3 \tan\theta_3 - \sec^2\theta_3 - F_3 = 0 \qquad \text{------ 4.4.2.}$$

but $\sec^2\theta_3 = 1 + \tan^2\theta_3$

substituting for $\sec^2\theta_3$ in 4.4.2

$$\tan^2\theta_3 - 2 R_3 \tan\theta_3 - (1 + F_3) = 0$$

divide throughout by 2.0

$$\tfrac{1}{2}\tan^2\theta_3 - R_3\tan\theta_3 - \tfrac{1}{2}(1 + F_3) = 0$$

$$\therefore \tan\theta_3 = R_3 \pm \sqrt{R_3^2 + (1 + F_3)} \qquad \text{------ 4.4.3.}$$

The minus sign is inadmissable as it yields a negative value for $\tan\theta_3$.

Substituting for R_3 and F_3 in 4.4.3.we get

$$\tan\theta_3 = \frac{M_3}{T_3} + \sqrt{\left(\frac{M_3}{T_3}\right)^2 + \left(1 + \frac{P_{s3}}{f_{r3}}\right)} \qquad \text{------ 4.4.4.}$$

Substituting for $\tan\theta_3$ in 4.4.1 and rearranging

$$T_3 = \frac{bd^2}{3} f_{r3}\left(\frac{M_3}{T_3} + \sqrt{\left(\frac{M_3}{T_3}\right)^2 + 1 + \frac{P_{s3}}{f_{r3}}}\right) \qquad \text{------ 4.4.5.}$$

rearranging

$$\left\{\frac{T_3}{2Z_3 f_{r3}} - \frac{M_3}{T_3}\right\}^2 = \left(\frac{M_3}{T_3}\right)^2 + 1 + \frac{P_{s3}}{f_{r3}}$$

where Z_3 = elastic section modulus = $\frac{bd^2}{6}$

$$\therefore \left(\frac{T_3}{2Z_3 f_{r3}}\right)^2 - \frac{T_3}{Z_3 f_{r3}}\frac{M_3}{T_3} = 1 + \frac{P_{s3}}{f_{r3}}$$

$$\therefore \left(\frac{T_3}{2Z_3 f_{r3}\sqrt{1 + P_{s3}/f_{r3}}}\right)^2 - \frac{M_3}{Z_3 f_{r3}(1 + P_{s3}/f_{r3})} = 1 \qquad \text{------ 4.4.6.}$$

but by a similar derivation to that of equation 4.3.5

$$T_{u3} = 2Z_3 f_{r3}\sqrt{1 + \frac{P_{s3}}{f_{r3}}} \qquad \text{------ 4.4.7.}$$

and for the simple elastic relationship

$$f = \frac{M}{Z}$$

$$M_{u3} = Z_3(f_{r3} + P_{s3})$$

$$M_{u3} = Z_3 f_{r3}(1 + P_{s3}/f_{r3}) \qquad \text{------ 4.4.8.}$$

Substituting for T_{u3} and M_{u3} in 4.4.6 yields the general interaction form of

$$\left(\frac{T_3}{T_{u3}}\right)^2 + \frac{M_3}{M_{u3}} = 1 \qquad \text{------ 4.4.9.}$$

As for Mode 2, equations 4.4.5 and 4.4.7 can be modified

1) By the factor proposed by Hsu[20] to produce

$$T_3 = \frac{bd^2}{3}(0.85\, f_{r3})\left(\frac{M_3}{T_3} + \sqrt{\left(\frac{M_3}{T_3}\right)^2 + \frac{1 + P_{s3}}{0.85 x f_{r3}}}\right) \qquad \text{------ 4.4.10.}$$

and

$$T_{u3} = \frac{bd^2}{3}(0.85\, f_{r3})\sqrt{\frac{1 + P_{s3}}{0.85 x f_{r3}}} \qquad \text{------ 4.4.11.}$$

2) By the factor proposed by Martin to account for the spiral form of the failure plane.

$$T_3 = \frac{bd^2 f_{r3}}{3+(d/b)^{\frac{1}{2}}}\left(\frac{M_3}{T_3} + \sqrt{\left(\frac{M_3}{T_3}\right)^2 + 1 + \frac{P_{s3}}{f_{r3}}}\right) \qquad \text{------ 4.4.12.}$$

$$T_{u3} = \frac{bd^2 f_{r3}}{3+(d/b)^{\frac{1}{2}}}\sqrt{1 + \frac{P_{s3}}{f_{r3}}} \qquad \text{------ 4.4.13.}$$

Chapter 5

Comparison of Theoretical and Experimental Results

5.1. Introduction

In the following chapter the theoretical solutions obtained from the equations proposed in Chapter 4.are compared with the experimental results of the author and other investigators. They are presented in tabular form in Tables 5.1 to 5.19. A brief description of the analysis of each set of results is given followed by a discussion on the relationship between the experimental and theoretical results.

The analysis of all results was carried out by use of computer programs. The programs were written in Fortran computer language and were run on an I.C.L. 1900 series machine. Copies of 3 of the programs used for Mode I failure are given in the appendix.

5.2. Analysis of Results

5.2.1. Author's Beams

Tables 5.1 to 5.5 show the author's experimental results compared with the theoretical solutions for Modes 3, 2, 1, and pure bending.

T_3 has been calculated using equation 4.4.12 with 2 values for the modulus of rupture strength f_{r3}. The first is that measured from the modulus of rupture tests and the second has been obtained using the following expression based upon that proposed by Hsu[20].

$$\left.\begin{aligned} f_{r3} &= 0.76\ (1 + \frac{6450}{d^2})\ (f'_c)^{\frac{1}{3}}\ N/mm^2 \\ f_{r3} &= 20.9\ (1 + \frac{10}{d^2})\ (f'_c)^{\frac{1}{3}}\ lbs/in^2 \end{aligned}\right\} \quad 5.1$$

for $d > 100$ mm (4 in.)

$$\left.\begin{aligned} f_{r3} &= \frac{5.34\ (f'_c)^{\frac{1}{3}}\ N/mm^2}{(d)^{\frac{1}{3}}} \quad \text{or} \\ f_{r3} &= \frac{20.9 \times 2.4\ (f'_c)^{\frac{1}{3}}\ lbs/in^2}{(d)^{\frac{1}{3}}} \end{aligned}\right\} \quad 5.2$$

for $d \leq 100$ mm (4 ins.)

The cylinder strength f'_c in the above expression has been calculated from the cube crushing strength using the relationship

$$f'_c = 0.8\ U_w \qquad \text{——— } 5.3$$

Equation 4.4.12(a) refers to that equation used with the computed modulus of rupture strength.

The strains recorded in the steel prior to testing have been used to analyse the distribution of the stresses due to prestress. The bar has been assumed to be located at a position from the soffit of the beam equal to one third of the depth. The stresses at the top and bottom of the beam are then given by

$$P_{s3} = \frac{P_{t1}}{bd} - \frac{P_{t1} \times e}{Z_3} \qquad \text{——— } 5.4$$

and

$$P_s = \frac{P_{t1}}{bd} + \frac{P_{t1} \times e}{Z_3} \qquad \text{——— } 5.5$$

This was thought to be a more reliable method of obtaining these stresses than using the strains recorded on the concrete. As mentioned in section 3.6 the author is of the opinion that the value of the strains recorded in the top of the beam during stressing are somewhat suspect.

The values of T_2 in Table 5.2 have been calculated using equation 4.3.9 in conjunction with 2 values of f_{r2}. As in the case of Mode 3 the first value is that obtained from the control specimens and the second is that given by the expressions:-

$$\left.\begin{aligned} f_{r2} &= 0.76\ \left(1 + \frac{6450}{b^2}\right)\ (f'_c)^{\frac{1}{3}}\ \text{N/mm}^2 \\ f_{r2} &= 20.9\ \left(1 + \frac{10}{b^2}\right)\ (f'_c)^{\frac{1}{3}}\ \text{lbs/in}^2 \end{aligned}\right\} \qquad \text{——— } 5.6$$

for $b > 100$ mm (4 in.)

or

$$f_{r2} = \frac{5.34(f'_c)^{\frac{1}{3}}}{(b)^{\frac{1}{3}}} \quad N/mm^2$$

$$f_{r2} = \frac{20.9 \times 2.4(f'_c)^{\frac{1}{3}}}{(b)^{\frac{1}{3}}} \quad lbs/in^2 \qquad \text{——— 5.7.}$$

for $b \leq 100$ mm (4 in.)

The above expressions are similar to those of 5.1 and 5.2 for Mode 3. For those beams failing in Mode 2 the effective depth of the section becomes equal to b, as rotation is now occurring about the side face of the beam. Thus substituting b for d in 5.1 and 5.2 yields 5.6 and 5.7.

Table 5.3 shows a comparison of the author's results for Mode 1 failure. Two solutions have been obtained using the measured and calculated values of f'_c and f_{r3}.

The first solution of d_n is that calculated from equation 4.2.1.41 in conjunction with equation 4.2.4.3 used to determine the value of θ. The resulting value of d_n was then substituted in equation 4.2.1.36 to determine the theoretical value of T. In addition the following values of the terms listed below have been used throughout the analysis

$b = 100$ mm (3.94 in.)

$d = 175$ mm (6.89 in.)

$d_1 = 116$ mm (4.59 in.)

$k_i = k_t = k_m = \frac{2}{3}$ - estimated

$P_s = 19.34$ N/mm^2 (2804 lbs/in^2) - Average value calculated from equation 5.5.

$R = 2.5$ - estimated

D_1 - from equation 4.2.3.1.

$A_{s1} = 388$ mm^2 (0.601 in^2)

$M_u = 17.09$ kN.m (151.12 kips.ins) - Average experimental value

$$m_1 = \frac{E_{sl}}{E_c}$$

where $E_{sl} = 18.75 \times 10^4$ N/mm^2 $(27.2 \times 10^6$ lbs/in$^2)$ - measured

$E_c = 2491 \sqrt{f'_c}$ N/mm^2 $(30000 \sqrt{f'_c}$ lbs/in$^2)$ - estimated

$C_1 = 0.375$ - estimated.

The values of f'_c and f_{r3} used in the second analysis were those given by equations 5.3 and 5.1 respectively. Equations 4.2.1.36(a) and 4.2.1.41(a) refer to those solutions determined using these computed values.

The theoretical solutions for the conditions of pure bending are shown in Table 5.4. All the terms listed above have been used in this calculation and the 2 solutions have again been obtained using the measured and computed values of f'_c and f_{r3}. The solution of d_n is identical to that for beams tested under a combination of bending moment and torsion, with the exception that all terms containing T in 4.2.1.41 are omitted. The value of M has been calculated using a modification of equation 4.2.1.33 shown below.

$$f_m = \frac{M + P_{tu} (d_1 - d_u)}{k_m b d_n^2 L_1} \qquad \text{——— 4.2.1.33.}$$

But for conditions of pure bending

$$f_m = f'_c$$

and for the author's beam $P_{tu} = 0$

Substituting for f_m and P_{tu} and rearranging

$$M_u = k_m b d_n^2 L_1 f'_c \qquad \text{——— 5.8.}$$

Equation 5.8(a) in Table 5.4 again refers to the use of the computed values of f'_c and f_{r3}.

A comparison between the solutions using a linear and non-linear stress - strain relationship for the concrete are shown in Table 5.5. The solution for d_n was obtained using equations

4.2.5.3, 11, and 12 in conjunction with the previously listed terms. A value of 3500 microstrains was taken as the ultimate strain E_{uc} in the concrete. This was estimated from the experimental results described in section 6.4 and shown in Fig. 6.4.3. The negative sign of equation 4.2.5.12 has been taken, indicating results lying on the rising portion of the curve. The theoretical values of f'_c and f_{r3} were used to determine the 2 solutions listed in the table.

5.2.2. Khalil's[19] Beams

A comparison of the results of 23 plain, prestressed beams tested by Khalil are shown in Tables 5.6 to 5.9. The letter U refers to uniformly prestressed beams and the letter E to eccentrically prestressed beams. The values of U_w, P_{s3}, and P_{s2} listed in Tables 5.6 to 5.9 are those given by Khalil. Two solutions for Modes 3, and 2 are given using 2 values of the modulus of rupture strength. The control specimens used by Khalil to determine his modulus of rupture strength measured 100 mm x 100 mm (4 in. x 4 in.) in section. The section size of his test specimens were 127 mm x 203 mm (5 in. x 8 in.). Tests reported by Hsu[20] and Wright[30] and shown in Fig. 2.1 have indicated that the modulus of rupture strength is dependent upon the depth of the specimen. For this reason it was decided to modify the strengths given by Khalil using equations 5.1 and 5.6. From these equations it can be seen that for a given value of f'_c

the modulus of rupture strength $\propto (1 + \frac{6450}{x^2})$

where x = depth of section (mm)

The modified values become :-

$$f_{r3} = \text{experimental value} \times \left\{ \frac{(1 + \frac{6450}{203^2})}{(1 + \frac{6450}{100^2})} \right\} \text{N/mm}^2 \quad \text{---- 5.9.}$$

$$f_{r2} = \text{experimental value} \times \left\{ \frac{\left(1 + \frac{6450}{127^2}\right)}{\left(1 + \frac{6450}{100^2}\right)} \right\} \text{ N/mm}^2 \quad \text{——— 5.10.}$$

The theoretical values of f_{r3} and f_{r2}, from equations 5.1 and 5.6 respectively, were used in the second analysis. The value of f'_c in both cases was that given by equation 5.3. The values of P_{s3} and P_{s2} were taken as those recorded by Khalil. As was the case with the author's beams, the theoretical values of T_3 and T_2 were determined from equations 4.4.12 and 4.3.9 respectively.

The results of beams failing in Mode I are shown in Table 5.8 . Two calculations were carried out using the recorded and computed values of f_{r3} to determine the value of θ. The difference between the two was, however, very small and those shown in the table were obtained using the computed value. The solution for d_n was obtained using equation 4.2.2.12. For Khalil's uniformly prestressed beams the compressive force resisted by the top steel has been ignored, and equation 4.2.2.12 then reduces to that of 4.2.2.15. Equation 4.2.2.4 or 5 has been solved to determine the torsional resistance T of the beam. The suffix (a) in Table 5.8 refers to the use of the computed value of f_{r3}.

The above analysis has been carried out using the following terms

$k_m = k_i = \frac{2}{3}$ - estimated

$A_{su} = A_{sl} = 77 \text{ mm}^2$ (0.1196 in^2)

$f'_c = 0.8\, U_w$ - equation 5.3

$R = 2.5$ - estimated

$E_c = 2491 \sqrt{f'_c}$ N/mm^2 (30,000 $\sqrt{f'_c}$ lbs/in^2)

$C_1 = 0.375$ - estimated

"U" Beams

$d_1 = 178$ mm (7.0 in.)

$d_u = 25$ mm (1.0 in.)

E_{su} = 19.41 x 10^4 N/mm^2 (28.15 x 10^6 lbs/in^2) --- given

E_{sl} = 10.68 x 10^4 N/mm^2 (15.5 x 10^6 lbs/in^2) --- given

D_l - from equation 4.2.3.1.

D_u = 0 - compressive force in top steel ignored

P_{tl} = 90 kN.(20.24 kips) --- given

P_{tu} = 86.6 kN (19.44 kips) - given

P_s = 6.9 N/mm^2 (1000 lbs/in^2) - given

M_u = 17.20 kN.m (152.0 kips.ins) - experimental

"E" Beams

d_l = 178 mm (7.0 in.)

d_u = 102 mm (4.0 in.)

E_{su} = 10.89 x 10^4 N/mm^2 (15.8 x 10^6 lbs/in^2) - given

E_{sl} = 13.93 x 10^4 N/mm^2 (20.2 x 10^6 lbs/in^2) - given

$D_l = D_u$ - from equation 4.2.3.1.

P_{tl} = 71.2 kN (16.0 kips.) - given

P_{tu} = 89.6 kN (20.20 kips.) - given

P_s = 12.6 N/mm^2 (1820 lbs/in^2) - given

M_u = 25.5 kN.m (226.0 kips.ins) - experimental

The theoretical solutions for beams tested under pure bending are shown in Table 5.9. The details of the analysis are identical to those described above with the exception of the format of the equation necessary to solve for M. This is a modification of equation 4.2.2.3 shown below

$$f_m = \frac{M + P_{tu}(d_l - d_u)}{k_m b d_n L_l - \dfrac{D_u A_{su} m_u (d_u - d_n)(d_l - d_u)}{d_n}} \qquad \text{------} \qquad 4.2.2.3$$

But for conditions of pure bending

$$f_m = f'_c$$

Substituting for f_m and rearranging

$$M_u = f'_c \left\{ k_m b d_n L_1 - \frac{D_u A_{su} m_u (d_u - d_n)(d_1 - d_u)}{d_n} \right\} - P_{tu}(d_1 - d_u) \quad \text{------} \quad 5.11.$$

For the "U" beams the terms involving A_{su} are eliminated.

5.2.3. Reynolds[8] Results

The theoretical results of 12 eccentrically prestressed beams tested by Reynolds are shown in Tables 5.10 and 5.11. The beams measuring 64 mm x 91 mm (2.5in. x 3.6 in.) were prestressed by 2 No. 5 mm (0.2 in.) diameter wires and tested under varying ratios of bending moment to torsion.

The values of f_{r2} in Table 5.10 were calculated using equations 5.3 and 5.7, and the value of P_{s2} is that given by Reynolds.

Only one solution is proposed for Mode 1 failure, that has been obtained using the computed values of f'_c and f_{r3} from 5.3 and 5.2 respectively. The solutions for d_n and T have been obtained (as with the author's beams) using equations 4.2.1.41(a) and 4.2.1.36(a) respectively.

The following additional terms have been used in the analysis of Reynolds' beams:-

$k_t = k_m = k_i = \frac{2}{3}$ - estimated

d_1 = 61 or 64 mm (2.4 or 2.5 in.)

A_{s1} = 41 mm^2 (0.0628 in^2)

$f'_c = 0.8\ U_w$ - equation 5.3

R = 2.5 estimated

$E_c = 2491\sqrt{f'_c}$ N/mm^2 ($30{,}000\sqrt{f'_c}$ lbs/in^2) - estimated

E_{sl} = 13.79 x 10^4 N/mm^2 (20.00 x 10^6 lbs/in^2) - estimated

P_{tl} = 36 kN. (8.1 kips.) - given

P_s = 12.4 N/mm^2 (1800 lbs/in^2) - given

C_1 = 0.375 - estimated

M_u = 2.43 kN.m (21.5 kips.ins) - average experimental value

$$D_1 = \frac{1.0}{(1.0 + {}^{M}/_{3}M_u)} \qquad \text{——5.12.}$$

Equation 5.12 is only an estimation of the bond slip factor for prestressing wires grouted in place. The author could find no experimental results on the relationship between the strain in bonded steel and the adjacent concrete. It is felt that for such conditions this factor is not equal to 1.0, although it is appreciated that it will be substantially greater than the factors used in the beams of the author and Khalil. The value proposed here varies from 1.0 to 0.75 for values of M/M_u ranging from 0 to 1.0.

5.2.4. Okada's[16] Results

Amongst the tests carried out by Okada et al, were 10 No. prestressed, plain concrete beams tested under varying combinations of bending moment and torsion. The beams were uniformly prestressed by a single 16 mm ($\frac{5}{8}$ in.) diameter bar and measured 100 mm x 200 mm (3.94 in. x 7.87 in.) in section. The experimental and theoretical results are compared in Tables 5.12 to 5.14.

The value of f_{r2} in Table 5.12 has been calculated using equation 5.7 with the value of f'_c obtained from the control specimens. P_{s2} is that value given by the investigator.

The theoretical solutions proposed for Mode 1 are those determined using the value of f_{r3} from equation 5.1 and the experimental value of f'_c. Equations 4.2.1.41 and 4.2.1.36 have been solved for d_n and T respectively. The suffix (a) has been omitted in this case

as the experimental value of f'_c has been used.

Shown below is a list of the terms used in the analysis of Okada's beams

$k_t = k_m = k_i = \frac{2}{3}$ - estimated

$d_1 = 100$ mm (3.937 in.) - given

$A_{sl} = 201$ mm^2 (0.3114 in^2) - given

$R = 2.5$ - estimated

$E_c = 2491 \sqrt{f'_c}$ N/mm^2 ($30{,}000 \sqrt{f'_c}$ lbs/in^2) - estimated

$E_{sl} = 19.3 \times 10^4$ N/mm^2 (28.00×10^6 lbs/in^2) - estimated

$P_{tl} = 148$ kN (33.17 kips) - given

$P_s = 7.38$ N/mm^2 (1070 lbs/in^2) - given

$C_1 = 0.375$ - estimated

$M_u = 16.24$ kN.m (143.75 kips.ins) - experimental

$$D_1 = \frac{1.0}{(1.0 + {}^{M}/_{3M_u})} \qquad \text{——— 5.12.}$$

D_1 has been estimated in the same manner as for Reynolds' results.

The analysis of the pure bending case (see Table 5.14) is very similar to that of the author's beams, equations 4.2.1.41 and 5.8 being used to solve for d_n and M_u respectively.

5.2.5. Zia's [9] Results

Zia reported tests, in pure torsion, on 68 pretensioned and plain concrete members consisting of rectangular, T, and I sections. Of the specimens tested 9 were rectangular prestressed beams 100 mm x 305 mm (4 in. x 12 in.) in section. Three of the beams were uniformly prestressed and the remaining 6 eccentrically prestressed. As a result of the shape of the section, and the fact that the beams were tested under a torsional moment only, the mode of failure in all cases was Mode 2. The theoretical results are compared with the experimental results in Table 5.15. The modulus of rupture value has been calculated using equation 5.7, and the torsional resistance T_2 using equation 4.3.9.(a). Knowing

the position and the force in each bar it was possible to calculate the prestressing stress P_{s2} using equations similar to those of 5.4 and 5.5.

5.2.6. Humphreys'[12] Results

The results of 57 prestressed rectangular beams tested under pure torsion are shown in Table 5.16. An average 100 mm (4 in.) cube strength was given for all beams in the series. The cylinder strength f'_c was determined using the relationship.

$$f'_c = 0.75\ U_w \qquad \text{——— 5.13.}$$

The beams were of varying cross-section and the uniform prestress was altered for each series as shown in the table. The results shown are the average of the number of beams shown in the first column. Equations 5.6 or 5.7 (depending on the size of b) were used to determine f_{r2}, and 4.3.9(a) was solved to estimate the torsional resistance T_2.

5.3. Discussion of Results

5.3.1. Author's Results

The theoretical solutions for the author's beams show good comparison with the experimental results as shown in Tables 5.1 to 5.4. It is apparent, however, that a better correlation is obtained using a concrete strength based upon the cube strength, rather than that strength obtained from the control specimens. This is particularly so for the case of those beams failing in Mode 1, shown in Table 5.3. This may be due to the fact that, the coefficient of variation on the cube strengths (shown in Table 3.1) is slightly less than that of the cylinder strenghts. It is also possible that the Cowan[25] criteria of failure, on which the Mode 1 failure is based, may be related to some function of the cube strength rather than to the cylinder strength. The difference between the two solutions is less defined

for Modes 3, and 2 as can be seen in Tables 5.1 and 5.2. This is not altogether unexpected as the expressions for f_{r3} and f_{r2} are functions of $\sqrt[3]{f'_c}$. Any change in the value of f'_c will be less significant in these cases than for Mode 1 where the strength is directly proportional to f'_c. This reduction in the difference may also be a result of the fact that in this case the failure criteria is not based upon that proposed by Cowan.

The failure mechanism of beam No. S.A.3 described in section 3.3 was observed to be of a Mode 2 nature. The theoretical solution for Mode 3, however, was less than that for Mode 2 and the results have therefore been included in Table 5.1. The opposite was true for beam No. S.A.4 where the observed failure was one of Mode 3 and the theoretical solution predicted a Mode 2 failure. This inconsistency is probably due to the fact that at this point the mode of failure is changing from Mode 3 to Mode 2. Although the theory assumes a sudden change between the two modes it is obvious that in practice this is not the case. The true solution is thought to lie somewhere between the two, with the compression hinge forming at some angle between the vertical and horizontal faces of the beam.

The theoretical solutions for Mode 2 failure (Table 5.2) show reasonable agreement with the experimental results for beams No.s S.A.4, 5, and 6. For the remainder of the beams shown the theoretical results, in general, appear to be appreciably lower than the experimental results. This phenomenon is thought to be related to the method by which the void for the prestressing bar was produced. In all beams after and including S.A.7 the prestressing bar was cast in-situ, previously the void had been preformed by a rubber tube (see 2.6.1. to 2.6.3.). It is thought

Beam No.	U_{w_2} N/mm^2 (lbs/in^2)	f_{r3} N/mm^2 (lbs/in^2)	f_{r3} equ^n.5.1 N/mm^2 (lbs/in^2)	P_{s3} N/mm^2 (lbs/in^2)	Experimental M kN.m (kips.ins)	Experimental T kN.m (kips.ins)	Ratio M/T	Theory equ^n.4.4.12. T_3 kN.m (kips.ins)	Ratio $\frac{T\ exp.}{T_3\ theo}$	Theory equ^n.4.4.12(a) T_3 kN.m (kips.ins)	Ratio $\frac{T\ exp.}{T_3\ theo.}$
1	48.24 (6995)	3.04 (441)	3.10 (449)	0 (0)	-0.15 (-1.28)	2.86 (25.27)	0.05	2.05 (18.12)	1.39	2.08 (18.45)	1.37
2	46.37 (6724)	2.61 (378)	3.06 (443)	0 (0)	0.86 (7.64)	3.18 (28.10)	0.27	2.42 (21.38)	1.31	2.83 (25.05)	1.12
3	43.80 (6351)	3.10 (449)	3.00 (435)	0 (0)	1.30 (11.53)	3.63 (32.14)	0.36	3.12 (27.59)	1.12	3.02 (26.73)	1.20

TABLE 5.1 Comparison of Author's Results - Mode 3

Beam No.	U_w N/mm^2 (lbs/in^2)	f_{r2} N/mm^2 (lbs/in^2)	f_{r2} equ^n.5.7 N/mm^2 (lbs/in^2)	P_{s2} N/mm^2 (lbs/in^2)	Experimental M kN.m (kips.ins)	Experimental T kN.m (kips.ins)	Ratio M/T	Theory equ^n.4.3.9 T_2 kN.m (kips.ins)	Ratio $\frac{T\ exp.}{T_2\ theo}$	Theory equ^n.4.3.9(a) T_2 kN.m (kips.ins)	Ratio $\frac{T\ exp.}{T_2\ theo.}$
4	51.22 (7427)	4.40 (638)	3.97 (575)	6.97 (1010)	1.89 (16.75)	3.40 (30.12)	0.56	3.29 (29.15)	1.03	3.07 (27.14)	1.11
5	53.09 (7695)	3.32 (482)	4.02 (583)	9.71 (1408)	2.43 (21.52)	3.40 (30.12)	0.71	3.07 (27.14)	1.11	3.46 (30.63)	0.98
6	52.24 (7575)	3.90 (566)	3.99 (579)	8.90 (1290)	2.87 (25.43)	3.85 (34.09)	0.75	3.29 (29.14)	1.17	3.34 (29.58)	1.15
7	52.02 (7543)	3.59 (520)	3.99 (579)	8.01 (1161)	3.29 (29.10)	4.42 (39.14)	0.74	3.00 (26.58)	1.47	3.22 (28.54)	1.37
8	61.50 (8917)	3.58 (519)	4.21 (610)	9.01 (1306)	3.83 (33.87)	4.42 (39.14)	0.87	3.13 (27.67)	1.42	3.48 (30.77)	1.27
9	60.94 (8836)	3.26 (473)	4.21 (610)	10.87 (1576)	4.96 (43.87)	4.19 (37.12)	1.18	3.16 (27.99)	1.40	3.71 (32.83)	1.19
10	57.26 (8302)	3.92 (568)	4.11 (596)	8.43 (1222)	7.53 (66.64)	4.76 (42.14)	1.58	3.24 (28.67)	1.47	3.34 (29.60)	1.42
11	56.14 (8141)	3.57 (517)	4.10 (593)	8.42 (1221)	13.23 (117.09)	4.38 (38.72)	3.02	3.05 (26.95)	1.44	3.33 (29.49)	1.31
20	47.21 (6845)	3.32 (482)	3.86 (560)	8.72 (1265)	10.60 (93.83)	3.86 (34.17)	2.75	2.95 (26.09)	1.31	3.25 (28.74)	1.19

TABLE 5.2 Comparison of Author's Results Mode 2

Beam No.	U_w N/mm^2 (lbs/in^2)	f'_c N/mm^2 (lbs/in^2)	f'_c equ^n.5.3 N/mm^2 (lbs/in^2)	Experimental M kN.m (kips.ins)	Experimental T kN.m (kips. ins)	Ratio M/T	Theory equ^n.4.2.1.41 d_n mm (ins.)	Theory equ^n.4.2.1.36 T kN.m (kips.ins)	Ratio T exp. / T theo.	Theory equ^n. 4.2.1.41(a) d_n mm (ins.)	Theory equ^n. 4.2.1.36(a) T kN.m (kips.ins)	Ratio T exp. / T theo.
13	57.33 (8313)	37.39 (5422)	45.86 (6650)	16.70 (147.75)	4.20 (37.20)	3.97	66.0 (2.60)	2.93 (25.94)	1.43	64.0 (2.52)	3.52 (31.11)	1.20
14	56.18 (8146)	37.55 (5445)	44.94 (6517)	18.19 (160.99)	3.63 (32.14)	5.01	64.3 (2.53)	2.49 (22.08)	1.46	62.5 (2.46)	2.93 (25.89)	1.24
17	55.47 (8043)	40.68 (5899)	44.37 (6434)	18.59 (164.53)	1.80 (15.96)	10.31	65.5 (2.58)	1.52 (13.43)	1.19	64.8 (2.55)	1.64 (14.52)	1.10
18	54.87 (7956)	45.67 (6622)	43.90 (6365)	15.70 (138.98)	2.47 (21.83)	6.37	70.1 (2.76)	2.70 (23.91)	0.91	69.6 (2.74)	2.58 (22.84)	0.96
19	49.21 (7137)	36.34 (5269)	39.38 (5710)	17.08 (151.12)	2.47 (21.83)	6.92	67.6 (2.66)	1.96 (17.32)	1.26	67.1 (2.64)	2.11 (18.63)	1.17
21	45.86 (6650)	44.52 (6455)	36.69 (5320)	14.91 (131.99)	2.95 (26.07)	5.06	71.6 (2.82)	3.18 (28.11)	0.93	72.9 (2.87)	2.65 (23.43)	1.11

TABLE 5.3 Comparison of Author's Results - Mode 1 - Dowel Force

Beam No.	U_w N/mm^2 (lbs/in^2)	f'_c N/mm^2 (lbs/in^2)	f'_c equ^n.5.3 N/mm^2 (lbs/in^2)	Experimental		Ratio	Theory equ^n. 4.2.1.41. d_n mm (ins.)	Theory equ^n.5.8 Mu kN.m (kips.ins)	Ratio $\frac{Mu\ exp.}{Mu\ theo}$	Theory equ^n. 4.2.1.41(a) d_n mm (ins.)	Theory equ^n.5.8(a) Mu kN.m (kips.ins)	Ratio $\frac{Mu\ exp.}{Mu\ theo}$
				M kN.m (kips.ins)	T kN.m (kips.ins)	M/T						
16	49.84 (7227)	41.83 (6065)	39.88 (5782)	17.20 (152.25)	0 (0)	∞	70.1 (2.76)	17.65 (156.22)	0.97	70.4 (2.77)	16.89 (149.46)	1.02
22	44.89 (6509)	35.72 (5179)	35.91 (5207)	16.95 (150.00)	0 (0)	∞	70.9 (2.79)	15.21 (134.62)	1.11	70.9 (2.79)	15.27 (135.14)	1.11

TABLE 5.4 Comparison of Author's Results - Pure Bending

Beam No.	Ratio $\frac{T\ exp.}{T\ theo.}$	
	Linear	Non Linear
13	1.20	1.25
14	1.24	1.26
17	1.10	1.08
18	1.17	1.17
19	0.96	0.98
21	1.11	1.15

TABLE 5.5 General Comparison of Linear and Non-Linear Theories - Mode 1

Author's Beams - Dowel Force

that with the bar cast in place there may be a dowel action set up after the first crack has been formed. It is possible that this dowel action has the effect of delaying failure to an extent when the concrete in the compression zone fails by crushing. This may also account for the shape of the principal tensile strain curves shown in Fig. 3.13. Those of beams Nos. S.A. 7, 8, 10, and 11 can be seen to continue for some time after the graph has ceased to become linear. With reference to Fig. 3.13 the theoretical failure loads for the above mentioned beams have been plotted on this graph. The loads, on the whole, coincide closely with the points at which their respective graphs become non-linear. Although experimental observations did not indicate cracking in these beams before failure it is possible that such cracks, although present, were not visible. No dowel action was thought to have occurred in those beams in which the void was preformed. In such cases the bar has room to move in the void and disrupture will therefore take place immediately after the formation of the first crack.

The theoretical solutions for Mode I, (see Table 5.3) using a computed value of f'_c, show good comparison with the experimental results. The experimental to theoretical ratio for Nos. S.A.13 and 14 are however, somewhat higher than the remainder. It is possible that these beams, failing under a relatively lower M/T ratio than the remainder, were in fact failing in some mode between 2 and 1. As was the case for beams S.A.3 and 4 failing between Modes 2 and 3, there is thought to be some transition between the different modes. In this case the theoretical solution for Mode 1 predicts an ultimate load lower than the experimental load, and that for Mode 2 predicts a higher ultimate load.

Table 5.5 shows a comparison between the theoretical solutions obtained using a linear and a non-linear stress-strain relationship for

the concrete. There can be seen from the table to be very little difference between the two theories. The relationship

$E_c = 2491 \sqrt{f'_c}$ N/mm^2 ($30{,}000 \sqrt{f'_c}$ lbs/in^2) used for the linear approach can therefore be assumed to be a good representation of the behaviour of the author's concrete tested under the conditions described.

A comparison between the dowel force, and the no dowel force theories is shown in Table 5.18. The no dowel force solution has been carried out using equation 4.2.2.4 or 5 to determine the torsional resistance. The computed values of f_{r3} and f'_c have been used in the analysis of both sets of results. In addition, the factors listed in 5.2.1 used for the dowel force theory have also been adopted in the no dowel force approach. It can be seen from the table that the presence of a dowel force considerably increases the torsional resistance of the beam. If the dowel force is ignored then the predicted collapse load may be as much as 50% below the experimental load.

In the solution for the angle of inclination, θ, of the compression hinge (see 4.2.4) it was assumed that the M/T ratios at cracking and ultimate were the same. This was not the case with the author's beams due to the way in which the loads were applied. It has been shown, during the theoretical analysis, that a 10% change in the value of tan θ will only effect the resulting torsional resistance by as little as 1%. This is a result of the format of the 2 equations (i.e. 4.2.1.37 and 38) containing $\tan\theta$, used to obtain a value of d_n. In this case the factor $(R.D_1-1)$ is very nearly equal to zero as D_1 is in general, approximately equal to 0.4. The term C_d, containing $\tan\theta$, therefore has very little effect on the value of Rd.

As a result of the relatively high M/T ratios the term T tan θ contained in the denomination of equation 4.2.1.38 tends to be small compared with M. The overall change in the value of Rd is therefore very small for a large change in tan θ. A comparison between the values of tan θ obtained using the ratios M_c/T_c and M/T is given in Table 5.19. The largest change in tan θ occurred in beam No. S.A.13. This yielded an increase of 70% in its value by using the two different ratios. Even such a large increase will only effect the predicted torsional load by approximately 7%.

The theoretical analysis has also shown that a small change in the value of d_n will produce a similar change in the value of T. This is to be expected from the form of equation 4.2.1.36 which can be seen to vary almost directly with d_n.

The means and coefficients of variation for the author's results, based upon the concrete strengths computed from the cube strengths, are presented in Table 5.17. The coefficient of variation is comparable with that of the concrete cube strengths (see Table 3.1).

5.3.2. Khalil's Results

The results of Khalil's beams for Modes 2 and 3 show good correlation with the theoretical loads (see Tables 5.6 and 5.7). The difference produced using the modified modulus of rupture value and that obtained from the cube strength is less marked than with the author's beams.

The failure mechanism of beam No. E_T was reported by Khalil to be one of Mode 2. The theoretical solutions proposed here predicted a lower collapse load for Mode 3 than for Mode 2. As explained in section 5.3.1 the true mechanism of failure probably lies between the two. The experimental to theoretical ratio for this beam is therefore appreciably higher than the remainder.

Prestressing was effected by means of post-tensioned, unbonded wires placed in preformed ducts in the beam. It was therefore thought that no dowel action would take place in the beams. Consequently those failing in Mode 2 would collapse immediately after the formation of the first crack. This is substantiated by the fact that the theoretical collapse loads for this mode are close to the experimental loads as shown in Table 5.7.

The theoretical solutions for Mode 1 shown in Table 5.8 have been predicted using the no dowel force theory. The experimental results show reasonable agreement with the theory although the coefficient of variation of 16% (see Table 5.17) is rather high.

In general the theoretical results tend to be high for the low M/T ratios and low for the high M/T ratios. It is possible that the relationship $E_c = 2491 \sqrt{f'_c}$ N/mm^2 ($30{,}000 \sqrt{f'_c}$ lbs/in^2) does not hold true for this particular concrete. A figure of $E_c = 3740 \sqrt{f'_c}$ N/mm^2 ($45{,}000 \sqrt{f'_c}$ lbs/in^2) may be more applicable in this case. Such a change would have the effect of reducing the value of T in the proposed theoretical solutions. It is also possible that a non-linear relationship for the concrete may effect Khalil's results to a greater degree than the author's. Many of Khalil's beams were tested under lower M/T ratios than the author's. It may be that the concrete in these beams had a higher E_c value than those tested under higher bending moments. This would result in a reduction in the theoretical load for those beams in the low M/T range and a possible increase for those in the high range.

Unlike the prestressing steel in the author's beams there was a non-linear stress-strain relationship in the steel over the tested range. The values of the modulus of elasticity used (see 5.2.2)

Beam No.	U_w N/mm^2 (lbs/in^2)	f_{r3} equ^n.5.9 N/mm^2 (lbs/in^2)	f_{r3} equ^n.5.1 N/mm^2 (lbs/in^2)	P_{s3} N/mm^2 (lbs/in^2)	Experimental M kN.m (kips.ins)	Experimental T kN.m (kips.ins)	Ratio M/T	Theory equ^n. 4.4.12 T_3	Ratio $\frac{T\ exp.}{T_3\ theo.}$	Theory equ^n. 4.4.12(a) T_3	Ratio $\frac{T\ exp.}{T_3\ theo.}$
E_T	61.50 (8900)	3.04 (441)	3.20 (465)	0 (0)	0 (0)	5.39 (47.7)	0	3.74 (33.09)	1.44	3.94 (34.89)	1.37

TABLE 5.6 Comparison of Khalil's Results Mode 3

Beam No.	U_w N/mm^2 (lbs/in^2)	f_{r2} equ^n.5.10 N/mm^2 (lbs/in^2)	f_{r2} equ^n.5.3 N/mm^2 (lbs/in^2)	P_{s2} N/mm^2 (lbs/in^2)	Experimental M kN.m (kips.ins)	Experimental T kN.m (kips.ins)	Ratio M/T	Theory equ^n. 4.3.9. T_2 kN.m (kips.ins	Ratio $\frac{T\ exp.}{T_2\ theo.}$	Theory equ^n. 4.3.9(a) T_2 kN.m (kips.ins)	Ratio $\frac{T\ exp.}{T_2\ theo.}$
U_T	50.6 (7350)	3.95 (573)	3.64 (528)	6.90 (1000)	0 (0)	5.50 (48.70)	0	5.66 (50.09)	0.97	5.35 (47.39)	1.03
U_8	58.5 (8500)	3.80 (551)	3.82 (554)	6.90 (1000)	4.28 (37.90)	5.40 (47.80)	0.79	5.51 (48.78)	0.98	5.53 (48.96)	0.98
E_{11}	49.5 (7200)	3.12 (452)	3.62 (525)	6.28 (910)	4.38 (38.80)	5.51 (48.80)	0.80	4.68 (41.40)	1.18	5.18 (45.80)	1.07
E_1	58.0 (8400)	3.80 (551)	3.81 (552)	6.28 (910)	10.50 (93.20)	6.00 (53.00)	1.75	5.35 (47.34)	1.12	5.36 (47.40)	1.12

TABLE 5.7. Comparison of Kahlil's Results – Mode 2

Beam No.	U_w N/mm^2 (lbs/in^2)	f'_c equ^n.5.3 N/mm^2 (lbs/in^2)	Experimental M kN.m (kips.ins)	Experimental T kN.m (kips.ins)	Ratio M/T	Theory equ^n. 4.2.2.12(a) d_n mm (ins)	Theory equ^n. 4.2.2.5(a) T kN.m (kips.ins)	Ratio $\frac{T\ exp.}{T\ theo.}$
U_1	53.7 (7800)	43.0 (6240)	8.28 (73.40)	4.90 (43.50)	1.69	101.1 (3.98)	5.10 (45.12)	0.96
U_6	53.5 (7750)	42.7 (6200)	10.2 (91.10)	3.98 (35.30)	2.58	95.8 (3.77)	4.50 (39.80)	0.89
U_2	54.8 (7950)	43.9 (6360)	11.8 (104.80)	3.39 (30.10)	3.48	87.1 (3.43)	3.81 (33.71)	0.89
U_5	50.2 (7280)	40.2 (5824)	12.62 (111.80)	2.98 (25.80)	4.33	83.6 (3.29)	3.10 (27.45)	0.94
U_3	51.0 (7400)	40.8 (5920)	14.31 (127.10)	2.80 (24.80)	5.13	70.1 (2.76)	2.36 (20.91)	1.19
U_4	53.1 (7700)	42.5 (6160)	14.40 (127.70)	2.16 (19.20)	6.65	71.9 (2.83)	2.28 (20.19)	0.95
E_{13}	46.5 (6720)	37.1 (5376)	12.15 (107.80)	4.57 (40.50)	2.66	105.2 (4.14)	4.70 (41.57)	0.97
E_2	58.5 (8500)	46.9 (6800)	15.10 (133.20)	4.24 (37.30)	3.57	86.6 (3.41)	4.28 (37.87)	0.99

TABLE 5.8. Comparison of Khalil's Results - Mode 1 - No Dowel Force

Beam No.	U_w N/mm^2 (lbs/in^2)	f'_c equ^n.5.3 N/mm^2 (lbs/in^2)	Experimental		Ratio M/T	Theory equ^n. 4.2.2.12(a) d_n mm (ins)	Theory equ^n. 4.2.2.5(a) T kN.m (kips.ins)	Ratio $\frac{T\ exp.}{T\ theo.}$
			M kN.m (kips.ins)	T kN.m (kips.ins)				
E_{15}	46.5 (6720)	37.1 (5376)	15.70 (139.00)	3.57 (31.60)	4.40	87.9 (3.46)	3.38 (29.90)	1.06
E_3	57.3 (8300)	45.8 (6640)	16.90 (149.50)	3.23 (28.60)	5.23	80.8 (3.18)	3.55 (31.42)	0.91
E_4	58.0 (8400)	46.3 (6720)	19.00 (168.00)	2.74 (24.30)	6.91	69.1 (2.72)	2.65 (23.49)	1.03
E_5	55.2 (8000)	44.1 (6400)	18.60 (164.50)	2.22 (19.70)	8.35	73.9 (2.91)	2.58 (22.87)	0.86
E_{10}	46.5 (6720)	37.1 (5376)	20.40 (180.40)	2.40 (21.20)	8.50	64.3 (2.53)	1.79 (15.87)	1.34
E_6	59.3 (8580)	47.3 (6864)	23.10 (204.50)	2.34 (20.70)	9.89	52.3 (2.06)	1.61 (14.24)	1.45
E_7	55.5 (8050)	44.4 (6440)	22.00 (194.90)	1.98 (17.50)	11.14	56.9 (2.24)	1.62 (14.35)	1.22
E_8	57.0 (8250)	45.5 (6600)	22.30 (197.20)	1.75 (15.50)	12.72	56.1 (2.21)	1.52 (13.49)	1.15

TABLE 5.8 Continued. Comparison of Khalil's Results Mode 1 - No Dowel Force

Beam No.	U_w N/mm^2 (lbs/in^2)	f'_c equ^n.5.3 N/mm^2 (lbs/in^2)	Experimental		Ratio M/T	Theory equ^n. 4.2.2.12 d_n mm (ins)	Theory equ^n.5.11 M_u kN.m (kips.ins)	Ratio $\frac{M_{u.exp.}}{M_{u\ theo.}}$
			M kN.m (kips.ins)	T kN.m (kips.ins)				
U_B	60.4 (8750)	48.3 (7000)	17.20 (152.20)	0 (0)	∞	54.6 (2.15)	21.94 (194.20)	0.78
E_B	59.2 (8570)	47.3 (6850)	25.50 (226.00)	0 (0)	∞	47.2 (1.86)	23.39 (206.97)	1.09

TABLE 5.9 - Comparison of Khalil's Results - Pure Bending

were those recommended by Khalil. Although these values vary for each layer of steel, depending upon the initial prestressing force, no account has been taken of the change in these values under the applied load. The only significant change will occur in the lower layers of steel in both the U and E beams. The tensile forces resisted by the steel will reduce its modulus of elasticity under high bending moments. A non-linear stress-strain relationship for the steel may therefore help to reduce the coefficient of variation of the results. If this relationship were adopted an increase in the modulus of elasticity for beams tested under low M/T ratios would result in an increase in the theoretical load. The reverse is true for beams under high M/T ratios. Although this on its own may not apparently improve the results a combination of non-linear stress - strain relationships in both the steel and the concrete could effect the results. Numerical analysis has shown, that the theoretical solution for low M/T ratios is less sensitive to changes in the modulus of elasticity values than are those for high M/T ratios. A 30% change in the value of E_c produces a 4% variation in T for a beam with an M/T ratio of 1.7. A similar change in E_c results in a 15% change in T for a beam failing under an M/T ratio of 12.7.

The assumption made in 5.2.2 concerning the relationship between the cube strength and the cylinder strength (i.e. $f'_c = 0.8\ U_w$) may not hold true for this particular concrete. Khalil assumed the relationship $f'_c = 0.84\ U_w$ but for consistency the author has used the relationship of equation 5.3.

Khalil's beams were loaded at a predetermined M/T ratio, the ratio at cracking being very nearly equal to that at ultimate. The assumption made in 4.2.4 concerning the inclination of the compression hinge at failure is therefore correct.

The effect of d_n upon the theoretical value of T is dependent upon the M/T ratio. A 1% change in d_n will produce a 5% variation in T for low M/T ratios and a 1% variation for high M/T ratios.

Table 5.18 shows a comparison between the dowel force and the no dowel force theories for Khalil's beams. The dowel force solutions were obtained using equations 4.2.1.28 and 4.2.1.15 for the E beams and equations 4.2.1.41 and 4.2.1.36 for the U beams. The dowel force theory predicts ultimate loads as much as 80% above the experimental loads. This difference is, however, more pronounced at the low M/T ratios. In those beams which failed under high M/T ratios, the theoretical loads were as little as 14% above the experimental values. In some cases the loads predicted by the dowel force theory were closer approximations to the experimental loads than those predicted by the no dowel force theory. It is possible that under high bending moments there is a certain amount of dowel action taking place. This could be due to the fact that at these high bending moments the deflection of the beam is sufficient to cause the prestressing bar to move to the top of its void. Once in contact with the concrete there may be sufficient friction between the two to allow a limited dowel force to be set up in the steel. It is very unlikely that this force will be as large as that produced in the steel bar of the author's beams. It may be large enough, however, to arrest the failure of the beam and hence increase, to a small extent, its carrying capacity. This phenomenon may account for the relatively high values of the experimental to theoretical ratio for those beams failing under high bending moments.

5.3.3. Reynolds' Results

The theoretical solutions for Modes 2 and 1 (see Tables 5.10 and 11) are in general approximately 25% above the experimental loads. The coefficients of variation (see Table 5.17) of 7% and 9% for Modes 2 and 1 respectively are, however, acceptable. The cube crushing strength of Reynolds' concrete was lower than that used by both Khalil and the author. The relationship between the cylinder strength and the cube strength used previously may not be applicable in this case. A factor of $f'_c = 0.75\ U_w$ may be more suited to the concrete of this investigation.

Prestressing was carried out by means of 2 No. 5 mm (0.2 in.) diameter wires grouted in position. The fact that the wires were grouted indicates the possibility of a dowel action occuring in the beam. It is considered unlikely that the dowel force resisted by a prestressed wire will be as great as that resisted by a steel bar. The flexibility of a wire, even when stressed, will be greater than that of a steel bar, and consequently the dowel force it will be able to resist will be reduced. The theoretical solutions proposed in Table 5.11 have been calculated using the same approach as for the author's beams. The flexibility of the wire and the resulting reduction in dowel force could account for experimental results being below those calculated. There is also some doubt as to the value of the bond slip factor of prestressed wires grouted in position. As mentioned in 5.2.3 no experimental evidence on the subject was available, and the factor obtained from equation 5.12 is only an estimation. The values computed from this equation may be too large for Reynolds' beams which would account for the high theoretical solutions.

The information available, concerning the properties of the steel and the concrete, was very limited. The factors used for

Beam No.	U_w N/mm^2 (lbs/in^2)	f_{r2} equ^n.5.7 N/mm^2 (lbs/in^2)	P_{s2} N/mm^2 (lbs/in^2)	Experimental		Ratio M/T	Theory equ^n. 4.3.9(a) T_2 kN.m (kips. ins)	Ratio $\frac{T\ exp.}{T\ theo.}$
				M kN.m (kips.ins)	T kN.m (kips.ins)			
1	44.14 (6400)	4.39 (636)	6.21 (900)	0.68 (6.00)	0.55 (4.90)	1.22	0.66 (5.80)	0.85
2	44.14 (6400)	4.39 (636)	6.21 (900)	0.68 (6.00)	0.55 (4.90)	1.22	0.66 (5.80)	0.85
3	44.14 (6400)	4.39 (636)	6.21 (900)	0.81 (7.20)	0.49 (4.35)	1.66	0.66 (5.89)	0.75

TABLE 5.10 Comparison of Reynolds' Results - Mode 2

Beam No.	U_w N/mm^2 (lbs/in^2)	f'_c equ^n.5.3 N/mm^2 (lbs/in^2)	Experimental		Ratio M/T	Theory equ^n. 4.2.1.41(a) d_n mm (ins.)	Theory equ^n. 4.2.1.36(a) T kN.m (kips.ins)	Ratio $\frac{\text{T exp.}}{\text{T theo.}}$
			M kN.m (kips.ins)	T kN.m (kips.ins)				
4	44.83 (6500)	35.86 (5200)	0.99 (8.80)	0.48 (4.25)	2.07	37.3 (1.47)	0.65 (5.75)	0.74
5	44.83 (6500)	35.86 (5200)	1.36 (12.00)	0.47 (4.20)	2.86	34.3 (1.35)	0.57 (5.01)	0.84
6	44.83 (6500)	35.86 (5200)	1.49 (13.20)	0.40 (3.50)	3.77	36.8 (1.45)	0.53 (4.67)	0.75
7	46.21 (6700)	36.97 (5360)	1.53 (13.50)	0.41 (3.60)	3.75	39.1 (1.54)	0.60 (5.29)	0.68
8	46.21 (6700)	36.97 (5360)	1.75 (15.50)	0.42 (3.75)	4.13	34.5 (1.36)	0.52 (4.58)	0.82
9	46.21 (6700)	36.97 (5360)	1.62 (14.30)	0.40 (3.45)	4.14	35.1 (1.38)	0.50 (4.39)	0.79
10	48.97 (7100)	39.17 (5680)	1.93 (17.10)	0.40 (3.45)	4.96	30.5 (1.20)	0.42 (3.75)	0.92
11	48.97 (7100)	39.17 (5680)	1.86 (16.50)	0.32 (2.80)	5.89	33.3 (1.31)	0.40 (3.53)	0.79
12	48.97 (7100)	39.17 (5680)	2.03 (18.00)	0.31 (2.70)	6.67	31.0 (1.22)	0.34 (2.98)	0.89

TABLE 5.11 Comparison of Reynolds Results – Mode 1 – Dowel Force

determining the modulus of elasticity of both materials (see 5.2.3) have only been estimated, and may not in fact be correct. It is also possible that a non-linear stress-strain relationship for one or both of the materials may be more applicable in this case.

The loads on the test specimens were applied simultaneously and as a result the M/T ratio was constant throughout the test. The assumption, made in section 4.2.9 concerning the relationship between the M/T ratio at cracking and ultimate is therefore correct.

The results obtained using the no dowel force theory are shown in Table 5.18. Equation 4.2.2.15 was solved for d_n and 4.2.2.4 or 5 used to determine T. The factors, listed in section 5.2.3, used for the dowel force approach were again used with the exception of the bond slip factor. As it was considered that there was no dowel force then it must also be assumed that there was no bond between the steel and the concrete. The factor given by equation 4.2.3.1 and used for both the author's and Khalil's beams was therefore used. As with the case previously, the dowel force theory predicts a higher failure load than the no dowel force approach. It is apparent that the no dowel force theory is more applicable to those beams failing under low M/T ratios. As mentioned previously this could be due to the flexibility of the prestressing wire which may be reduced as the applied bending moment is increased. A reduction in the flexibility would mean an increase in the dowel force. This is substantiated by the fact the dowel force theory is more applicable to the beams in the high M/T range.

5.3.4. Okada's Results

The prestressing steel used in Okada's beams was a single 16 mm ($\frac{5}{8}$ in.) diameter bar. It was not reported whether or not the

bar was grouted after stressing. For the purpose of this analysis the bond slip factor has been taken as that obtained from equation 5.12.

The variation of the experimental to theoretical ratio (see Table 5.12) for Mode 2 is very small the coefficient of variation being 6% (see Table 5.17). The fact that the average value of this ratio is greater than 1.0 is possibly due to the effect of a dowel action. A similar effect was reported in the discussion on the author's results in section 5.3.1. Another factor which may have influenced the results was the concrete crushing strength. In all previous calculations the cylinder crushing strength has been calculated from the cube strength using equation 5.3. Okada has only reported an average cylinder strength for all his beams tested in this series. Had a cube strength been reported it may have yielded a different cylinder strength when substituted into equation 5.3.

Since only 2 of Okada's beams were considered to fail in Mode I (see Table 5.13) it is not very meaningful to draw any conclusions from the results. The theoretical results do, however, show good agreement with those obtained from the experiments. This indicates that the assumptions made concerning the dowel force and bond slip factor are probably correct. The theoretical results for the cases of pure bending are somewhat less than those obtained from the experiments. This may suggest a need for a reduction in the modulus of elasticity value of the steel for the cases of high bending moments.

Those results obtained from the no dowel force theory (see Table 5.18) show an average reduction of 25% in the predicted collapse load. As with Reynolds' beams, the bond slip factor in this case was taken as that obtained from equation 4.2.3.1.

Beam No.	f'_c N/mm^2 (lbs/in^2)	f_{r2} equ^n.5.7 N/mm^2 (lbs/in^2)	P_{s2} N/mm^2 (lbs/in^2)	Experimental		Ratio M/T	Theory equ^n. 4.3.9(a) T_2 kN.m (kips.ins)	Ratio $\frac{T\ exp.}{T_2\ theo.}$
				M kN.m (kips.ins)	T kN.m (kips.ins)			
P_s1	39.6 (5740)	3.92 (568)	7.38 (1070)	0 (0)	4.34 (38.45)	0	3.59 (31.76)	1.21
P_s2	39.6 (5740)	3.92 (568)	7.38 (1070)	0 (0)	4.51 (39.95)	0	3.59 (31.76)	1.26
P_s3	39.6 (5740)	3.92 (568)	7.38 (1070)	1.82 (16.14)	4.40 (38.98)	0.41	3.59 (31.76)	1.23
P_s4	39.6 (5740)	3.92 (568)	7.38 (1070)	1.71 (15.17)	4.15 (36.69)	0.41	3.59 (31.76)	1.16
P_s5	39.6 (5740)	3.92 (568)	7.38 (1070)	4.03 (35.63)	4.03 (35.63)	1.0	3.59 (31.76)	1.12
P_s6	39.6 (5740)	3.92 (568)	7.38 (1070)	3.89 (34.39)	3.89 (34.39)	1.0	3.59 (31.76)	1.08

TABLE 5.12 – Comparison of Okada's Results – Mode 2

Beam No.	f'_c N/mm^2 (lbs/in^2)	Experimental		Ratio M/T	Theory equ^n. 4.2.1.41 d_n mm (ins)	Theory equ^n. 4.2.1.36 T kN.m (kips.ins)	Ratio $\frac{T\ exp.}{T\ theo.}$
		M kN.m (kips.ins)	T kN.m (kips.ins)				
P_s7	39.6 (5740)	8.12 (71.87)	3.36 (29.72)	2.42	71.1 (2.80)	3.26 (28.82)	1.03
P_s8	39.6 (5740)	8.24 (72.93)	3.39 (29.98)	2.43	70.6 (2.78)	3.23 (28.62)	1.05

TABLE 5.13 - Comparison of Okada's Results - Mode 1 - Dowel Force

Beam No.	f'_c N/mm^2 (lbs/in^2)	Experimental		Ratio M/T	Theory equ^n. 4.2.1.41 d_n mm (ins)	Theory equ^n.5.8 M_u kN.m (kips.ins)	Ratio $\frac{M_u\ exp.}{M_u\ theo.}$
		M_u kN.m (kips.ins)	T kN.m (kips.ins)				
P_s9	39.6 (5740)	16.24 (143.75)	0 (0)	∞	60.7 (2.39)	12.33 (109.13)	1.32
P_s10	39.6 (5740)	15.05 (133.17)	0 (0)	∞	63.8 (2.51)	12.76 (112.96)	1.18

TABLE 5.14 - Comparison of Okada's Results - Pure Bending

The M/T ratio was kept constant throughout the test and as before the assumption made in 4.2.4 concerning this factor can be assumed to be correct.

5.3.5. Zia's Results

Table 5.15 shows a comparison of tests by Zia, in pure torsion, on 9 rectangularly prestressed, pretensioned, beams. The overall mean of the experimental to theoretical ratio is low, being 0.84, although the coefficient of variation of 5% (see Table 5.17) is good. The reported value of the cylinder crushing strength is exceptionaly large. This value is approximately 40% higher than the average computed cylinder strengths of all other investigators reported in this section. Such a difference would effect the computed modulus of rupture value by 10% and hence alter the mean of the ratio from 0.84 to 0.94. As no cube strengths were reported it was not possible to compare the cylinder strengths obtained from equation 5.3 with those of other investigators.

It is not clear whether the prestressing wire used in Zia's beams is producing a dowel force great enough to effect the failure loads in Mode 2. From the results shown in Table 5.15 it is doubtful whether this is the case.

5.3.6. Humphreys' Results

Humphreys' results (see Table 5.16) on 57 prestressed rectangular beams tested in pure torsion show good correlation with the theoretical solutions. A summary of the means and coefficients of variation for the various beam sizes is given in Table 5.17.

Humphreys reported an average 100 mm (4 in.) cube strength for all the beams tested throughout his investigation. To obtain an equivalent cylinder crushing strength it was decided to use a relationship of $f'_c = 0.75\ U_w$. This should be compared with the factor of 0.8 used for the results on 150 mm (6 in.) cube strengths.

Beam No.	f'_c N/mm^2 (lbs/in^2)	f_{r2} equ^n.5.7 N/mm^2 (lbs/in^2)	P_{s2} N/mm^2 (lbs/in^2)	Experimental		Ratio M/T	Theory equ^n.4.3.9(a) T_2 kN.m (kips.ins)	Ratio $\frac{T\ exp.}{T_2 theo.}$
				M kN.m (kips.ins.)	T kN.m (kips.ins)			
OR 1	55.52 (8050)	4.37 (634)	7.02 (1018)	0 (0)	4.99 (44.20)	0	6.21 (54.93)	0.80
OR 2	55.52 (8050)	4.37 (634)	7.02 (1018)	0 (0)	5.25 (46.50)	0	6.21 (54.93)	0.85
OR 3	56.55 (8200)	4.40 (638)	6.95 (1008)	0 (0)	5.28 (46.72)	0	6.21 (55.00)	0.85
2R 1	58.62 (8500)	4.45 (645)	7.18 (1041)	0 (0)	5.41 (47.90)	0	6.32 (55.97)	0.86
2R 2	58.90 (8540)	4.46 (647)	7.18 (1041)	0 (0)	5.77 (51.04)	0	6.34 (56.09)	0.91
2R 3	58.90 (8540)	4.46 (647)	7.18 (1041)	0 (0)	5.56 (49.24)	0	6.34 (56.09)	0.88
2.5R1	58.90 (8540)	4.46 (647)	6.94 (1007)	0 (0)	5.16 (45.64)	0	6.27 (55.52)	0.82
2.5R2	58.90 (8540)	4.46 (647)	6.94 (1007)	0 (0)	5.34 (47.24)	0	6.27 (55.52)	0.85
2.5R3	58.90 (8540)	4.46 (647)	6.94 (1007)	0 (0)	4.86 (43.04)	0	6.27 (55.52)	0.78

TABLE 5.15. Comparison of Zia's Results Mode 2

Beam No.	Beam size mm (ins.)	U_w N/mm^2 (lbs/in^2)	f_{r2} equ^n. 5.6or5.7 N/mm^2 (lbs/in^2)	P_{s2} N/mm^2 (lbs/in^2)	Experimental		Ratio M/T	Theory equ^n. 4.3.9(a) T_2 kN.m (kips.ins)	Ratio T exp. / T theo.
					M kN.m (kips.ins)	T kN.m (kips.ins)			
P2 A,B,C, D	127x127 (5x5)	60.21 (8730)	3.79 (549)	8.70 (1261)	0 (0)	2.86 (25.30)	0	3.52 (31.13)	0.81
P3 A,B,C	127x127 (5x5)	60.21 (8730)	3.79 (549)	12.34 (1790)	0 (0)	3.31 (29.33)	0	4.00 (35.41)	0.84
P4 A,B,C	127x127 (5x5)	60.21 (8730)	3.79 (549)	19.17 (2780)	0 (0)	4.69 (41.47)	0	4.77 (42.23)	0.98
P5 A,B, C,X	127x127 (5x5)	60.21 (8730)	3.79 (549)	24.92 (3613)	0 (0)	5.36 (47.44)	0	5.34 (47.22)	1.00
P6 A,B,C	127x127 (5x5)	60.21 (8730)	3.79 (549)	30.50 (4423)	0 (0)	5.98 (52.95)	0	5.83 (51.63)	1.03
P7 A,B,C	127x127 (5x5)	60.21 (8730)	3.79 (549)	42.07 (6100)	0 (0)	5.10 (45.17)	0	6.75 (59.70)	0.76
PR2 A,B,C	127x254 (5x10)	60.21 (8730)	3.79 (549)	6.01 (872)	0 (0)	6.05 (53.50)	0	6.73 (59.56)	0.90
PR3 A	127x254 (5x10)	60.21 (8730)	3.79 (549)	14.14 (2050)	0 (0)	8.23 (72.80)	0	9.10 (80.56)	0.90

TABLE 5.16 Comparison of Humphreys' Results Mode 2

Beam No.	Beam Size mm (ins)	U_w N/mm^2 (lbs/in^2)	f_{r2} equ^n. 5.6or 5.7 N/mm^2 (lbs/in^2)	P_{s2} N/mm^2 (lbs/in^2)	Experimental		Ratio M/T	Theory equ^n. 4.3.9(a) T_2 kN.m (kips.ins)	Ratio $\frac{T\ exp.}{T_2\ theo.}$
					M kN.m (kips. ins)	T kN.m (kips. ins)			
PR4 A,B,C	127x254 (5x10)	60.21 (8730)	3.79 (549)	18.12 (2627)	0 (0)	9.23 (81.70)	0	10.06 (89.04)	0.92
PR6 A,B,C	127x254 (5x10)	60.21 (8730)	3.79 (549)	29.24 (4240)	0 (0)	11.22 (99.27)	0	12.35 (109.34)	0.91
PS2 A,B,C	127x381 (5x15)	60.21 (8730)	3.79 (549)	4.15 (602)	0 (0)	9.00 (79.70)	0	9.41 (83.29)	0.96
PS4 A,B,C	127x381 (5x15)	60.21 (8730)	3.79 (549)	15.31 (2220)	0 (0)	14.22 (125.87)	0	14.61 (129.32)	0.97
PS6 A,B,C	127x381 (5x15)	60.21 (8730)	3.79 (549)	26.37 (3823)	0 (0)	19.15 (169.50)	0	18.35 (162.41)	1.04
PT2 A,B,C	76 x229 (3x9)	60.21 (8730)	4.48 (650)	4.26 (617)	0 (0)	2.10 (18.56)	0	2.32 (20.55)	0.90
PT4 A,B,C	76x229 (3x9)	60.21 (8730)	4.48 (650)	11.84 (1717)	0 (0)	3.31 (29.28)	0	3.17 (28.08)	1.04
PT6 A,B,C	76x229 (3x9)	60.21 (8730)	4.48 (650)	18.41 (2670)	0 (0)	4.23 (37.46)	0	3.76 (33.24)	1.13

TABLE 5.16 Continued Comparison of Humphreys' Results. Mode 2

Beam No.	Beam Size mm (ins)	U_w N/mm^2 (lbs/in^2)	f_{r2} equ^n. 5.6or5.7 N/mm^2 (lbs/in^2)	P_{s2} N/mm^2 (lbs/in^2)	Experimental		Ratio M/T	Theory equ^n.4.3.9(a) T_2 kN.m (kips.ins.)	Ratio $\frac{T\ exp.}{T_2\ theo.}$
					M kN.m (kips.ins)	T kN.m (kips. ins)			
PU2 A,B,C	76x305 (3x12)	60.21 (8730)	4.48 (650)	4.43 (643)	0 (0)	3.52 (31.18)	0	3.20 (28.29)	1.10
PU4 A,B,C	76x305 (3x12)	60.21 (8730)	4.48 (650)	11.36 (1647)	0 (0)	4.88 (43.22)	0	4.26 (37.69)	1.15
PU6 A,B,C	76x305 (3x12)	60.21 (8730)	4.48 (650)	23.17 (3360)	0 (0)	5.83 (51.63)	0	5.63 (49.81)	1.04

TABLE 5.16 Continued. Comparison of Humphreys' Results Mode 2

Investigator	Beam size mm (ins)	Number of Beams	Mode of Failure	Mean $\frac{T\ exp.}{T\ theo.}$	% Coeff. Variation
Author (preferred results) Dowel force	100x175 (3.9x6.9)	3	3	1.23	10%
		9	2	1.22	11%
		6	1	1.13	9%
Khalil (preferred results) No Dowel Force	127x203 (5x8)	1	3	1.37	
		4	2	1.05	6%
		16	1	1.05	16%
Reynolds Dowel Force	64x91 (2.5x3.6)	3	2	0.82	7%
		9	1	0.80	9%
Okada Dowel Force	100x200 (3.9x7.9)	6	2	1.18	6%
		2	1	1.04	1%
Zia	102x305 (4x12)	9	2	0.84	5%
Humphreys	127x127 (5x5)	20	2	0.90	13%
	127x254 (5x10)	10	2	0.91	1%
	127x381 (5x15)	9	2	0.99	4%
	76x229 (3x9)	9	2	1.02	11%
	76x305 (3x12)	9	2	1.10	5%
Total + Pure Bending Tests		131	Average	1.02	17%

TABLE 5.17

General Comparison of Results

Investigator	Beam No.	Ratio $\frac{T\ exp.}{T\ theo.}$	
		Dowel Force	No Dowel Force
Author	13	1.20	2.27
	14	1.24	2.14
	17	1.10	1.33
	18	0.96	1.33
	19	1.17	1.62
	21	1.11	1.66
Reynolds	4	0.74	
	5	0.84	1.12
	6	0.75	1.01
	7	0.68	0.90
	8	0.82	1.35
	9	0.79	1.17
	10	0.92	1.73
	11	0.79	1.24
	12	0.89	1.50
Okada	P_s7	1.03	1.26
	P_s8	1.05	1.30

Investigator	Beam No.	Ratio $\frac{T\ exp.}{T\ theo.}$	
		Dowel Force	No Dowel Force
Khalil	U_1	0.59	0.96
	U_6	0.57	0.89
	U_2	0.60	0.89
	U_5	0.67	0.94
	U_3	0.79	1.19
	U_4	0.74	0.95
	E_{13}	0.60	0.97
	E_2	0.55	0.99
	E_{15}	0.66	1.06
	E_3	0.58	0.91
	E_4	0.67	1.03
	E_5	0.64	0.86
	E_{10}	0.92	1.34
	E_6	0.94	1.45
	E_7	0.89	1.22
	E_8	0.88	1.15

TABLE 5.18

General Comparison of Dowel Force and No Dowel Force Theories

Beam No.	Cracking		Ultimate	
	M_c/T_c	tan θ	M/T	tan θ
13	12.50	0.273	3.97	0.781
14	12.50	0.273	5.01	0.649
17	12.50	0.273	10.31	0.325
18	4.90	0.667	6.37	0.532
19	5.50	0.620	6.92	0.510
21	12.50	0.290	5.06	0.675

TABLE 5.19

Comparison of tan θ using Cracking and Ultimate Moments – Author's Beams

It is not certain whether the factor mentioned above is applicable to the concrete used in this series of tests.

Humphreys' beams were prestressed in a similar manner to the author's, the prestressing bar being left unbonded but cast in place in the beam. There may have been a dowel action present which was similar to that thought to have occurred in the author's beams. This phenomenon is not verified by the theoretical results which are generally slightly above those obtained from experiments. The reasons for this are not fully understood although it is possible that the computed modulus of rupture value is greater than that actually occurring.

5.3.7. The Modulus of Rupture Value

All the modulus of rupture values used in the theoretical analysis of all results, have been obtained from one of the equations listed below:-

5.1, 5.2, 5.6, 5.7, 5.9, 5.10.

The equations are all based upon the expression proposed by Hsu,[20] and indicate that the modulus of rupture value increases with a decrease in the depth of the section. The results of tests by Hsu and Wright[30] regarding the effect of beam size on the modulus of rupture value are shown in Fig. 2.1. As mentioned in section 2.4 the dimensions of the section of the modulus of rupture beams used by the author were identical to those of the prestressed beams. For those beams failing in Modes 1 and 3 the modulus of rupture beam was tested with its larger dimension vertical, and with its smaller dimension vertical for those failing in Mode 2. If the depth of the section is effecting the modulus of rupture value then there should be a noticeable increase in its value for those beams failing in Mode 2. With reference to Table 3.1, however, this is not the case.

There is only an average increase of 10% in the value as opposed to one of 35% predicted by the theory. The reasons for this are not clear although it should be noted that in all the tests carried out by Hsu and Wright their specimens were square in section. It is possible, therefore, that the shape of the section, in addition to its depth, is effecting the modulus of rupture value. This phenomenon clearly needs more investigation but it was not considered beneficial, in this case, to persue this line of thought any further.

From the discussions presented in this chapter it may be concluded that in general the computed modulus of rupture values show fairly good agreement with the experimental results. It is realized, however, that one equation cannot represent the properties and behaviour of all types of concrete. In many cases a better correlation may be obtained by adjusting the values of the constants in equations 5.1, 5.2, 5.6, and 5.7 to suit different types of concrete.

5.3.8. The Angle of Inclination of the Compression Hinge

The theoretical solutions of θ, the angle of inclination of the compression hinge, for the author's, Khalil's, and Reynolds' beams are shown in Fig. 5.1. The curves have been plotted using equation 4.2.4.3 in conjunction with the average values of P_s/f_{r3} for the respective beams. Disrupture of the author's beams, failing in Mode 1, was so complete that it was not possible to accurately determine the crack angles in the top of the beam. As no other experimental evidence was available no experimental crack angles are shown in Fig. 5.1.

It has been shown in the discussion on the author's beams that a large change in θ only effects the theoretical solution by a small amount. This is a result of the high M/T ratios and the low values of the bond slip factor occurring in these beams.

The solution will become more sensitive to tan θ for

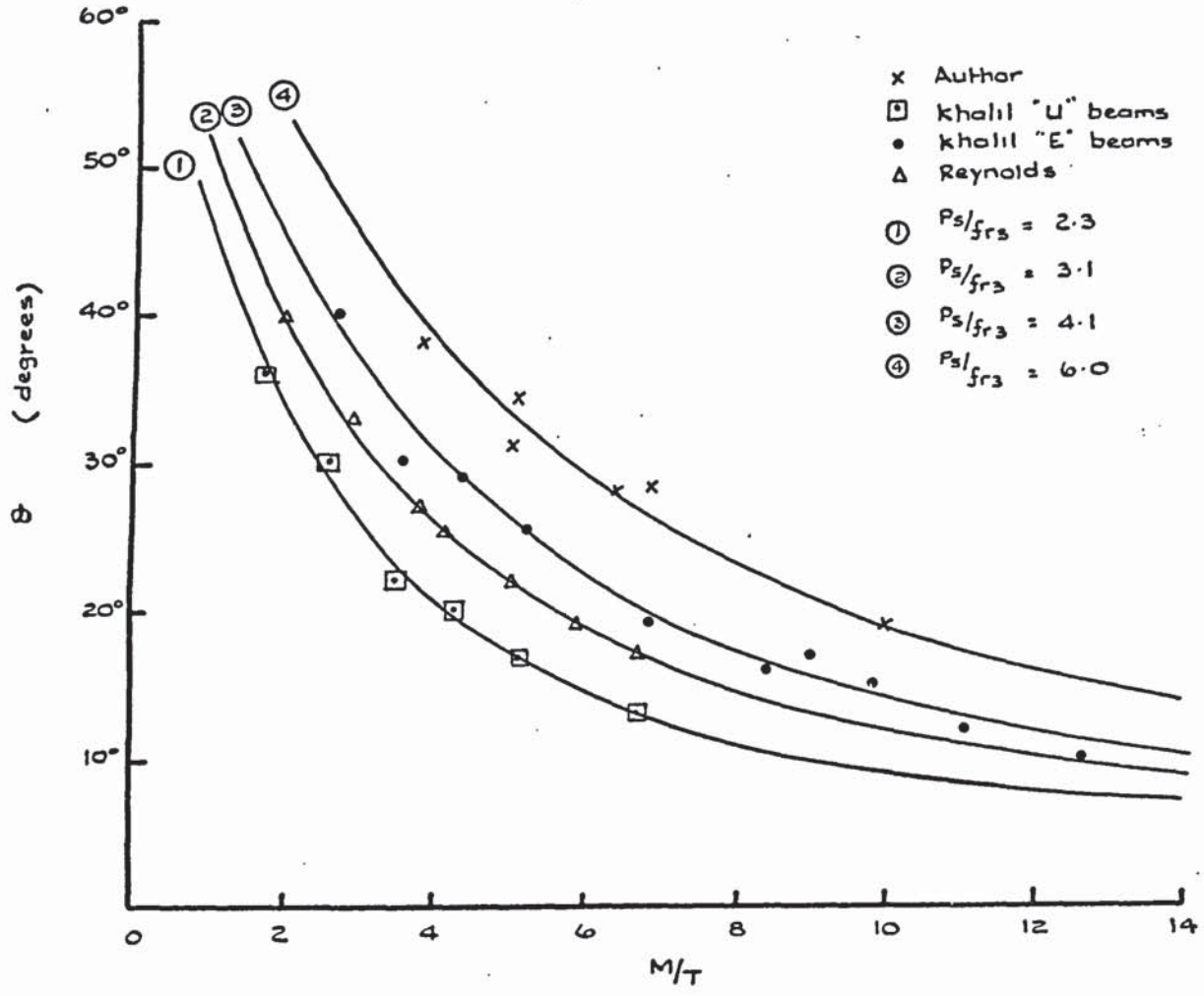

Fig. 5.1. Theoretical solutions for angle of inclination of compression hinge. - Mode 1.

both the lower M/T ratios and when the bond slip factor is significantly greater than 0.4. In this case the factor $(R.D_1-1)$ (equation 4.2.1.40) is no longer zero and the term containing $\tan\theta$ in the numerator will become predominant.

It is realized that the assumption made in 4.2.4 regarding the fact that the crack travels vertically up the side faces is not strictly correct. From the results presented in this chapter it is evident that this assumption does not significantly effect the accuracy of the theoretical solution.

Chapter 6

Subsidiary Tests

6.1. Hollow Cylinders

Summary

22 hollow cylinders, of identical mix, were tested under varying ratios of compressive stress to shear stress. The results indicate that, for all conditions of loading, failure is governed by a principal tensile strain criteria. The results of the tests are also compared with those of other investigators.

6.1.1. Introduction

The need for a failure criteria for concrete subjected to a combination of shear and compressive stresses became evident during the analysis of the prestressed beams failing in Mode 1. Failure in this case occurs in the top of the beam as a result of the compressive stresses due to bending and prestress, combined with the torsional shear stresses.

The object of these tests was to formulate a failure criteria which was applicable to the Mode 1 type of failure occuring in the prestressed beams. It was originally intended to carry out the entire series of tests under high ratios of direct stress to shear stress. However, the unexpected low failure load of the first 4 cylinders led to an investigation covering the whole range of this ratio.

6.1.2. Experimental Work

The author wishes to thank Manchester University, and in particular Dr. Goode, [37] for the loan of much of the apparatus necessary to carry out these experiments. Both the test rig and the moulds for the hollow cylinders were manufactured at Manchester for the purpose of carrying out tests of a similar nature to those

described in this chapter.

6.1.2.1. Test Specimens

The specimens (See Fig. 6.1.1.) consisted of hollow concrete cylinders of 200 mm (8 in.) outside diameter, 150 mm (6 in.) inside diameter, and with an over-all length of 914 mm (36 in.). In order that failure would not occur in the ends of the specimen due to pressure from the torque bands, a 150 mm (6 in.) length at either end was filled with concrete to form a solid plug.

The mixing and curing conditions were identical to those of the prestressed beams except for the following:-

(1) Due to lack of storage space in the laboratory it was not possible to store sufficient aggregate to complete the entire series of tests. Supplies of the first batch were exhausted after the casting of cylinders Nos 7, and 8, and a second batch was obtained from the same quarry. A comparison between the gradings of both batches is shown in Table 2.2. The lack of fines in the second batch resulted in a mix of very poor workability. It was therefore decided to adjust the relative weights of fine and course aggregate. From the original weight of coarse aggregate required for a 1 : $1\frac{1}{2}$: 3 mix, 13% was removed and replaced by fines. Of the amount removed, 3% consisted of aggregate retained on a $\frac{3}{8}$ in. sieve, and the remaining 10%, of aggregate retained on a $^{3}/_{16}$ in. sieve. The resulting mix had good workability and resulted in a concrete of similar strength to that used previously.

(2) All specimens were vibrated by means of a table vibrator. The relatively thin walls of the hollow cylinders made it impossible to use the internal poker vibrator. The steel moulds, in which the cylinders were cast, contained a collapsable central core which was removed 7 hours after casting. This procedure

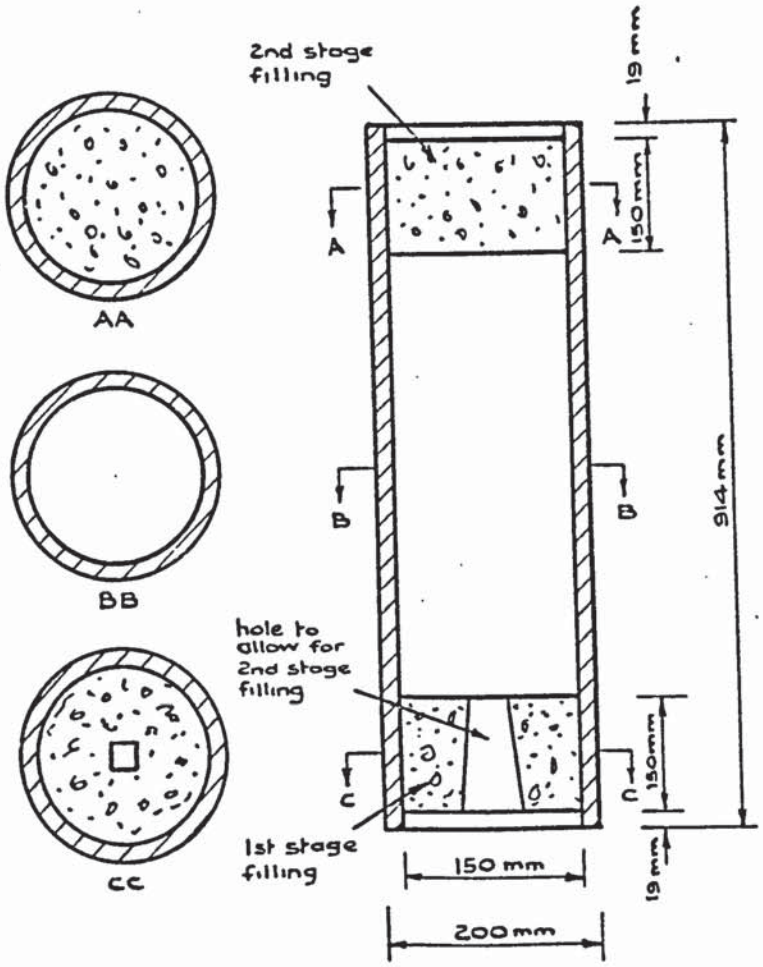

Fig. 6.1.1. Details of hollow cylinder specimens.

reduced the possibility of cracking by removing the restraint to shrinkage.

With each casting of 2 hollow cylinders the following control specimens were made:-

(1) 3 No. 150 mm (6 in.) cubes to determine the cube strength U_w.

(2) 6 No. 300 mm (12 in.) x 150 mm (5 in.) diameter cylinders to determine f'_c the cylinder crushing strength, and f_{sp} the split cylinder strength.

After 24 hours all specimens were removed from their moulds, placed in the curing tank, and removed 28 days later to be prepared for testing on the 29th and 30th days.

6.1.2.2. Test Rig.

The general layout and features of the test rig are shown in Plate 6.1.1. The bottom thrust bearing was designed to eliminate both torsional restraints, and bending restraints, produced by the non alignement of the vertical load.

The axial load was applied through a 1000 kN (100 ton) jack of the same type used in the main series. The torque was applied by means of a 50 kN (5 ton) jack through friction bands fitted with brake lining material, and clamped around either end of the cylinder. The load was recorded on a 50 kN (5 ton) tensile proving ring similar to that described in 2.9.

Lateral support to the cylinder was provided by needle bearings placed between 2 cylindrical steel surfaces, one attached to the frame of the main test rig and the other to the torsion band. This arrangement allowed the specimen to rotate freely during the test but prevented any lateral movement from taking place.

6.1.2.3. Instrumentation

Electrical resistance wire gauges, type 7A, were used to

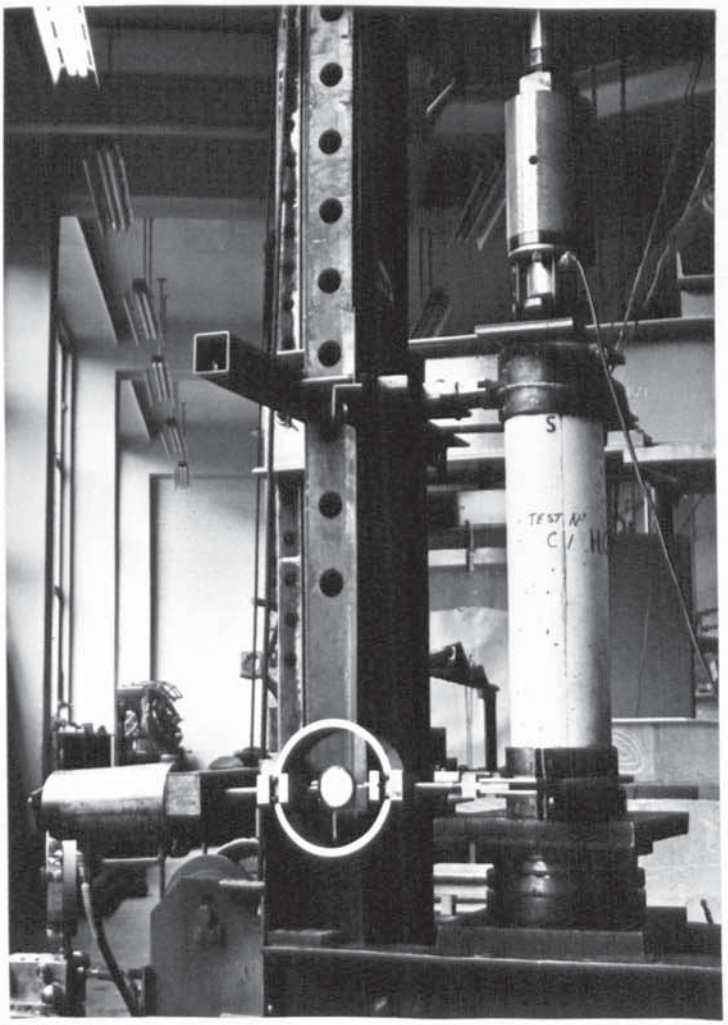

Plate 6.1.1. General layout of hollow cylinder test rig

measure all the strains on the surface of the cylinders. In all but 1 test a 45° strain rosette was employed, 3 of which were placed at points equidistant around the circumference of the cylinder at its mid height. In the remaining case 5 gauges were placed, along the vertical axis of the cylinder, at its mid height, at points equally spaced around the circumference. The reasons for doing this are explained in 6.1.3.1. The methods of fixing the gauges and measuring the strains are identical to those described in 2.10.2.

6.1.2.4. Preparation of the Cylinder for Testing

Prior to the commencement of the first test the upper plate of the thrust bearing was accurately levelled by means of a Dumpy Field Level. Wooden blocks, cut accurately to size, and placed under the corners of the plate ensured that it remained level whilst the cylinder was being positioned on the rig. The use of these same blocks in all subsequent tests provided a quick and accurate method of levelling the plate.

The cylinder, with the lower torque band attached, was placed on a layer of Plaster of Paris on the plate and held, with its axis vertical, until the plaster had set. The upper torque band was then attached together with the top bearing plate which was bedded with Plaster of Paris. A small vertical load applied through the jack ensured that any surplus plaster was squeezed out. A final check was made on the position of the cylinder by means of a plumb bob to ensure that it was located centrally beneath the jack. The needle bearings of the lateral supports were then placed in position and packing pieces inserted to ensure that the bearings were effective. Finally the torque bars were attached connecting the torque bands to the main frame of the test

rig. The upper bar was fixed rigidly to the support whilst the lower one was connected, via the proving ring, to the hydraulic jack.

6.1.2.5 Loading Proceedure

Those cylinders tested under pure axial load were loaded in increments of 20 kN (2 ton) until failure. The remaining cylinders were tested under a predetermined direct stress to shear stress ratio. This ratio was kept constant throughout each individual test by applying alternate increments of axial and torsional load.

6.1.3. Description of Tests

6.1.3.1. Cylinders Tested Under Direct Compression

No. H.C.6.

Failure was sudden and explosive and occurred at a stress almost 50% below that of its cylinder crushing strength. A close examination of the fragments revealed that tensile cracks had formed on one face of the cylinder with the formation of debris on the opposite face, indicating a crushing type failure. Although no definate conclusions could be drawn, due to the extent of disruption of the specimen, it was thought that this type of failure could be caused by an eccentrically applied load. The additional bending moment produced by such a load would result in a similar failure pattern to that observed.

No. H.C.7.

Great care was taken in this test to ensure that the load was applied axially, the cylinder being aligned with the jack by means of a theodolite. Failure again occurred at a stress considerably lower than that of the cylinder strength, and its sudden explosive nature prevented any conclusions being drawn

from the nature of the crack pattern.

No. H.C.8.

In order to substantiate the fact that a concentric load was being applied, 5 strain gauges were attached to the cylinder as described in 6.1.2.3. Any notable difference in the gauge readings would indicate an eccentrically applied load. Readings were taken at each increment of loading until failure. Vertical tension cracks appeared in the bottom of the cylinder at a load similar to that of previous tests. Slight honeycombing and segregation had however taken place in this region during casting which would probably account for the low load. Analysis of the strain gauge readings indicated that a concentric vertical load was being applied to the specimen.

Nos.H.C.9 and 10.

Both specimens were cast from the first mix to be made with the new supply of aggregate. As mentioned in 6.1.2.1 the resulting mix was badly graded producing a concrete of lower strength in comparison with previous tests. Failure, although occurring at a load lower than previously, was again associated with the formation of vertical tension cracks in the bottom of the cylinder.

Nos. H.C.11 and 12.

The mode of failure was similar to that obtained from earlier tests with vertical tension cracks appearing in the top of the cylinder as shown in Plate 6.1.2.

The position of these cracks suggested that the concrete plug, cast into the cylinder to prevent crushing by the torque bands, could be influencing the failure. In all direct compression tests to this stage of testing the torque bands had been omitted, and in nearly every case failure had occurred in either the upper or

lower regions of the cylinder. The plug, inserted after the cylinder had been cast, was left 19 mm ($\frac{3}{4}$ in.) short of the extremities to allow for the upstand on the loading plates. A small inaccuracy in the position of the plug, leaving it closer to the end than intended, would result in the loading plate bearing on the plug and not on the cylinder walls. On application of the load there would be a tendancy for the plug to be forced towards the central section of the cylinder. Such a movement could possibly be responsible for the formation of vertical tension cracks. Differential shrinkage between the plug and the cylinder may also have occurred which would tend to weaken the cylinder at this section. By attaching the collars of the torque arms it was hoped to strengthen the cylinder at the ends, and thus ensure that failure occurred in the central section.

H.C. No's. 13 and 14

In addition to attaching the collars, strain gauges in the form of 45° rosettes were attached to the cylinders, as described in 6.1.2.3. The collars prevented failure at the extremities of the cylinder, but in both cases vertical tension cracks appeared in the central section as shown in Plate 6.1.3.

6.1.3.2. Cylinders Tested Under Combined Direct and Shear Stresses

The remaining cylinders were tested under varying ratios of direct stress to shear stress.

It is not proposed to describe, in detail, each individual test. In every case failure was initiated by the formation of a tension crack inclined at some angle $\gamma°$ to the longitudinal axis of the cylinder. The value of $\gamma°$ was observed to decrease with an increase in the direct stress to shear stress ratio as shown in

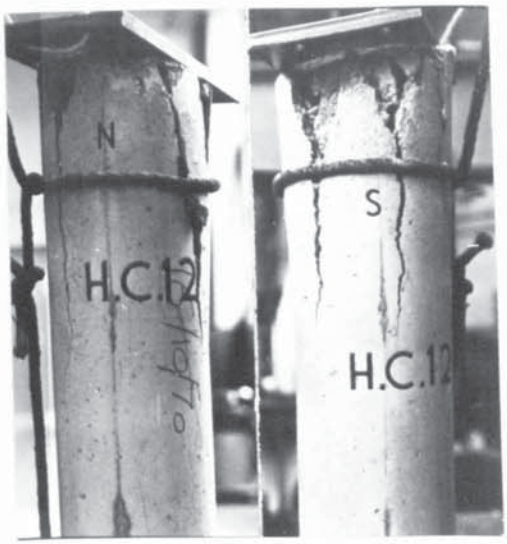

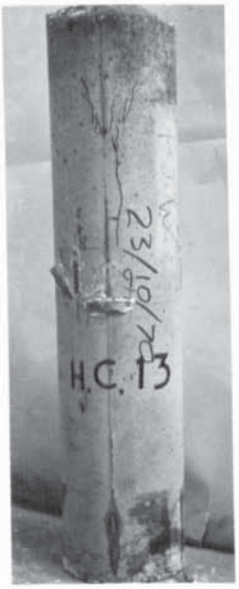

Plate 6.1.2. H.C.12 at failure. Plate 6.1.3. H.C.13 at failure.

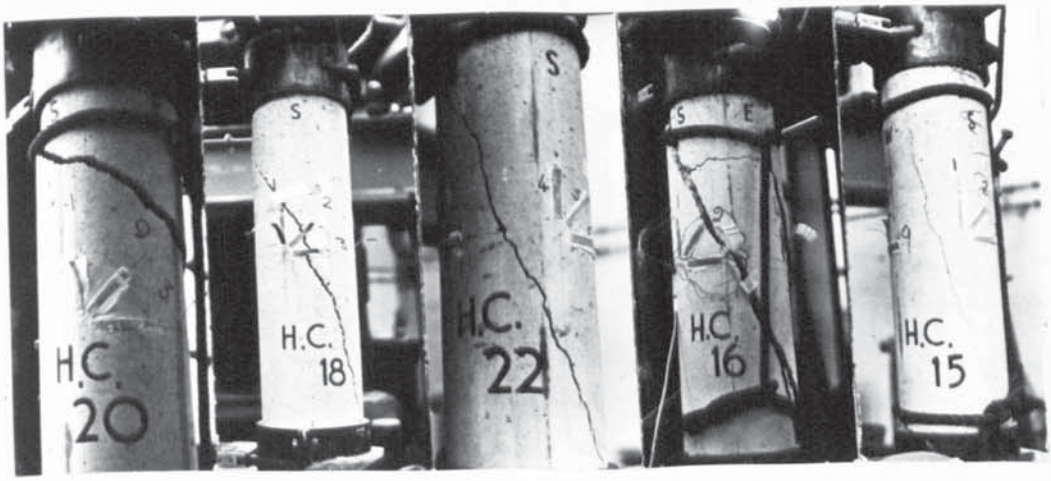

Plate 6.1.4. Hollow cylinders at failure showing variation of crack angle.

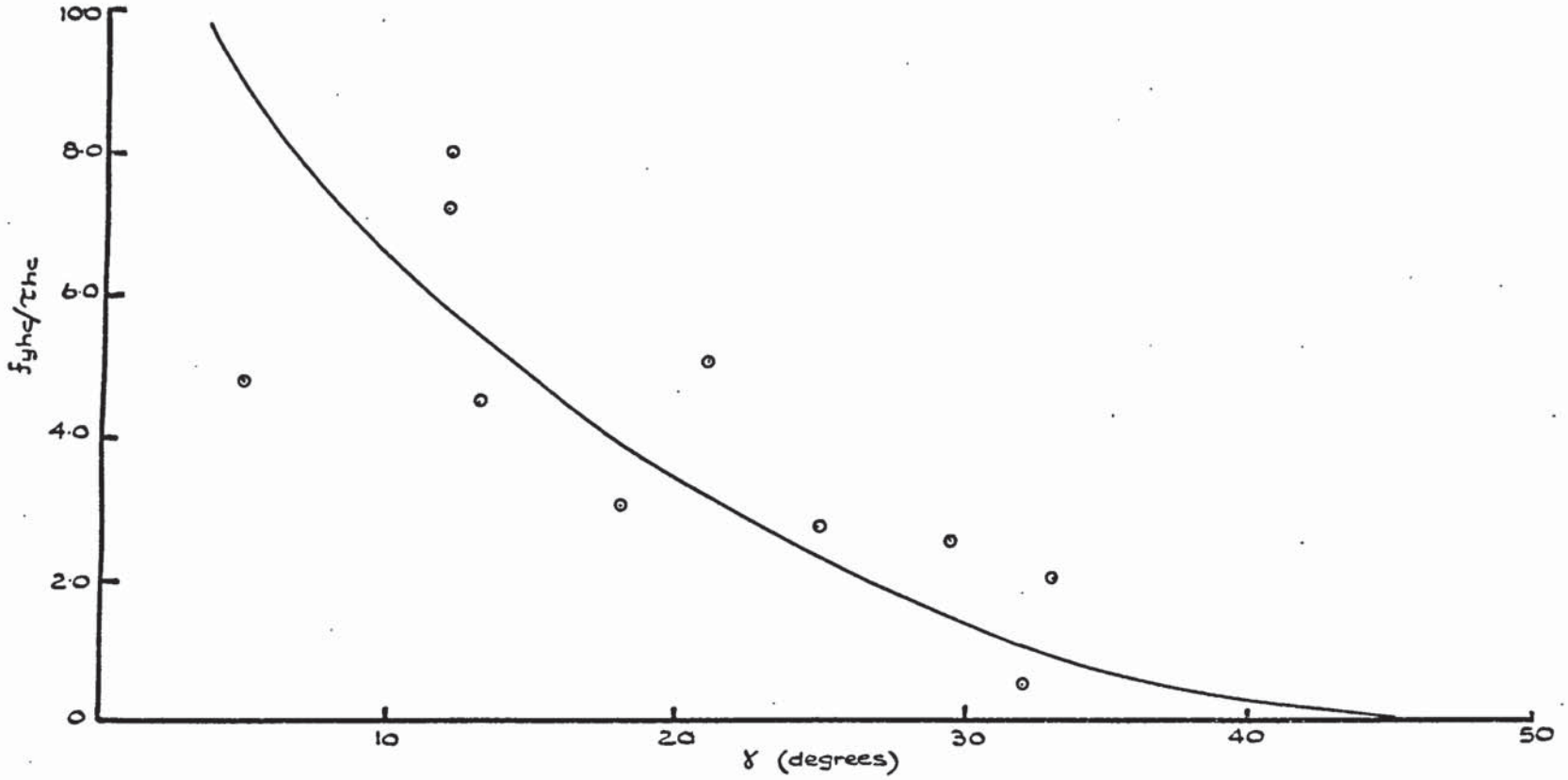

Fig. 6.1.3. Variation of crack angle with stress ratio.

Fig. 6.1.3. and Plate 6.1.4.

6.1.5. Theory

Failure is considered to be governed by a principal tensile strain criteria as proposed by St. Venant [24] The loads acting on the cylinder (see Fig. 6.1.4.(A)) produce stress conditions on an element as shown in Fig. 6.1.4.(B). The stresses consist of:-

1) A direct stress f_{yhc} due to the axial load.

2) A lateral stress f_{xhc} induced by the axial load.

3) A shear stress τ_{hc} resulting from the torsional load.

Using Mohrs' Strain Circle see Fig. 6.1.4.(C) we have, from the geometry of the circle

$$ON = ON' = \frac{\varepsilon_{yhc} + \varepsilon_{xhc}}{2}$$

$$OR = \sqrt{\left(\frac{\varepsilon_{yhc} + \varepsilon_{xhc}}{2}\right)^2 + \left(\frac{\phi_{hc}}{2}\right)^2}$$

$$LN' = NM = OM - ON$$

But $OM = OR$

$$\therefore LN' = NM = OR - ON$$

$$\varepsilon_{1hc} = \varepsilon_{xhc} + LN'$$

$$\varepsilon_{2hc} = \varepsilon_{yhc} + NM$$

$$\therefore \varepsilon_{1hc} = \varepsilon_{xhc} + \tfrac{1}{2}\sqrt{(\varepsilon_{yhc} + \varepsilon_{xhc})^2 + \phi_{hc}^2} - \tfrac{1}{2}(\varepsilon_{yhc} + \varepsilon_{xhc})$$

$$\therefore \varepsilon_{1hc} = \tfrac{1}{2}\sqrt{(\varepsilon_{yhc} + \varepsilon_{xhc})^2 + \phi_{hc}^2} - \tfrac{1}{2}(\varepsilon_{yhc} - \varepsilon_{xhc}) \quad --- 6.1.1.$$

and

$$\varepsilon_{2hc} = \tfrac{1}{2}\sqrt{(\varepsilon_{yhc} + \varepsilon_{xhc})^2 + \phi_{hc}^2} + \tfrac{1}{2}(\varepsilon_{yhc} - \varepsilon_{xhc}) \quad --- 6.1.2.$$

Now assuming a linear stress-strain relationship for the concrete in

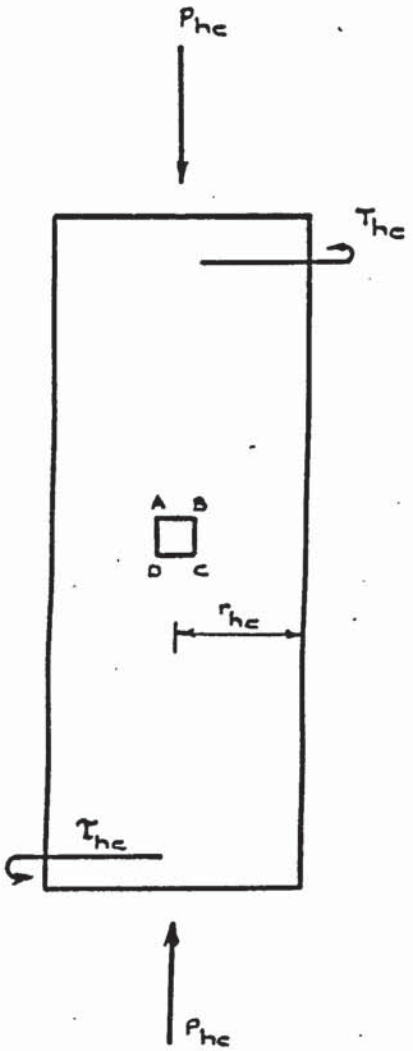

Fig. 6.1.4. a. Loading condition of hollow cylinder.

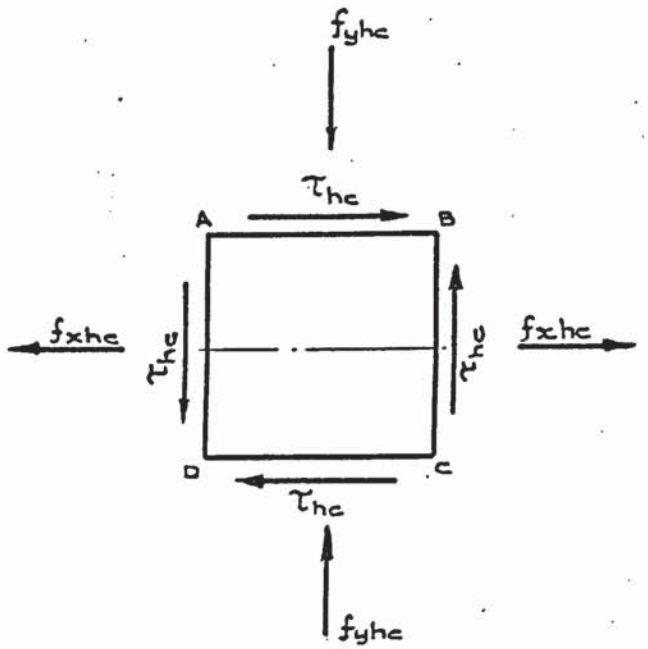

Fig. 6.1.4. b. Stresses acting on an element.

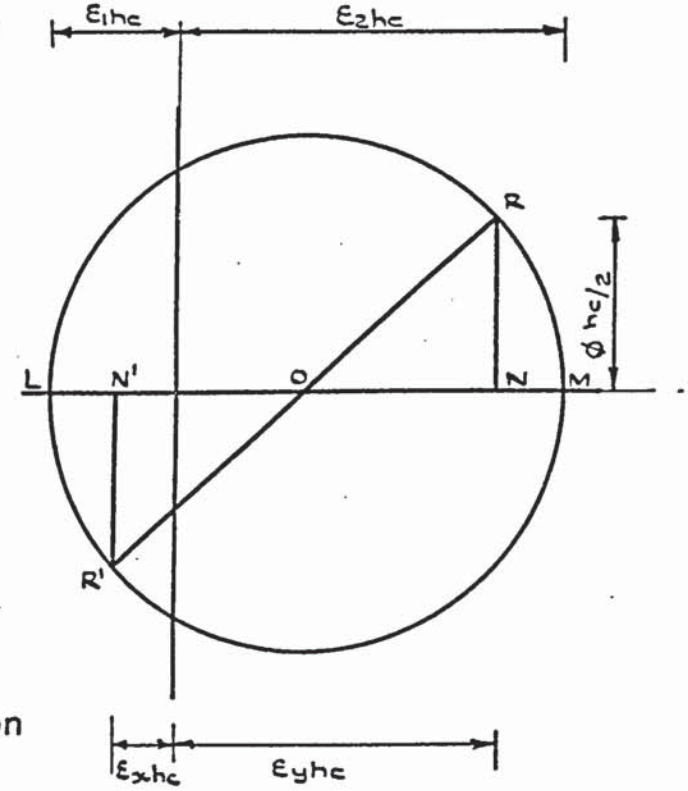

Fig. 6.1.4. c Mohr's strain circle.

both tension and compression we have

$$\varepsilon_{yhc} = \frac{P_{hc}}{A_{hc}\ E_c} \qquad \text{--- 6.1.3.}$$

$$\varepsilon_{xhc} = \frac{P_{hc} \cdot \sigma_c}{A_{hc}\ E_c} \qquad \text{--- 6.1.4.}$$

$$\phi_{hc} = \frac{\tau_{hc}}{G_c} = \frac{\tau_{hc}\ \ 2\,(1 + \sigma_c)}{E_c} \qquad \text{--- 6.1.5.}$$

and $$\tau_{hc} = \frac{T_{hc} \times r_{hc}}{J_{hc}} \qquad \text{--- 6.1.6.}$$

Substituting for ε_{yhc}, ε_{xhc}, ϕ_{hc} in 6.1.1 we get

$$\varepsilon_{1hc} = \tfrac{1}{2}\sqrt{\left(\frac{P_{hc}}{E_c A_{hc}} + \frac{P_{hc}\,\sigma_c}{E_c A_{hc}}\right)^2 + \left(\frac{2\tau_{hc}(1 + \sigma_c)}{E_c}\right)^2} - \tfrac{1}{2}\left(\frac{P_{hc}}{E_c A_{hc}} - \frac{\sigma_c P_{hc}}{E_c A_{hc}}\right)$$

$$\therefore\ \varepsilon_{1hc} + \frac{P_{hc}}{2\,E_c A_{hc}}(1-\sigma_c) = \tfrac{1}{2}\sqrt{\left(\frac{P_{hc}}{E_c A_{hc}} + \frac{P_{hc}\,\sigma_c}{E_c A_{hc}}\right)^2 + \left(\frac{2\,\tau_{hc}(1+\sigma_c)}{E_c}\right)^2}$$

Squaring both sides we get.

$$\frac{\varepsilon_{1hc}^{\ 2} + \varepsilon_{1hc}\,P_{hc}(1 - \sigma_c)}{E_c A_{hc}} + \left(\frac{P_{hc}}{4\,E_c\,A_{hc}}\right)^2 (1 - 2\,\sigma_c + \sigma_c^{\ 2})$$

$$= \tfrac{1}{4}\left\{\left(\frac{P_{hc}}{E_c A_{hc}}\right)^2 + \frac{2P_{hc}^{\ 2}\,\sigma_c}{E_c^{\ 2}\,A_{hc}^{\ 2}} + \left(\frac{P_{hc}^{\ 2}\,\sigma_c^{\ 2}}{E_c A_{hc}}\right)^2 + \left(\frac{2\,\tau_{hc}(1 + \sigma_c)}{E_c}\right)^2\right\}$$

simplifying we get

$$\varepsilon_{1hc}^{\ 2} + \frac{\varepsilon_{1hc}\,P_{hc}}{E_c A_{hc}}(1 - \sigma_c) - \frac{\sigma_c P_{hc}^{\ 2}}{E_c^{\ 2} A_{hc}^{\ 2}} = \frac{\tau_{hc}^{\ 2}}{E_c^{\ 2}}\ (1 + \sigma_c)^2 \qquad \text{--- 6.1.7.}$$

- Since experimental results for the uniaxial tensile strength were not available split cylinder strengths have been used assuming they are approximately equal.

also

$$f_t = \varepsilon_{1hc} E_c \qquad \text{--- 6.1.8.}$$

and

$$f_{yhc} = \frac{P_{hc}}{A_{hc}} \qquad \text{--- 6.1.9.}$$

substituting f_t and f_{yhc} in 6.1.7 we get

$$\left(\frac{f_t}{E_c}\right)^2 + \frac{f_t f_{yhc}}{E_c^2}(1 - \sigma_c) - \frac{\sigma_c f_{yhc}^2}{E_c^2} = \frac{\tau_{hc}^2 (1 + \sigma_c)^2}{E_c^2}$$

from which

$$\tau_{hc} = \sqrt{f_t^2 + \frac{f_t f_{yhc}(1 - \sigma_c) - \sigma_c f_{yhc}^2}{(1 + \sigma_c)^2}} \qquad \text{--- 6.1.10}$$

But $$\tau_{hc} = \frac{T_{hc} r_{hc}}{J_{hc}}$$

$$\therefore \quad T_{hc} = \frac{J_{hc}}{r_{hc}} \sqrt{\frac{f_t^2 + f_t f_{yhc}(1 - \sigma_c) - \sigma_c f_{yhc}^2}{(1 + \sigma_c)^2}} \qquad \text{--- 6.1.11.}$$

Thus the torsional load T_{hc} required to cause failure under a direct stress f_{yhc} can be calculated using equation 6.1.11.

6.1.5. Discussion of Theory and Results

The results of all the control specimens together with their respective test specimens are given in tabular form in Table 6.1.1. Fig. 6.1.5 shows the test results plotted in the dimensionless form τ_{hc}/f_{sp}: f_{yhc}/f_{sp}. The 2 theoretical curves have been obtained using 2 values of Poisson's ratio, 0.10, and 0.14. These values were obtained from the results of the direct compressive tests No's. H.C. 13 and 14. Fig. 6.1.6 shows the graph Poisson's ratio against direct compressive stress and indicates that its value increases from approximately 0.10 to 0.14 as the compressive stress is increased. The majority of the test results can be seen to lie within the limits of the 2 theoretical curves. The curves representing the principal tensile stress criteria[24] and the Cowan Slip Plane criteria[25] have also been plotted in Fig. 6.1.5. Prior to carrying

No.	Control Specimens			Cylinder Stress at Failure		Crack Angles at Failure	
	U_w N/mm^2 (lb/in^2)	f_c' N/mm^2 (lb/in^2)	f_{sp} N/mm^2 (lb/in^2)	f_{yhc} N/mm^2 (lb/in^2)	τ_{hc} N/mm^2 (lb/in^2)	Experimental	Theoretical
1	44.5 (6402)	34.55 (5010)	2.34 (339)	15.10 (2190)	3.14 (455)	5	
2				15.45 (2241)	3.44 (499)	13	
3	35.4 (5134)	20.79 (3015)	1.88 (272)	12.30 (1783)	1.72 (249)	12	
4							
5	44.94 (6517)	30.43 (4413)	2.25 (326)	17.03 (2470)	1.89 (274)		
6				16.68 (2419)			
7	33.20 (4815)	28.29 (4102)	1.86 (269)	18.26 (2648)			
8				19.67 (2852)			

TABLE 6.1.1. Test Results of Control Specimens and Hollow Cylinders

$$f_{yhc} = \frac{\text{Direct Load}}{\text{Area}} = \frac{P_{hc}}{7\pi}$$

$$\tau_{hc} = \frac{T_{hc} \times r_{hc}}{J_{hc}}$$

where T_{hc} = Load x Lever Arm

Lever Arm = 381 mm (15 in.)

r_{hc} = 102 mm (4 in.)

$J_{hc} = 1.14 \times 10^8$ mm^4 (275 in.^{4})

	Control Specimens			Cylinder Stress at Failure		Crack Angles at Failure	
No.	U_w N/mm^2 (lb/in^2)	f_c' N/mm^2 (lb/in^2)	f_{sp} N/mm^2 (lb/in^2)	f_{yhc} N/mm^2 (lb/in^2)	τ_{hc} N/mm^2 (lb/in^2)	Experimental	Theoretical
9	26.25 (3806)	15.90 (2306)	1.78 (258)	11.59 (1681)			
10				14.03 (2037)			
11	41.08 (5948)	31.99 (4639)	2.63 (381)	18.61 (2699)			
12				18.26 (2648)			
13	39.21 (5686)	37.27 (5405)	1.83 (266)	23.18 (3361)			
14				33.01 (4787)			
15	45.29 (6568)	37.89 (5495)	2.71 (393)	24.58 (3565)	3.07 (445)	12	10
16				20.02 (2903)	4.99 (723)	21	10

$$f_{yhc} = \frac{\text{Direct Load}}{\text{Area}} = \frac{P_{hc}}{7\pi}$$

$$\tau_{hc} = \frac{T_{hc} \times r_{hc}}{J_{hc}}$$

where T_{hc} = Load x Lever Arm

Lever Arm = 381 mm (15in.)

r_{hc} = 102 mm (4 in.)

$J_{hc} = 1.14 \times 10^8$ mm^4 ($275 in.^4$)

TABLE 6.1.1. Continued Test Results of Control Specimens and Hollow Cylinders

	Control Specimens			Cylinder Stress at Failure		Crack Angles at Failure	
No.	U_w N/mm^2 (lb/in^2)	f_c' N/mm^2 (lb/in^2)	f_{sp} N/mm^2 (lb/in^2)	f_{yhc} N/mm^2 (lb/in^2)	τ_{hc} N/mm^2 (lb/in^2)	Experimental	Theoretical
9	26.25 (3806)	15.90 (2306)	1.78 (258)	11.59 (1681)			
10				14.03 (2037)			
11	41.08 (5948)	31.99 (4639)	2.63 (381)	18.61 (2699)			
12				18.26 (2648)			
13	39.21 (5686)	37.27 (5405)	1.83 (266)	23.18 (3361)			
14				33.01 (4787)			
15	45.29 (6568)	37.89 (5495)	2.71 (393)	24.58 (3565)	3.07 (445)	12	10
16				20.02 (2903)	4.99 (723)	21	10

$$f_{yhc} = \frac{\text{Direct Load}}{\text{Area}} = \frac{P_{hc}}{7\pi}$$

$$\tau_{hc} = \frac{T_{hc} \times r_{hc}}{J_{hc}}$$

where T_{hc} = Load x Lever Arm

Lever Arm = 381 mm (15in.)

r_{hc} = 102 mm (4 in.)

$J_{hc} = 1.14 \times 10^8 \text{ mm}^4 (275 \text{in.}^4)$

TABLE 6.1.1. Continued Test Results of Control Specimens and Hollow Cylinders

	Control Specimens			Cylinder Stress at Failure		Crack Angles at Failure	
No.	U_w N/mm^2 (lb/in^2)	f_c' N/mm^2 (lb/in^2)	f_{sp} N/mm^2 (lb/in^2)	f_{yhc} N/mm^2 (lb/in^2)	τ_{hc} N/mm^2 (lb/in^2)	Experimental	Theoretical
17	37.00 (5365)	33.36 (4838)	2.01 (292)	13.34 (1935)	4.45 (645)	18	13
18				5.79 (840)	2.93 (425)	33	31
19	42.21 (6121)	34.72 (5035)	1.86 (269)	3.16 (458)	3.12 (453)	32	30
20				0 (0)	1.56 (226)	55	46
21	40.80 (5920)	31.37 (4549)	2.28 (330)	21.95 (3183)	1.28 (185)		12
22				10.19 (1477)	3.97 (546)	26	19

$$f_{yhc} = \frac{\text{Direct Load}}{\text{Area}} = \frac{P_{hc}}{7\pi}$$

$$\tau_{hc} = \frac{T_{hc} \times r_{hc}}{J_{hc}}$$

where T_{hc} = Load x Lever Arm

Lever Arm = 384 mm(15in.)

r_{hc} = 102 mm (4 in.)

$J_{hc} = 1.14 \times 10^8 mm^4 (275 in.^4)$

TABLE 6.1.1. Continued Test Results of control Specimens and Hollow Cylinders

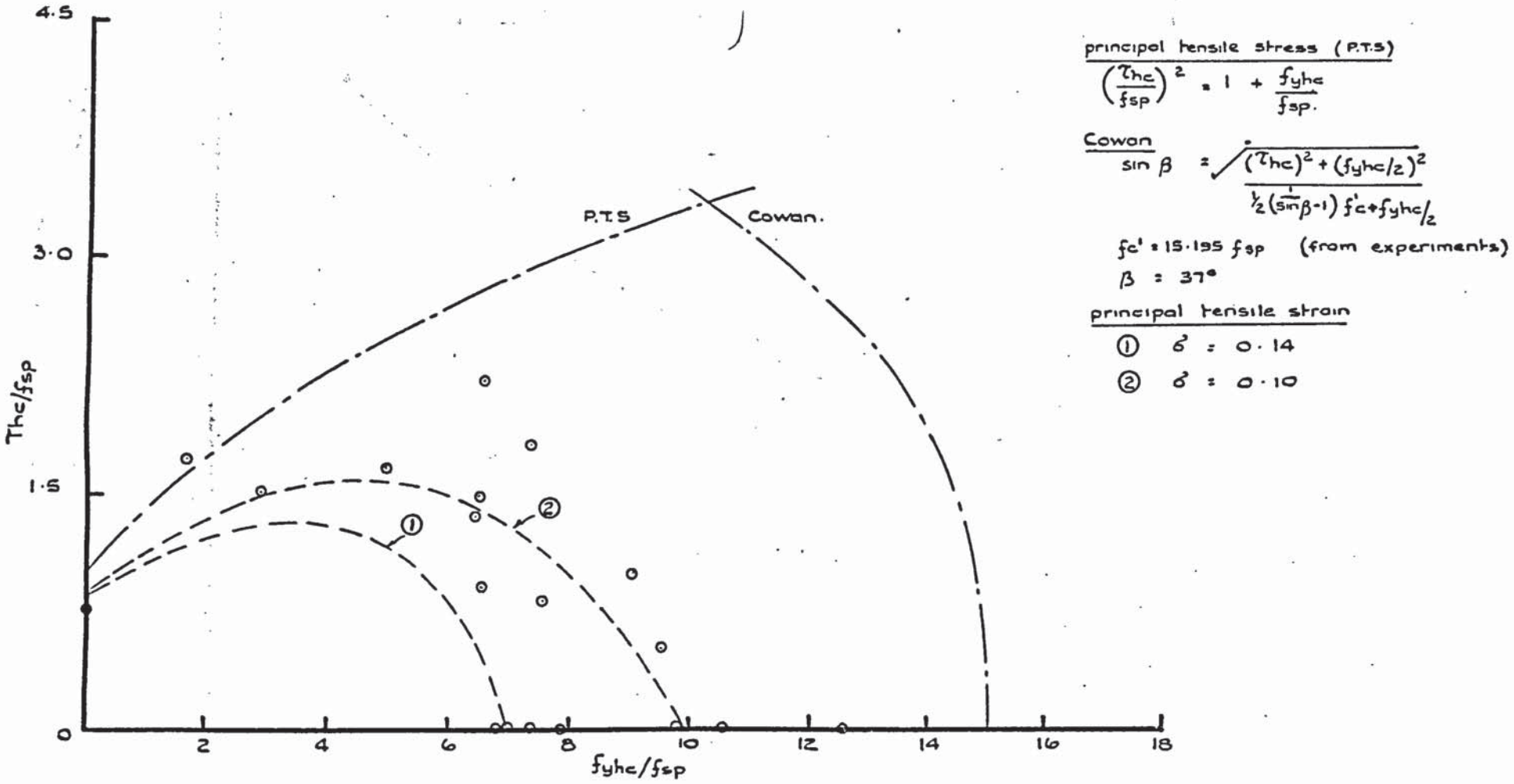

principal tensile stress (P.T.S)

$$\left(\frac{\tau_{hc}}{f_{sp}}\right)^2 = 1 + \frac{f_{yhc}}{f_{sp}}$$

Cowan

$$\sin\beta = \sqrt{\frac{(\tau_{hc})^2 + (f_{yhc}/2)^2}{\frac{1}{2}\left(\frac{1}{\sin\beta} - 1\right) f'_c + f_{yhc}/2}}$$

$f_c' = 15.195\, f_{sp}$ (from experiments)

$\beta = 37°$

principal tensile strain

① $\delta = 0.14$

② $\delta = 0.10$

Fig. 6.1.5. Comparison of experimental & theoretical results – hollow cylinders

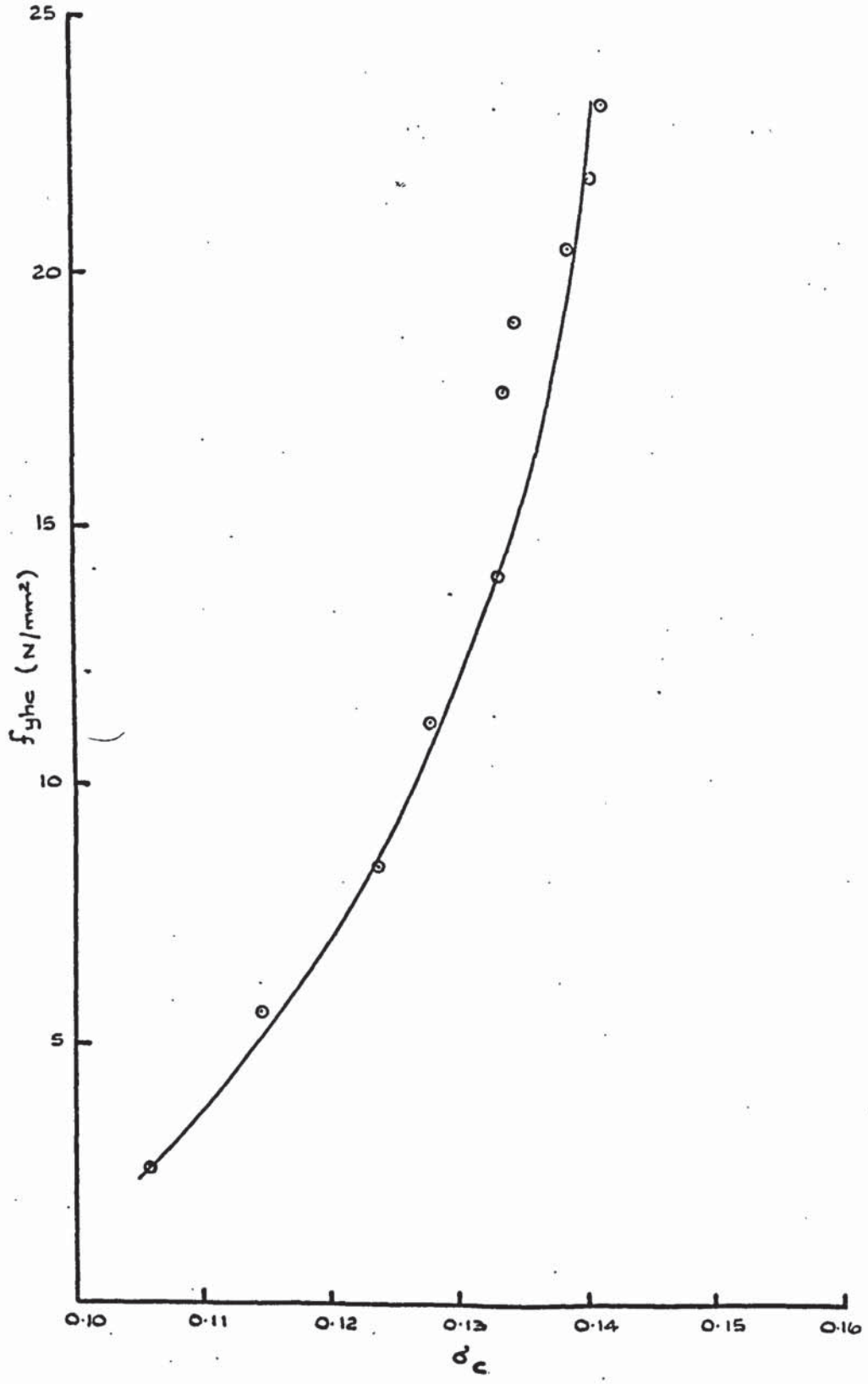

Fig. 6.1.6. Variation of Poisson's ratio with compressive stress.

out this investigation it was thought that the results produced would lie close to the Cowan criteria curve. The graph shows clearly that this is not so.

In Fig. 6.1.7 the maximum principal compressive and tensile stresses have been plotted against the maximum principal compressive and tensile strains respectively for 5 cylinders ranging from pure torsion to pure compression. In a series of direct compression tests carried out on standard 150 mm (6 in.) diameter cylinders. (see 6.4) the limiting strains recorded are shown in Table 6.4.1. Using the minimum average strain of 1800 microstrains, to allow for the difference in test conditions between them and the hollow cylinders, it can be seen from Fig. 6.1.7.that this limit is not reached. In all 3 tests carried out under pure compression, where strain readings were taken, the maximum strain recorded by any one gauge was only 2,000 microstrains. If the limiting tensile strain is taken as 75 microstrains then from Fig 6.1.7 it is apparent that this value is reached in every case. This limiting value was calculated from the elastic relationship

E_c = Stress/Strain

Where E_c = 28600 N/mm^2 (4.15 x 10^6 lb/in^2) and the ultimate tensile stress = f_{sp} = 2.1 N/mm^2(310lb/in^2).

The value of f_{sp} has been taken as the average of all those shown in Table 6.1.1. The value of E_c was obtained from the average of all the tests carried out with the prestressed beams.

The slope of the tensile strain curve can be seen to decrease as the compressive stress to shear stress ratio is increased. In pure torsion (No. H.C.20) the line is almost straight reaching a maximum tensile strain of 75 microstrains. The slope of the curve for No. H.C. 15, where the ratio is 8.0, is much less,

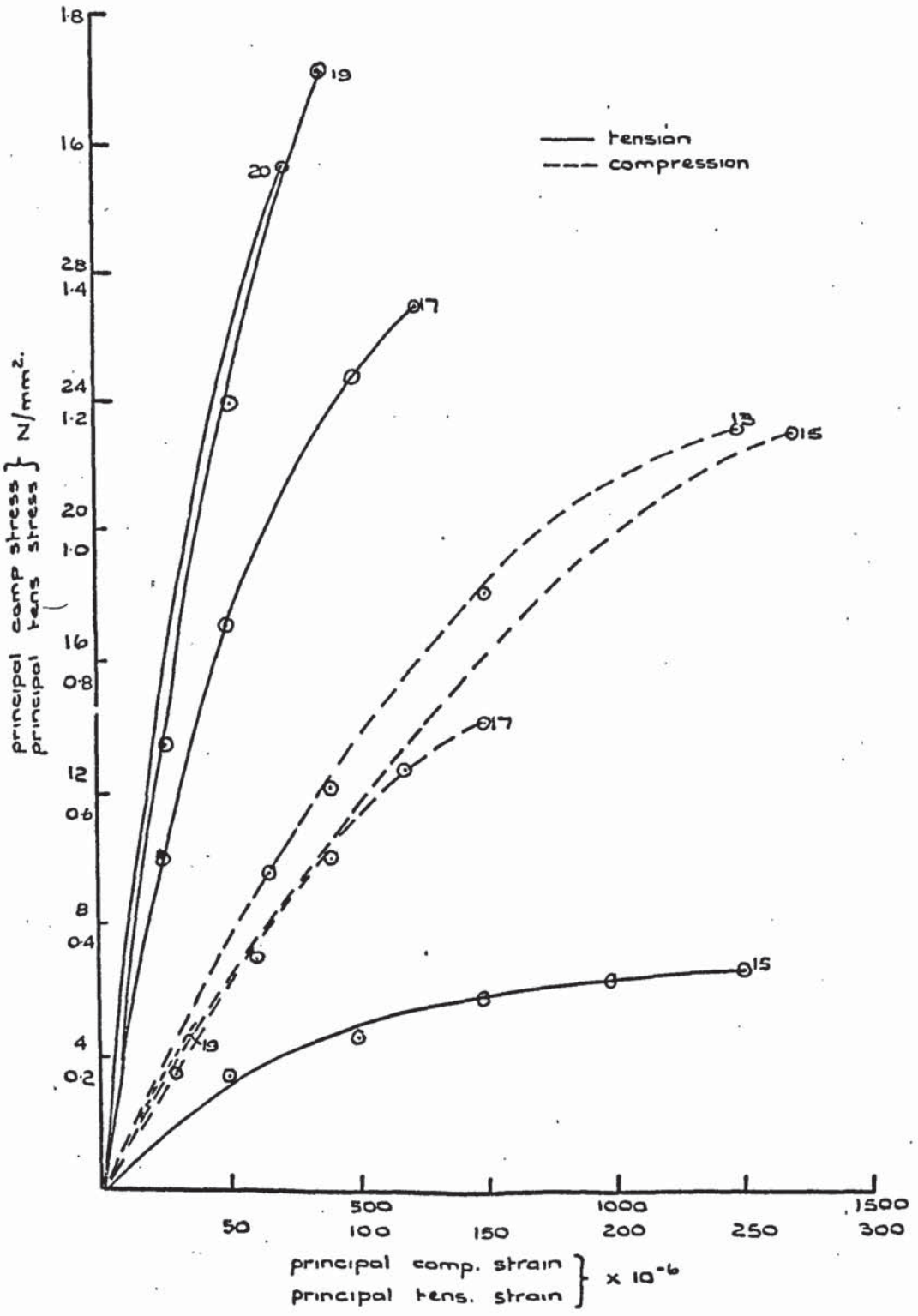

Fig. 6.1.7. Principal stresses / Principal strains – hollow cylinders.

and reaches a maximum tensile strain of 250 microstrains. This indicates that although failure is governed by the principal tensile strain, it is not purely an elastic mode of failure as in the case of pure torsion. The slope of the compressive strain curve is not effected by the value of the compressive stress to shear stress ratio. In every case the line is almost straight, a phenomenon not characteristic of a compression type failure.

Goode[37] reported tests on 39 hollow cylinders of varying strengths tested under different combinations of direct compression and torsion.

He concluded that Mohr's[24] theory (of which Cowan's is a simplification) with the adoption of Leon's[26] parabolic envelope, provided a good representation of the failure of his cylinders.

Also reported, in graphical form, were the results of similar tests by other investigators which are shown, in Fig. 6.1.8, in the non dimensional form $f_{yhc}/f'_c : \tau_{hc}/f'_c$. Comparison between these results and the 2 modes of failure discussed here, namely the Cowan Slip Plane Criteria, and the principal tensile strain criteria are also shown. The principal tensile strain criteria curve has been plotted using values of 0.067 and 0.10 for the tensile to compressive strength ratio and Poisson's ratio respectively. The results show a large amount of scatter and many of them, particularly those reported by Tsuboi and Suenaga could be assumed to follow the principal tensile strain criteria. A better comparison between the results and the tensile strain criteria could be obtained by using the tensile strength instead of the compressive strength of the concrete. It was, however, considered unprofitable to persue this line of enquiry in relation to the main objective of prestressed concrete in torsion and bending. All the results of other investigators were obtained from Goode's paper in which the tensile strengths

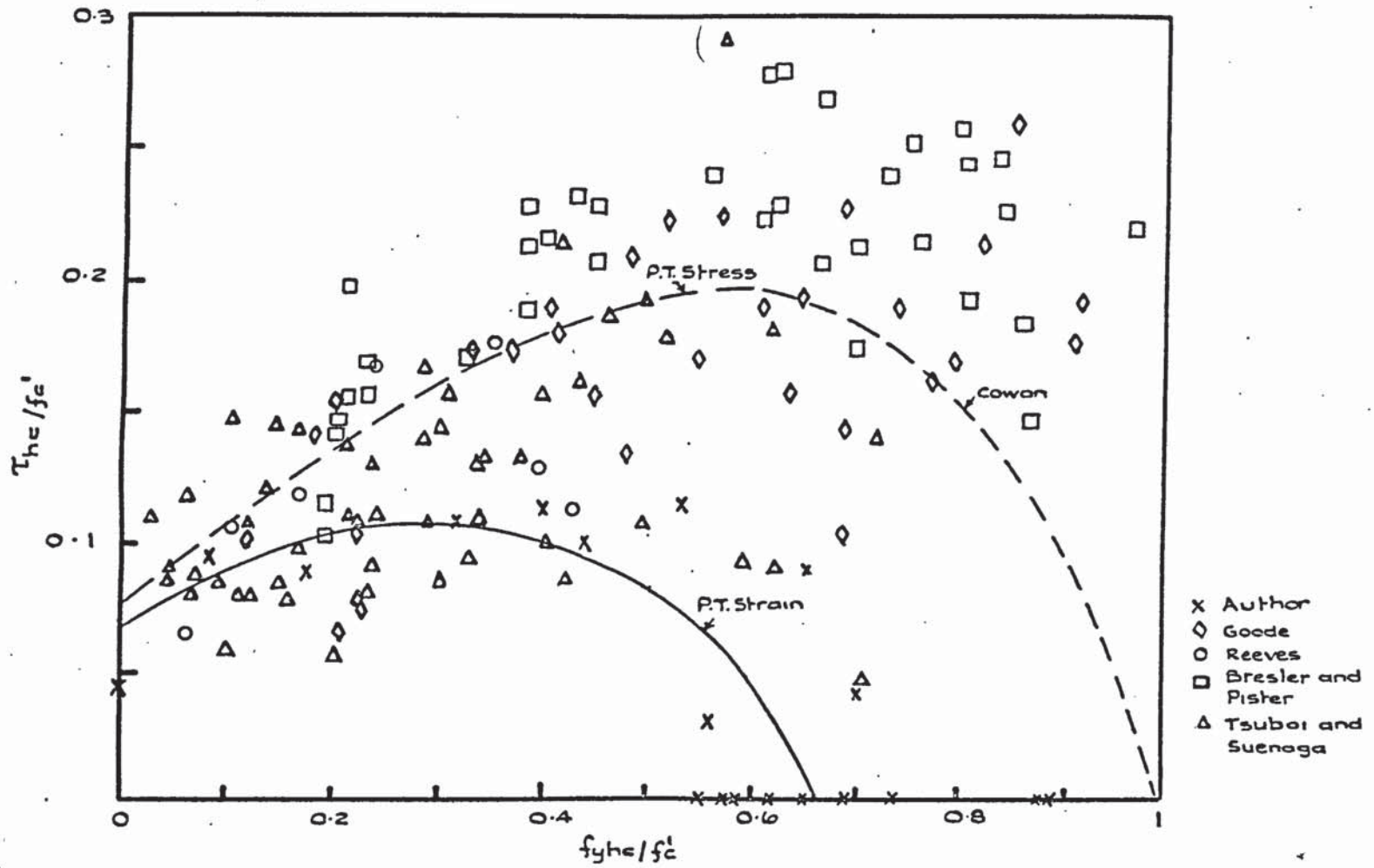

Fig. 6.1.8. General comparison of results.

of only his tests were reported.

One reason for the scatter is probably due to the strength of the concrete. A low strength concrete may be able to reach it's maximum compressive stress before the ultimate value of the lateral tensile strain has been reached. With a higher strength concrete however, this may not occur, the higher load required to produce compressive failure inducing lateral strains greater than the ultimate tensile strains.. This is not always the case, however, as those cylinders reported by Goode, and made from a high strength mix still tended to follow the criteria predicted by Cowan. The value of Poisson's ratio is obviously an important factor when considering a principal tensile strain criteria, and a variation of the value could explain some of the scatter.

6.1.6. Conclusions

The purpose of this series of tests was to formulate a criteria for the failure of concrete under combined torsion and direct stress. This criteria, it was hoped, would be applicable to the failure, in Mode I, of the prestressed beams in the main series of tests. Experimental evidence showed, however, that the mode of failure of the cylinders was based on a tensile strain criteria, while failure of the beams appeared to be based on the Cowan slip plane criteria.

The principal tensile strain criteria proposed here may have only limited application, and did not appear relevant to the main objective of testing prestressed beams in bending and torsion. Further work on the failure criteria was then conducted based on the Cowan slip plane approach and described in 6.2. The theory put forward here is a purely elastic one, but it is obvious from the results presented that this does not hold true for all cases, in particular

those in which the f_{yhc}/τ_{hc} ratio is high. For such cases, to be strictly correct, consideration should be given to a non linear stress-strain relationship for the concrete. The value of Poisson's ratio has been shown to be critical, and has also been shown to increase as the compressive stress increases. A more rigorous solution would therefore involve an expression with Poissons's ratio as a variable and not as a constant as has been shown.

The theoretical solution proposed does however agree reasonably well with the experimental results.

6.2 Split Cube Test

Summary

20 No. 150 mm (6 in.) split cubes of identical mix were tested under varying ratios of direct stress to shear stress.

6.2.1. Introduction

The following series of tests was carried out as a sequel to those carried out on the hollow cylinders described in 6.1. Once again the object of the tests was to formulate a failure criteria which was applicable to the failure of the prestressed beams in Mode 1. This type of failure is basically a slip plane mechanism and it was hoped, that the conditions produced by splitting the cube, and applying varying ratios of direct and shear stress would be analogous to the failure conditions.

6.2.2. Experimental Work

6.2.2.1. Test Specimens

20 No. 150 mm (6 in.) cubes were cast along with the following control specimens:-

1) 3 No. 150 mm (6 in.) cubes to determine U_w the uniaxial cube crushing strength.

2) 3 No. 300 mm (12 in.) x 150 mm (6 in.) diameter cylinders to determine f'_c the uniaxial cylinder crushing strength.

3) 3 No. 300 mm (12 in.) x 150 mm (6 in.) diameter cylinders to determine f_{sp} the split cylinder tensile strength.

The mixing and curing conditions were identical to those of the main series of tests.

6.2.2.2. Cube Splitting

The cubes were split in half by subjecting them to a compressive load, applied through knife edge loading points as shown in Plate 6.2.1. Care was required when setting up the specimen to ensure that the loading points were correctly positioned at the centre of the

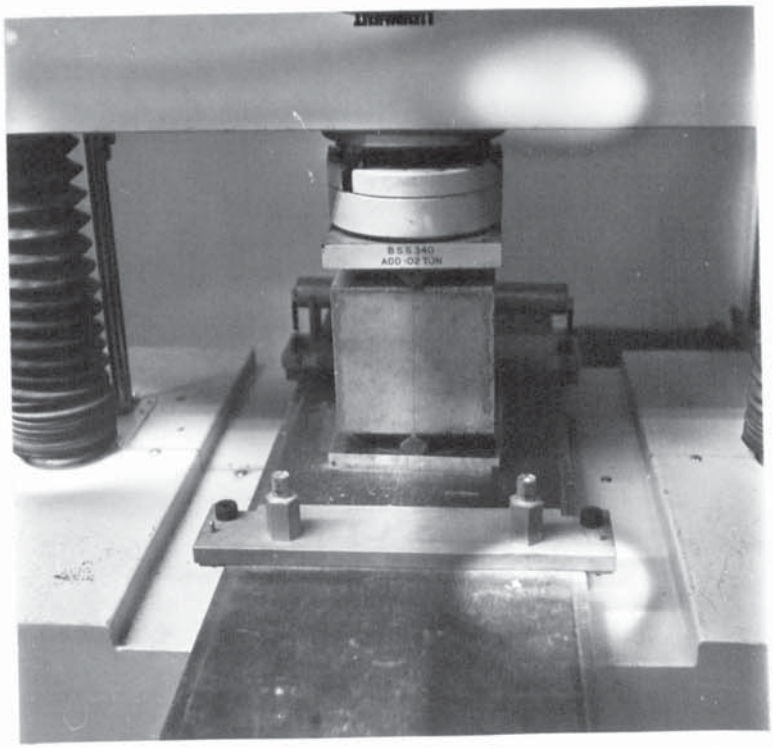

Plate 6.2.1. Cube splitting apparatus

cube. This type of arrangement produced a fairly even failure plane at the centre of the cube, with a relatively small amount of localized crushing at the loading points.

6.2.2.3. Test Rig

The nature of the tests to be carried out necessitated a rig which was capable of applying to the split cube, a vertical compressive force and a horizontal shear force. As it was also decided that the Denison machine should be used to apply the vertical load, it was also necessary for the apparatus to be able to fit onto the base of the machine.

The final design was that shown in Fig. 6.2.1, and Plates 6.2.2 and 6.2.3. The shear force was applied by a 300 kN (30 ton) manually operated hydraulic jack, the load being read off on a pressure gauge whose calibration chart is shown in Fig. 6.2.2. The jack was held laterally in position by the side plates which were welded to the main base of the rig. To ensure that the shear force was applied to the centre of the upper half of the fractured cube a channel was welded onto the base of the rig, on which the jack could rest. Reaction to the jack was supplied by a back plate which was also welded to the base of the rig. The lower half of the cube was held in position by a "cube holder" designed to support the cube up to a position just below the fracture line. The shear force was transmitted to the cube by means of a piece of angle fitting over the one face, and top of the cube as shown. The compression load from the Denison was applied via a 12 mm ($\frac{1}{2}$ in.) plate, 3 No. 75 mm (3 in.) diameter rollers, and the above mentioned angle. The whole apparatus was fixed to the base of the machine by 4 No. 12 mm ($\frac{1}{2}$ in.) diameter pins required to prevent any lateral movement of the rig during testing.

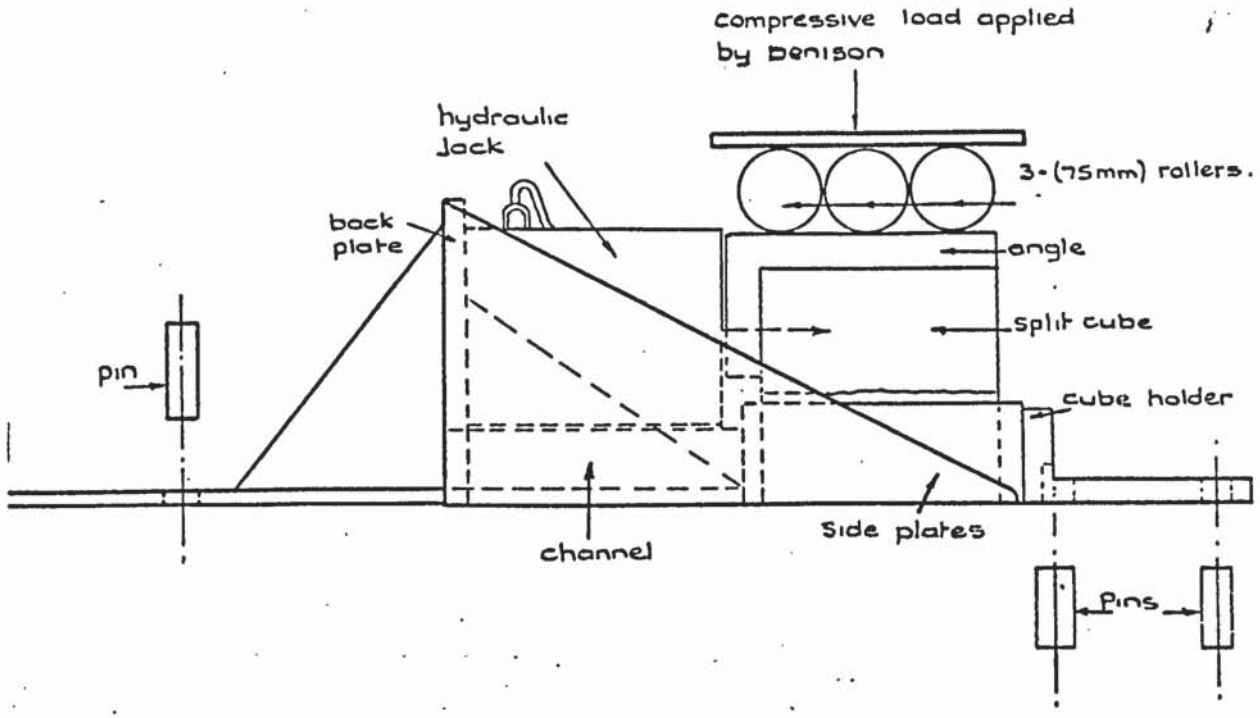

side view

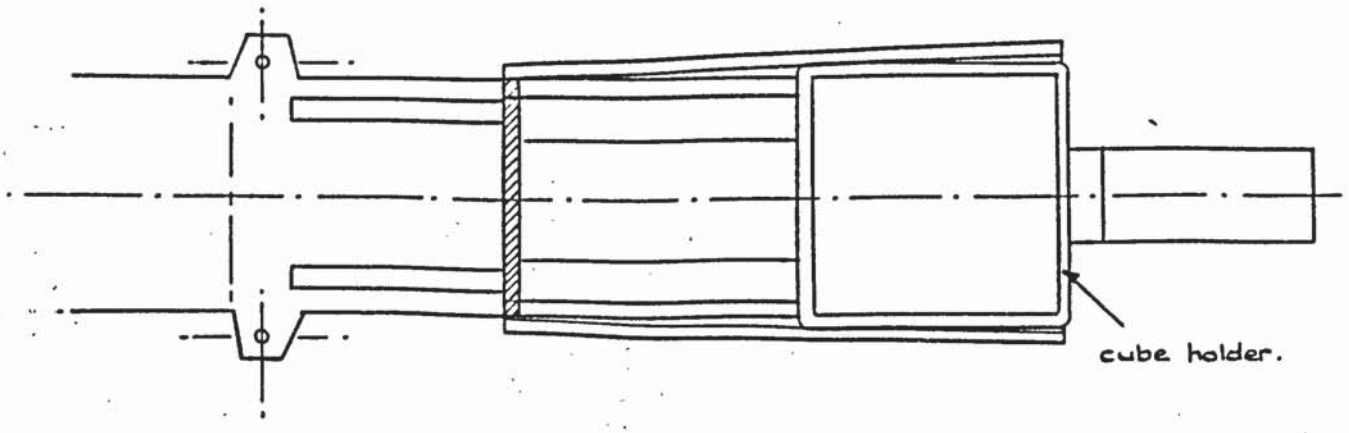

plan

Fig. 6.2.1. Split cube apparatus.

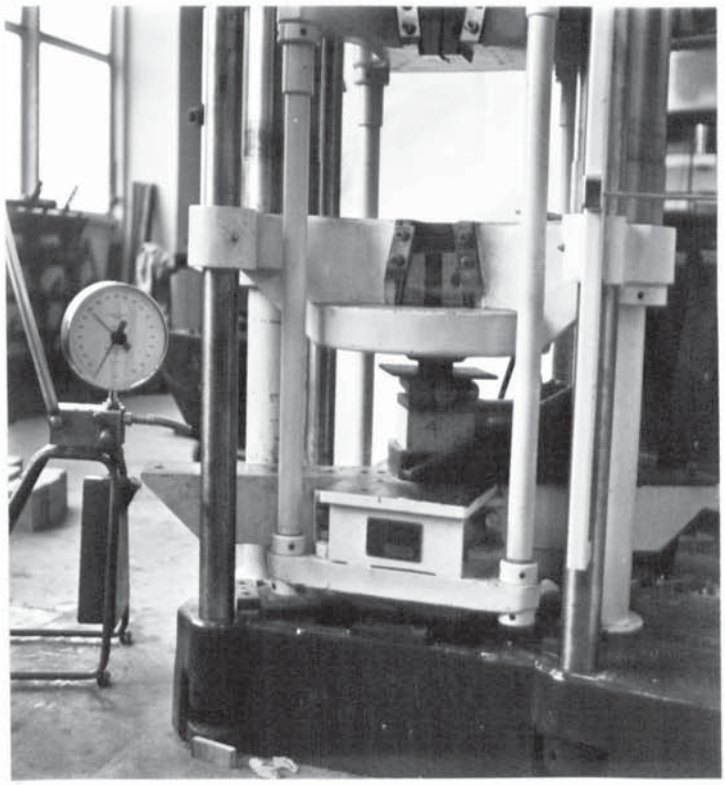

Plate 6.2.2. General view of split cube test rig

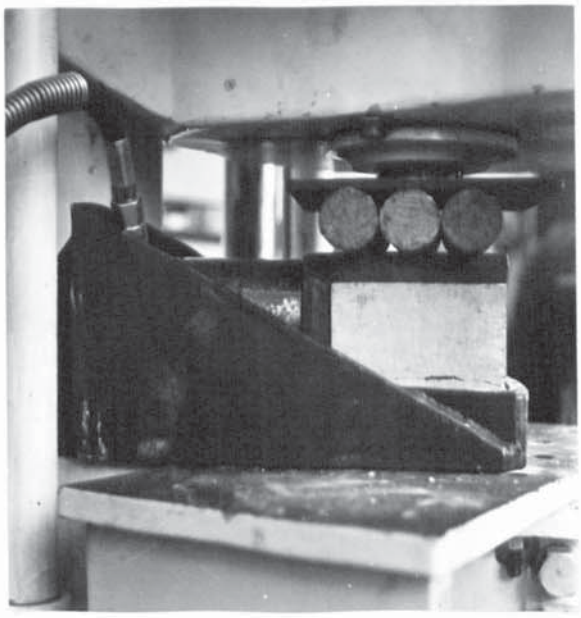

Plate 6.2.3. Detail of split cube test rig

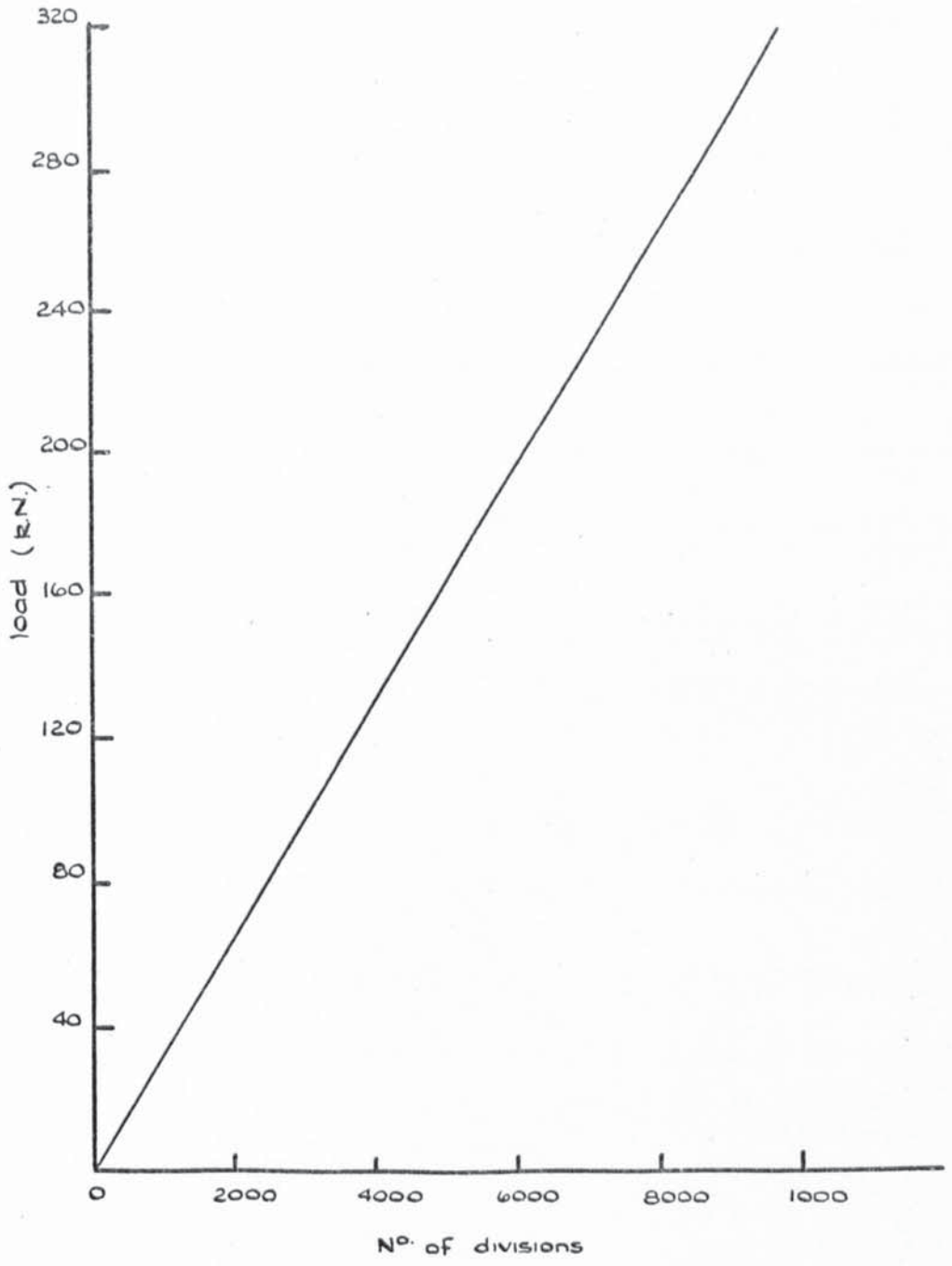

Fig. 6.2.2. Proving ring calibration chart

6.2.2.4. Description of Tests

Prior to testing all the cubes were split using the method described in 6.2.2.2. Failure was sudden and violent, although very little debris was produced enabling the two halves to be placed easily back together again before testing.

A predetermined axial load was applied to each specimen, and the shear force then applied until failure. Failure was considered to have taken place when the reading on the shear force jack began to fall rapidly, the maximum recorded load being taken as the failure load.

Failure of specimens tested under low compressive loads tended to be governed purely by the frictional forces set up between the two faces. The mechanism was simply one of the two halves being pushed over one another, with no aggregate failure and very little failure of the aggregate cement paste bond.

An increase in the compressive load produced a slightly different mode of failure, with a small amount of debris appearing on the failure surface. A closer examination revealed a breakdown in the aggregate cement paste bond with the actual aggregate still remaining intact.

As the compressive load was increased even more, the amount of debris produced became greater. In addition to the failure of the bond it was now apparent that a certain amount of the weaker aggregate was failing in shear.

A further increase in load resulted in more of the aggregate failing with the appearance of small diagonal tension cracks in the bottom half of the cube. These cracks became even more prominent at higher loads and also began to appear in the top half of the cube.

With each successive increase the proportion of aggregate failure on the surface increased.

Typical patterns of failure can be seen in Plate 6.2.4 where the bottom halves of several cubes are shown. The relatively clean, almost undamaged failure surface of No. 6 tested under very low compressive loads, can be compared against those of Nos. 1 and 4. No. 1, tested under relatively low compressive loads is predominatly a bond failure whereas the slightly rougher texture of No. 4 indicates the beginning of aggregate failure. The start, and enlargening of the tensile crack with increase in load can be seen in Nos. 7, 13, 14, and 11.

6.2.3. Discussion of Results

The results of the tests and control specimens are, shown in tabular form in Table 6.2.1, and in graphical form in Fig. 6.2.3. The cube splitting strength f_{sc} shown in the table, is calculated from the expression(38).

$$f_{sc} = \frac{2 \times \text{load}}{\pi \times \text{Area of Failure surface}}$$

The general trend of the results indicates an increase in the shear strength of the specimen for an increase in the applied compressive force. The rate of increase does, however, appear to reduce as the higher compressive loads are approached.

The distribution of the shear stress across the failure plane of the cube has been assumed to be linear. In the case of the prestressed beam a parabolic distribution of stresses in the compression zone has been assumed, which for the same load, will give a peak stress $1\frac{1}{2}$ times greater than that resulting from uniform distribution. The modified curve shown in Fig. 6.2.3 has been obtained by multiplying the measured shear stress by $1\frac{1}{2}$.

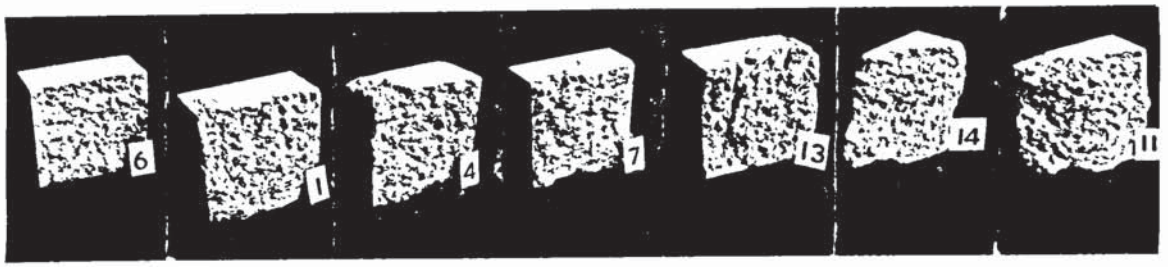

Plate 6.2.4. Typical failure patterns of split cubes

U_w = 56.0 N/mm^2(8120 lbs/in^2) f_c' = 39.1 N/mm^2 (5670 lbs/in^2)

f_{sp} = 2.38 N/mm^2 (345 lbs/in^2)

No.	Direct Compressive Stress N/mm^2 (lbs/in^2)	Shear Stress N/mm^2 (lbs/in^2)	Cube Splitting Stress N/mm^2 (lbs/in^2)
1	1.77 (257)	3.77 (547)	2.11 (306)
2	2.66 (386)	4.65 (674)	2.21 (320)
3	3.54 (513)	5.40 (783)	2.11 (306)
4	4.43 (642)	9.13 (1324)	2.44 (354)
5	5.32 (771)	7.57 (1098)	2.18 (316)
6	0.89 (129)	2.70 (392)	1.97 (286)
7	6.20 (899)	9.13 (1324)	2.09 (303)
8	7.07 (1028)	8.11 (1176)	2.66 (386)
9	7.97 (1156)	10.10 (1465)	2.04 (296)
10	9.75 (1414)	11.70 (1697)	2.61 (378)
11	10.65 (1544)	Limit of Jack	2.72 (394)
12	4.43 (624)	7.31 (1060)	2.61 (378)
13	8.86 (1284)	10.32 (1496)	2.42 (351)
14	9.30 (1349)	12.54 (1818)	2.44 (354)
15	9.75 (1414)	11.30 (1639)	2.64 (383)

TABLE 6.2.1. Test Results – Split Cubes

U_w = 56.0 N/mm^2(8120 lbs/in^2) f_c' = 39.1 N/mm^2 (5670 lbs/in^2)

f_{sp} = 2.38 N/mm^2 (345 lbs/in^2)

No.	Direct Compressive Stress N/mm^2 (lbs/in^2)	Shear Stress N/mm^2 (lbs/in^2)	Cube Splitting Stress N/mm^2 (lbs/in^2)
16	10.19 (1478)	9.75 (1414)	2.45 (355)
17	10.63 (1541)	11.47 (1663)	2.43 (352)
18	10.65 (1544)	Limit of Jack	2.47 (358)
19	8.86 (1285)	13.60 (1972)	2.35 (341)
20	10.19 (1478)	13.29 (1927)	2.46 (357)

TABLE 6.2.1. Continued Test Results - Split Cubes

If the results followed the Cowan Slip Plane Criterea,[25] then we would expect the failure envelope to be tangential to the cylinder compression circle at an angle of 37°. This can be clearly seen in Fig. 6.2.3 as not to be the case. Under normal test conditions however, the concrete has a certain tensile strength, but in this case, as the failure plane has already been formed by splitting the cube, the tensile strength has been effectively reduced to zero. The effect of this reduction on the failure envelope is not certain, but it would seem a logical step to adjust the origin of the curve, along the 'x' axis only, until it became tangential to the stress circle. The effects of this for both the measured and modified curves are shown in Figs. 6.2.4 and 6.2.5 respectively. The observed results show very good agreement with the Cowan line although the resulting apparent tensile strength is very high. The modified curve, however, although giving a tensile strength very close to that measured, does not follow so closely the Cowan curve, the angle of the tangent to the circle being 56°. It should be noted, however, that the line of both curves in the high compressive load region had to be estimated, which could give rise to certain inaccuracies, as it is in this region that the envelopes are tangential to the circle.

It is not all together certain that the effect of splitting the cube is purely to reduce the tensile strength of the specimen. It may be that it is also causing a reduction in the compressive strength, in which case it would be justifiable to adjust the origin of the curve in both the 'x' and 'y' directions. The outcome of this for the measured results is shown in Fig. 6.2.6. Once again the envelope follows fairly closely the Cowan line, the angle of the tangent to the curve being 37°, and the apparent increase in tensile strength relatively small. A slight increase in the tensile strength is to be expected, because the original curve (see Fig. 6.2.3) does not pass through the origin, and if continued back cuts the axis at

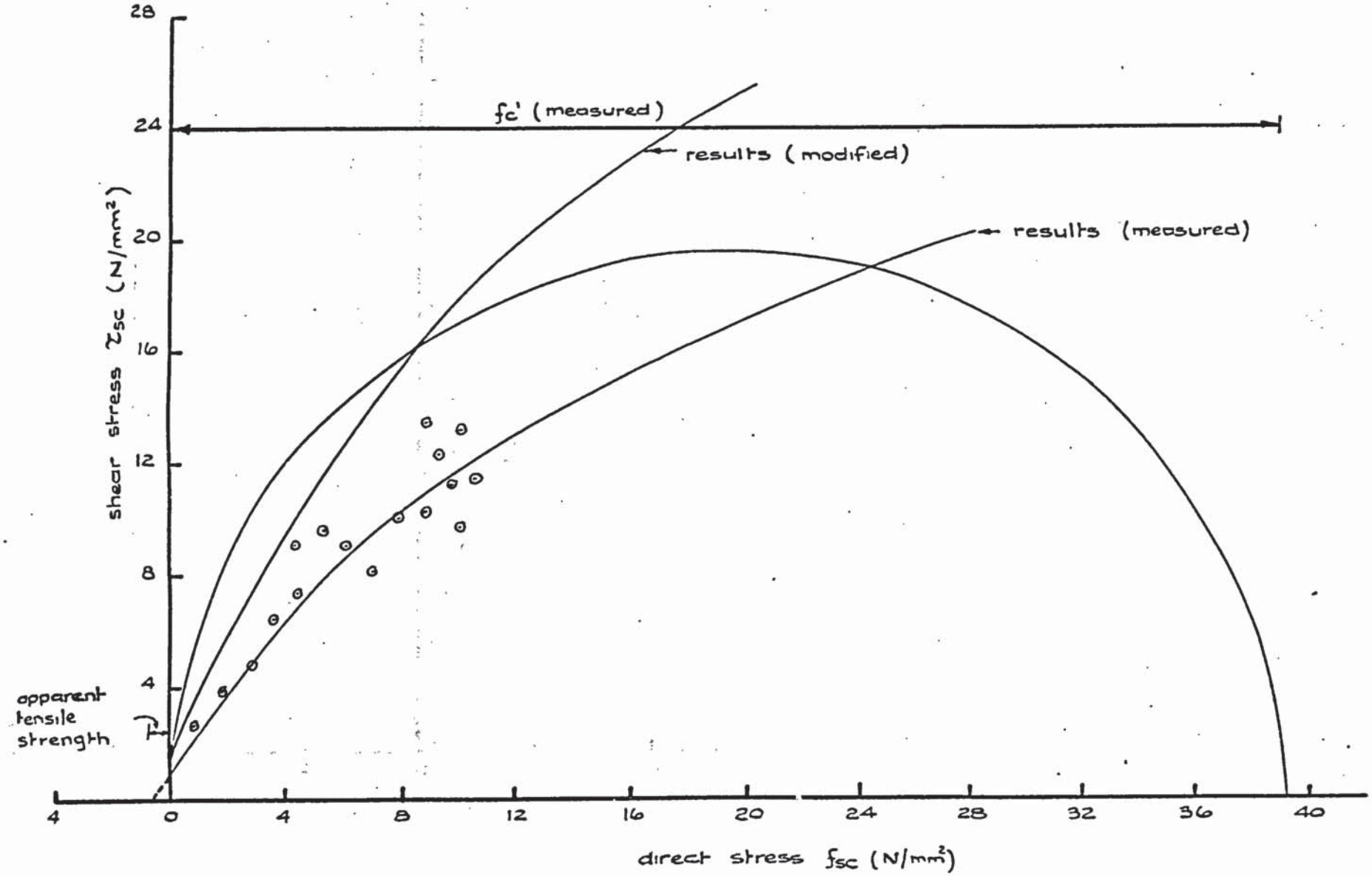

Fig. 6.2.3. - Split cube results

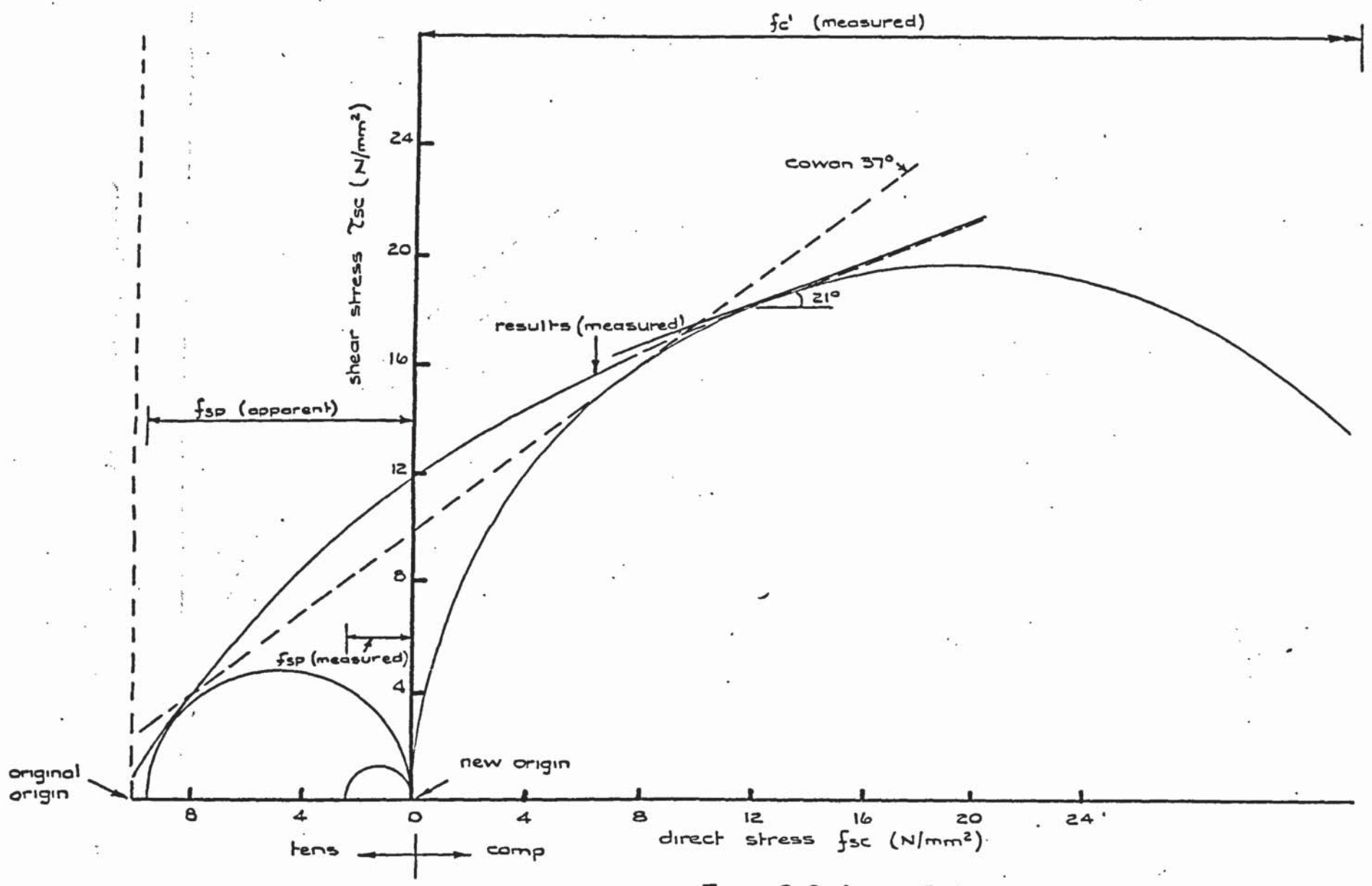

Fig. 6.2.4. Split cube results

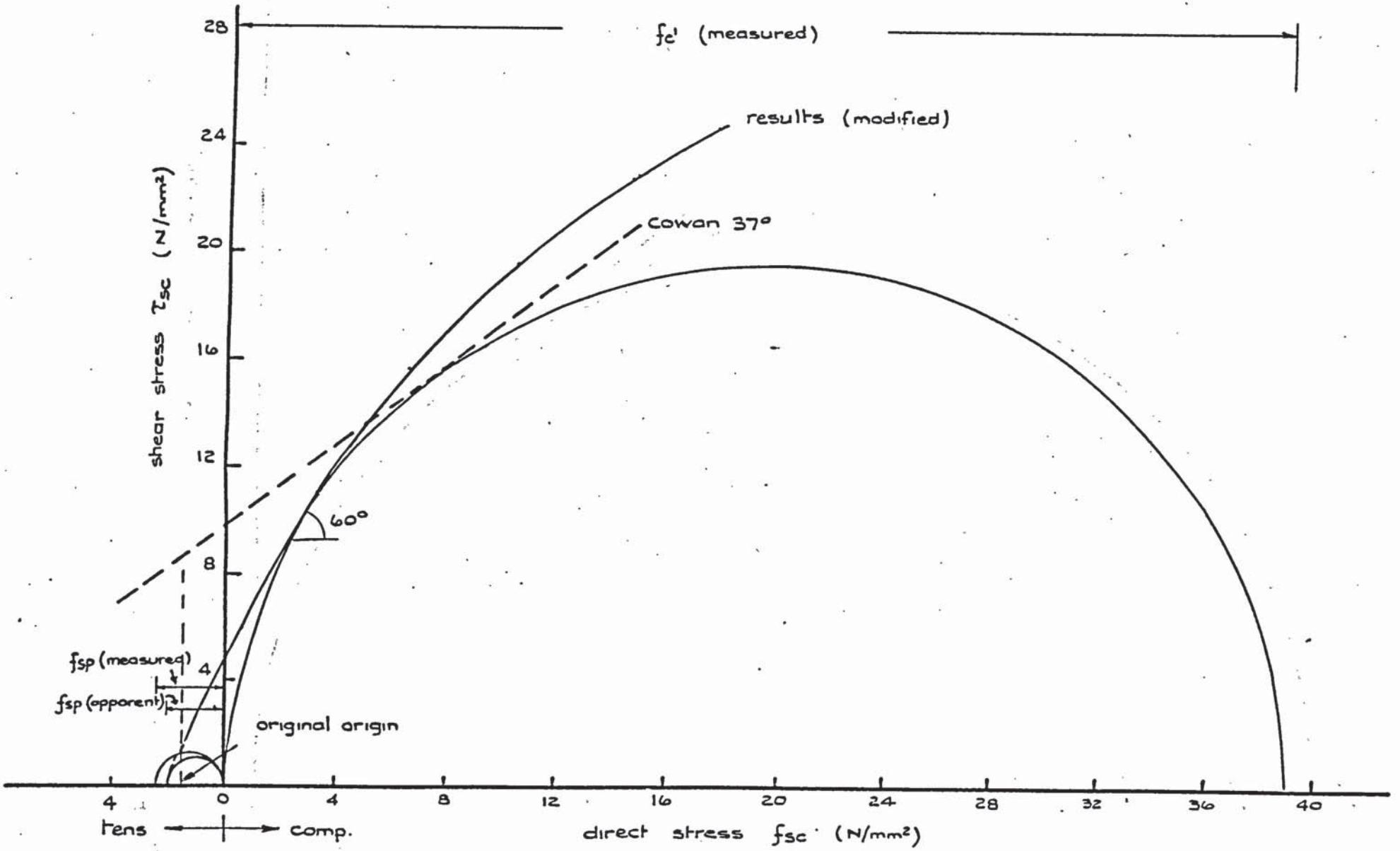

Fig. 6.2.5 · Split cube results

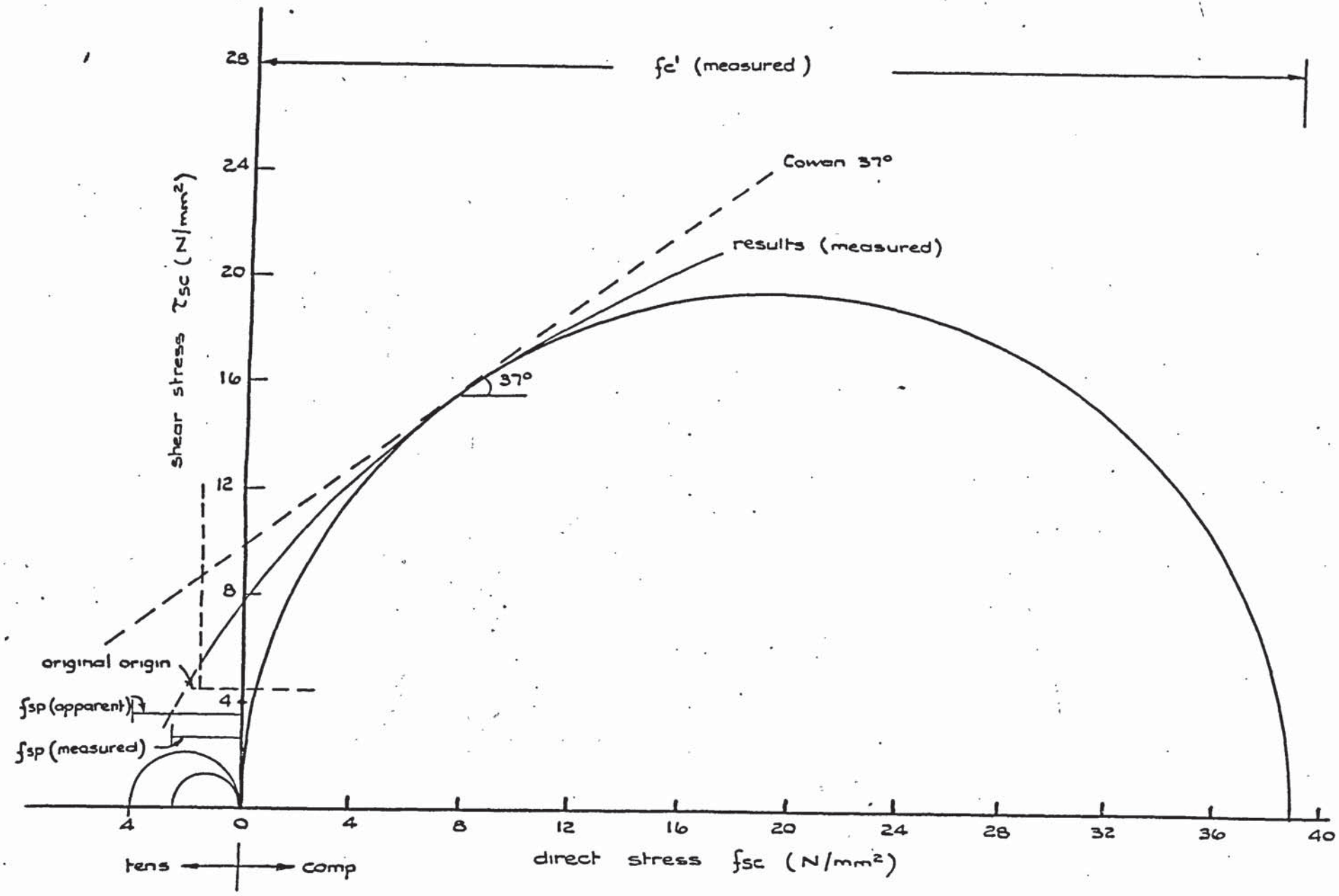

Fig. 6.2.6. Split cube results

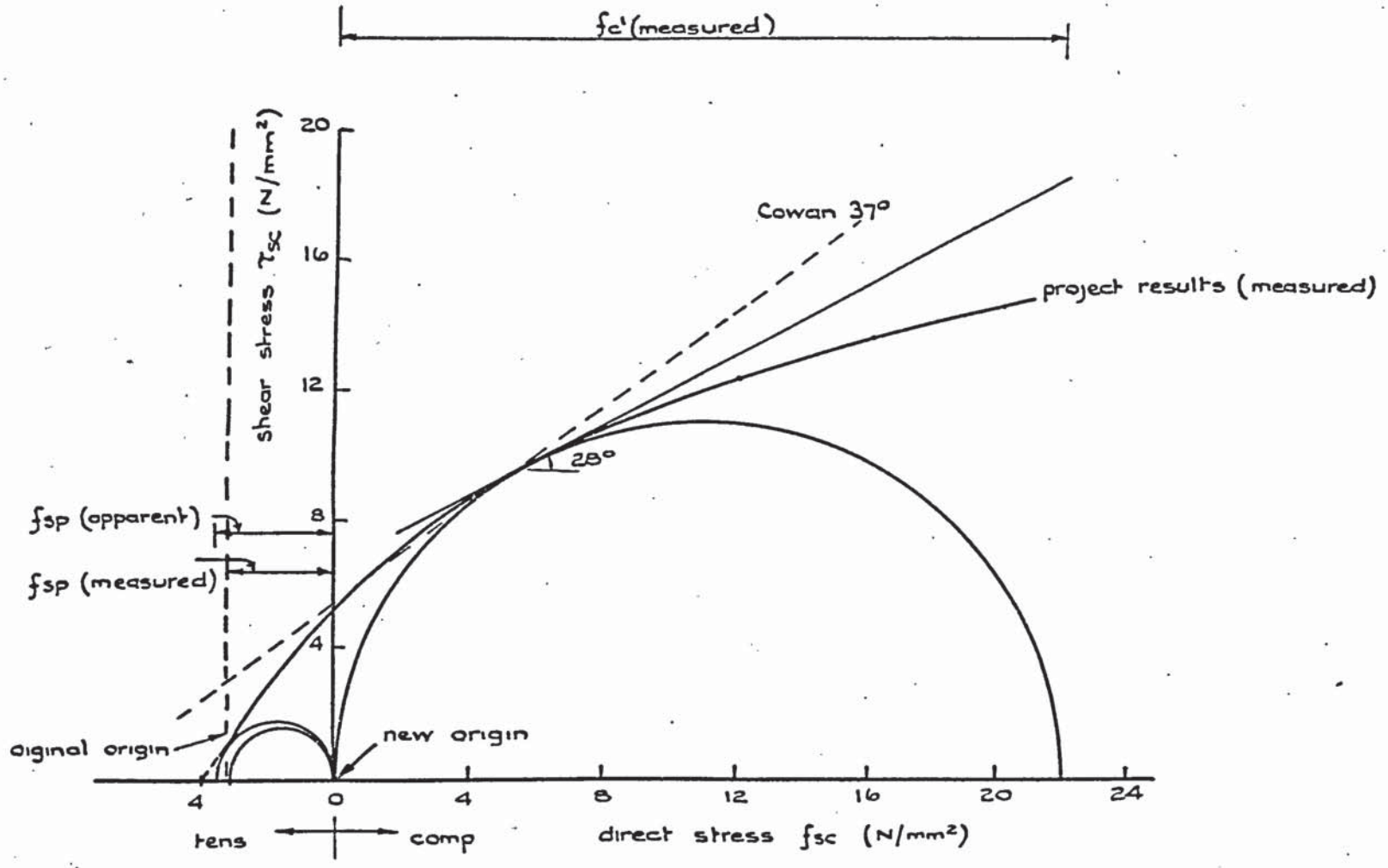

Fig. 6.2.7. Split cube results. (Project students.)

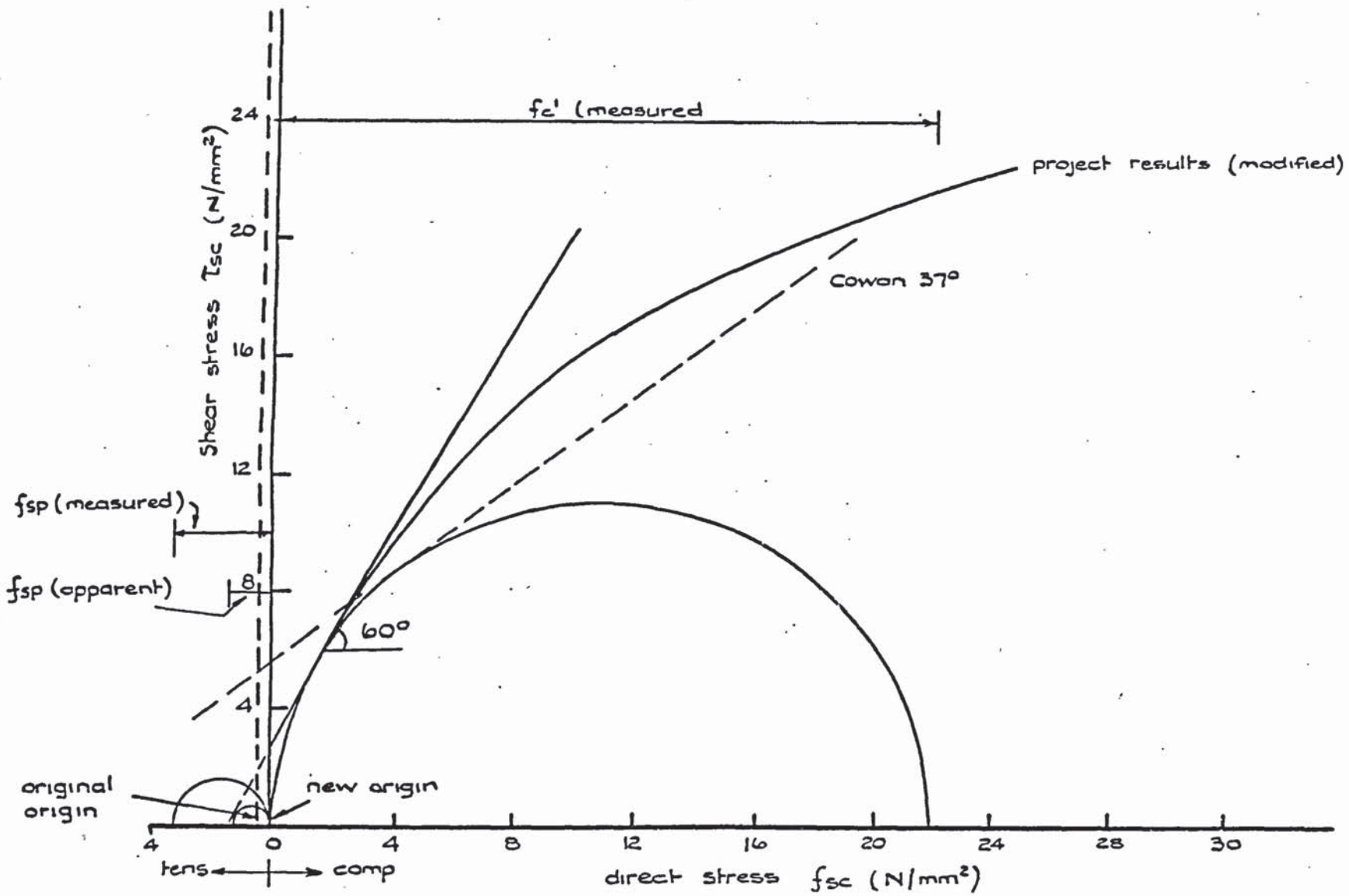

Fig. 6.2.8. Split cube results (Project students)

a value of 0.7 N/mm^2. The adjustment of the origin in both directions applied to the modified curve produces the same conditions as those shown in Fig. 6.2.5. No adjustment in the vertical direction is required to enable the curve to become tangential to the circle.

The results of work carried out by final year undergraduate students under the supervision of the author and his tutor are shown in Figs. 6.2.7 and 6.2.8. They tested 32 No. cubes of identical mix to those of the author, but cured for only 7 days. The general trend of the results is similar to those described previously, the shear stress at high compressive loads being somewhat lower than before.

The adjustments required to bring both curves tangential to the stress circle are in a horizontal direction only. The measured results show close agreement with the Cowan line, the angle of the tangent being 28°. The apparent increase in tensile strength is very small and is close to the value of 0.8 N/mm^2 obtained from the fact that the original curve does not pass through the origin. Comparison with the modified curve (see Fig. 6.2.8) is not so good, the angle of the tangent being 60°, and the resulting tensile strength somewhat lower than that measured.

6.2.4. Conclusions

The results obtained from the tests do not prove conclusively that the type of failure produced is analogous to that of the Cowan slip plane criteria. It is felt, however, that there is some relationship between the two mechanisms, although its actual form is not yet certain. The main difference between the two is that the failure surface of the cubes was preformed by splitting, which obviously effects the tensile strength of the specimen. Good agreement is obtained (see Fig. 6.2.7) using the results of the project students and adjusting the origin by an amount equal to the measured split cylinder strength. This is not the case with the authors results where the best agreement is obtained

(see Fig. 6.2.6) by adjusting the origin in both directions. The concrete strengths obtained by the students, however, are questionable. The 7 day cylinder crushing strength of 22 N/mm^2 is reasonable compared with the 28 day strength of 39 N/mm^2 obtained by the author. The split cylinder strength of 3.2 N/mm^2, on the other hand, appears rather high when compared with that of 2.4 N/mm^2 obtained after 28 days. The results of two sets of tests is not felt to be sufficient enough to draw any definite conclusions on the effect of the splitting of the cube. Had time permitted the author would have liked to continue with the tests in this field. It would have been most beneficial had results been obtained with much higher compressive loads to enable the "falling off" point of the curve to be determined. To do this would have required a larger capacity jack to apply the shear force, and almost certainly, a new test rig, the design of which would have taken up valueable time.

Tests on cubes which had not previously been split would also be of great interest, hence eliminating the problem of loss in tensile strength. It is felt, though, with such a test, that the cube may not fail along the desired plane, which was the main reason for splitting the cube prior to testing. Work along these lines is being carried out within the department but unfortunately no results are available at the time of writing.

6.3. The Direct Tension Test

Summary

20 No. 150 mm (6 in.) diameter x 300 mm (12 in.) solid cylinders were tested by various methods in an attempt to determine the direct tensile strength of the concrete. In all the tests carried out failure occurred at, or near one end of the specimen at a stress about 50% lower than the split cylinder strength. It was concluded that a state of triaxial tension was being developed at the end of the specimen resulting in the low failure load.

6.3.1. Introduction

The theoretical solutions for the failure of the prestressed beams in Modes 2 and 3 are based upon a tensile strength of concrete. It was necessary therefore to have an accurate knowledge of the tensile strength of the concrete used throughout this investigation. There are two methods in common use at the moment of determining a tensile strength of concrete, namely, the cylinder splitting test, and the modulus of rupture test. Opinions differ however as to which, if any, of the two tests give a true indication of the tensile strength of the concrete. It is well known[48,50,51] that the modulus of rupture gives a higher failing strength than the cylinder splitting strength, Ward [51] reported a ratio of 1.35 between modulus of rupture and indirect tension strengths. The reasons for this difference is the variation in stress distribution between the two types of specimens. Blakey and Beresford[52] indicated that in a flexure test the stress distribution in the compression zone may be linear, but in the tension zone it may be either a second or third order parabola. Evans [48] also reported that it was possible to balance the internal forces in a flexural beam at failure only as long as the direct tension strength was not less than 59% of the flexural strength. Tests by Hsu[20] and Wright[30] have shown that the value of modulus

of rupture is dependent on the size of specimen used.

The stress distribution in the split cylinder test is somewhat complex, but if certain assumptions are made, as explained by Wright[53] a simplified stress analysis leads to the widely accepted formula.

$$\text{Tensile Strength} = \frac{\text{load at failure}}{\text{half circumference x length of cylinder}}$$

Chapman[54] has shown, however that results obtained from this test depend upon the width and type of packing pieces employed. He also indicated that a tensile failure will only occur if the ratio of true compressive strength to true tensile strength is greater than 8.

For a true uniaxial tensile strength, the specimen should be loaded in such a manner so as to produce a state of uniform tensile stress across the critical section.

The object of the work described here was to develop a suitable uni-axial tension test employing standard 150 mm (6 in.) diameter cylinders as test specimens.

6.3.2. Review of Previous Work

More than 30 different testing techniques have been employed to apply a uni-axial tension force to a test specimen. All these methods may, however, be divided into four main categories, namely:-

6.3.2.1.) Specimens with enlarged ends

a) tensile briquets

b) large tension specimens

6.3.2.2.) Specimens with embedded bars

6.3.2.3.) Frictional gripping techniques

6.3.2.4.) Adhesives

6.3.2.1. Specimens with enlarged ends

The tensile briquet used originally as a standard test for cement performance was the first method adopted. The small size of the

specimen lead to many disadvantages however, and more recent tests were carried out using enlarged specimens. The main disadvantages of this system are:-

1) eccentricity due to non-alignment of the centre line of the specimen with the applied load.

2) stress concentrations around the grips.

Evans [48] carried out strain measurements on opposite sides of several different sizes of briquet. He concluded that the strain distribution on these specimens depended to a large extent on the original location of the specimen in the grips.

6.3.2.2. Specimens With Embedded Bars

Basically this method involves casting a bar, or bars into the end of the specimen through which a direct tensile load can be applied. Great care must be taken when setting the bars in place to ensure that no inherent eccentricity is produced. The method becomes very tedious when a large number of specimens are to be tested.

6.3.2.3. Friction Gripping Techniques

This method is probably one of the most widely used today, and work is still continuing to improve it.

In 1926 D. Abrams[55] produced the first of such grips. These grips comprised pieces of steel pipe split into quarters and lined with leather. Friction was produced by tightening the tangential connecting bolts. The majority of the specimens tested however, failed in the region of the grips.

It is considered that the most effective method for gripping a direct tension specimen is that designed by O'Cleary and Byrne[56]. Self-centering "lazy tongs" were used to grip the prismatic specimen with reduced centre section and reinforced ends.

Recent modifications have been made to this system by Ward and Johnston and Sidwell [57].

6.3.2.4. Adhesives

A relatively new method of applying a direct tensile force is to attach the test specimen to the loading system by means of a suitable adhesive. Chapman (58) carried out a series of tests using a necked prismatic specimen with glued end plates. Hsu (20) reported tests on 150 mm (6 in.) diameter cylinders, a slice of concrete being removed from either end, and steel plates attached by means of an epoxy resin.

6.3.3. Experimental Work

6.3.3.1. Test Specimens

As mentioned previously the purpose of the tests was to develop a simple uni-axial tension test using standard 150 mm (6 in.) diameter cylinders. With each prestressed beam cast three standard cylinders were included in the control specimens for the purpose of this test.

6.3.3.2. Description of Apparatus and Tests

Alterations were continually being made to the apparatus after the completion of each test. It is now proposed to describe the tests in sequence, at the same time making reference to the changes made in the testing equipment.

Early tests were carried out using a friction grip apparatus similar to that of Abrams (55) and shown in Fig. 6.3.1.

The grips consisted of pieces of 150 mm (6 in.) steel pipe 100 mm (4 in.) in depth, cut in two, and serrated on their inner surface. The specimen was gripped by tightening radial bolts passing through a heavy end plate in which the grips were seated. Load from the machine was transferred to the grips by a type of universal joint manufactured in the university workshop.

Abrams used leather packing pieces in his grips to prevent failure within the grips due to the stress concentrations produced there. He reports however, that the majority of specimens tested in this manner

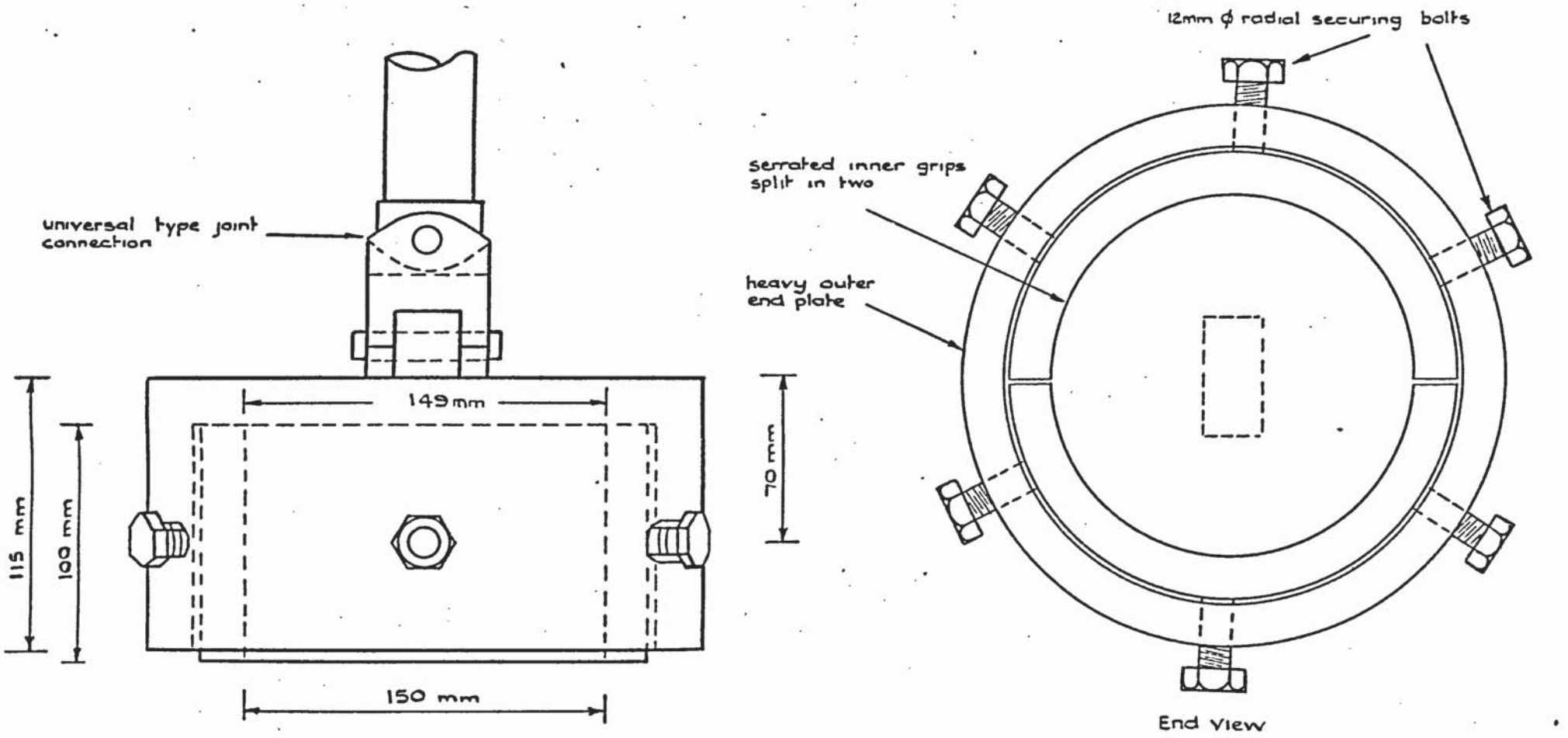

Fig. 6.3.1. Friction grip apparatus.

failed in the vicinity of the grip, but assumed that the failing stress very nearly represented the true tensile strength of the material. It is felt that there must be stress concentrations induced near the grips where the stress changes from pure tensile to pure compressive. This, it is thought causes the specimen to fail at a stress lower than its pure tensile stress. The "lazy tong" grips developed by Johnston and Sidwell [57] eliminates this phenomena. The change of axial tensile stress from unity to zero within the grip being gradual and continuous, and the lateral compressive stress falling to zero near the inner extremity of the grip. The grips however, can only be used on rectangular specimens and would not be applicable to the cylinders. It was therefore decided to try and produce this effect with the circular grips by tapering them. They were machined to measure 149 mm in diameter at their outer extremity and 150 mm at their inner extremity. With all cylinders tested in this manner failure occurred within the grips. Plaster of Paris was used to bed the specimen in the grips to help distribute the load more evenly and remove any high or low spots on the surface of the cylinder. Failure again occurred within the grips. A typical test is shown in Plate 6.3.1. The joints used to transmit the load to the cylinders were not true universal joints and it was felt that the load applied may not be purely axial. The universal joints required for this purpose were too large to allow the apparatus to be accommodated in the Dennison testing machine and as a result a new line of approach was decided upon.

Tests by Hsu [20] have shown that failure in uni-axial tension at the centre section of a cylinder may be produced by attaching end plates to the specimens by means of a epoxy resin. Using the end plates shown in Fig. 6.3.2. and bolting them to the universal joints it was

possible to place the whole apparatus in the testing machine as shown in Plate 6.3.2.

A 130 mm (5 in.) slice was removed from the end of one of the cylinders by means of a carborundum saw, and the other end cleaned using a "Grinderette" abrasive machine and a de-greasing agent "Tetrachlorethylene". An epoxy resin manufactured by "Araldite Ltd." of the type AV.123B in conjunction with a hardener type H.V.953B was used to adhere the steel plates to the concrete specimen. Care was taken to ensure that the plates were aligned at right angles to the axis of the cylinder, and weights were placed on top during the curing period to ensure good bond.

Failure occurred in the bond between the glue and the concrete at the end which had not been sawn.

The next test was carried out using a cylinder which had been reduced to 180 mm (7 in.) in length by removing slices off both ends. All ends and plates were de-greased and the same glue as before used. The end plate again pulled away from the specimen at the concrete, glue interface, but it was now apparent that although adhesion between the cement paste and glue was successful, no such adhesion was occurring with the particles of aggregate.

The glue manufacturers were contacted and a new adhesive type GY278 with hardener HY850 was recommended. This proved less reliable than the previous method.

Another glue type AY103 with hardener HY951 was advised by the manufacturers who also advised the etching of the steel plates with sulphuric acid. Despite increasing the curing time from 4 hours at 60°C to 15 hours at room temperature and 4 hours at 60°C, there was no bond between steel and glue.

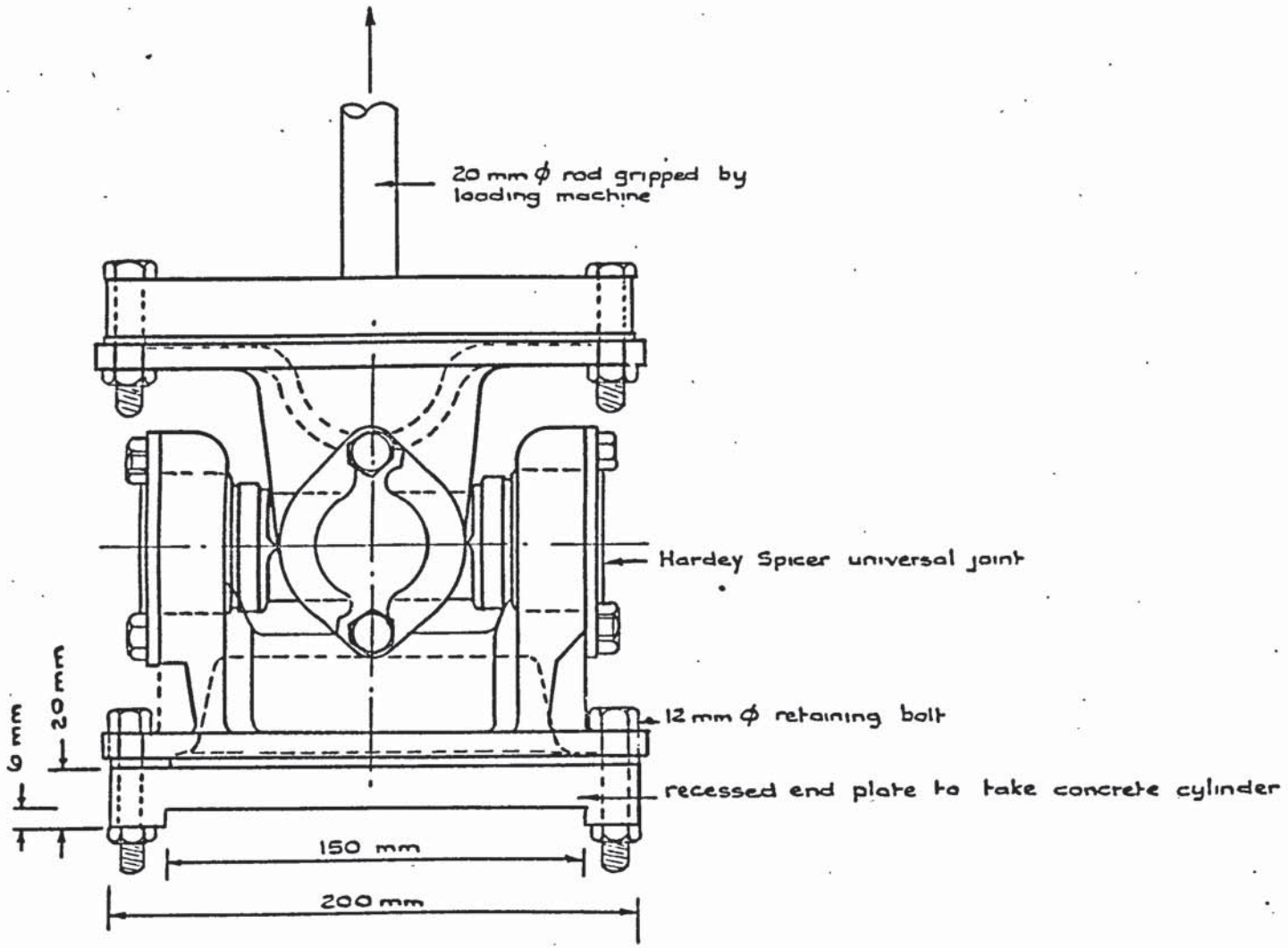

Fig. 6.3.2. Detail of recessed end plates and joint for adhesive test.

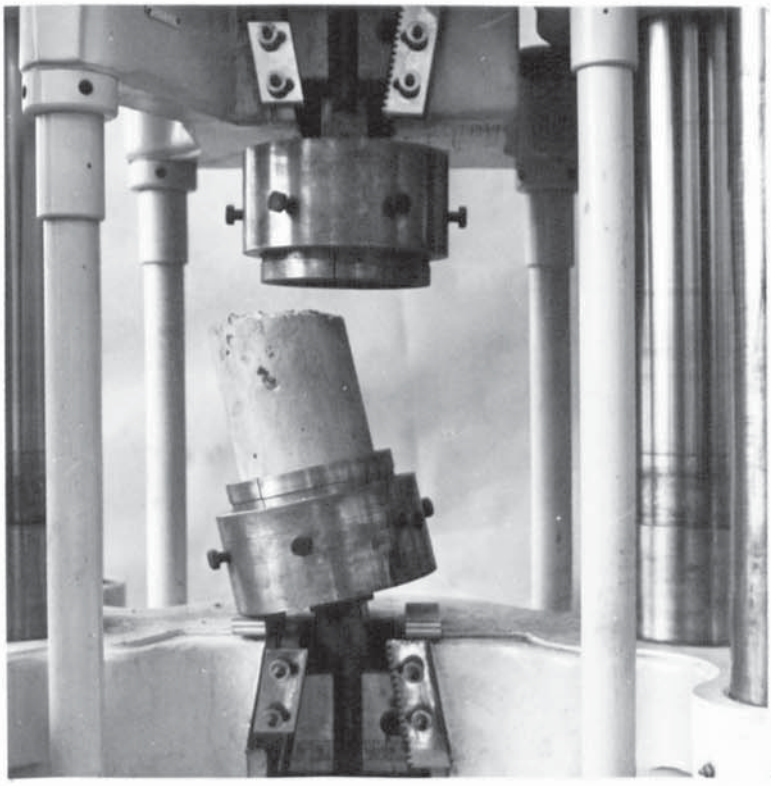

Plate 6.3.1. - Direct tension test - friction grips

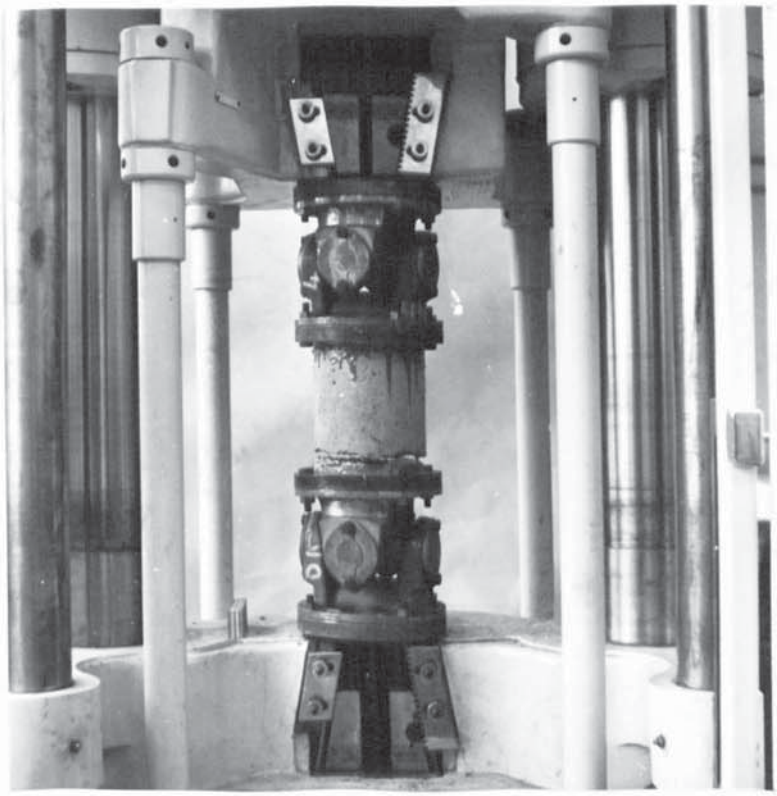

Plate 6.3.2. - Direct tension test - adhesive technique

Fig. 6.3.3. Location of failure plane recessed plates

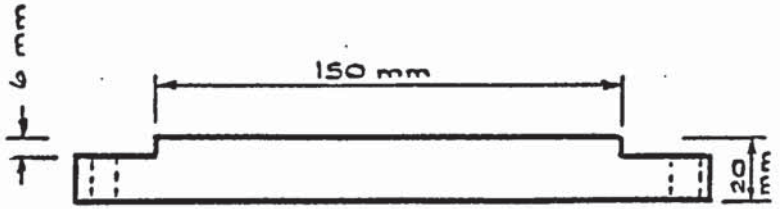

Fig.6.3.4. Modified end plates with upstand.

The question of whether the strength of a vertically cast cylinder varies throughout its depth was still in doubt. To try and clarify this a cylinder was cut in half, and, using the bottom half only and following the same procedure as before the test was carried out. The result was identical to that of previous tests, the critical section being at the upper end of the cylinder. It is unlikely that the strength of the cylinder varies from top to bottom and it was still thought that the lateral restriction supplied by the end plates was causing premature failure. The fact that the last three cylinders all failed in the top was not sufficient evidence to support the fact that the weaker section was at this point.

It was noticed from the photographs, see Plate 6.3.3 of Hsu's apparatus that his end plates were of the same diameter as his cylinders. From the brief description of the tests given in the report this appeared to be the only obvious difference between the authors apparatus and that of Hsu. It was therefore decided to modify the end plates to the shape shown in Fig. 6.3.4 in an attempt to eliminate the end restraint. Using the bottom half of a cylinder whose ends had been sand blasted, failure again occurred very close to the extremity, but in this case it took place at the lower end.

Due to time limitations it was now decided to discontinue work on this particular experiment.

6.3.4. Conclusions

The results of all the tests carried out are shown in Table 6.3.1. The time of casting to time of testing may vary considerably in many cases. This is because all cylinders tested were used only as a means of testing the apparatus and not as control specimens for specific tests.

The tendency for all the cylinders, with end plates attached

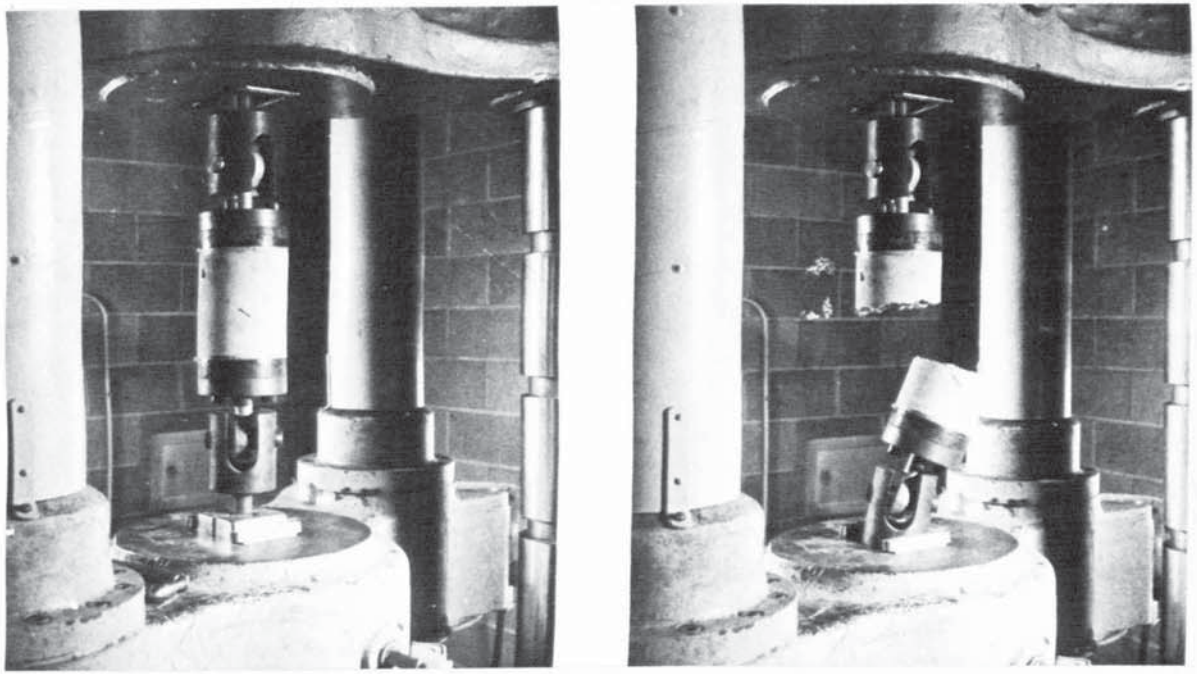

Plate 6.3.3. - Direct tension apparatus used by Hsu[20]

No.	Date Cast	Date Test	Strength in N/mm^2 (lbs/in^2) At Date			Failure Stress N/mm^2 (lbs/in^2)	Remarks
			Date	Cube Strength	Split Cylinder		
1(F)	24/2/69	30/10/69	18/11/69	65.0 (9400)	3.24 (470)	0.98 (142)	Slipping in grips
2(F)	14/1/67	30/10/69	25/7/69	38.36 (5562)	2.34 (340)	1.53 (222)	Fracture in grips
3(F)	24/2/69	31/10/69	18/11/69	65.0 (9400)	3.24 (470)	1.48 (214)	"
4(F)	" "	" "	" "	"	"	1.31 (190)	Plaster of Paris used failure still in grips
5(F)	" "	9/12/69	" "	"	"	1.94 (281)	Tappered grips Failure in grips
6(A)	" "	13/5/70	" "	"	"	0.65 (95)	Slice from 1 end No adhesion concrete to glue
7(A)	" "	14/5/70	" "	"	"	1.09 (158)	Slice from 1 end Partial adhesion conc. to glue
8(A)	" "	15/5/70	" "	"	"	1.19 (173)	Slices off both ends - No adhesion aggregate to glue

TABLE 6.3.1. Test Results - Direct Tension Tests

Key: (F) denotes friction grips

(A) denotes adhesive grips

No.	Date Cast	Date Test	Strength in N/mm^2 (lbs/in^2) At Date			Failure Stress N/mm^2 (lbs/in^2)	Remarks
			Date	Cube Strength	Split Cylinder		
9(A)	24/2/69	18/5/70	18/11/69	65.0 (9400)	3.24 (470)	1.40 (203)	Slices off both ends New glues used
10(A)	" "	" "	" "	"	"	1.38 (200)	No adhesion concrete to glue
11(A)	" "	19/5/70	" "	"	"	0.13 (20)	New glues - end plates etched, no adhesion
12(A)	" "	5/6/70	" "	"	"	1.29 (186)	New glues - concrete etched - no adhesion aggregate to glue
13(A)	" "	" "	" "	"	"	1.04 (150)	
14(A)	5/11/69	22/6/70	12/12/69	46.7 (6724)	1.26 (183)	1.23 (178)	Ends sand blasted new glues - no adhesion glue to concrete
15(A)	" "	" "	" "	"	"	1.26 (182)	
16(A)	8/4/70	30/6/70	8/5/70	57.3 (8313)	2.72 (395)	2.24 (324)	Adhesion achieved glue type AV121 + HY991 - Failure near end

TABLE 6.3.1. Test Results - Direct Tension Tests Continued

Key: (F) denotes friction grips

(A) denotes adhesive grips

No.	Date Cast	Date Test	Strength in N/mm^2 (lbs/in^2) At Date			Failure Stress N/mm^2 (lbs/in^2)	Remarks
			Date	Cube Strength	Split Cylinder		
17(A)	6/5/70	8/7/70	5/6/70	52.6 (7632)	3.39 (493)	1.82 (264)	Failure near end
18(A)	22/4/70	10/7/70	22/5/70	56.2 (8146)	2.61 (379)	1.72 (249)	Failure near end at top
19(A)	20/5/70	20/7/70	18/6/70	49.8 (7229)	3.38 (491)	1.64 (238)	Flat end plates, failure near end at top
20(A)	22/4/70	20/7/70	22/5/70	56.2 (8146)	2.61 (379)	1.41 (204)	Recessed end plates - failure as before
21(A)	24/2/69	30/7/70	18/11/69	65.0 (9400)	3.24 (470)	1.43 (218)	" " " " " "
22(A)	" "	" "	" "	"	"	1.36 (198)	Flat end plates - failure as before
23(A)	" "	31/7/70	" "	"	"	1.55 (224)	Upstand end plate - failure in bottom

TABLE 6.3.1. Continued

Test Results - Direct Tension Tests

Key: (F) denotes friction grips
(A) denotes adhesive grips

by adhesive, to fail prematurely at the ends was due to the lateral restraint supplied by the plates. This problem could have been overcome by reducing the central section, but as mentioned previously the purpose of the experiment was to develop a test using standard 150 mm (6 in.) cylinders. One other possible way of overcoming this may by to place a layer of a third material between the steel and the concrete. This material, possibly a hard rubber, must allow the concrete to increase in area as it is stretched, yet at the same time remain adhered to the steel on its other face. It is suggested that future work in this field be carried out along these lines.

The friction grip technique may indeed be a better line of approach to the problem, but as mentioned previously the apparatus available did not allow this part of the work to be continued. If perfected it would certainly be more practical than the adhesive method, as a great deal of time and preparation would be required to prepare the cylinders for such a test.

6.4 The Stress - Strain Relationship of The Concrete

Summary

12 No. 300 mm (12 in.) x 150 mm (6 in.) diameter cylinders were tested under simple compression. A stress - strain relationship for the concrete was determined together with a ratio between the cube compressive strength and the cylinder compressive strength.

6.4.1. Introduction

The analysis of beams failing in Mode 1 required a knowledge of the stress - strain relationship of the concrete. In addition, the values of the "peak" strains and ultimate strains produced under direct compression were required. It was not possible to determine these values from the Young's Modulus tests carried out in the main series. The type of apparatus used (see 2.10.2) did not enable the strains near failure of the cylinder, to be recorded.

A large amount of work has been carried out in investigating the stress - strain relationship of concrete. As yet no general solution, applicable to all types of concrete, is available. The nature of this curve is dependent upon many factors, the most important of which are the strength of concrete, the type of aggregate, and the rate of loading. Clearly any equation taking account of all these variables would need to be complex. Many equations, both simple and involved, have been put forward in an attempt to represent this curve, and several of these are shown in Fig. 6.4.5.

That proposed by Desayi and Krishnan[39] shows fairly good agreement with results obtained by Whitney[40] and Hognestad.[41]. Saenz[42] however, points out that this equation is only a simplification of the one proposed by himself. The same equation is also the

basis of that put forward by the European Concrete Committee. In both cases the assumption is made that the value of the ratio between the initial tangent modulus and the secant tangent modulus is 2.0. This, Saenz purports is not the case, since it does in fact vary from 4.0 for low strength concretes to 1.3 for high strength concretes. Hognestad, Prentis [43] and Smith [44] all proposed similar methods of determining the shape of the curve by means of numerical differentiation.

The method of testing is also a point over which many experimenters appear to disagree. The stress-strain relationship obtained from a cylinder under concentric loading is thought, by some, not to be a true representation of the conditions occurring in a beam under flexure. Sturman[45] carried out tests on rectangular concrete prisms both concentrically and eccentrically loaded. He found a marked difference in the resulting stress - strain curves. The peak of the eccentric curve occurred at a point which had a strain 50% higher, and a stress 20% higher than comparable points on the concentric curve. The differences in the 2 tests, pointed out by Saenz, include:-

1) The differences in the normal stresses and strains developed.
2) The influence of flexural shear stresses and strains.
3) The rate of loading on different fibres.
4) The type of failure and type of restraint.

Despite these differences, however, he concluded that their effect on the shape of the curve was very small. Only in the case of low strength concretes would there be a pronounced difference. Tests conducted by Smith and Young[46] and Hognestad[41] appear to support this view. The cylinders tested by Hognestad failed suddenly shortly after the maximum load was reached. He concluded that this

was due to the sudden release of energy stored in the machine, which in turn was related to the stiffness of the machine.

The author decided that, due to the large degree of uncertainty regarding the stress - strain curve, a seperate investigation into this relationship would be desirable.

The average ratio between cylinder compressive strength, and cube compressive strength, measured during the tests on the prestressed beams, was 0.73. This was considered somewhat low as a value of 0.80 is that generally accepted by most investigators. The results from this series of tests were also used, therefore, as a means of substantiating this value.

6.4.2. Experimental Work

6.4.2.1. Test Specimens

12 No. 300 mm (12 in.) x 150 mm (6 in.) diameter cylinders were cast together with 12 No. 150 mm (6 in.) cubes. The cylinders, capped 12 hours after casting, were tested to determine f'_c , and the cubes tested to determine U_w. In addition, the tests on the cylinders were used as a means of determining a stress - strain relationship for the concrete. The mixing and curing conditions were identical to those of the main series. The method of vibration used previously had been by external poker vibrator, and it was thought that this may be having some effect on the cylinder strength to cube strength ratio. It was therefore decided, in this particular test, to carry out vibration by means of a table vibrator.

6.4.2.2. Details of Tests and Apparatus

Strains in the concrete were measured by means of electrical resistance gauges of the same type used previously. Two gauges were fixed at the mid height of each cylinder, parallel to its vertical axis, and on opposite sides of a diameter. Details of the gauges and

methods of fixing are described in 2.10.2.

Use was made of an ultra violet recorder to record the strains instead of the Peekel arrangement used in all previous tests. This arrangement allowed a continuous stress - strain plot to be produced up to a point at, or near the failure of the cylinder. The type of recorder used was a 6 channel, type S.E.2005, manufactured by S.E. Laboratories (Engineering) Ltd. Each of the 2 gauges on the cylinder formed 1 arm of a Wheatstone Bridge Circuit as shown in Fig. 6.4.1. The 3 dummy gauges were of the same type as the active gauge, and were all attached to a single concrete cube. A constant voltage of 8V was supplied to each bridge circuit by means of a voltage regulator. Each of the 2 bridge circuits were connected to individual channels on the recorder.

Calibration was carried out using a simple 2 point bending test as shown in Fig. 6.4.2. Two gauges were fixed along side one another to the underside of a stainless steel bar. One of them completed 1 of the bridge circuits which was then connected to the U.V. recorder. The second gauge was attached to a Peekel strain recorder. A change in the strain on the bar produced a trace on the U.V. recorder and a corresponding direct strain reading on the Peekel box. As both gauges were recording identical strains it was possible to relate the amplitude of the trace on the U.V. recorder to a direct strain reading. The average results of several test was taken and a straight line relationship up to 4000 micro-strains obtained. The second bridge circuit was calibrated in a similar manner. The deflection of the trace produced by a change in resistance of the active gauge was dependant upon the sensitivity of the galvanometer and the size of the voltage supply. Both these were fixed so that the maximum expected strain of 5000

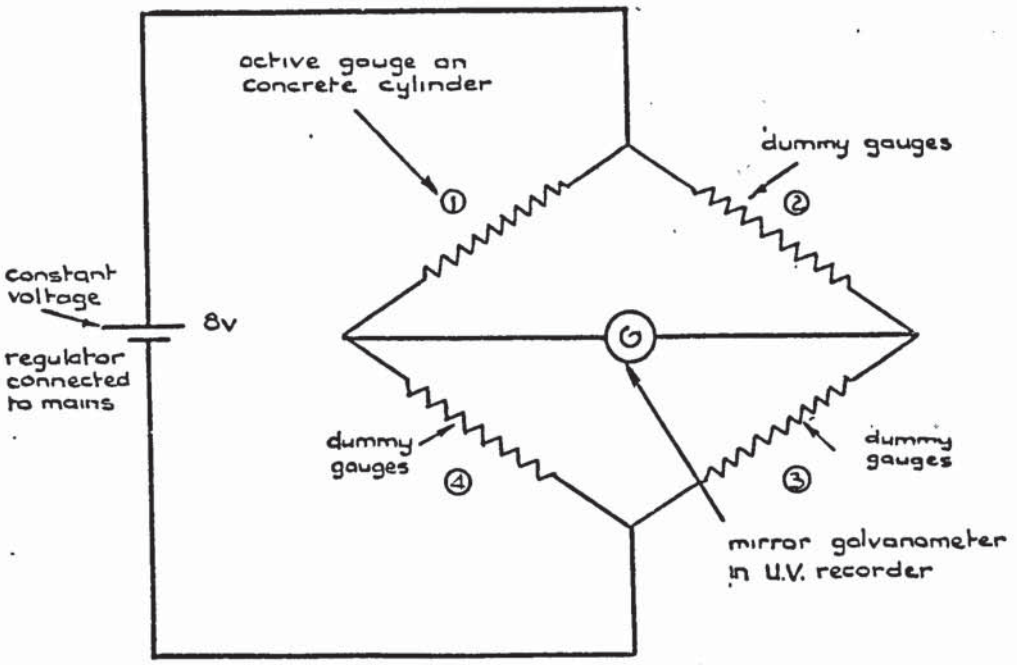

Fig. 6.4.1. Circuit diagram for U.V. recorder

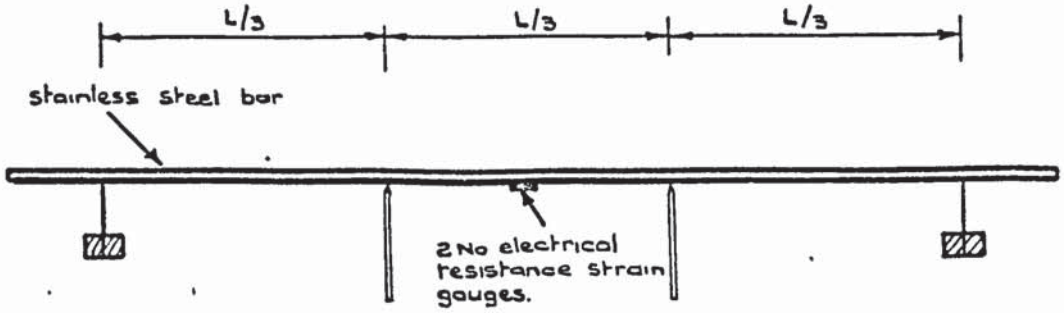

Fig. 6.4.2. Third point bending test for calibration of UV recorder.

microstrains produced the maximum deflection of 140 mm on the recorder.

Testing was carried out in a variable capacity Denison testing machine, the rate of loading for both cubes and cylinders being in accordance with B.S. 1881. Knowing the rate of loading and the speed of the paper leaving the recorder it was possible to graduate the vertical scale of the graph in terms of stress.

6.4.3. Theory

The assumed idealized form of the stress - strain curve for concrete is shown, in dimensionless form, in Fig. 6.4.4. In order to obtain a solution the following assumptions were made

1) The curve is parabolic

2) The slope of the curve at the point (1, 1) is zero.

Now the equation of a parabola can take the form

$$ax^2 + bx = y^2 + cy \qquad 6.4.1.$$

where

$$y = {}^{f_p}/_{f'_c} \qquad x = {}^{\varepsilon_c}/_{\varepsilon_{uc}}$$

d.w.r.t.x we get

$$2y \cdot \frac{dy}{dx} + c \cdot \frac{dy}{dx} = 2ax + b \qquad 6.4.2$$

at the point (1, 1) ${}^{dy}/_{dx} = 0$

$$\therefore 0 = 2a + b \qquad 6.4.3.$$

at the point (0, 0) ${}^{dy}/_{dx} = S_c$

$$\therefore c.S_c = b \qquad 6.4.4.$$

when x = 1, y = 1, then 6.4.1. becomes

$$a + b = 1 + c \qquad 6.4.5.$$

equating equations 6.4.3., 6.4.4, and 6.4.5, we get

$$c = \frac{2}{S_c - 2}$$

$$b = \frac{2 S_c}{S_c - 2}$$

$$a = \frac{S_c}{2 - S_c}$$

substituting for a, b, c, x, and y in 6.4.1. and rearranging we get

$$\frac{\varepsilon_c}{\varepsilon_{uc}} = 1 \pm \sqrt{1 + \left(\frac{2 - S_c}{S_c}\right)\left({}^{f_p}/_{f'_p}\right)^2 - \frac{2}{S_c}\left({}^{f_p}/_{f'_c}\right)} \qquad 6.4.8.$$

The minus sign represents the rising part of the curve, and the plus sign the falling part.

The failure loads of all specimens along with the highest recorded strains in each cylinder are given in Table 6.4.1. Fig.6.4.3 represents the average of all 24 stress - strain graphs obtained from the U.V. recorder.

The dimensionless form of the stress - strain curve is shown in Fig. 6.4.4. and compared with the theoretical curves obtained from equation 6.4.8. The theoretical curves have been plotted using 2 values of S_c, the slope of the stress - strain curve at the origin. The initial tangent modulus, Ec, was that measured from the curve in Fig. 6.4.3. The dynamic modulus of elasticity, Ed, was calculated using the relationship [47].

$$E_c = 1.6\, E_d - 44.$$

Both theoretical curves show fairly close agreement with that measured, the variation in S_c appearing to have very little effect on their shapes.

Comparison is made in Fig. 6.4.5 between the authors theoretical curve and those proposed by other investigators mentioned

150 mm Cubes	150 mm diameter Cylinders			
U_{w_2} N/mm^2 (lbs/in^2)	Maximum Recorded Strain (Microstrains)		Average $\frac{① + ②}{2}$	f_c' N/mm^2 (lbs/in^2)
	1	2		
39.93 (5790)	2501	3284	2893	34.50 (5003)
41.88 (6073)	3329	3838	3584	37.44 (5429)
41.88 (6073)	No readings			23.34 (3384)
42.59 (6176)	4520	4855	4688	29.20 (4234)
42.59 (6176)	3364	3820	3592	29.77 (4317)
41.92 (6078)	1414	2178	1796	31.57 (4578)
44.67 (6477)	3657	5355	4506	30.11 (4366)
43.12 (6252)	1035	3856	2446	37.10 (5380)
41.26 (5983)	3140	4338	3739	28.53 (4137)
40.46 (5867)	2018	6319	4169	32.70 (4742)
43.07 (6245)	3847	5105	4476	26.16 (3793)
37.72 (5469)	1898	5034	3466	33.88 (4913)
41.76 (6055)	Average		3577	31.19 (4523)
4%	% coeff. var.		25%	14%

$f_c'/U_w = 0.75$

TABLE 6.4.1.

Experimental Results – Stress – Strain Relationship

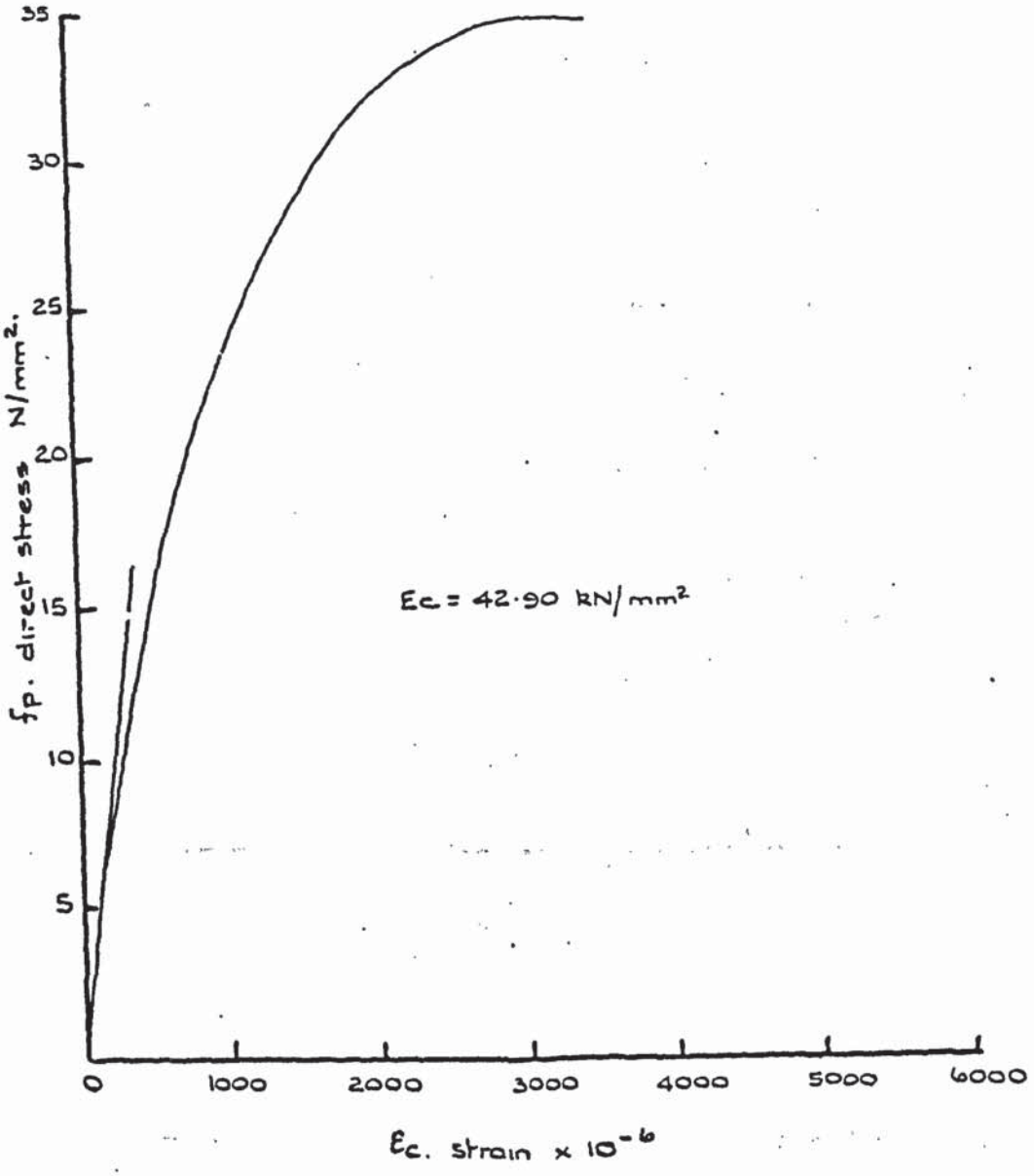

Fig. 6.4.3. Experimental curve.

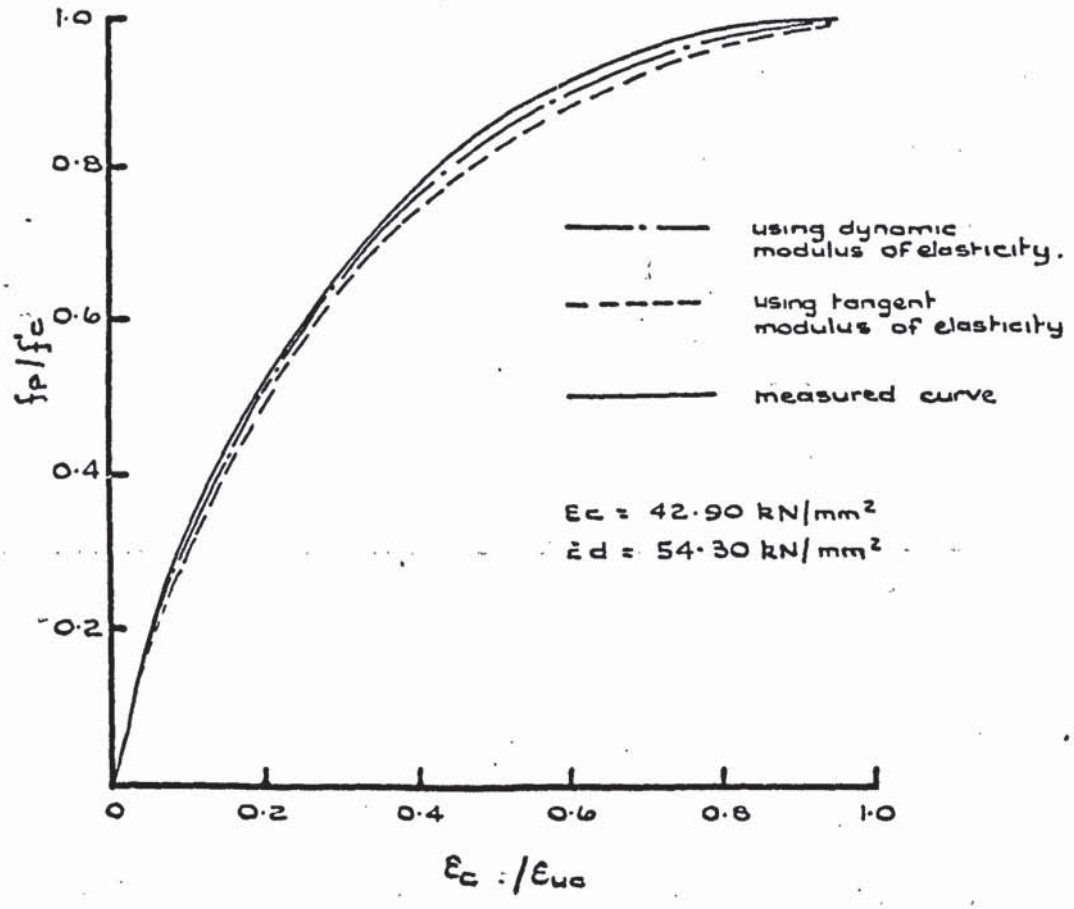

Fig. 6.4.4. Comparison of experimental and theoretical curves.

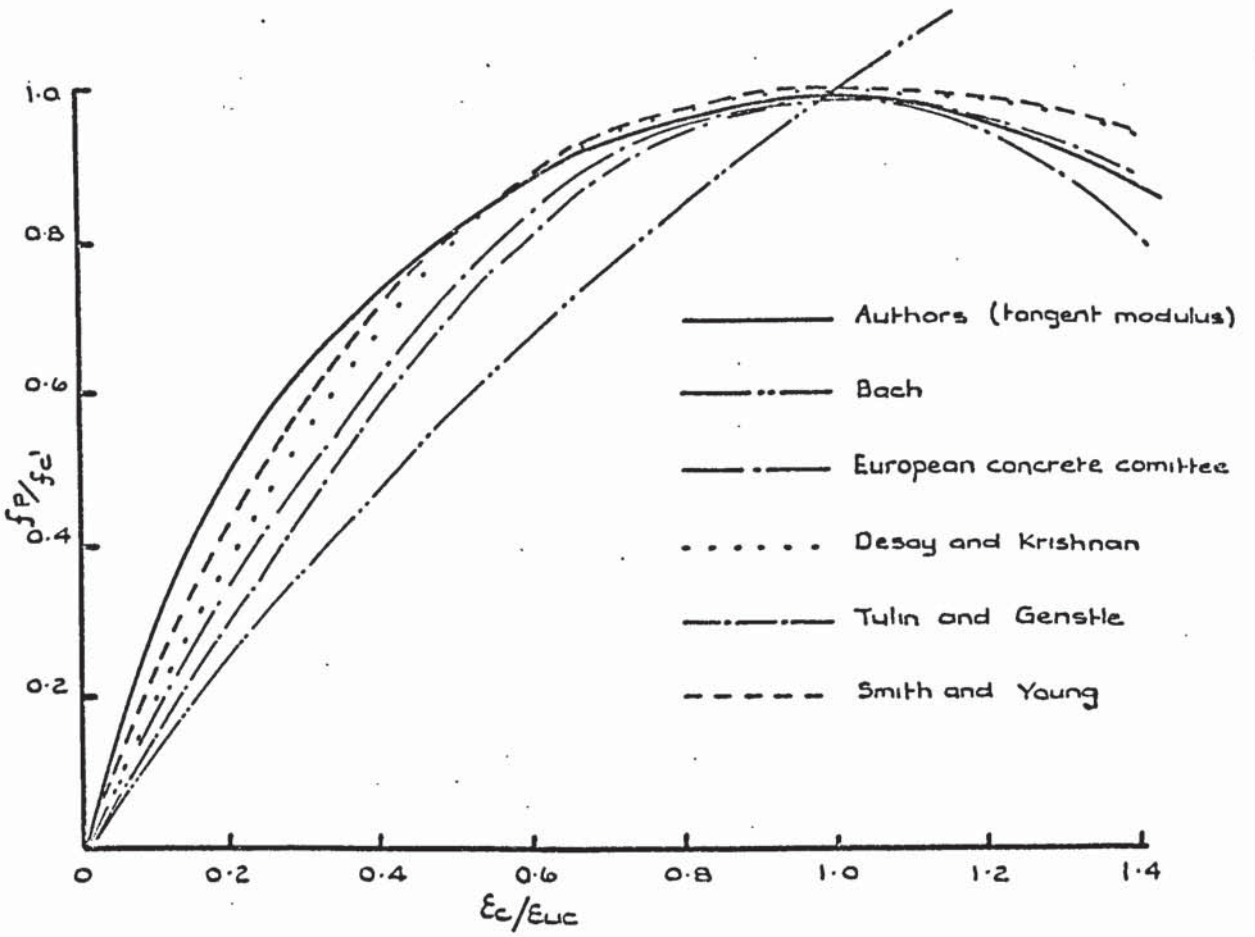

Source	Formula for axial stress f_p	Dimensionless form for f_p/f'_c
Bach	$C_1\varepsilon_c^{\,n}$	$(\varepsilon_c/\varepsilon_{uc})^{0.8}$
European Concrete Committee	$E_c\varepsilon_c^{\,n}(1-\varepsilon_c/2\varepsilon_{uc})$	$(\varepsilon_c/\varepsilon_{uc})(2-\varepsilon_c/\varepsilon_{uc})$
Desayi and Krishnan	$E_c\varepsilon_c/(1+(\varepsilon_c/\varepsilon_{uc})^2)$	$(\varepsilon_c/\varepsilon_{uc})2/(1+(\varepsilon_c/\varepsilon_{uc})^2)$
Tulin and Gerstle	$E_c\varepsilon_c/(C_2+(\varepsilon_c/\varepsilon_{uc})^n$	$(\varepsilon_c/\varepsilon_{uc})3/(2+(\varepsilon_c/\varepsilon_{uc})^3)$
Smith and Young	$E_c\varepsilon_c\, e^{-\varepsilon_c/\varepsilon_{uc}}$	$(\varepsilon_c/\varepsilon_{uc})\, e^{1-\varepsilon_c/\varepsilon_{uc}}$

Fig. 6.4.5. Formulas for ascending branch of stress - strain curve and comparison with authors.

in 6.4.2. The authors curve tends to be slightly steeper than any of those shown, although agreement is still satisfactory. Good comparison between a particular set of results and theoretical solutions proposed by other experimenters is not always to be expected. The nature of the curve, as mentioned in 6.4.2, is dependent upon many factors, and one theoretical curve will not necessarily fit more than one set of results.

It is also realized that conditions produced in the test described here may not be analogous to those in the prestressed beam. The method of testing, as referred to in 6.4.2, is considered by many to effect the shape of the curve. Opinions on this matter, however, tend to differ. Had time allowed the author would have liked to clarify this point by carrying out a series of tests on beams in flexure.

It is not certain whether or not the theoretical solution for the falling part of the curve is a good representation of the experimental results. As the cylinder approached failure extensive cracking on its outer surface was responsible for the failure of many of the strain gauges. It was therefore impossible to obtain any satisfactory results on the falling branch of the curve.

Despite these uncertainties it is still felt that the proposed solution is a good approximation of the behaviour of the concrete used in this investigation.

The average cube compressive strength to cylinder compressive strength ratio obtained from the tests was 0.75. This is in good agreement with that of 0.73 obtained from the prestressed beam tests. The unusually low value does not appear, therefore, to be connected with the method of vibration of the specimens. There are many factors effecting this ratio and it would require an

exhaustive investigation before a comprehensive solution could be reliably obtained.

Chapter 7

Conclusions

From the work carried out by the author concerning the behaviour of eccentrically prestressed rectangular beams under combined bending and torsion, the following conclusions have been drawn.

1) The test rig, designed by the author to apply varying ratios of bending moment and torsion to a rectangular beam, proved to be satisfactory.

2) From the tests carried out on 22 No. prestressed beams under M/T ratios ranging from pure torsion to pure bending, 3 distinct modes of failure were observed.

3) Under very low M/T ratios failure occurs by rotation about a compression hinge in the bottom face of the beam. This takes place immediately after the formation of the first crack and is referred to as a Mode 3 failure. Such a mode has not been observed before in rectangular prestressed beams although it has been noted in reinforced concrete. A small increase in bending moment increases the compressive stress in the top of the beam and this stress results in an increase in the torsional resistance. This increase reaches a maximum of approximately 50% of its capacity in pure torsion.

The theory proposed for this mode of failure is of the form:-

$$\left(\frac{T_3}{T_{u3}}\right)^2 - \frac{M_3}{M_{u3}} = 1.$$

The theory is based on a simple elastic approach and assumes that the critical stress occurs at the top of the beam.

4) Under higher M/T ratios the failure mechanism (referred to as a Mode 2 failure) changes to one of rotation about a compression hinge on the side face of the beam. This is caused by the relief, under higher bending moments, of the compressive stresses due to prestress in the lower part of the beam. The result is a lowering of the position of the critical stress and a subsequent rotation about a hinge on the side of the beam. Failure again occurs after the formation of the first crack. There is no notable increase in the torsional resistance with an increase in the bending moment for beams failing in this mode. The torsional resistance of beams failing in Mode 2 will be increased if the compressive stress due to prestress in the bottom of the beam is increased.

The theoretical solution proposed for this mode is of the form

$$\frac{T_2}{T_{u2}} = 1$$

The theory is again based on an elastic approach and assumes that the critical stress is situated at the centre of the longer side. There is evidence to suggest that in some cases a dowel action is produced which results in a compressive failure of the concrete.

5) When approximately 90% of the ultimate moment in pure bending has been applied the failure mechanism changes to one of a compressive failure of the concrete in the top of the beam. This is referred to as a Mode 1 failure. All beams failing in this mode show extensive cracking before failure. A small increase in the bending moment results in a large decrease in the torsional resistance of the beam. The theoretical solution is based upon the equilibrium of a cracked section about a skew axis and is of the form

$$T = k_t \, bd_n \, L_1 \, f'_c \left\{ \frac{0.2}{\sqrt{\left(\frac{f_m}{2f_v}\right)^2 + 1} - 0.3\left(\frac{f_m}{f_v}\right)} \right\}$$

The failure of the concrete in the top of the beam under the combination of direct stresses and torsional shear stresses is considered to be governed by the Cowan[25] criteria of failure.

6) The torsional stiffness of the prestressed concrete beams before cracking is little influenced by the presence of flexure.

7) The results of tests on 22 No. hollow cylinders tested under varying ratios of compressive stress to shear stress indicated a mode of failure governed by a principal tensile strain criteria. The results were not considered applicable to the behaviour of the concrete in the top of those beams failing in Mode 1.

8) Tests were carried out on 20 No. split cubes subjected to differing ratios of direct stress to shear stress. The results indicated a possible relationship between the mode of failure obtained from experiments and the Cowan slip plane criteria.

9) An investigation was carried out concerning the direct tensile strength of the concrete. Tests were conducted on 20 No. standard 150 mm (6 in.) diameter cylinders under conditions of simple tension. Despite making many modifications to the techniques employed in gripping the ends of the cylinders, failure always occurred at or near one end of the specimen. In all cases it was concluded that failure was the result of a state of triaxial tension.

10) From the results of tests in simple compression on 12 No. standard 150 mm (6 in.) diameter cylinders a non-linear stress - strain relationship for the concrete was proposed. The solution was used in conjunction with the theoretical solution for Mode 1 to predict the ultimate load of the author's beams. It was conoluded, however, that for the conditions occurring in these beams a non-linear relation-

ship yielded results very close to those obtained using a linear relationship.

11) Results from tests on modulus of rupture beams indicated a possible relationship between the modulus of rupture strength and the shape of the section. This is in addition to that relationship which is thought to exist between the modulus of rupture strength and the depth of the section.

12) The theoretical solutions proposed show good correlation with the author's results for all modes of failure. The overall average and coefficient of variation of the experimental to theoretical ratio is 1.14 and 11% respectively.

13) Theoretical solutions for beams with and without a dowel force are proposed. The inclusion of a dowel force is shown to increase the torsional resistance of a beam by up to 50%. The magnitude of the dowel force is dependent upon the type of prestressing steel used (i.e. steel strands or bars) and whether or not it is free to move in its void.

14) The theoretical solutions for all modes of failure have been compared with a total of 131 results taken from the author and other investigators. For some results in Mode 1 the dowel force has been included where appropriate. The overall average and coefficient of variation of the experimental to theoretical ratio is 1.02 and 17% respectively.

7.1 Recommendations for Future Work

From the results obtained in this investigation the following recommendations for future work are proposed.

1) The effect of a dowel force on those beams failing in Mode 2, under low M/T ratios, and its relationship to the type of prestressing steel used (i.e. steel strands or bars).

2) The effect of the shape and size of the beam section

on the modulus of rupture value and its application to the failure of those beams governed by the tensile strength of the concrete.

3) The effect of the relationship between the strain in the steel and the adjacent concrete for beams with both bonded and unbonded reinforcement.

4) An investigation into the relationship between the cube crushing strength and the cylinder crushing strength of the concrete and its application to those beams whose failure is governed by the compressive strength of the concrete.

5) The difference in the dowel forces resisted by prestressed wires and bars for those beams failing in Mode 1.

6) The effect of the geometry and shape of the cross - section on the ultimate strength of members failing under all ratios of bending moment to torsion.

7) The effect of the addition of web reinforcement on the behaviour of prestressed beams under combined bending and torsion.

8) A study of the behaviour of prestressed concrete beams under combined, bending, torsion, and shear.

References

1. St. Venant. Nadai, A. "Theory of flow and fracture of solids". V.1 McGraw-Hill 1950. pp. 208.

2. Miyamoto, T. "Torsional strength of reinforced concrete". Concrete and Constructional Engineering. (London) V.22. 1927. pp. 637.

3. Turner, L. and Davies, V. C. "Plain and reinforced concrete in torsion". Selected Engineering Paper. No. 165. Inst. Civ. Engrs. 1934.

4. Marshall, W. T. and Tembe, N. R. "Experiments on plain and reinforced concrete in torsion". Struct. Engr. (London). V.19. 1941. pp. 177.

5. Nadai, A. "Theory of flow and fracture of solids". V.1. McGraw-Hill 1950. pp. 494-499.

6. Nylander, H. "Vridning och vridningsinspanning vid betongkonstruktioner". (torsion and torsional restraint of concrete structures). States Komitte for Byggnadsforskning. Stockholm, Bulletin No. 3. 1945.

7. Cowan, H. J. and Armstrong, S. "Experiments on the strength of reinforced and prestressed concrete beams and of concrete-encased steel joists in combined bending and torsion". Mag. Conc. Res. V.7. No. 19. March 1955. pp. 3 - 20.

8. Reynolds, G. C. "The strength of prestressed concrete grillage bridges". C. and C.A. Technical Report. TRA/268. June 1957.

9. Zia, P. "Torsional strength of prestressed concrete members". Proc. Amr. Conc. Inst. V.32 No. 10. April 1961. pp. 1337-1359.

10. Gardner, R. P. M. "The behaviour of prestressed concrete I beams under combined bending and torsion". C. and C.A. Technical Report TRA/39. Feb. 1960.

11. Reeves, J. S. "Prestressed concrete T beams under combined bending and torsion". C. and C.A. Technical Report. TRA/364. Dec. 1962.

12. Humphreys, R. "Torsional properties of prestressed concrete". Struct. Engr. V. 35. No. 6. June 1957. pp. 213-224

13. Swamy, M. "The behaviour and ultimate strength of prestressed concrete hollow beams under combined bending and torsion". Mag. Conc. Res. V.14. No. 40. March 1962.

14. Van der Vlugt.and Rowe. "Reports on the torsional strength of prestressed concrete". 3rd Congress F.I.P. Berlin. 1958. Discussions. pp.44.

15. Gersch, C and Moore, W. H. "Flexure, shear and torsion tests on prestressed concrete I beams". Highway Research Board Bulletin 339. 1962.

16. Okada, K. Nishibayashi, S. and Abe, T. "Experimental studies of the strength of rectangular reinforced and prestressed concrete beams under combined flexure and torsion". Transactions of the Japanese Society of Civil Engineers No. 121. July 1966. pp. 39-51.

17. Bishara, A. "Prestressed concrete beams under combined bending torsion and shear". Proc. Amr. Conc. Inst. V66. July 1969 pp. 525-538.

18. Gausel, E. "Ultimate strength of prestressed concrete I beams in combined torsion, bending, and shear". Summary Paper. Proc. Amr. Conc. Inst. V.67. No. 9. Sept. 1970 pp.675-678.

19. Khalil, M. G. A. "Ultimate strength of prestressed concrete beams in combined bending and torsion". Ph.D. Thesis Leeds University. September 1967.

also

Evans, R. H. and Khalil, M. G. A. "The behaviour and strength of prestressed concrete rectangular beams subjected to combined

bending and torsion". Struct. Engr. V.48. No. 2. Feb 1970. pp. 59-73.

20. Hsu, T. T. C. "Torsion of structural concrete - plain concrete rectangular sections". Special Publication SP-18. Amr. Conc. Inst. Detroit 1968. pp. 203-258.
21. Hsu, T. T. C. "Torsion of structural concrete - uniformly pre-stressed rectangular members without web reinforcement". J. Prestr. Conc. Inst. V.13. No.2. April 1968. pp. 34-44.
22. Zia, P. "What do we know about torsion in concrete members?" J. Struct. Div. Proc. Amr. Soc. Civ. Eng. V.96. No. ST6. June 1970. pp. 1191.
23. Mukherjee, P. R. and Warwaruk, M. "Torsion, bending and shear in prestressed concrete". J. Struct. Div. Proc. Amr. Soc. Civ. Eng. V.97. No. ST4. April 1971. pp. 1063.
24. Nadai, A. "Theory of flow and fracture of solids". V.1 McGraw-Hill 1950. pp. 207-228.
25. Cowan, H. J. "The strength of plain, reinforced, and prestressed concrete under the action of combined stresses". Mag. Conc. Res. V.5. No. 14. Dec. 1953. pp. 75-86.
26. Leon, A. Cowan, H. J. and Lyalin, I. M. "Reinforced and prestressed concrete in torsion". Arnold 1965. pp. 55.
27. Bresler, B. and Pister, K. S. "Strength of concrete under combined stresses". Proc. Amr. Conc. Inst. V.55. No. 3. Sept. 1958. pp. 321-345.
28. Griffith, A. A. "The phenomena of rupture and flow in solids". Philosophical Transactions of the Royal Society. V.221A. 1920. pp. 163-168.
29. Newman, K. "Criteria for the behaviour of plain concrete under complex states of stress". Proc. Int. Confr. on the Structure of Concrete. London 1965.

30. Wright, P. J. F. "The effect of the method of test on the flexural strength of concrete". Mag. Conc. Res. No.11. Oct.1952. pp.67-76.

31. Hsu, T. T. C. and Mattock, A. H. "A torsion test rig". J. P.C.A. Res. and Devp. Labs. V.7. No. 1. Jan. 1965. pp. 2-9. P.C.A. Development Department Bulletin D91.

32. Collins, M. P. Walsh, P. F., Archer, F. E. and Hall, A. S. "Ultimate strength of reinforced concrete beams subjected to combined torsion and bending". Special Publication SP-18. Amr. Conc. Inst. Detroit 1968. pp. 379-402.

33. Cowan, H. J. "Reinforced and prestressed concrete in torsion". Arnold. 1965. pp. 17-20.

34. Lessig, N. N. "The determination of the load bearing capacity of rectangular reinforced concrete sections subject to combined torsion and bending". Study No.5, Conc. and Reinf. Conc. Inst. (Moscow)1959. pp. 5-28.

35. Ryder, G. H. "Strength of materials" 2 nd. Edit. Cleaver-Hume. London 1958. pp 50-54.

36. Martin, L. H. "Ultimate strength in bending and torsion of plain and reinforced concrete". Building Science. to be published.

37. Goode, C. D. and Helmy, M. A. "The strength of concrete under combined shear and direct stress". Mag. Conc. Res. V.19 No.59 Jan. 1967. pp. 105-112.

38. "Recommendations for an international code of practice for reinforced concrete. An Amr. Conc. Inst. and C. and C.A. publication.

39. Desayi, P. and Krishnan, S. "Equation of the stress-strain curve of concrete". Proc. Amr. Conc. Inst. V.61 No. 3 March 1964. pp. 345-350.

40. Whitney, C. S. "Plastic theory of reinforced concrete design". Transactions of Amr. Soc. Civ. Eng. V.107. 1942. pp. 251-282.

41. Hognestad, E., Hanson, N. W. and McHenry, D. "Concrete stress distribution in ultimate strength design". Proc. Amr. Conc. Inst. V52. No. 4 Dec. 1955. pp. 455-480.

42. Saenz, L. P. Discussion to references No. 41 Proc. Amr. Conc. Inst. V.61. Sept. 1964. pp.1229-1235.

43. Prentis, J. M. "The distribution of concrete stress in reinforced and prestressed concrete beams when tested to destruction by a pure bending moment". Mag. Conc. Res. No.5. Jan. 1951. pp. 73-77.

44. Smith, R. G. "The determination of the compressive stress-strain properties of concrete in flexure". Mag. Conc. Res. V.12. No.36. Nov. 1960.

45. Sturman, G. H., Shah, S. P. and Winter, G. "The effect of flexural strain gradients on microcracking and stress-strain behaviour of concrete". Proc. Amr. Conc. Inst. V.62. No.7. July 1965. pp. 805-822.

46. Smith, G. M. and Young, L. E. "Ultimate flexural analysis based on stress-strain curves of cylinders". Proc. Amr. Conc. Inst. V.53. No.6. Dec. 1956. pp. 597-610.

47. Draft British Standard Code of Practise for the structural use of concrete. Sept. 1969. pp.49.

48. Evans, R. H. "Extensibility and modulus of rupture of concrete". Struct. Eng. V.24. No.12. Dec.1946. pp. 636-639.

50. Gonnerman, H. F. and Shuman, E. C. "Compression, flexure, and tension tests on plain concrete." Proc. A.S.T.M. V.28. Pt.2. 1928. pp. 527-552.

51. Ward, M. A. "The testing of concrete materials by precisely controlled uniaxial tension". Ph.D. thesis. University of London. 1964.

52. Blakey, F. A. and Beresford, F. A. Discussion to paper No. 6012. Proc. Inst. Civ. Eng. V4. No.6. Nov. 1955. pp. 849-853.

53. Wright, P. J. F. "Comments on an indirect tensile test on concrete cylinders". Mag. Conc. Res. V.7. No. 20. July 1955.

54. Chapman, G. P. "The cylinder splitting test". Concrete. Feb. 1968. pp. 77-85.

55. Abrams, D. Discussion by Proudley, G. E. to a paper by Johnston, A. M. "Concrete in tension". Proc. A.S.T.M. V.26 Pt.II. 1926. pp.441.

56. O'Cleary, P. P. and ;Byrne, J. G. "Testing concrete and mortar in tension". Engineering. V. 189. No. 4900.18. March1960. pp. 384-385.

57. Johnston, C. D. and Sidwell, E. H. "Testing concrete in tension and compression". Mag. Conc. Res. V.20. No. 65. Dec. 1968. pp. 221-228.

58. Chapman, G. P. "The deformation and failure of concrete". Ph.D. Thesis University of Birmingham 1965.

APPENDIX

Program No. 1

Used to Solve for Beams Containing a Dowel Force and 2 Layers of Tensile Reinforcement

```
      MASTER PRCONSKEW3
      READ(1,3)J
    3 FORMAT(I0)
      B=5.0
      D=8.0
      D1=7.0
      FY=235200.0
      TK=0.667
      BMK=0.667
      ESC=15800000.0
      EST=20200000.0
      WRITE(2,4)B,D,D1,AST,FY,TK,BMK,ES,ASC
    4 FORMAT(2X,1HB,1X,F7.4,3X,1HD,1X,F7.4,3X,2HD1,1X,F7.4,3X,3HAST,1X,F
     16.4,3X,2HFY,1X,F8.0,3X,2HTK,1X,F6.4,3X,3HBMK,1X,F6.4,/3X,2HES,1X,F
     210.0,3X,3HASC,1X,F6.4)
      WRITE(2,5)
    5 FORMAT(/2X,2HBM,8X,1HT,8X,2HDS,8X,2HFC,8X,3HPTC,8X,2HPT,8X,2HEC,5X
     1,3HT1A,5X,4HT1AM,5X,2HDN,5X,3HRA1,5X,3HRAM)
      DO 11 I=1,J
      READ(1,6)BM,T,FC,PTC,PT,EC,DS,EST,ESC,FR1
    6 FORMAT(10F0.0)
      FC=0.9523*FC
      EC=30000.0*SQRT(FC)
      IF(DS.EQ.4.0)GO TO 83
      BMULT=152000.0
      DFT=0.8/(1.0+BM/BMULT)
      DFC=1.34/(1.0+BM/BMULT)
      AST=0.1196*DFT
      ASC=0.1196*DFC
      BMU=B*D*D*1000.0/6.0
      GO TO 84
   83 BMULT=226000.0
      DFT=0.8/(1.0+BM/BMULT)
      AST=0.1196*DFT
      ASC=0.1196*DFT
      PTS=1820.0
   84 FM=BM-BMU
      FM=BM/T
      ANGC=1.0+(PTS/FR1)
      ANG=SQRT((FM*FM)+(ANGC))-FM
      ANGL=ATAN(ANG)
      FC1=SIN(ANGL)/COS(ANGL)
   76 FC2=BM+PTC*(D1-DS)+T*FC1
      R1=EST/EC
      R2=ESC/EC
      P=AST/(B*D1)
      RP1=R1*P
      RP2=R2*P
      DN=D1*(-RP2+SQRT(RP2*RP2+(2.0*RP2)))
      A=DN
   75 A=A-0.01
      GO TO 86
   85 A=A+0.01
   86 AL1=D1-0.375*A
      AL2=DS-0.375*A
      FAD=AL1*(2.5*DFT-1.0)+AL2*(2.5*DFC-1.0)
      FAC1=(T*FC1)/((AL1*AL1)+(AL2*AL2))
      FAC2=(PT+PTC)-(FAC1*FAD)
```

Program No. 1 (Continued)

```
      FAC3=FC2-((AL1-AL2)*AL2*(2.5*DFC-1.0)*FAC1)
      FAC4=FAC2/FAC3
      FAC5=AL1*FAC4
      IF(FAC5.GT.0.98)GO TO 85
      SKAL=2.0*B*A*A*(1.0-FAC5)/3.0
      SKAR=(AST*(D1-A)*R1)+(ASC*R2*(DS-A)*(1.0-((DS-A)*FAC4)))
      DIFFA=SKAL-SKAR
      WRITE(2,72)ANGL,FC2,FC3,FAC1,FAC2,FAC3,FAC4,FAC5,FAC,SKAL,SKAR,A
   72 FORMAT(12F15.6)
      IF(SKAL.GT.SKAR)GO TO 75
      G=0.9*D1
      AL1=D1-0.375*G
      AL2=DS-0.375*G
      FGD=AL1*(2.5*DFT-1.0)+AL2*(2.5*DFC-1.0)
      FGC1=(T*FC1)/((AL1*AL1)+(AL2*AL2))
      FGC2=(PT+PTC)-(FGC1*FGD)
      FGC3=FC2-((AL1-AL2)*AL2*(2.5*DFC-1.0)*FGC1)
      FGC4=FGC2/FGC3
      FGC5=AL1*FGC4
      SKGL=2.0*B*G*G*(1.0-FGC5)/3.0
      SKGR=(AST*(D1-G)*R1)+(ASC*R2*(DS-G)*(1.0-((DS-G)*FGC4)))
      DIFFG=SKGL-SKGR
      WRITE(2,73)G,AL1,AL2,FGC1,FGC2,FGC3,FGC4,FGC5,FGC,SKGL,SKGR
   73 FORMAT(11F15.6)
      BB=A
      A=G
      G=BB
      PRODA=DIFFA*DIFFG
      IF(PRODA.LT.0.00)GO TO 7
      WRITE(2,8)
    8 FORMAT(5X,11HNO SOLUTION)
    7 C=(A+G)/2.0
      AL1=D1-0.375*C
      AL2=DS-0.375*C
      FCD=AL1*(2.5*DFT-1.0)+AL2*(2.5*DFC-1.0)
      FCC1=(T*FC1)/((AL1*AL1)+(AL2*AL2))
      FCC2=(PT+PTC)-(FCC1*FCD)
      FCC3=FC2-((AL1-AL2)*AL2*(2.5*DFC-1.0)*FCC1)
      FCC4=FCC2/FCC3
      FCC5=AL1*FCC4
      SKCL=2.0*B*C*C*(1.0-FCC5)/3.0
      SKCR=(AST*(D1-C)*R1)+(ASC*R2*(DS-C)*(1.0-((DS-C)*FCC4)))
      DIFFC=SKCL-SKCR
      WRITE(2,74)C,AL1,AL2,FCC1,FCC2,FCC3,FCC4,FCC5,FCC,SKCL,SKCR
   74 FORMAT(11F15.6)
      IF(DIFFC.GT.0.00)GO TO 9
      GO TO 10
    9 A=C
      GO TO 12
   10 G=C
   12 AMING=A-G
      IF(AMING.GT.0.001)GO TO 7
      DN=A
      AL1=D1-0.375*DN
      AL2=DS-0.375*DN
      IF(T.EQ.0.000)GO TO 88
      GRD1=AL2*(AL1-AL2)/(AL1*AL1+AL2*AL2)
      GRD2=BM+PTC*(D1-DS)
      GRD3=(TK*B*DN*AL1)-(ASC*R2*(DS-DN)*(D1-DS)/DN)
      GRD4=(TK*B*DN*AL1)/(T*(1.0+GRD1))
```

Program No. 1 (Continued)

```
      GRD=(GRD2*GRD4)/(GRD3*2.0)
      ERD=TK*B*DN*AL1*FC*0.2
      ERD=ERD/(1.0+GRD1)
      T1A=ERD/(SQRT(1.0+(GRD*GRD))-(0.6*GPD))
      T1AM=5.0*ERD/(SQRT(4.0*GRD*GRD+12.50))
      RA1=T/T1A
      RAM=T/T1AM
   88 BMT=(2.0*B*DN*AL1*FC/3.0)-(PTC*(D1-DS))
      WRITE(2,27)BM,T,DS,FC,PTC,PT,EC,T1A,T1AM,DN,RA1,RAM,BMT
   27 FORMAT(/2X,F8.0,2X,F8.0,2X,F7.4,2X,F6.0,2X,F7.0,2X,F7.0,2X,F8.0,2X
     1,F8.0,2X,F8.0,2X,F7.4,2X,F7.5,2X,F7.5,2X,F10.2)
   11 CONTINUE
      STOP
      END

MENT, LENGTH  1007, NAME  PRCCNSKEW3
```

Program No. 2

Used to Solve for Beams Containing a Dowel Force and 1 Layer of Tensile Reinforcement

```
      MASTER KHALILU3
      READ(1,3)J
    3 FORMAT(I0)
      B=3.9370
      D=6.8897
      D1=4.5931
      FY=235200.0
      TK=0.667
      BMK=0.667
      ES=27200000.0
      DS=0.0
      WRITE(2,4)B,D,D1,AST,FY,TK,BMK,ES,ASC
    4 FORMAT(2X,1HB,1X,F7.4,3X,1HD,1X,F7.4,3X,2HD1,1X,F7.4,3X,3HAST,1X,
     16.4,3X,2HFY,1X,F8.0,3X,2HTK,1X,F6.4,3X,3HBMK,1X,F6.4,/3X,2HES,1X,
     210.0,3X,3HASC,1X,F6.4)
      WRITE(2,5)
    5 FORMAT(/2X,2HBM,8X,1HT,8X,2HDS,8X,2HFC,8X,3HPTC,8X,2HPT,8X,2HEC,5
     1,3HT1A,5X,4HT1AM,5X,2HDN,5X,3HRA1,5X,3HRAM)
      DO 11 I=1,J
      READ(1,6)BM,T,FC,PTC,PT,EC,FR1
    6 FORMAT(7F0.0)
      EC=30000.0*SQRT(FC)
      IF(DS.EQ.0.000)GO TO 87
      IF(DS.EQ.4.0)GO TO 83
      BMULT=152000.0
      DFC=1.34/(1.0+BM/BMULT)
      AST=0.1196*DFT
      ASC=0.1196*DFC
      BMU=B*D*D*1000.0/6.0
      GO TO 84
   83 BMULT=226000.0
      DFT=0.8/(1.0+BM/BMULT)
      AST=0.1196*DFT
      ASC=0.1196*DFT
      BMU=B*D*D*1820.0/6.0
   84 BM=BM-BMU
   87 BMULT=151125.0
      DFT=0.8/(1.0+BM/BMULT)
      AST=0.601*DFT
      PTS=2804.0
      FM=BM/T
      ANGC=1.0+(PTS/FR1)
      ANG=SQRT((FM*FM)+(ANGC))-FM
      ANGL=ATAN(ANG)
      FD1=(2.5*DFT-1.0)
   76 FC1=FD1*T*SIN(ANGL)/COS(ANGL)
      FC2=BM+PTC*(D1-DS)+T*SIN(ANGL)/COS(ANGL)
      R=ES/EC
      P=AST/(B*D1)
      RP=R*P
      DN=D1*(-RP+SQRT(RP*RP+(2.0*RP)))
      A=DN
   75 A=A-0.01
      GO TO 86
   85 A=A+0.01
   86 AL=D1-0.375*A
      FAC=1.0-(((PTC+PT)*AL-FC1)/FC2)
```

Program No. 2 (Continued)

```
      RP1=RP/FAC
      SKAL=A/D1
      SKAR=-0.75*RP1+SQRT((0.75*RP1)*(0.75*RP1)+(1.5*RP1))
      DIFFA=SKAL-SKAR
      WRITE(2,72)ANGL,FC1,FC2,A,FAC,SKAL,SKAR
   72 FORMAT(1H0,F15.6,2X,F15.6,2X,F15.6,2X,F15.6,/2X,F15.6,2X,F15.6,2X
     1F15.6)
      IF(SKAL.GT.SKAR)GO TO 75
      G=0.9*D1
      AL=D1-0.375*G
      FAC=1.0-(((PTC+PT)*AL-FC1)/FC2)
      RP1=RP/FAC
      SKGL=G/D1
      SKGR=-0.75*RP1+SQRT((0.75*RP1)*(0.75*RP1)+(1.5*RP1))
      DIFFG=SKGL-SKGR
      WRITE(2,73)G,AL,FAC,SKGL,SKGR
   73 FORMAT(1H0,F15.6,2X,F15.6,2X,F15.6,/2X,F15.6,2X,F15.6)
      BB=A
      A=G
      G=BB
      PRODA=DIFFA*DIFFG
      IF(PRODA.LT.0.00)GO TO 7
      WRITE(2,8)
    8 FORMAT(5X,11HNO SOLUTION)
    7 C=(A+G)/2.0
      AL=D1-0.375*C
      FAC=1.0-(((PTC+PT)*AL-FC1)/FC2)
      RP1=RP/FAC
      SKCL=C/D1
      SKCR=-0.75*RP1+SQRT((0.75*RP1)*(0.75*RP1)+(1.5*RP1))
      DIFFC=SKCL-SKCR
      WRITE(2,74)C,AL,FAC,SKCL,SKCR
   74 FORMAT(1H0,F15.6,2X,F15.6,2X,F15.6,/2X,F15.6,2X,F15.6)
      IF(DIFFC.GT.0.00)GO TO 9
      GO TO 10
    9 A=C
      GO TO 12
   10 G=C
   12 AMING=A-G
      IF(AMING.GT.0.001)GO TO 7
      DN=A
      AL=D1-0.375*DN
      IF(T.EQ.0.000)GO TO 77
      GRD=(BM*PTC*(D1-DS))/(2.0*T)
      ERD=TK*B*DN*AL*FC*0.2
      T1A=ERD/(SQRT(1.0+(GRD*GRD))-(0.6*GRD))
      T1AM=5.0*ERD/(SQRT(4.0*GRD*GRD+12.50))
      RA1=T/T1A
      RAM=T/T1AM
   77 BMT=(2.0*B*DN*AL*FC/3.0)-(PTC*(D1-DS))
      WRITE(2,27)BM,T,DS,FC,PTC,PT,EC,T1A,T1AM,DN,RA1,RAM,BMT
   27 FORMAT(/2X,F8.0,2X,F8.0,2X,F7.4,2X,F6.0,2X,F7.0,2X,F7.0,2X,F8.0,2X
     1,F8.0,2X,F8.0,2X,F7.4,2X,F7.5,2X,F7.5,2X,F10.2)
   11 CONTINUE
      STOP
      END
```

EGMENT, LENGTH 771, NAME KHALILU3

Program No. 3

Used to Solve for Beams Containing No Dowel Force

```
      MASTER NODOWEL
      READ(1,3)J
    3 FORMAT(I0)
      B=3.937
      D=7.874
      D1=3.937
      EST=28000000.0
      PT=33170.0
      FC=5724.0
      EUC=0.0045
      FY=235200.0
      EUS=0.01
      TK=0.667
      BMK=0.667
      DS=0.00
      WRITE(2,4)B,D,D1,EUC,AST,FY,EUS,TK,BMK,ES,ASC
    4 FORMAT(2X,1HB,1X,F7.4,3X,1HD,1X,F7.4,3X,2HD1,1X,F7.4,3X,3HEUC,
     11X,F5.4,3X,3HAST,1X,F6.4,3X,2HFY,1X,F8.0,3X,3HEUS,1X,F5.4,3X,
     22HTK,1X,F6.4,3X,3HBMK,1X,F6.4,/2X,2HES,1X,F10.0,3X,3HASC,1X,F6.4)
      WRITE(2,5)
    5 FORMAT(/2X,2HBM,8X,1HT,8X,2HDS,8X,2HFC,8X,3HPTC,8X,2HPT,8X,2HEC,
     15X,5HT1ASV,5X,5HT1ASH,5X,2HDN)
      DO 11 I=1,J
      READ(1,6)BM,T
    6 FORMAT(2F0.0)
      IF(DS.EQ.0.000)GO TO 97
      IF(DS.EQ.4.0)GO TO 83
      BMULT=152000.0
      DFT=0.8/(1.0+BM/BMULT)
      DFC=1.34/(1.0+BM/BMULT)
      AST=0.1196*DFT
      ASC=0.1196*DFC
      ASC=0.000
      PTS=1000.0
      R=EST/EC
      GO TO 84
   83 BMULT=226000.0
      DFT=0.8/(1.0+BM/BMULT)
      AST=0.1196*DFT
      ASC=0.1196*DFT
      PTS=1820.0
      R=ESC/EC
      GO TO 84
   97 BMULT=143748.0*3.0
      DFT=1.0/(1.0+BM/BMULT)
      AST=DFT*0.3115
      ASC=0.000
      PTS=1070.0
      FR1=434.0
   84 EC=30000.0*SQRT(FC)
      R=EST/EC
      RT=EST/EC
      RC=ESC/EC
      P=AST/(B*D1)
      RP=R*P
      DN=D1*(-RP+SQRT(RP*RP+(2.0*RP)))
      IF(T.EQ.0.000)GO TO 87
   86 FM=BM/T
```

Program No. 3 (Continued)

```
      ANGC=1.0+(PTS/FR1)
      ANG=SQRT((FM*FM)+(ANGC))-FM
      ANGL=ATAN(ANG)
      GO TO 88
   87 ANGL=0.000
   88 SKW1=2.00*B/(COS(ANGL)*3.0)
      SKW2=RT*AST/COS(ANGL)
      SKW3=ASC*(1.0-RC)/COS(ANGL)
      SKW4=(PT+PTC)/((BM*COS(ANGL))+(T*SIN(ANGL))+(PTC*(D1-DS)*COS(ANGL
     1))
      SKW5=2.00*B/3.00
      SKW6=ASC*(D1-DS)*(RC-1.0)
      WRITE(2,71)RP,DN,ANGL,SKW1,SKW2,SKW3,SKW4,SKW5,SKW6,ASC
   71 FORMAT(1HO,2HRP,1X,F15.6,3X,2HDN,1X,F15.6,3X,4HANGL,1X,F15.6,3X,4
     1HSKW1,1X,F15.6,/3X,4HSKW2,1X,F15.6,3X,4HSKW3,1X,F15.6,3X,4HSKW4,1X
     2F15.6,3X,4HSKW5,1X,F15.6,/3X,4HSKW6,1X,F15.6,3X,3HASC,1X,F15.6)
      A=DN
      AL=D1-0.375*A
      SKWAL=SKW1*A*A
      SKWAR=SKW2*(D1-A)+SKW3*(A-DS)+A*SKW4*((A*SKW5*AL)+((A-DS)*SKW6/A)
      DIFFA=SKWAL-SKWAR
      WRITE(2,72)A,AL,SKWA1,SKWAL,SKWAR,DIFFA
   72 FORMAT(1HO,1HA,1X,F15.6,3X,2HAL,1X,F15.6,3X,5HSKWA1,1X,F15.6,3X,5
     1HSKWAL,1X,F15.6,/3X,5HSKWAR,1X,F15.6,3X,5HDIFFA,1X,F15.6)
      G=0.9*D1
      AL=D1-0.375*G
      SKWGL=SKW1*G*G
      SKWGR=SKW2*(D1-G)+SKW3*(G-DS)+G*SKW4*((G*SKW5*AL)+((G-DS)*SKW6/G)
      DIFFG=SKWGL-SKWGR
      WRITE(2,73)G,AL,SKWG1,SKWGL,SKWGR,DIFFG
   73 FORMAT(1HO,1HG,1X,F15.6,3X,2HAL,2X,F15.6,3X,5HSKWG1,1X,F15.6,3X,5
     1HSKWGL,1X,F15.6,/3X,5HSKWGR,1X,F15.6,3X,5HDIFFG,1X,F15.6)
      BB=A
      A=G
      G=BB
      PRODA=DIFFA*DIFFG
      IF(PRODA.LT.0.0)GO TO 7
      WRITE(2,8)
    8 FORMAT(5X,2HNO,1X,8HSOLUTION)
    7 C=(A+G)/2.0
      AL=D1-0.375*C
      SKWCL=SKW1*C*C
      SKWCR=SKW2*(D1-C)+SKW3*(C-DS)+C*SKW4*((C*SKW5*AL)+((C-DS)*SKW6/C)
      DIFFC=SKWCL-SKWCR
      WRITE(2,74)C,AL,SKWC1,SKWCL,SKWCR,DIFFC
   74 FORMAT(1HO,1HC,1X,F15.6,3X,2HAL,1X,F15.6,3X,5HSKWC1,1X,F15.6,3X,5
     1HSKWCL,1X,F15.6,/3X,5HSKWCR,1X,F15.6,1X,5HDIFFC,1X,F15.6)
      IF(DIFFC.GT.0.00)GO TO 9
      GO TO 10
    9 A=C
      GO TO 12
   10 G=C
   12 AMING=A-G
      IF(AMING.GT.0.001)GO TO 7
      DN=A
      AL=D1-0.375*DN
      IF(T.EQ.0.000)GO TO 77
      FP=BMK*B*DN*AL
      FP1=ASC*(DN-DS)*(D1-DS)*(RC-1.0)/DN
```

Program No. 3 (Continued)

```
      FP=EP+EP1
      FM=(BM+PTC*(D1-DS))/EP
      IF(DN.LE.B)GO TO 24
      GTSH=0.5*B*B*(DN-(B/3.0))/T
      GO TO 81
   24 GTSH=0.5*DN*DN*(B-(DN/3.0))/T
   81 FSH=FM*GTSH
      GTS1=0.2*FC*T*GTSH
      GTS2=SQRT(1.0+(FSH*FSH/4.0))-(0.3*FSH)
      WRITE(2,82)FM,GTSH,FSH,GTS1,GTS2
   82 FORMAT(5F15.5)
      T1ASH=GTS1/GTS2
      RASH=T/T1ASH
   77 BMT=(2.0*B*DN*AL*FC/3.0)-(PTC*(D1-DS))
      WRITE(2,27)BM,T,DS,FC,PTC,PT,EC,T1ASV,T1ASH,DN,RASH,BMT
   27 FORMAT(/2X,F8.0,2X,F8.0,2X,F7.4,2X,F6.0,2X,F7.0,2X,F7.0,2X,F8.0,2X
     1,F8.0,2X,F8.0,2X,F7.4,2X,F7.5,2X,F10.2)
   11 CONTINUE
      STOP
      END

SEGMENT, LENGTH   892, NAME  NODOWEL
```